AD NUMBER

AD357974

CLASSIFICATION CHANGES

TO: unclassified

FROM: confidential

LIMITATION CHANGES

TO:

Approved for public release, distribution unlimited

FROM:

Distribution authorized to DoD only; Administrative/Operational Use; Mar 1965. Other requests shall be referred to Director, Atomic Support Agency, Washington, DC 20301.

AUTHORITY

HQ DNA/IMTI ltr dtd 8 Jun 1994; HQ DNA/IMTI ltr dtd 8 Jun 1994

AD 357974L

Operation

TUMBLER

NEVADA PROVING GROUNDS

April-June, 1952

Projects 1.3 and 1.5

FREE-AIR AND GROUND-LEVEL PRESSURE MEASUREMENTS

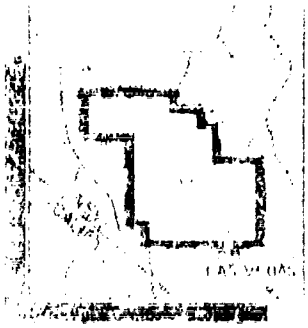

ARMED FORCES SPECIAL WEAPONS PROJECT
WASHINGTON, D. C.

Operation TUMBLER

NEVADA PROVING GROUNDS

April-June, 1952

Projects 1.3 and 1.5

FREE-AIR AND GROUND-LEVEL PRESSURE MEASUREMENTS

SPECIAL WEAPONS PROJECT

CONFIDENTIAL

[redacted]

U. S. MILITARY AGENCIES MAY OBTAIN COPIES OF THIS REPORT DIRECTLY FROM DDC. OTHER QUALIFIED USERS SHALL REQUEST THROUGH

Director
Defense Atomic Support Agency
Washington, D. C. 20301

This document contains information affecting the national defense of the United States within the meaning of the Espionage Laws, Title 18 U. S. C. Sections 793 and 794. The transmission or the revelation of its contents in any manner to an unauthorized person is prohibited by law.

FORMERLY RESTRICTED DATA
HANDLE AS RESTRICTED DATA IN FOREIGN DISSEMINATION
SECTION 144b, ATOMIC ENERGY ACT 1954

[redacted]

EXCLUDED FROM AUTOMATIC REGRADING; DOD DIR 5200.10 DOES NOT APPLY

[redacted]

CONFIDENTIAL

[redacted]

This document consists of 261 pages

No. [redacted] of 305 copies, Series A

(21 Report no.

OPERATION TUMBLER

Projects 1.3 and 1.5

FREE-AIR AND GROUND-LEVEL PRESSURE MEASUREMENTS

REPORT TO THE TEST DIRECTOR

by

C. J. Aronson
J. F. Moulton, Jr.
J. Petes
E. J. Culling
E. R. Walthall

November 1952

(17) Rept no. NOL-1166

NAVAL ORDNANCE LABORATORY REPORT 1166

U. S. Naval Ordnance Laboratory
White Oak, Silver Spring 19, Maryland

[redacted]

CONFIDENTIAL

[redacted]

Reproduced Direct from Manuscript Copy by
AEC Technical Information Service
Oak Ridge, Tennessee

Inquiries relative to this report may be made to

Chief, Armed Forces Special Weapons Project
P. O. Box 2610
Washington, D. C.

ABSTRACT

The Naval Ordnance Laboratory participated in all four air burst shots of Operation TUMBLER at the Nevada Proving Grounds by measuring free-air peak pressures and pressure variation with time by means of rocket smoke-trail photography and by measuring pressure-time data at ground level by means of Bendix inductance gages using an FM transmission system.

As the free-air data scaled well, a reliable composite free-air pressure-distance curve from 6 to 800 psi has been obtained in terms of 1 KT (Radiochemical) at sea level. Efficiencies in free-air were estimated to be of the order of 45 per cent compared to cast TNT spheres at about the 20 psi level.

Data from the gages in the ground show that the first three shots fell between the so-called "Fair" and "Good" height-of-burst curves while data from the last shot fell between the "Poor" and "Fair" curves. The optimum height of burst for the test conditions was found to be zero for pressure levels greater than 12 psi and to follow the empirical relation $H_{op} = \frac{19,690}{14.7 + p}$ between 12 and 3 psi where p is the overpressure in psi and H'_{op} is in ft for 1 KT(RC) at sea level.

Long rise times were encountered on the fourth shot except at low pressure ranges, and rounding or chopping-off of the peak shock occurred on all shots in the regular region in varying amounts. Shots 2 and 3 which were at nearly scaled heights gave ground level data which scaled well.

Decay constants and impulses calculated from particle displacement measurements scaled well with high explosives results; but the free-air pressure-time curves themselves were arrived at by such smoothing processes that no fine structure of the pressure-time history could be determined from them.

Comparisons with high explosives data indicated the importance of the height of the measuring system above the ground level. Calculations based on the free-air pressure curve and ideal reflection theory showed that in the regular region on Shots 1 and 2 the ground level pressures could have been reasonably well predicted, but that predictions for the Shot 4 results would have been too high. This fact showed up in other phases of the analysis the most outstanding of which was the direct evidence of a precursor shock, ahead of the incident shock, on TUMBLER 4. This phenomenon is shown to be similar to certain underwater explosion effects and to have been predictable on the basis of acoustic theory if a heated layer of air near the ground were assumed to exist.

PREFACE

This report on the work of the Naval Ordnance Laboratory group on Operation TUMBLER (Projects 1.3 and 1.5) presents all the data thus far extracted from the records. Most of the information has been checked at least once, and it is not planned to re-examine it unless questions are raised on specific points. There are, particularly on the particle-displacement motion picture records, some data which have not been completely analyzed; however, it is not believed that such data will alter the conclusions of this report.

It should be noted that enough of the data presented in the preliminary reports, Annexes II and XXI to the Operation TUMBLER Preliminary Report of 15 May 1952, have been revised for presentation in this report to make both of these preliminary annexes of questionable value as references; and it is strongly recommended that existing copies of them be destroyed. These revisions are not expected to modify the basic conclusions previously presented, but they are important in any consideration where the data are to be compared in detail with data from other projects or from other operations.

This report was prepared as Naval Ordnance Laboratory Report 1166 for publication and distribution by the Armed Forces Special Weapons Project as WT-513.

ACKNOWLEDGMENTS

Planning for the Naval Ordnance Laboratory's participation was done by Dr. G. K. Hartmann, Dr. P. M. Fye, Dr. J. E. Ablard, Dr. W. E. Morris, Mr. C. J. Aronson, Mr. J. F. Moulton, Jr., and Mr. Joseph Petes. Administrative details were capably handled by LCDR J. D. McClendon with advice and assistance in planning by CDR F. E. Somers and Mr. Joseph Shisko. Mr. J. R. Mitchell successfully met the difficult problems imposed on logistics by the stringent time scale of the operation. He was aided in this by the Supply and Fiscal Department of the Naval Ordnance Laboratory and by Major C. W. Burns of the J-4 Division of the Test Command.

Appreciation is sincerely expressed to the Military Effects Tests Group and the office of Program One which spared no pains to smooth out the administrative and technical difficulties encountered in the field by Projects 1.3 and 1.5. In particular the work of Lt. Col. G. B. Page, Dr. H. Scoville, Jr., and CDR D. C. Campbell made this well-run operation a pleasant, and it is believed a most worth while experience. Appreciation is also expressed to Edgerton, Germeshausen, and Grier, Inc., whose excellent photography was the source of all Project 1.5 data. Their cooperation made the results available rapidly and simplified the work of the NOL group appreciably.

The authors are indebted to the following persons who competently aided in the analysis of the data for this report:

LCDR J. D. McClendon
P. Hanlon
F. Theilheimer
T. A. Flynn
R. L. Varwig
LT(jg) C. C. Little
F. J. Oliver
C. L. Karmel
C. A. Dixon

Preparation of material in form for publication was done by:

M. M. Case
J. R. Mitchell
M. M. Fox
S. Woolston
R. Q. Hiser
L. A. Grymes
J. W. Culbertson
R. B. Granet
E. L. Rankin
M. Simon
V. Sorrell
E. Zdanis

CONTENTS

ABSTRACT 3

PREFACE 5

ACKNOWLEDGMENTS 7

ILLUSTRATIONS 13

TABLES 19

CHAPTER 1 INTRODUCTION 23

1.1 General Objectives 23
1.2 Objectives of Projects 1.3 and 1.5 23
1.3 Methods 24
1.4 Test Conditions 24
1.4.1 Inductance Gages 24
1.4.2 Rocket Lines 25
1.5 Summary of Instrument Performance 25
1.6 Conversion Factors and Scaling 25
1.7 Personnel and Responsibilities 28
1.8 Costs of Projects 1.3 and 1.5 29

CHAPTER 2 GROUND LEVEL PRESSURE-TIME MEASUREMENTS (PROJECT 1.3) 31

2.1 Instrumentation 31
2.1.1 General 31
2.1.2 Gages 31
2.1.3 Oscillator-Amplifier 39
2.1.4 Recording System 40
2.1.5 Power 42
2.1.6 Playback and Data Reduction 42
2.1.7 System Errors 46
2.1.8 Recommendations for Instrumentation . . 47
2.2 Results 49
2.2.1 TUMBLER 1 52
2.2.2 TUMBLER 2 60
2.2.3 TUMBLER 3 61
2.2.4 TUMBLER 4 76
2.2.5 Comparison of Data 88

CONTENTS (CONT.)

CHAPTER 3 PHOTO-OPTICAL PRESSURE MEASUREMENTS (PROJECT 1.5) . . 90

3.1 Background and Basic Theory 90
3.1.1 The Shock Velocity Method of Peak Pressure Determination 90
3.1.2 The Particle Displacement Method of Pressure-Time Determination 91
3.2 Instrumentation 92
3.2.1 The Smoke Rocket Detection Grid 92
3.2.2 Photographic Instrumentation 93
3.3 Results 93
3.3.1 Pressure-Distance Results - TUMBLER 1 . . 95
3.3.2 Pressure-Distance Results - TUMBLER 2 . .102
3.3.3 Pressure-Distance Results - TUMBLER 3 . .106
3.3.4 Pressure-Distance Results - TUMBLER 4 . .109
3.3.5 Free-air Pressure-Time Results-TUMBLER 1 .112
3.3.6 Free-air Pressure-Time Results-TUMBLER 4 .113
3.3.7 Determination of the Decay Parameter, θ .125
3.3.8 Accuracy of Results 126

CHAPTER 4 REDUCED RESULTS 132

4.1 Ground Level Data 132
4.2 Photo-Optical Data in Free Air 133
4.2.1 Arrival Time of the Shock Wave in Free Air 133
4.2.2 Pressure-Distance in Free Air 146
4.2.3 Pressure-Time in Free Air 146
4.2.4 Reduced Decay Parameter, θ 150

CHAPTER 5 DISCUSSION OF RESULTS 151

5.1 Height-of-Burst Comparisons 151
5.1.1 Height-of-Burst, TUMBLER and High Explosives 151
5.1.2 Height-of-Burst, TUMBLER vs Previous Operational Instructions 155
5.2 The Precursor of TUMBLER 4 161
5.2.1 Description of the Phenomenon 161
5.2.2 Arrival Time of the Precursor Along the Ground. 164
5.2.3 Analysis of Results 165
5.2.4 Discussion and Conclusions 168
5.3 Comparison with Regular Reflection Theory . .171
5.3.1 Method 171
5.3.2 Results in Regular Region 172

CONTENTS (CONT.)

5.4 TNT Efficiencies of TUMBLER Weapons 173
5.4.1 Comparison of Free-air Data with TNT 173
5.4.2 TNT Efficiencies at Ground Level 173
5.5 Positive Impulse in Free Air Compared with TNT . . 179

CHAPTER 6 CONCLUSIONS AND RECOMMENDATIONS 182

6.1 Conclusions on Systems Used 182
6.1.1 Pressure-Time Measurements on the Ground 182
6.1.2 Peak Pressure Measurements in Free Air by the Shock Velocity Method 182
6.1.3 Pressure-Time Measurements in Free Air by the Particle Displacement Method . . . 182
6.2 Conclusions on Experiments 183
6.3 Recommendations 185

APPENDIX A MEASUREMENT OF PEAK PRESSURE BY INDENTER GAGES DAMPED WITH SILICONE AND WITH BAFFLE CHAMBER (By F. J. Oliver) 186

A.1 Field Experiments 186
A.2 Analysis 189
A.3 Conclusion 189

APPENDIX B DETERMINATION OF PRESSURE-TIME CURVES FROM OBSERVED PARTICLE MOTION IN BLAST WAVES (By F. Theilheimer) . . 191

B.1 Introduction 191
B.2 Analysis of Photographic Records 191
B.3 Determination of Pressure-Time Curves 193
B.4 Derivation of Equation (B.3) 195
B.5 Check on the Accuracy of the Procedure 197

LIST OF REFERENCES 199

TABULAR DATA 202

ILLUSTRATIONS

1.1 Area F - Test Layout, Project 1.5a and 1.5b, TUMBLER 1 26
1.2 Area T-7 - Test Layout, Project 1.5a and 1.5b, TUMBLER 2-4 27

2.1 Blast Line Layouts for Operation TUMBLER 32
2.2 Cable Laying 33
2.3 Bendix Gage and its Construction 33
2.4 Transient Response of Bendix Gages 35
2.5 Gage Calibration Set-up 36
2.6 Top View of Cover Plate Baffle 37
2.7 Oscillator Amplifier Chassis and Gage on Cover Plate Baffle 37
2.8 Oscillator-Amplifier and Cable Schematic 38
2.9 Instrument Trailer in Revetment 39
2.10 Inside View of Instrumentation Trailer 40
2.11 Block Diagram Showing Signal Paths and Interlaced Station Hookup 41
2.12 Timing and Fiducial Marker System 43
2.13 Power System and Remote Control Relay Utilization 44
2.14 Magnetic Tape Playback Block Diagram 45
2.15 Non-Linearity Correction for Impulse 48
2.16 Symbols for Characteristic Waveforms 51
2.17 Records, TUMBLER 1, Stations F-200 through F-203 53
2.18 Records, TUMBLER 1, Stations F-204 through F-208 54
2.19 Records, TUMBLER 1, Stations F-209 through F-211 55
2.20 Peak Positive Overpressure, P_c, Ground Level, TUMBLER 1 . . 56
2.21 Peak Negative Pressure, P_e, Ground Level, TUMBLER 1 . . . 57
2.22 Positive Impulse, Ground Level, TUMBLER 1 58
2.23 Positive Phase Duration, t_4, Ground Level, TUMBLER 1 . . . 59
2.24 Negative Phase Duration, t_8, Ground Level, TUMBLER 1 . . . 59
2.25 Arrival Time of Initial Disturbance, t_1, Ground Level, TUMBLER 1 60
2.26 Records, TUMBLER 2, Stations 7-200 through 7-201T 62
2.27 Records, TUMBLER 2, Stations 7-213 through 7-204 63
2.28 Records, TUMBLER 2, Stations 7-205 through 7-206T 64
2.29 Peak Positive Overpressure, P_c, Ground Level, TUMBLER 2 . . 65
2.30 Peak Negative Pressure, P_e, Ground Level, TUMBLER 2 . . . 65
2.31 Positive Impulse, Ground Level, TUMBLER 2 66
2.32 Positive Phase Duration, t_4, Ground Level, TUMBLER 2 . . . 66
2.33 Negative Phase Duration, t_8, Ground Level, TUMBLER 2 . . . 66
2.34 Arrival Time of Initial Disturbance, t_1, Ground Level, TUMBLER 2 67
2.35 Records, TUMBLER 3, Stations 7-200 through 7-201T 68
2.36 Records, TUMBLER 3, Stations 7-213 through 7-205 69

Preceding Page Blank

ILLUSTRATIONS (CONT.)

2.37 Records, TUMBLER 3, Stations 7-206T through 7-209 70
2.38 Records, TUMBLER 3, Stations 7-210 through 7-Q2 71
2.39 Peak Positive Overpressure, P_c, Ground Level, TUMBLER 3 72
2.40 Peak Negative Pressure, P_e, Ground Level, TUMBLER 3 73
2.41 Positive Impulse, Ground Level, TUMBLER 3 74
2.42 Arrival Time of Initial Disturbance, t_1, Ground Level, TUMBLER 3 75
2.43 Positive Phase Duration, t_4, Ground Level, TUMBLER 3 . . . 75
2.44 Negative Phase Duration, t_8, Ground Level, TUMBLER 3 . . . 76
2.45 Records, TUMBLER 4, Stations 7-200 through 7-213 78
2.46 Records, TUMBLER 4, Stations 7-202 through 7-205 79
2.47 Records, TUMBLER 4, Stations 7-206T through 7-209 80
2.48 Records, TUMBLER 4, Stations 7-210 through 7-Q2 81
2.49 Peak Positive Overpressure, P_c, Ground Level, TUMBLER 4 82
2.50 Peak Negative Pressure, P_e, Ground Level, TUMBLER 4 83
2.51 Positive Impulse, Ground Level, TUMBLER 4 84
2.52 Positive Phase Duration, t_4, Ground Level, TUMBLER 4 . . . 85
2.53 Arrival Times, t_1, t_2, t_3, and t_9, Ground Level, TUMBLER 4 86
2.54 Expanded Scale of Arrival Times, t_1, t_2, and t_3, Ground Level, TUMBLER 4 87

3.1 Rocket Launcher with 85° Firing Angle 94
3.2 Assembled Smoke Rockets with Mk 3 Motor (Left), Mk 4 Motor (Right), TUMBLER 1-4 94
3.3 Planes of Measurement used in Free-air Pressure-Distance Analyses 96
3.4 Free-air Shock Wave Time-of-Arrival Curve, TUMBLER 1 . . . 97
3.5 Shock Wave Time-of-Arrival Curve Along the Ground, TUMBLER 1 98
3.6 Height of Mach Stem vs Distance from Ground Zero, TUMBLER 1 99
3.7 Atmospheric Pressure, P_o, and Sound Velocity, C_o, vs Altitude, TUMBLER 1 100
3.8 Peak Shock Overpressure in Free Air vs Distance, TUMBLER 1 101
3.9 Free-air Shock Wave Time-of-Arrival Curve, TUMBLER 2 . . .103
3.10 Atmospheric Pressure P_o, and Sound Velocity, C_o, vs Altitude, TUMBLER 2 104
3.11 Peak Shock Overpressure in Free Air vs Distance, TUMBLER 2 105
3.12 Free-air Shock Wave Time-of-Arrival Curve, TUMBLER 3 . . .107

ILLUSTRATIONS (CONT.)

3.13 Atmospheric Pressure, P_o, and Sound Velocity, C_o, vs Altitude, TUMBLER 3 108
3.14 Peak Shock Overpressure in Free Air vs Distance, TUMBLER 3 110
3.15 Free-air Shock Wave Time-of-Arrival Curve, TUMBLER 4 111
3.16 Atmospheric Pressure, P_o, and Sound Velocity, C_o, vs Altitude, TUMBLER 4 114
3.17 Peak Shock Overpressure in Free Air vs Distance, TUMBLER 4 115
3.18 Particle Displacement Layout, TUMBLER 1 116
3.19 Particle Displacement Layout, TUMBLER 4 116
3.20 Particle Displacement vs Time, TUMBLER 1 117
3.21 Particle Displacement vs Time, TUMBLER 4 118
3.22 K and Z at Constant Times, TUMBLER 1 119
3.23 K and Z at Constant Times, TUMBLER 4 120
3.24 $P_{n,m}$ vs X, TUMBLER 1 121
3.25 $P_{n,m}$ vs X, TUMBLER 4 122
3.26 Pressure-Time in Free Air, TUMBLER 1 123
3.27 Pressure-Time in Free Air, TUMBLER 4 124
3.28 Effect of a Nearby Surface on Smoke Trail Particle Motion 130
3.29 Particle Displacement Smoke Trails Before Shock Arrival, TUMBLER 1 131
3.30 Particle Displacement Smoke Trails After Shock Arrival, TUMBLER 1 131

4.1 Peak Positive Overpressure vs Ground Range, Data Reduced to 1 KT at Sea Level 134
4.2 Positive Impulse vs Ground Range, Data Reduced to 1 KT at Sea Level 135
4.3 Peak Negative Pressure vs Ground Range, Data Reduced to 1 KT at Sea Level 136
4.4 Arrival Times, t_1 and t_2 vs Ground Range, Data Reduced to 1 KT at Sea Level 137
4.5 Positive Duration vs Ground Range, Data Reduced to 1 KT at Sea Level 138
4.6 Peak Positive Overpressure vs Slant Range, Data Reduced to 1 KT at Sea Level 139
4.7 Positive Impulse vs Slant Range, Data Reduced to 1 KT at Sea Level 140
4.8 Peak Negative Pressure vs Slant Range, Data Reduced to 1 KT at Sea Level 141
4.9 Arrival Times, t_1 and t_2 vs Slant Range, Data Reduced to 1 KT at Sea Level 142

ILLUSTRATIONS (CONT.)

4.10 Positive Duration vs Slant Range, Data Reduced to 1 KT at Sea Level 143
4.11 Composite Reduced Free-air Arrival Time Curves, TUMBLER 1-4 145
4.12 Composite Reduced (1 KT(RC) at Sea Level) Free-air Pressure-Distance Curve, TUMBLER 1-4 147
4.13 Reduced p vs t for TUMBLER 1 and 4 at a Reduced Distance of 541 ft for 1 KT(RC) at Sea Level 148
4.14 Q vs Distance, Reduced to 1 KT(RC) at Sea Level, TUMBLER 1 and 4 (Free Air) 149

5.1 Height of Burst vs Horizontal Distance for 1 KT(RC) Bomb, Curves Based on TUMBLER Data 152
5.2 Height of Burst vs Horizontal Distance for 1 KT(RC) Bomb, Comparison with High Explosives and Effect of Gage Height 153
5.3 Height of Burst vs Horizontal Distance for 1 KT(RC) at Sea Level for 50-15-5 psi 156
5.4 Height of Burst vs Horizontal Distance for 1 KT(RC) at Sea Level for 40-12-4 psi 157
5.5 Height of Burst vs Horizontal Distance for 1 KT(RC) at Sea Level for 30-10-3 psi 158
5.6 Height of Burst vs Horizontal Distance for 1 KT(RC) at Sea Level for 25-8 psi 159
5.7 Height of Burst vs Horizontal Distance for 1 KT(RC) at Sea Level for 20-6 psi 160
5.8 Precursor Sequence, 0.2512 sec, TUMBLER 4 162
5.9 Precursor Sequence, 0.2906 sec, TUMBLER 4 162
5.10 Precursor Sequence, 0.4189 sec, TUMBLER 4 163
5.11 Precursor Sequence, 0.5867 sec, TUMBLER 4 163
5.12 Sketch Showing Construction of Reference Frame for Precursor Measurements 166
5.13 Time-of-Arrival of Precursor and Reflected Shock Wave, TUMBLER 4 167
5.14 Reflection of a Spherical Wave by a Medium of Higher Wave Velocity 170
5.15 One of the Family of Curves Showing P_r vs P_s for Ideal Reflection of Shocks from a Rigid Surface 174
5.16 Pressures in the Regular Reflection Region, TUMBLER 1, 2, and 4 175
5.17 Free-air Pressure Reduced to 1 KT of TNT at Sea Level . . . 176
5.18 Free-air Positive Impulse (Reduced to 1 KT(RC) at Sea Level) - Particle Displacement Method Compared with TNT . . 180

ILLUSTRATIONS (CONT.)

A.1 Arrangement of Indenter Gage with Baffle Chamber 187
A.2 Comparison of Inductance and Indenter Gages, TUMBLER 3 and 4 188

B.1 Smoke Trails Before Passing of Shock 192
B.2 Tables Required for Complete Pressure-Time Analysis 194

TABLES

1.1 Characteristics of TUMBLER Shots 1 through 4 202

2.1 Carbon Paper Distribution 203
2.2 TUMBLER 1 - Phase Durations, Positive Impulses, and Pressures (Ground Level) 204
2.3 TUMBLER 1 - Distances and Times (Ground Level) 205
2.4 TUMBLER 2 - Phase Durations, Positive Impulses, and Pressures (Ground Level) 206
2.5 TUMBLER 2 - Distances and Times (Ground Level) 206
2.6 TUMBLER 3 - Phase Durations, Positive Impulses, and Pressures (Ground Level) 207
2.7 TUMBLER 3 - Distances and Times (Ground Level) 208
2.8 TUMBLER 4 - Distance and Arrival Times (Ground Level) . . . 209
2.9 TUMBLER 4 - Positive Impulses and Pressures (Ground Level) . 210
2.10 TUMBLER 4 - Phase Durations and Rise Times (Ground Level). . 211

3.1 Photographic Details 212
3.2 Absolute Time-of-Arrival of Shock in Free Air and Mach Region, TUMBLER 1 213
3.3 Peak Overpressure - Shock Velocity - Distance, TUMBLER 1 . . 214
3.4 Absolute Time-of-Arrival of Shock in Free Air, TUMBLER 2 . . 215
3.5 Peak Overpressure - Shock Velocity - Distance, TUMBLER 2 . . 214
3.6 Absolute Time-of-Arrival of Shock in Free Air, TUMBLER 3 . . 216
3.7 Peak Overpressure-Shock Velocity-Distance, TUMBLER 3 . . . 217
3.8 Absolute Time-of-Arrival of Shock in Free Air, TUMBLER 4 . . 218
3.9 Peak Overpressure-Shock Velocity-Distance, TUMBLER 4 . . . 219
3.10 X's and Z's in Feet (Film 13083) TUMBLER 1 220
3.11 X's and Z's in Feet (Film 13383) TUMBLER 4 220
3.12 $Z_n - Z_j$, $X_n - X_j$ in Feet, TUMBLER 1 221
3.13 $Z_n - Z_j$, $X_n - X_j$ in Feet, TUMBLER 4 221
3.14 Calculated K, $\left(\frac{\partial X}{\partial Z}\right)_t$, TUMBLER 1 222
3.15 Calculated K, $\left(\frac{\partial X}{\partial Z}\right)_t$, TUMBLER 4 222
3.16 Calculated Pressure, $P_{n,m}$, and Distance, X, TUMBLER 1 . . . 223
3.17 Calculated Pressure, $P_{n,m}$, and Distance, X, TUMBLER 4 . . . 224
3.18 Free-air Pressure-Time, TUMBLER 1 225
3.19 Free-air Pressure-Time, TUMBLER 4 225
3.20 Decay Parameter, θ, for TUMBLER 1 and 4 226

4.1 TUMBLER 1 - Ground Level Data Reduced to 1 KT at Sea Level . 227
4.2 TUMBLER 2 - Ground Level Data Reduced to 1 KT at Sea Level . 228
4.3 TUMBLER 3 - Ground Level Data Reduced to 1 KT at Sea Level . 229
4.4 TUMBLER 4 - Ground Level Data Reduced to 1 KT at Sea Level . 230

TABLES (CONT.)

4.5 Reduced Time-of-Arrival of Shock in Free Air and Mach Region, TUMBLER 1 231
4.6 Reduced Time-of-Arrival of Shock in Free Air, TUMBLER 2 232
4.7 Reduced Time-of-Arrival of Shock in Free Air, TUMBLER 3 233
4.8 Reduced Time-of-Arrival of Shock in Free Air, TUMBLER 4 234
4.9 Reduced Time-of-Arrival of Shock in Free Air, GREENHOUSE (DOG) 235
4.10 Reduced Time-of-Arrival of Shock in Free Air, GREENHOUSE (EASY) 235
4.11 Reduced Free-air Overpressure vs Distance, TUMBLER 1 . . .236
4.12 Reduced Free-air Overpressure vs Distance, TUMBLER 2 . . .236
4.13 Reduced Free-air Overpressure vs Distance, TUMBLER 3 . . .237
4.14 Reduced Free-air Overpressure vs Distance, TUMBLER 4 . . .238
4.15 Composite Free-air Peak Overpressures vs Distance Reduced to 1 KT(RC) at Sea Level 239
4.16 Pressures at Reduced Distances, GREENHOUSE (DOG), (EASY) . .240
4.17 Free-air Pressure-Time Reduced to 1 KT(RC) at Sea Level TUMBLER 1 and 4 241
4.18 Values of Decay Parameter, θ, Reduced to 1 KT(RC) at Sea Level. 242

5.1 Distances at which Pressures Occur-Reduced to 1 KT(RC) at Sea Level. 243
5.2 Optimum Height of Burst for 1 KT at Sea Level. 243
5.3 Data for Figure 5.2 244
5.4 Arrival Time of Precursor and Reflected Shock, TUMBLER 4 . .245
5.5 Overlap of Ground Level and Free-air Measurements 245
5.6 TUMBLER 1 - Calculated vs Experimental Values of Reflected Pressures in the Regular Region 246
5.7 TUMBLER 2 - Calculated vs Experimental Values of Reflected Pressures in the Regular Region 246
5.8 TUMBLER 4 - Calculated vs Experimental Values of Reflected Pressures in the Regular Region 246
5.9 $P_s = p_o \left(\frac{1}{\quad} - 1\right)$ for TUMBLER 1 247
5.10 $P_s = p_o \left(\frac{1}{\quad} - 1\right)$ for TUMBLER 2 247
5.11 $P_s = p_o \left(\frac{1}{\quad} - 1\right)$ for TUMBLER 4 247
5.12 $P_f = p_o \left(\frac{\quad}{\quad} - 1\right)$ for TUMBLER 1 248
5.13 $P_f = p_o \left(\frac{\quad}{\quad} - 1\right)$ for TUMBLER 2 248
5.14 $P_f = p_o \left(\frac{\quad}{\quad} - 1\right)$ for TUMBLER 4 248

TABLES (CONT.)

5.15 Distances at which Pressure Levels occur in Free Air for 1 KT(TNT) at Sea Level 249
5.16 Comparison of TUMBLER Data with TNT in Free Air 250
5.17 Comparison of TUMBLER Data with TNT for Reflected Pressures 251
5.18 Comparison of Free-air Impulse Data for Scaled Nuclear and TNT Charges 252

6.1 Summary of Free-air TNT Equivalents for TUMBLER 252

A.1 TUMBLER 3 - Peak Pressure (Ground Level) 253
A.2 TUMBLER 4 - Peak Pressure (Ground Level) 254

CHAPTER 1

INTRODUCTION

1.1 GENERAL OBJECTIVES

As the result of blast measurements made on Operation BUSTER in the fall of 1951, questions arose as to the reliability of the height-of-burst curves presented in LA-743R[1] because the pressures measured were considerably less than expected and the rise times to the measured maximum pressures were much longer than would be expected from pure shock waves. These height-of-burst curves which were based on theory, shock-tube experiments, small-charge (HE) experiments, and a small amount of nuclear bomb data were used by military operational agencies to select the proper heights for detonating atomic weapons, the proper yield of weapon to achieve particular military objectives, and the criteria for the design of fuzes. The proper height-of-burst information was, therefore, considered essential to the national defense; and it was decided to conduct a series of atomic bomb tests to determine (a) if the BUSTER results were reproducible, (b) if the current scaling laws could be considered reliable, (c) whether the origin of the effects noted on BUSTER might be attributed to the absorption of thermal radiation by the ground, to ground shock, or to other phenomena, and (d) whether nuclear bombs at high heights of burst gave results comparable with predictions.

1.2 OBJECTIVES OF PROJECTS 1.3 AND 1.5

As part of this operation the Naval Ordnance Laboratory was asked to make two types of measurements (a) free-air peak pressures to serve as a basis for judging the blast effectiveness of the test weapons independent of ground conditions, i.e., to obtain knowledge of the weapons' characteristics so that they could be isolated from the characteristics introduced by the geometry and terrain (Project 1.5a); and (b) independent pressure-time measurements on the ground to check other methods of instrumentation for measuring the actual blast of the weapons at locations where military targets might exist (Project 1.3). Early in the preparation period a feasibility experiment (Project 1.5b), was added at the request of the NOL to use a photo-optical method for measuring pressure-time in the free air from the motion of rocket trails which were hit by the shock wave. The importance of this technique is that it might provide pressure-time data in a region where it would be almost impossible to locate gages by conventional methods. Such data would be most useful for an understanding of the blast char-

1/ See references, page 199

acteristics of atomic weapons. The methods employed in these projects will be described in brief below and in detail in Chapters 2 and 3.

1.3 METHODS

Because of the limited preparation time for this operation, about two months, existing instrumentation and proven methods were employed with as little modification as possible. The shock-velocity method for measuring free-air peak pressures from photographs of rocket smoke trails as seen through the shock wave had been previously used on Operations GREENHOUSE[2] and JANGLE[3]. The Bendix inductance gage system to obtain pressure-time data employed a combination of techniques many of which were used on Operations SANDSTONE[4], GREENHOUSE[2], and JANGLE[6]. Although it was not part of the original plan, the firing of Shots 3 and 4 provided suitable test conditions for indenter gages which are being developed by the NOL to measure peak pressure[7/8/9/10]. These shots were, therefore, instrumented by a limited number of indenter gages mounted near the Bendix pressure-time installations. Discussion of this work is limited to Appendix A.

1.4 TEST CONDITIONS

All bombs were dropped from aircraft at the Nevada Proving Grounds during April and May, 1952. The first shot was fired on 1 April 1952 over Frenchman Flat which was light colored, flat, smooth, and a relatively stable target area. The other three shots were fired on 15 and 22 April and 1 May over area T-7, near the site of the BUSTER shots, which was, in general, rougher, darker, and dustier than the Frenchman Flat area. Details of the location of the bursts, the size of the weapons as used for scaling data, and similar parameters of the shots are listed in Table 1.1.

1.4.1 Inductance Gages

All inductance gages were mounted flush with the ground 35 ft to one side of the blast-line towers, except that on Shots 3 and 4 two additional stations were installed in a region several hundred feet to the side of the blast line where the sage brush was less disturbed than that on the main blast line. The purpose of these additional stations (7-Q1 and 7-Q2) was to get data from terrain more similar to that of the BUSTER tests than the blast line terrain. The exact locations of all instruments relative to each burst (ground and slant ranges) were calculated on the basis of information given in Table 1.1 and are tabulated in the appropriate tables of results given in Chapter 2. (Although distances are given to the nearest 0.1 foot

in the tables, the precision is only about ± 1.0 foot; hence such data may be rounded off.)

1.4.2 Rocket Lines

Two rocket lines were employed on each shot - one for the shock-velocity measurements and one for the particle motion measurements. The layout of these launcher lines relative to the blast lines, the 200 stations, and the cameras are shown in Figs. 1.1 and 1.2.

1.5 SUMMARY OF INSTRUMENT PERFORMANCE

Projects 1.3 and 1.5 were exceptionally successful in that all inductance gages worked on all shots and all required film records of rocket trails were readable. Actually there were a few rockets on the first two shots which failed to smoke but this in no way reduced the reliability nor amount of significant data. Film broke on one camera used in Shot 2 but there was adequate coverage from a back-up camera. In general the results of the inductance gages checked those of other pressure-time gages, as indicated in the preliminary reports of other groups[11]. Free-air pressure distance curves were obtained from shock-velocity records on all shots so that a generalized reliable free-air curve was made. Free-air pressure-time curves were calculated from the particle motion films from two shots, and data are available for computing such information from the other two shots when and if the expenditure of the effort seems warranted. The indanter gage trials demonstrated a successful baffle for protecting the gage from sandblast, radiation, and other mechanical disturbances; it also demonstrated that additional laboratory work was needed for a complete understanding of the use of these gages.

1.6 CONVERSION FACTORS AND SCALING

To scale effects from one weight charge to another and from charges fired at different altitudes to sea level a certain number of almost arbitrary decisions have to be made as to the exact method to use. The method of scaling for altitude and kilotonnage used in this report is the one recommended by paragraph 7 of reference 16 which states that pressures at high altitude targets can be converted to those at sea level by multiplying the high altitude values by $\frac{14.7}{p_o}$ and that distances for a one KT bomb at sea level can be calculated from those at the target for a bomb of weight W_o by multiplying the distance by $\left(\frac{p_o}{14.7\ W_o}\right)^{1/3}$ where p_o is the atmospheric pressure at burst height. There has been some informal discussion as to whether p_o should

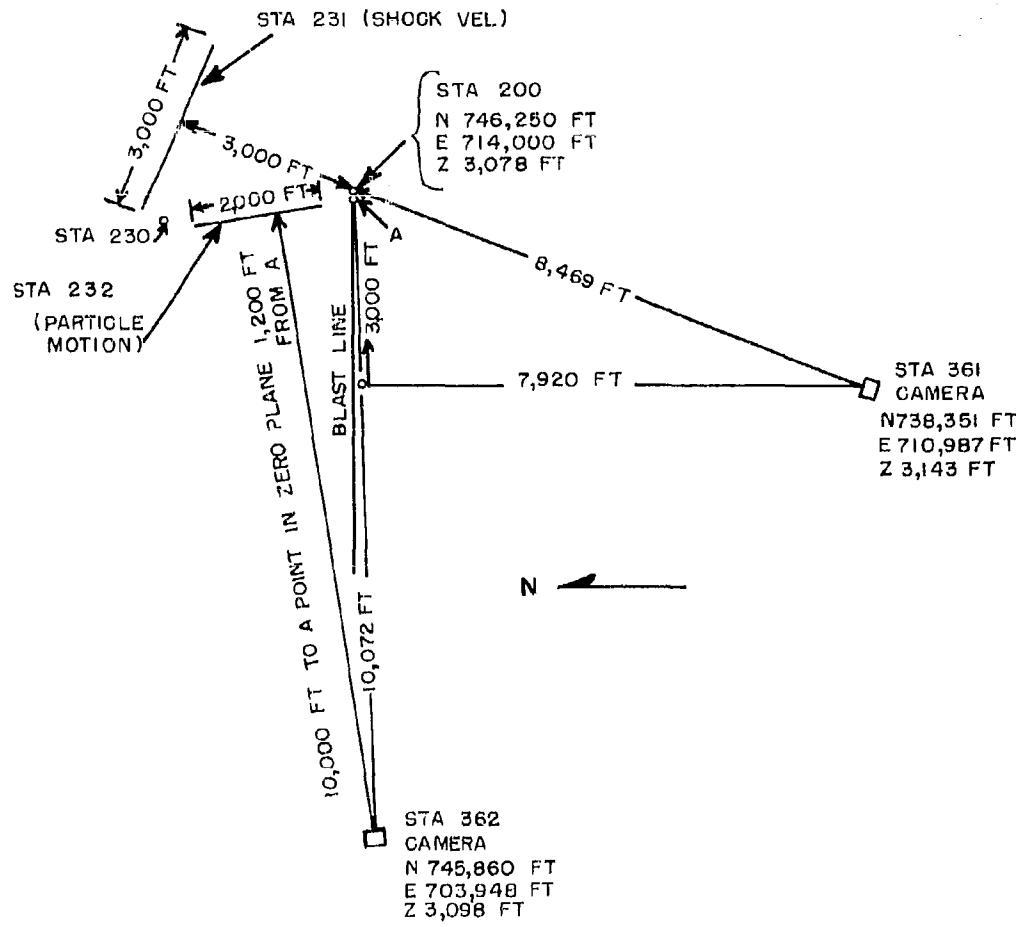

NOTE: (1) STA 231, LAUNCHERS AT 250 FT INTERVALS
(2) STA 232, LAUNCHERS AT 400 FT INTERVALS
(3) A, BASE POINT 70 FT, S 80-44-46 W FROM STA 200
(4) COORDINATES ARE THOSE OF NPG, MERCURY, NEVADA

Fig. 1.1 Area "F" Test Layout, Project 1.5a and 1.5b, TUMBLER 1

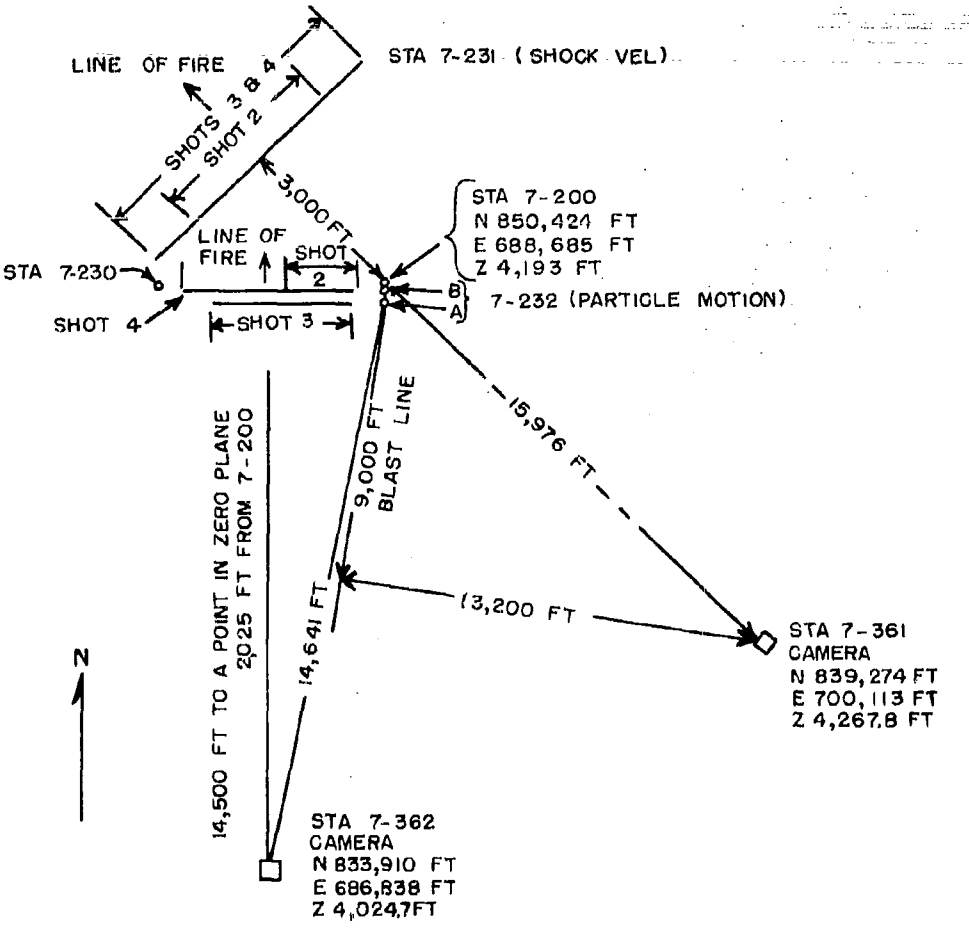

NOTE: (1) STA 7-231 SHOT 2; 3,000 FT LONG, LAUNCHERS AT 250 FT INTERVALS. SHOTS 3 & 4; 4,800 FT LONG, LAUNCHERS AT 400 FT INTERVALS.
(2) STA 7-232 SHOT 2; 1,200 FT LONG, 500 FT FROM POINT B TO 1st LAUNCHER. 1st 4 LAUNCHERS AT 200 FT INTERVALS. LAST 2 AT 400 FT INTERVALS. SHOT 4; 2,850 FT LONG, 600 FT FROM POINT "B" TO 1st LAUNCHER. 1st 4 LAUNCHERS AT 285 FT INTERVALS, LAST 4 AT 570 FT INTERVALS. SHOT 3; 2,280 FT LONG, 600 FT FROM POINT A TO 1st LAUNCHER. 1st 4 LAUNCHERS 285 FT INTERVALS. LAST 3 AT 570 FT INTERVALS.
(3) A 306 FT SO-46-41 E FROM STA 7-200
B 92 FT SO-46-41 E FROM STA 7-200
(4) COORDINATES ARE THOSE OF NPG, MERCURY, NEVADA

Fig. 1.2 Area T-7 Test Layout, Project 1.5a and 1.5b, TUMBLER 2-4

be the atmospheric pressure at burst height, target height, or some compromise value. Although the latter is probably most realistic, for reasons of uniformity with other projects and ease of computation the method of reference 16 is being used. No mention is made in reference 16 of methods of scaling time and impulse so that the following relations, based on methods similar to those discussed in references 17 and 19 are being used in this report (Table 1.1). (In all cases the atmospheric pressure at burst height is considered the suitable value to use.)

If I_1 and τ_1 prevail at a distance R_1, for certain values of p_1, c_1, and W_1, and it is desired to convert them for other atmospheric conditions and charge weights p_2, c_2, and W_2 at R_2, then

$$I_1 = I_2 \frac{c_2}{c_1} \left(\frac{W_1}{W_2}\right)^{1/3} \left(\frac{p_1}{p_2}\right)^{2/3} \qquad (1.1)$$

$$\tau_1 = \tau_2 \frac{c_2}{c_1} \left(\frac{W_1}{W_2}\right)^{1/3} \left(\frac{p_1}{p_2}\right)^{1/3} \qquad (1.2)$$

$$R_1 = R_2 \left(\frac{W_1}{W_2}\right)^{1/3} \left(\frac{p_2}{p_1}\right)^{1/3} \qquad (1.3)$$

$$\frac{c_2}{c_1} = \left(\frac{T_2 + 273}{T_1 + 273}\right)^{1/2} \qquad (1.4)$$

where I = Impulse
τ = Time
R = Distance
c = Velocity of sound
W = Weight of charge
p = Atmospheric pressure
T = Temperature, ^{o}C

It should be noted that the radio-chemical kilotonnages used are those provided by the Armed Forces Special Weapons Project on 31 July 1952 and do not agree with those based on fire-ball measurements which were given in the preliminary reports. For conversion to sea level the atmospheric pressure at sea level was assumed to be 14.7 psi, and the temperature was assumed to be 293°K (i.e. 20°C).

1.7 PERSONNEL AND RESPONSIBILITIES

To execute these projects the field party was sent out to Nevada

in three stages - an advance party to lay cable and receive shipping - the main party to set-up and conduct the experiments - and a shipping party to pack equipment for return to the NOL. The advance party of H. W. Baggott, C. L. Karmel, and E. G. Nacke was under the direction of LT G. W. Robinson, USN. The main party, under the direction of C. J. Aronson, was as follows:

C. J. Aronson	Project Officer (1.3 and 1.5)
J. F. Moulton, Jr.	Group Leader (1.5)
J. Petes	Group Leader (1.3)
H. W. Baggott	Cable and Power (1.3)
E. E. Burk	Electronic Technician (1.3)
E. J. Culling	Associate Group Leader (1.3)
P. Hanlon	Analysis (1.5)
C. L. Karmel	Instrumentation and Cabling (1.5)
C. C. Little (LTJG,USN)	Instrumentation and Analysis (1.3)
B. M. Loring (LT, USN)	Instrumentation (1.5)
J. D. McClendon(LCDR,USN)	Administration and Analysis (1.3 and 1.5)
J. R. Mitchell	Logistics (1.3 and 1.5)
E. G. Nacke	Cable and Power (1.3 and 1.5)
F. J. Oliver	Instrumentation and Analysis (1.3)
G. W. Robinson (LT, USN)	Cable and Power (1.3)
E. R. Walthall	Associate Group Leader (1.5)

The shipping party sent out by the Supply Department of the NOL comprised two packers, Curtis Becks and H. L. Terry, to prepare apparatus for the return shipment.

1.8 COSTS OF PROJECTS 1.3 AND 1.5

As a guide for the planning of future tests of this nature the following costs of this operation are listed.

Labor and Material	Fiscal 1952	$39,208
Capital Equipment		1,783
Communications		174
Shipping and Packing		18,759
Travel		12,754
Clerical, Supervisory, Maintenance		44,900
Reports, Analysis and Close-out work - Fiscal 1953		30,000 (est.)
TOTAL CHARGES AT THE NOL		$147,578
Trailer Shelters (2)		56,221
Rocket Control Shelters (2)		10,368

Cabling and Trenching F-Area	9,319	
Cabling and Trenching 7-Area	15,384	
Rocket Lines	1,600	
Camera Stations (2)	15,615	
Support Job Orders	10,000	
TOTAL CHANGES AT THE NPG		$118,507
TOTAL		$266,085

CHAPTER 2

GROUND LEVEL PRESSURE-TIME MEASUREMENTS (PROJECT 1.3)

2.1 INSTRUMENTATION

2.1.1 General

The instrumentation system used by the Naval Ordnance Laboratory on Operation TUMBLER was the system developed for Operation JANGLE[6] with minor modifications. The JANGLE system was an outgrowth of the system used on Operation GREENHOUSE[5] and used many of the same basic components. The system featured the use of frequency modulation for transmission of gage signals over long lengths of cable to a remote position where these signals were recorded on multi-channel magnetic tape recorders. The blast line layouts are shown in Figs. 2.1 and 2.2. The system has proved itself to be highly reliable and fairly free from the effects peculiar to atomic explosions.

2.1.2 Gages

The pressure gages used were modified Bendix Type TTP-3A variable reluctance pressure pickups (Fig. 2.3). The modification which was found advantageous for use on Operation GREENHOUSE was accepted and no further improvements were attempted. This modification consisted of adding a suitably restricted inlet tube to reduce air column and diaphragm ringing. These gages produced an oscillator frequency shift of approximately 7.5 per cent when nominal rated pressure was applied. Gages were used having nominal ratings of 5,10,15,20,30, 60, and 100 psi. In general these gages were used and calibrated for pressures up to 150 per cent of the nominal rating.

Sample gages of each pressure range, except 100 psi, were tested in the NOL shock tube, and the resulting transient characteristics observed. The gages exhibited ring frequencies from about 700 cps for a 5 psi gage to 1330 cps for a 60 psi gage. The diaphragm was essentially undamped and would ring for several cycles, but the amplitude of this oscillation was reduced materially by the choice of the suitably small inlet tube diameter.

For the 5, 10, and 15 psi gages this ring amplitude had a peak value not exceeding 10 per cent of the applied step of pressure. For pressures which had rise times longer than 2 to 3 msec this ring amplitude was considerably reduced. The higher range gages had greater

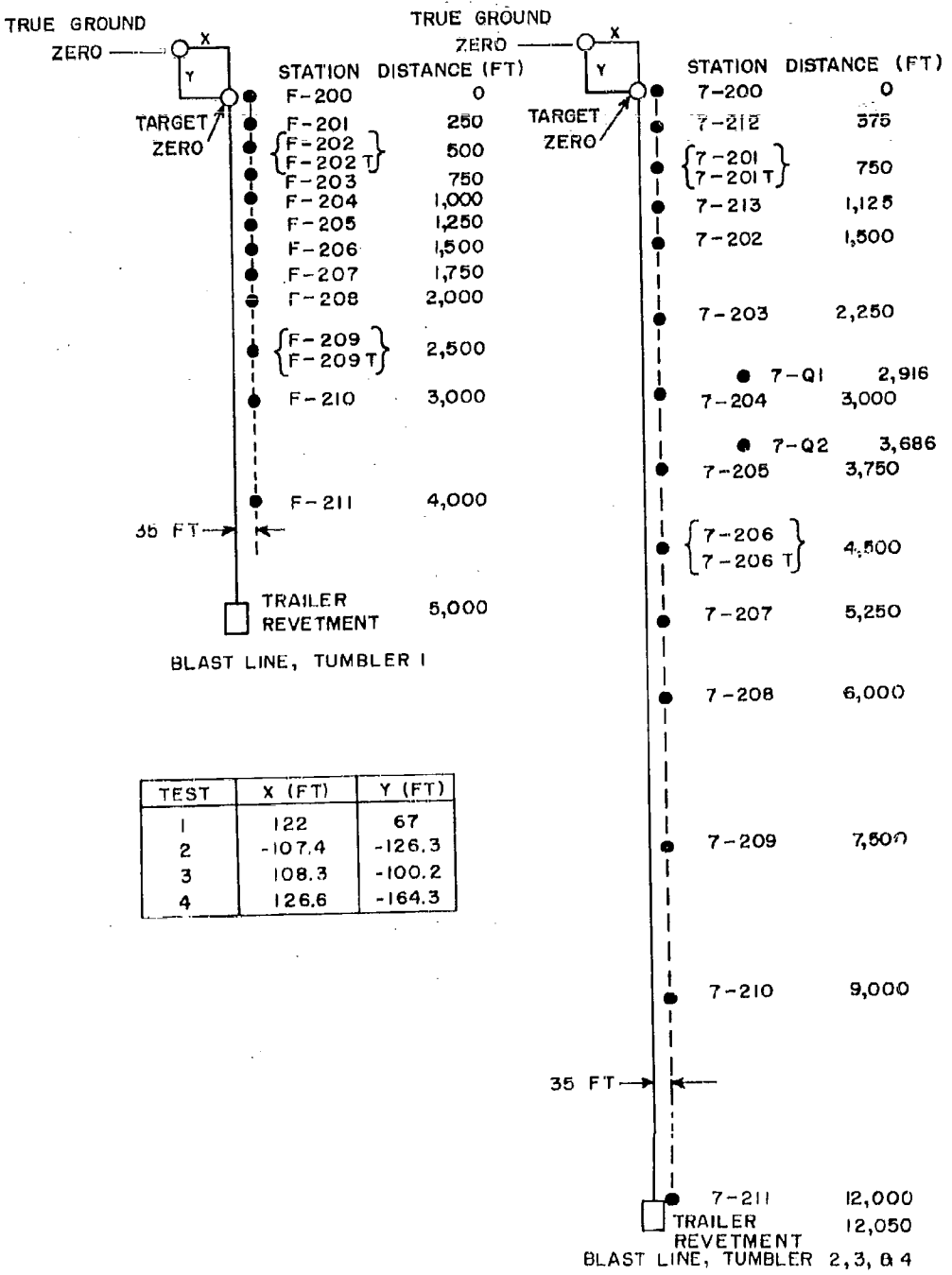

TEST	X (FT)	Y (FT)
1	122	67
2	-107.4	-126.3
3	108.3	-100.2
4	126.6	-164.3

Fig. 2.1 Blast Line Layouts for Operation TUMBLER

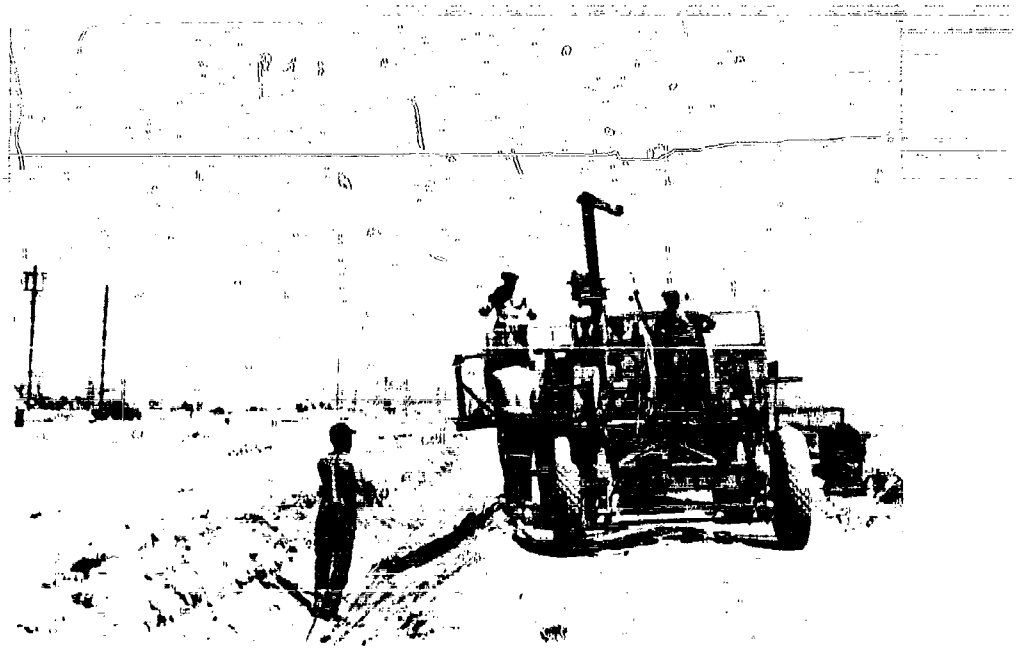

Fig. 2.2 Cable Laying

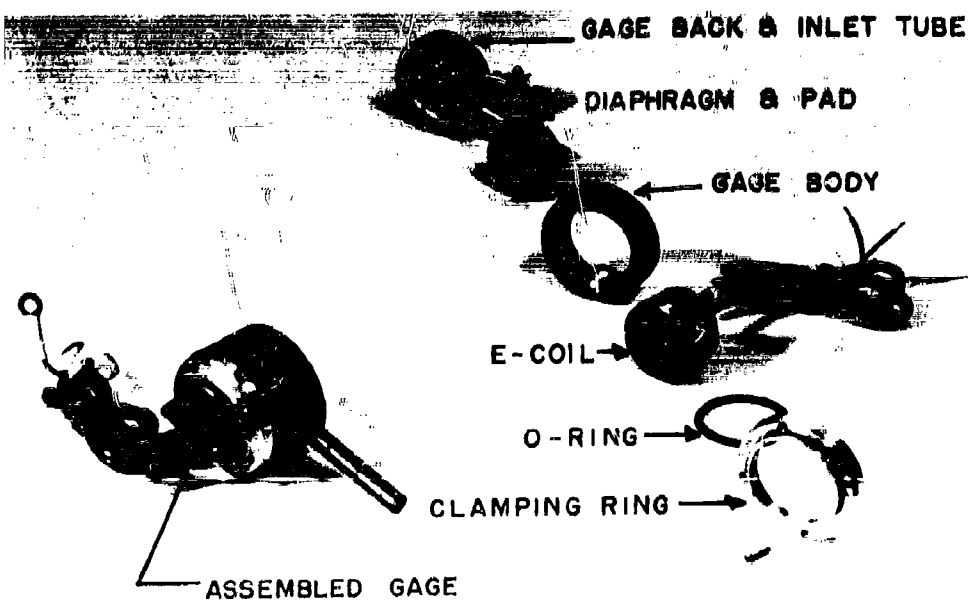

Fig. 2.3 Bendix Gage and Its Construction

ring amplitudes, more diaphragm damping, and exhibited some inlet tube ringing which produced a coupled resonance effect. (Fig. 2.4).

All gages were factory calibrated for a particular ambient temperature and pressure which were noted. Field calibrations, however, were taken and used for all measurements. This was thought advisable since the gages had a built-in air cavity, sealed at the time of manufacture, providing the reference pressure. This sealed air cavity made the gages sensitive to both ambient temperature and barometric pressure, so that the center frequency of each oscillator had to be set at the time of field calibration. Those changes in center frequency which resulted from variations in barometric pressure and temperature were used to locate the new pre-shock reference point on the non-linear gage calibration curve. The pressure standards used for field calibration were a mercury manometer up to 15 psi levels and a dead-weight calibrated Bourdon tube dial gage above 15 psi. A sketch of the calibration set-up is shown in Fig. 2.5.

The gage inlet tube was mounted flush with the surface of a steel cover plate (Fig. 2.6). A short length of rubber hose completed the seal and provided some shock mounting for the gage. Gage inlets were kept sealed until a few hours before the test. In locations where burning was assured, carbon paper was fastened over the inlet to be burnt off by the thermal energy before blast arrival. To increase the assurance of burning, the carbon paper was humped over the inlet tube providing a small area at least, with decreased angle of incidence (i.e. more nearly normal) to the thermal energy. This seemed to be an excellent way to protect the gages against dirt and sand entering the inlet tube before shot time. Although there was no operational evidence of sand causing gage malfunctioning, it was considered to be a hazard. The carbon paper protection proved to be satisfactory, and no disturbance of the pressure signal on the records could be attributed to the presence of the carbon paper or its residual ash. Table 2.1 gives the stations at which carbon paper was placed over the gage inlets for protection or on the cover plate as a control; the thermal results are also given. (In reference 26 for Operation BUSTER, Table C.3 shows that carbon paper was totally destroyed for a normally incident thermal energy of 2.9 cal/cm^2 and that laboratory tests indicated the critical value to be 0.78 cal/cm^2. On Operation TUMBLER in locations where normal incidence was assured, burning was found for thermal energies as low as 1.45 cal/cm^2; however, for a test patch of carbon paper with an angle of incidence that could have been as high as 82° from normal in an area of 9.0 cal/cm^2, no burning occurred. The computed normally incident energy for this station

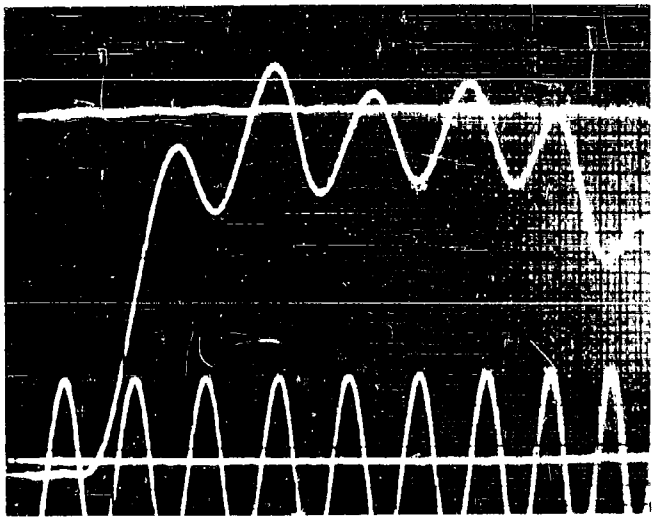

Gage N36 Output with 9.2 psi Step Applied for
5 msec by NOL Shock Tube. 1000 cps Timing Trace

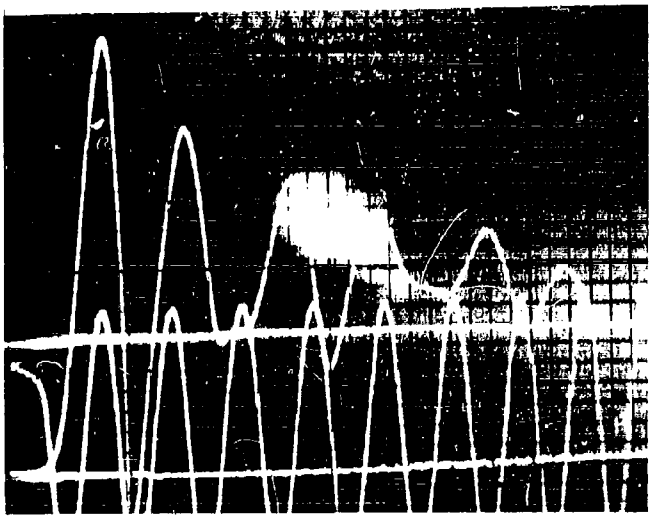

Gage N59 Output with 19.8 psi Step Applied for
5 msec by NOL Shock Tube. 1000 cps Timing Trace

Fig. 2.4 Transient Response of Bendix Gages

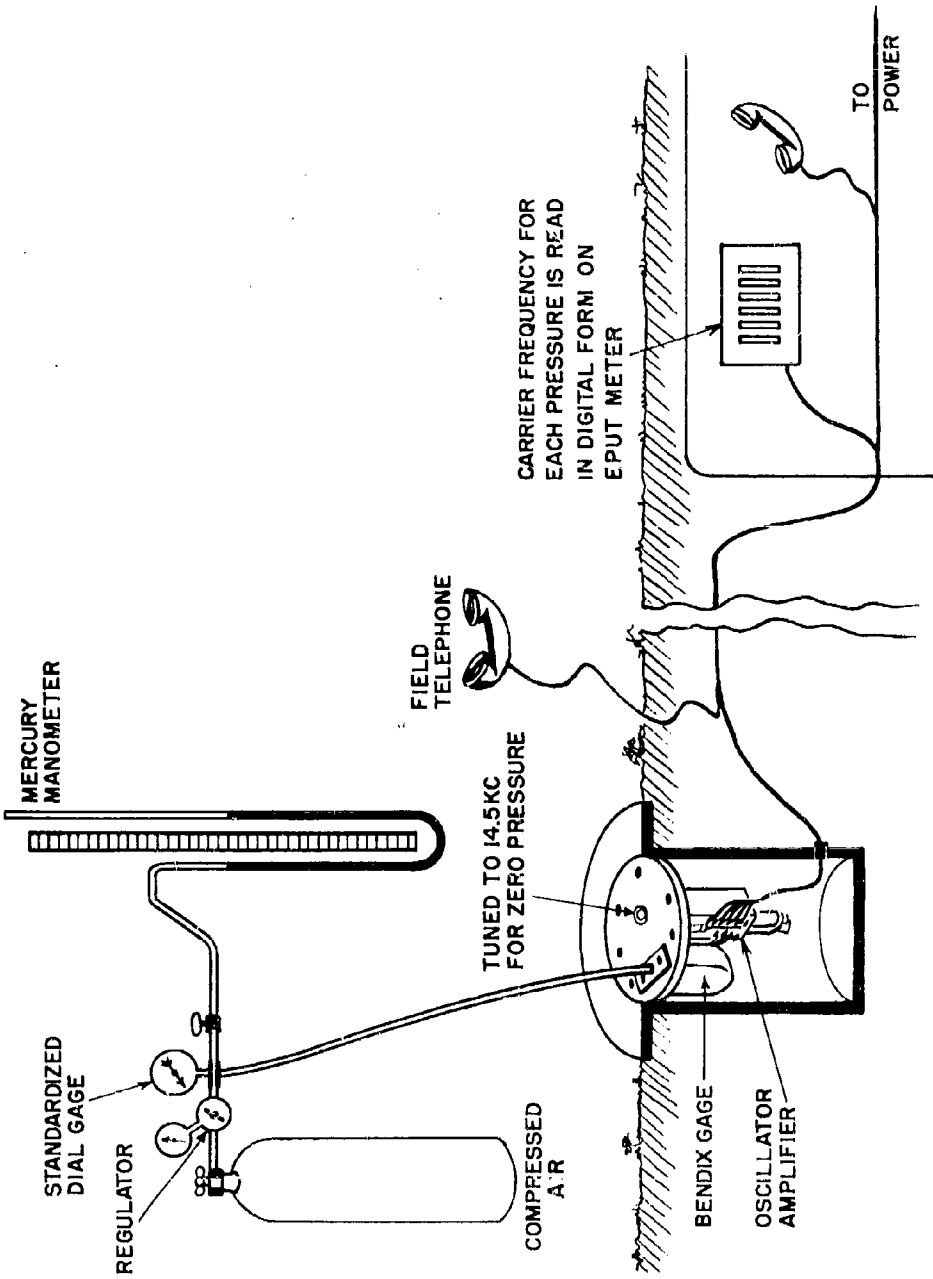

Fig. 2.5 Gage Calibration Set-up

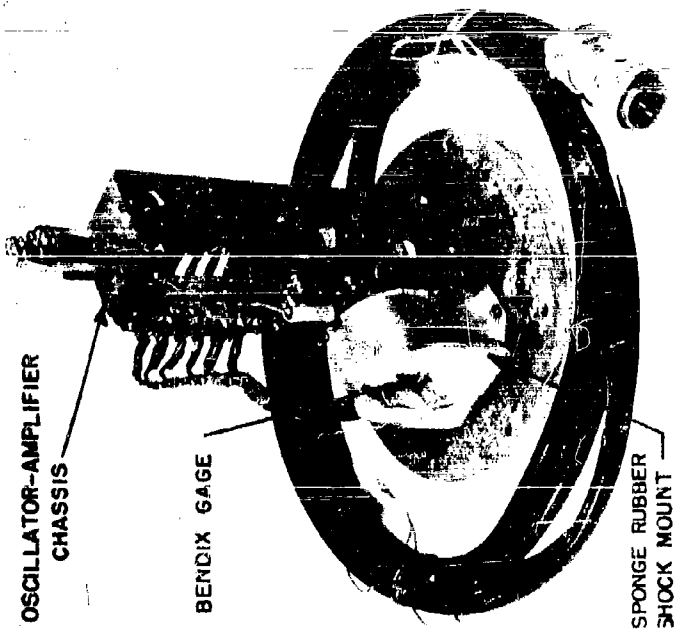

Fig. 2.7 Oscillator Amplifier Chassis and Gage on Cover Plate Baffle

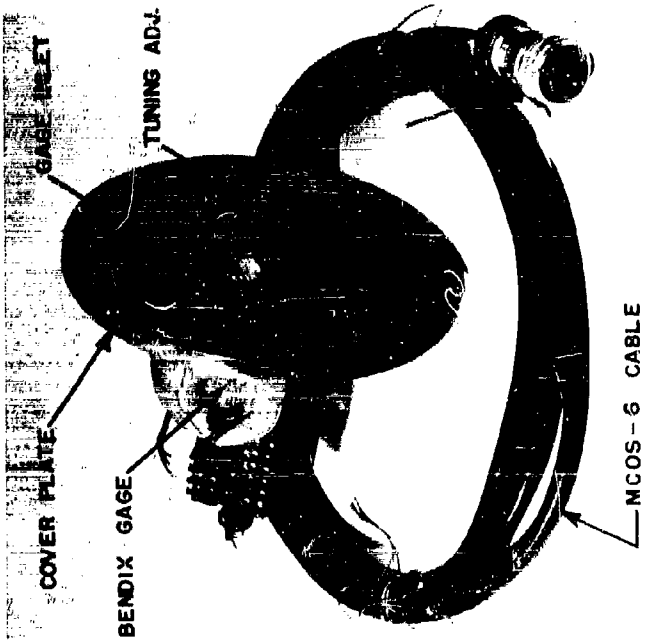

Fig. 2.6 Top View of Cover Plate Baffle

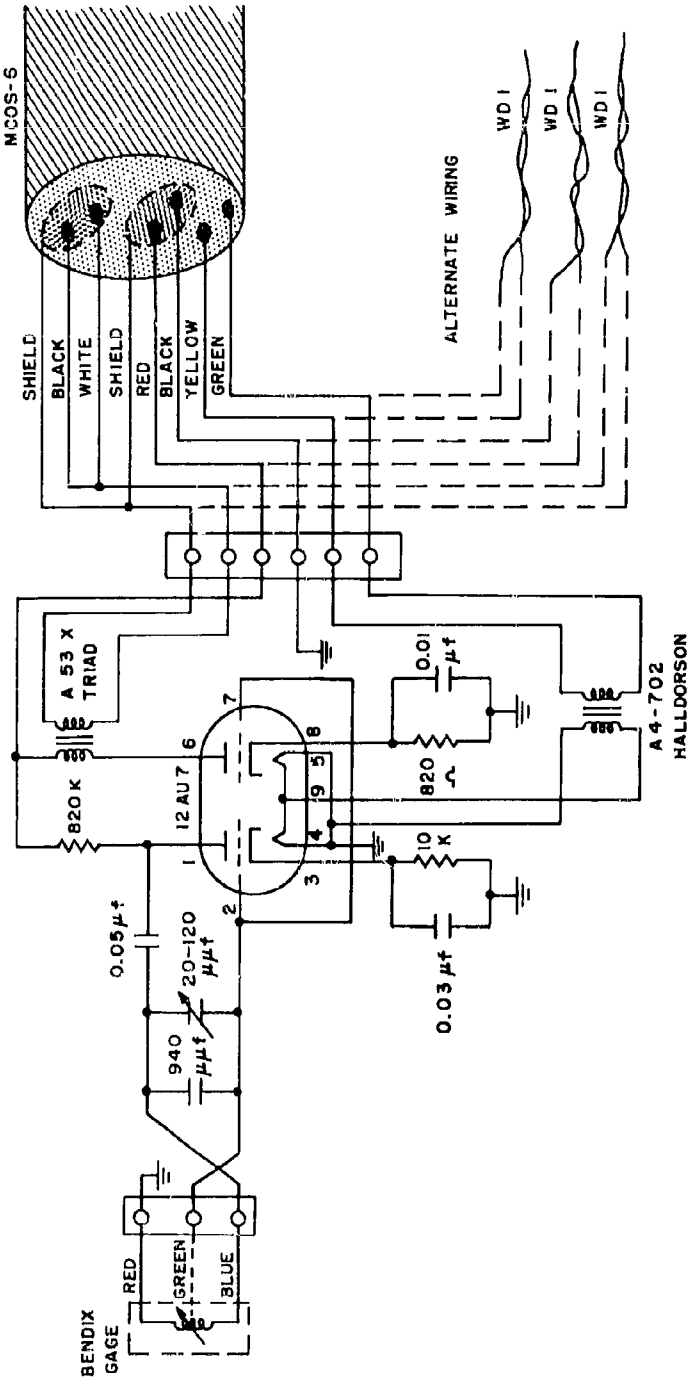

Fig. 2.8 Oscillator-amplifier and Cable Schematic

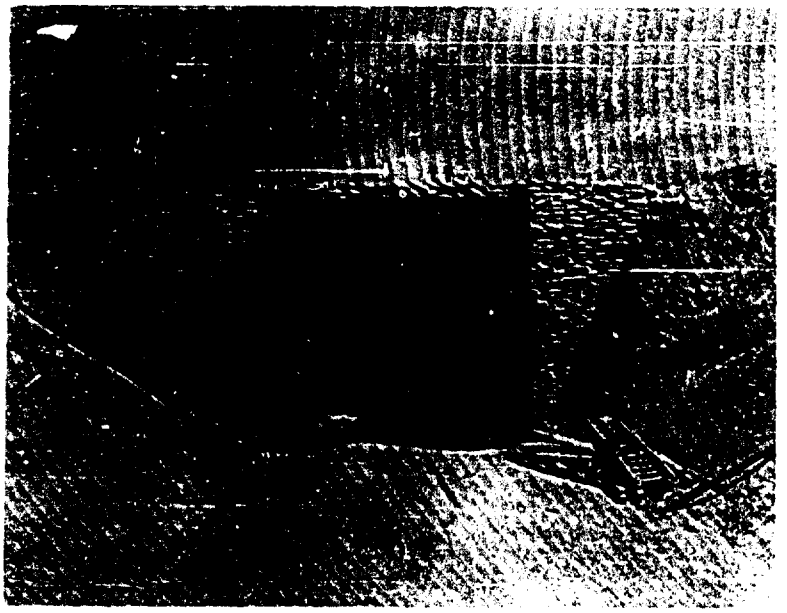

Fig. 2.9 Instrument Trailer in Revetment

was 1.26 cal/cm^2. Thermal data were taken from reference 11.)

2.1.3 Oscillator-Amplifier

In the field a one tube, shunt-feed, Hartley oscillator comprised the signal source, the tapped inductance of the gage providing the entire inductance for the 14,500 cps frequency-determining circuit. A triode amplifier was incorporated to insure adequate power for signal transmission. This oscillator-amplifier unit, except for simplified transmission line coupling and the addition of a by-pass condenser to insure vigorous oscillations at the expense of increased carrier distortion, was identical to the oscillator-amplifier system used and carefully studied for Operation JANGLE. A schematic diagram of the oscillator-amplifier showing cable utilization is shown in Fig. 2.8, and a photograph showing the oscillator-amplifier and gage mounted on the baffle cover-plate is given in Fig. 2.7.

Standard MCOS-6 cable was used except for two lines of unshielded WD-1 twisted pair telephone wires. The telephone wire was used experimentally to determine the feasibility of using it extensively in future tests. Its use would reduce cable costs materially. All cables were laid in trenches and covered to a depth of 18 in. to

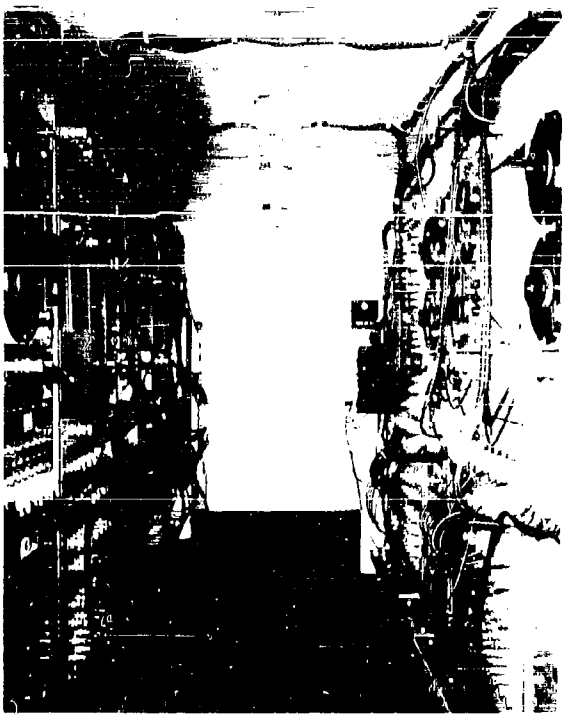

Fig. 2.10 Inside View of Instrumentation Trailer

afford mechanical and thermal protection (see Fig. 2.2).

2.1.4 Recording System

The system and equipment for recording the signals received over cables from the gage stations were the same as those used on Operation JANGLE[67]. The system was built around the Model S-3041 Ampex multichannel magnetic tape recorder. Eight of these recorders were assembled in a single instrument trailer, along with associated power, time base, fiducial marker, remote control, and other supporting equipment. (See Fig. 2.10). To protect the trailers from blast and radiation hazards, they were housed in underground revetments having inside dimensions 35 ft long, 11 ft wide, and 12.5 ft high (Fig. 2.9). Figure 2.11 is a block diagram showing the use of alternate recorders for back-up, and the interlaced station hookup to prevent loss of data from adjacent measuring stations in case of failure. The intelligence bandwidth of the recording system was 0 to 1500 cps,

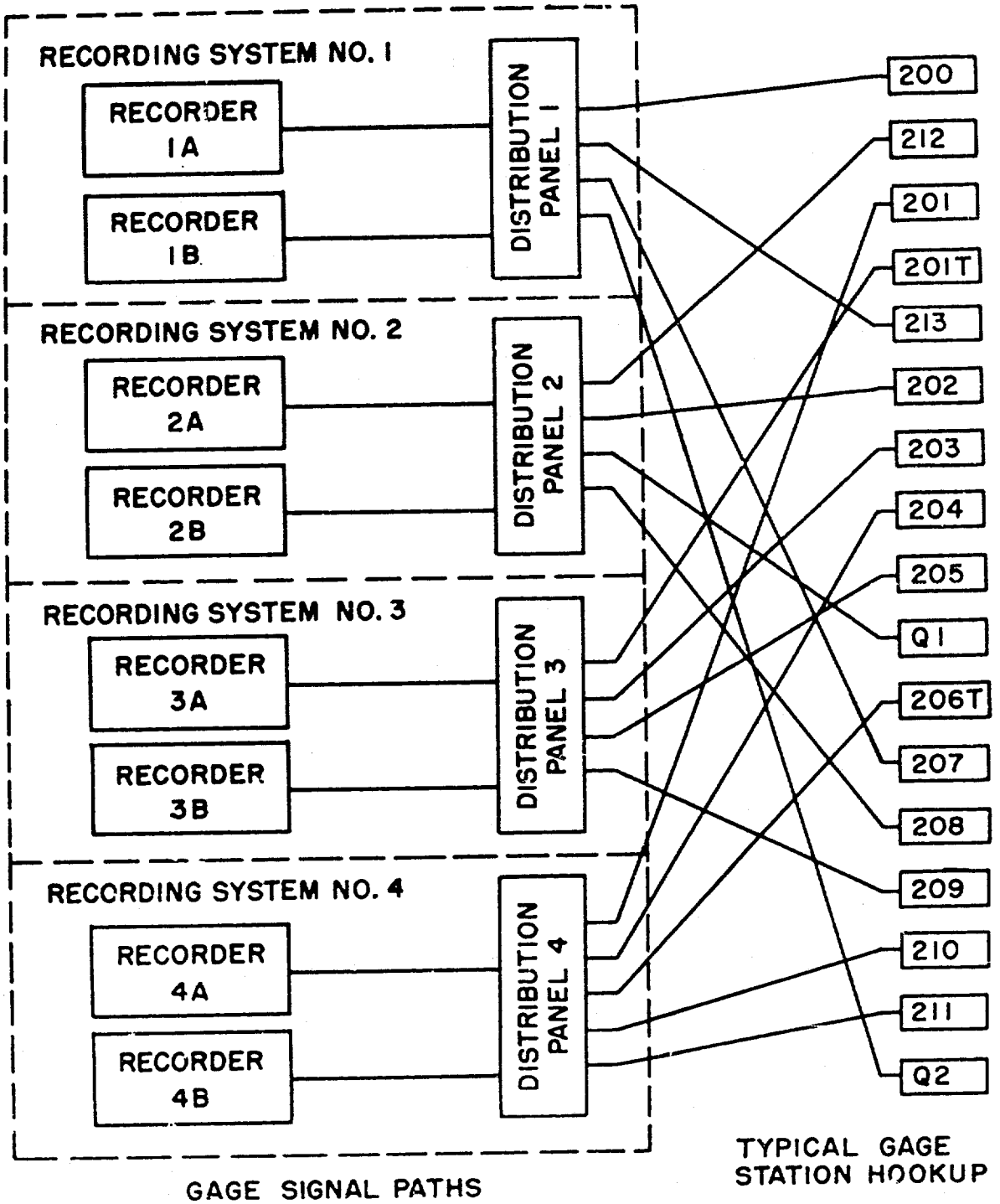

Fig. 2.11 Block Diagram Showing Signal Paths and Interlaced Station Hookup

leaving the pressure gage as the limiting factor in determining overall system response.

The time base equipment consisted of 400 cps and 1000 cps tuning forks, the outputs of which were recorded simultaneously on all tapes. Similarly, signals from two photo-electric circuits (Blue Boxes) generating zero-time marks, and two signals derived from a minus 2.5 second relay signal were recorded on all tapes to furnish common fiducial marks. This timing and fiducial marker system is shown in the block diagra of Fig. 2.12.

2.1.5 Power

Storage batteries provided power for all equipment during the tests giving complete independence from outside power sources. To reduce data loss in case of failure, four independent power systems supplied power to four complete recording systems. Except for fiducial and timing signals, each system could provide complete functioning of one quarter of the data channels. A block diagram showing the power system and utilization of the remote control relays is shown in Fig. 2.13.

2.1.6 Playback and Data Reduction

The magnetic tape records recovered from the instrument trailer were returned to the base camp where the reproducing equipment was set-up. (See Fig. 2.14). By use of an Ampex Model S-3042 Reproducer, the frequency modulated signals from individual data channels and the fiducial marker channel were recovered and fed simultaneously into two discriminators. The discriminator outputs were fed into separate galvanometers of a Century Oscillograph, Model 408, which provided continuous timing lines from a 100 cps tuning fork. During playback the magnetic tape reproducer speed was manually controlled, keeping the recorded 400 cps or 1000 cps time-base signals in step with a similar fork-generated signal in the playback equipment. In this way proper playback speed was assured, thus compensating for any tape shrinkage or variation in recorder speed.

The records were played back with an oscillograph paper speed of approximately 7 in. per sec for studying gross effects, measuring arrival times, positive durations, negative durations, and negative peak pressures. A paper speed of about 60 in. per sec was used to obtain better time-base resolution near the peak so that a judicious choice of the short duration positive peak could be made and

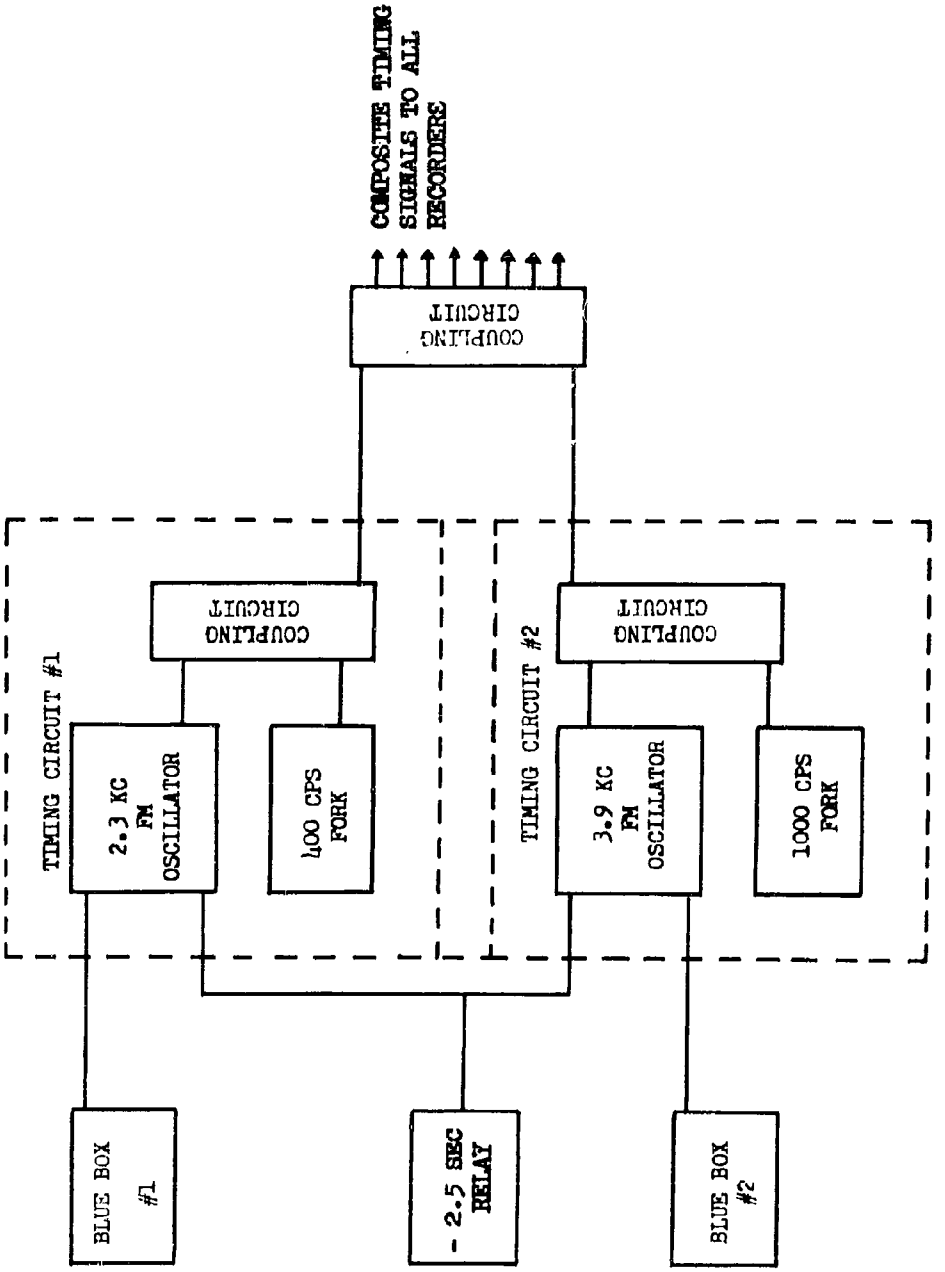

Fig. 2.12 Timing and Fiducial Marker System

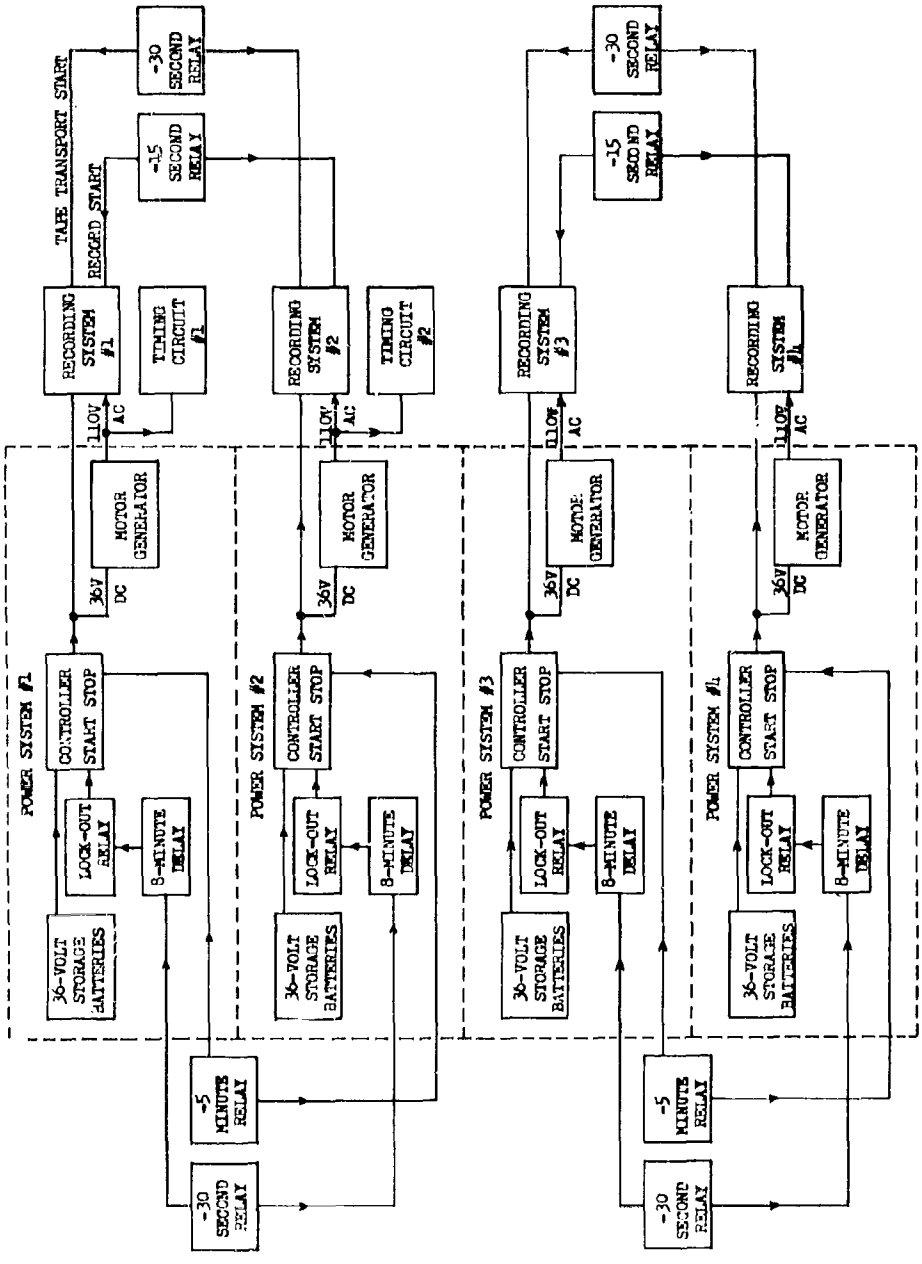

Fig. 2.13 Power System and Remote Control Relay Utilization

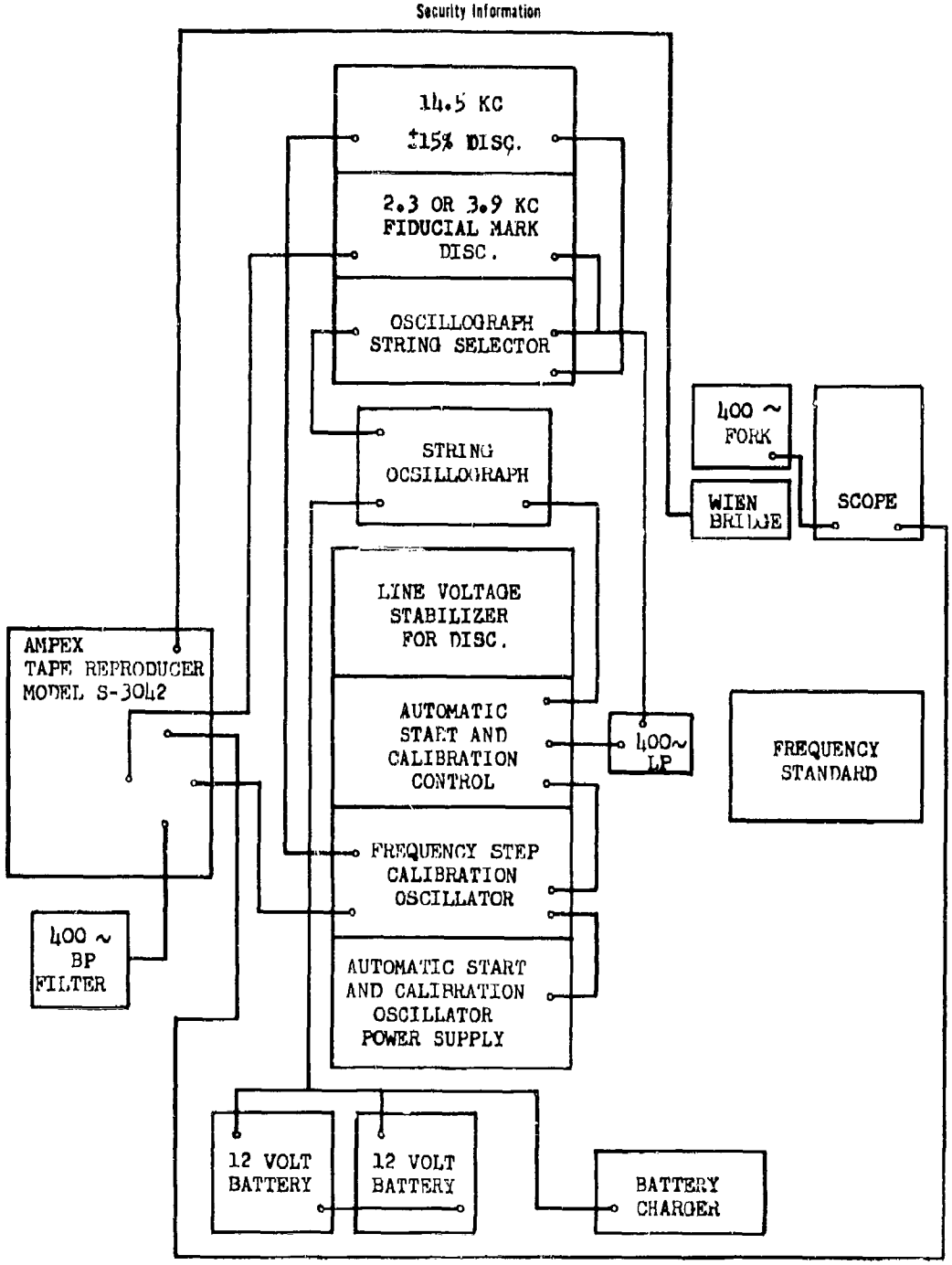

Fig. 2.14 Magnetic Tape Playback Block Diagram

the rise times measured.

Amplitude calibrations were provided automatically at the beginning of each oscillograph record by a step calibration generator. This unit produced eight equal steps of 290 cps each, covering the frequencies from 12,470 to 14,790 cps. To obtain pressure values from the records, the amplitude of the trace was measured, converted into a frequency value by means of simple ratios from the calibration signals, and then this frequency was converted into a pressure value by means of the gage calibration curve which plotted pressure versus oscillator frequency.

2.1.7 System Errors

It is estimated that an amplitude on the record could be converted to a pressure with an accuracy of $\pm$ 2.6 per cent of the pressure input or $\pm$ 1.4 per cent of nominal gage rating whichever was larger. Choice of the points to be read were subject to considerably greater variation because of the extraneous signals introduced by the instrumentation system and the irregularities in the pressure wave. The points read on all records obtained on this operation were points believed to be the most significant as selected by methods consistent with previous practices used at the NOL, which were based on known characteristics of the overall system as determined by laboratory and shock tube tests.

Measurement of the frequency of all vacuum-tube tuning forks used in controlling the time base was made with a crystal controlled oscillator with an accuracy of 1 part in 10^5. The short time stability of the three forks was sufficient to maintain an overall corrected time base accuracy of $\pm$ 0.1 per cent. The measurable correction was -0.392 per cent and was applied to all time measurements. The time base resolution on high-speed records was 0.2 msec and on low-speed records, 2 msec.

In the impulse calculations it was necessary to consider the fact that the oscillograms of the pressure waves were distorted somewhat because of the non-linearity of the gages. This resulted in the area under the p-t oscillograms being smaller than the areas would have been if the pressures had acted on gages with linear characteristics. The actual pressure-time histories could be reconstructed only by a tedious replotting of the records point by point. This replotting was avoided by assuming that the actual pressure-time functions were triangular and determining exact corrections for these assumed p-t curves, as shown in Fig. 2.15. These corrections were then applied to the area measurements of the actual p-t oscillograms.

The difference in the correction factor required for the triangular wave shape and the actual p-t curve was only a second order effect. A few records plotted point to point to check the validity of the assumption and procedure resulted in good agreement. The maximum correction for any record increased the area (and impulse) measured on the oscillogram by 15.7 per cent, while the average correction was about 7 per cent. The average of at least two readings was used for each record area measurement; the error in area measurement was estimated to be 3.6 per cent. Since the area was multiplied by the peak pressure, which had an accuracy of 2.6 per cent, the final impulse accuracy was approximately 4.5 per cent, i.e., 96 per cent of the impulse values had an accuracy of ± 4.5 per cent or better.

2.1.8 Recommendations for Instrumentation Improvement

Although the NOL system used for measuring pressure as a function of time on Operation TUMBLER had a high degree of reliability, several features are subject to improvement.

The signal-to-noise ratio should be increased by using wider frequency deviation, an improved tape recorder, or a flutter compensation scheme. This would increase the dynamic range of the system, a vital factor when amplitude predictions are uncertain.

A reduction in the number of conductors necessary to operate a gage station and the use of an inexpensive unshielded cable would reduce costs materially. Although the experimental channels operated on TUMBLER using unshielded cable showed no ill effects, there are unanswered questions about the possible effects of cross-talk when such cable is used on more than two channels.

Automatic control of the tape speed during playback instead of the present manual control would offer improved base line and time base stability.

More extensive use of automatic start, calibration, and record length control in playback would be desirable.

The gage is subject to considerable improvement. It would be desirable to use a gage with improved frequency response, better damping, better linearity, and one capable of producing wide frequency deviation. Since all known gages that fit into an FM system leave much to be desired, it would seem that work on this type gage might prove rewarding.

The data reduction for TUMBLER has all been done manually.

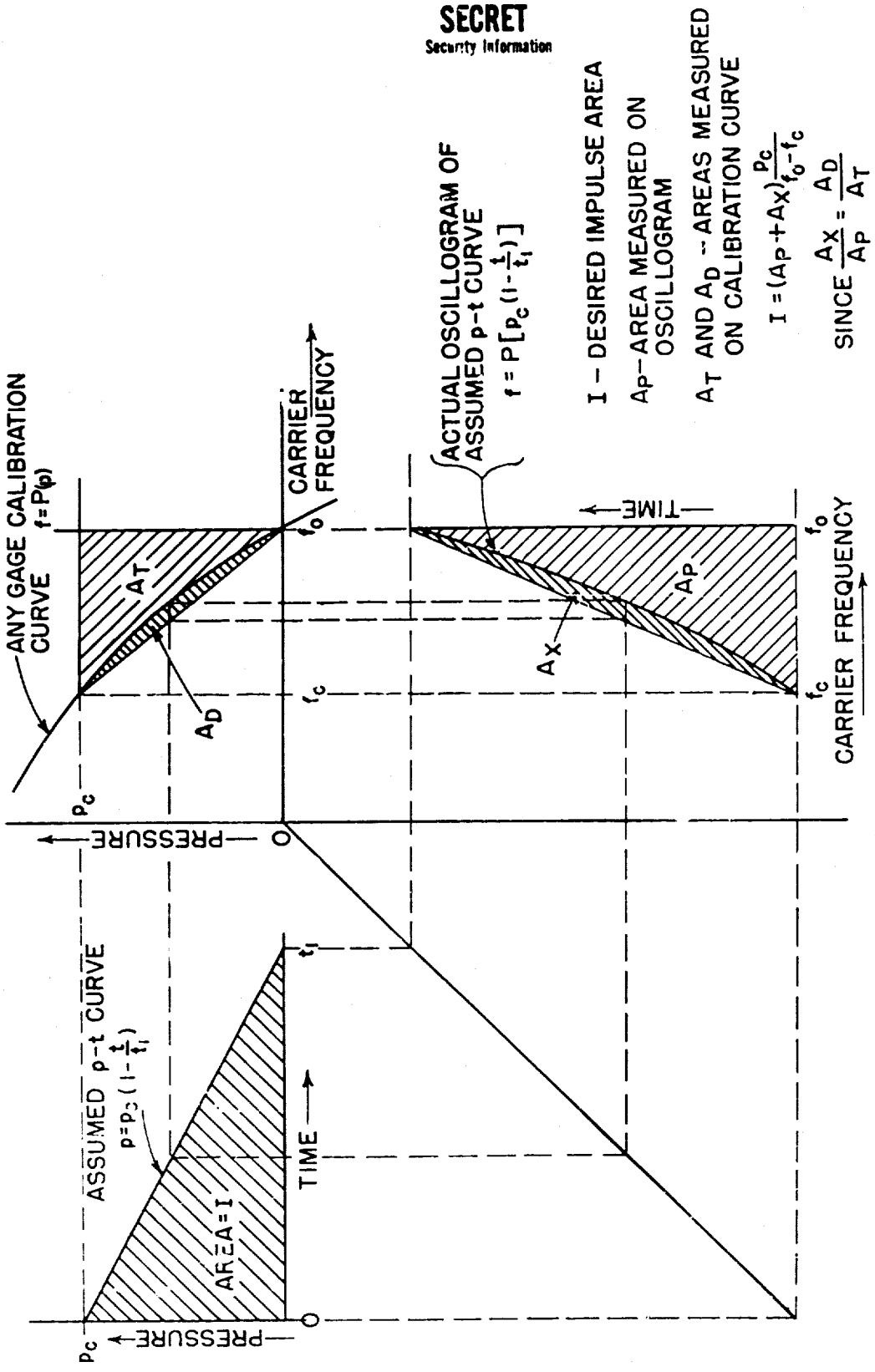

Fig. 2.15 Non-Linearity Correction for Impulse

For a large program some mechanization should be attempted. The use of a Tele-reader to transfer data to IBM cards is one approach. The burden of rapid data reduction in the field could be relieved somewhat by the use of an electronic integrator for impulse values and possibly by an electronic means of locating and computing peak pressure and time duration.

2.2 RESULTS

The complete instrumentation system functioned satisfactorily on this operation resulting in 59 records produced by the 59 gages used. These records* are reproduced throughout this chapter. Complete shock data were obtained from all records but one. The oscillator-amplifier at Station 7-201 on TUMBLER 3 behaved erratically approximately 50 milliseconds after the arrival of the shock wave producing spurious signals (Fig. 2.35), so that no determinations of positive phase duration and impulse, and negative phase duration and pressure were made from this record. However, no information was lost at this distance since the back-up station, 7-201 T, functioned properly.

The cable experiment described in Sec 2.1.3 proved to be highly successful. The stations using telephone wire for signal transmission (T appended to station designation) showed no difference in pick-up characteristics when compared to the stations using shielded MCOS-6 cable (see Fig. 2.26). Any extraneous signal which may have been picked up on TUMBLER 1, 2, and 3 had no effect on the FM signal; on TUMBLER 4, the telephone wire circuits were affected to the same degree as the MCOS-6 circuits.

---

* To show the complete pressure-time history at each station in a form suitable for publication the magnetic tape records were re-run using a low-speed paper feed on the string oscillograph thus compressing the time scale. The amplitude scale remained the same as on the oscillograph records used for data analysis. The high-speed record inserts of the initial peaks are photographic reproductions of careful tracings of the original high-speed records used for analysis and have approximately the same amplitude scale as the low-speed records. The reader is cautioned against scaling any of these reproduced records for quantitative values since gage calibration curves and correction values are not included in this report. The original data with all necessary curves and correction factors are available for study at the Naval Ordnance Laboratory.

To read the records obtained in this operation, considerable judgment had to be exercised in the choice of the points to be read so as to distinguish among background noise in the system, gage ringing, and true signals. In general, the procedures used in reading the records were as follows:

(a) Where there appeared to be a clean shock as shown in the records for TUMBLER 2, Stations 7-203 and 7-204 (Fig. 2.27), the peak pressure was considered to occur at the time and have the value indicated by smoothing a line through the center of the decaying signal from right to left until it intersected the initial signal rise. This decaying signal was due to gage ringing, and it was superimposed on the forcing function. The smoothing process was the attempt to extract the forcing function - in this case, the pressure signal - from the composite signal.

(b) Where there appeared to be excessive overshoot as in TUMBLER 2, Stations 7-205 and 7-206 (Fig. 2.28), the smoothing process was also used; however, the first upswing was weighted more heavily than in the above case. There was justification for this in terms of the system behavior and therefore the initial high amplitude spikes were considered to be a composite of gage ring and high short duration peaks of pressure. Indeed, high peaks of short duration had been recorded by other instrumentation systems at the onset of such records.

(c) Where there was a pecularity about the initial rise particularly careful judgment had to be used in establishing a smoothed line. On some records, such as on TUMBLER 1, Station F-202 (Fig. 2.17), smoothing was necessary to filter out the recorder and playback flutter; on other records, such as TUMBLER 4, Station 7-201 (Fig. 2.45) for instance, the smoothing was done only to establish the significant peak-pressure wave shape - the individual short duration peaks and oscillations were considered to be real pressure induced signals.

(d) In reading phase durations, some difficulty was experienced in determining the exact point where the signal trace intersected the base line. This was particularly true for negative phase durations where the intersection of the two traces took place at a very small angle because of the long durations and small amplitudes. Because of this lack of resolution, negative duration times may be in error by as much as 0.1 to 0.2 second. This may account for the large degree of scatter evident in the negative phase duration plots in Figs. 2.24, 2.33, and 2.44.

It must be re-emphasized that considerable judgment was required

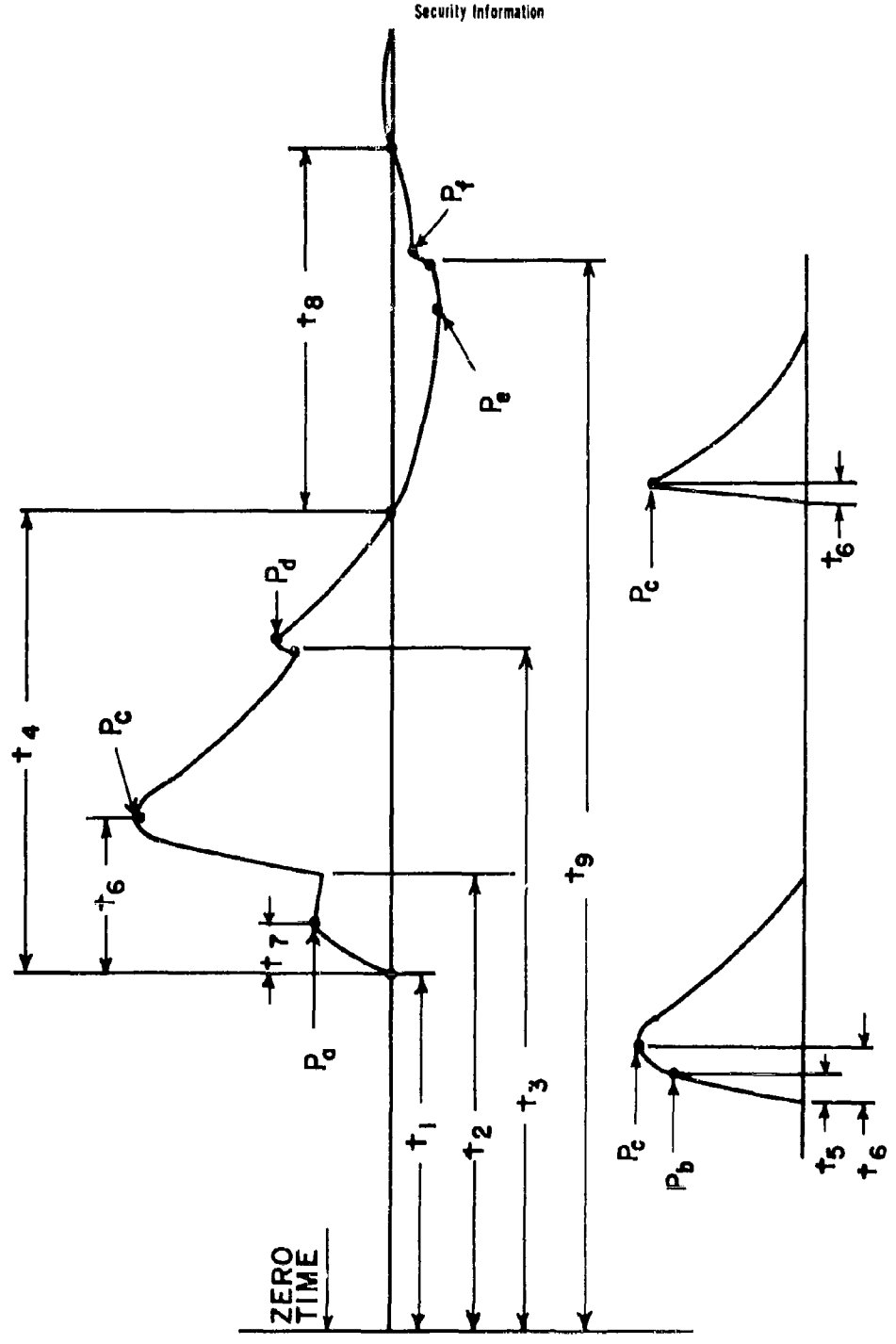

Fig. R.16 Symbols for Characteristic Waveforms

to interpret the records. The values read on all records obtained on this operation were read at points believed to be the most significant as selected by methods consistant with previous practices used at the NOL. This selection was based on known characteristics of the overall system as determined by laboratory and shock tube tests.

To assist in the interpretation of the tabulated and plotted data, the various points of interest read off the records are labeled and pictorially defined in Fig. 2.16.

2.2.1 TUMBLER 1

The high and low-speed records for TUMBLER 1 are shown in Figs. 2.17, 2.18, and 2.19; the numerical results obtained from the analysis of these records are summarized in Tables 2.2 and 2.3 and plotted in Figs. 2.20 through 2.25. A study of the high-speed records indicates that there was a definite difference between the rise time characteristics of the close-in and farther-out stations. The early stations, F-200 through F-203, showed a relatively long rise time to the maximum pressure value, averaging approximately 8.5 milliseconds. Within the resolution capabilities of the instrumentation, this rise appeared to take place with a double step in a manner very similar to that encountered at the close-in stations on TUMBLER 4. This suggests that these initial steps may have arisen in a similar fashion to the precursor phenomenon noted in TUMBLER 4 and discussed in Sec. 5.2. It should be noted that there was some corroborative photographic evidence of such a precursor in the results of Project 1.5 for TUMBLER 1. (See Sec. 5.2).

Stations F-205 through F-211 gave pressure-time records of the conventional variety with short rise times, averaging 1.3 milliseconds (which is about the response time of the system), and smooth decays. The oscillations at the early portions of these records were due to gage ringing caused by the rapid application of the pressure wave on the air column and the diaphragm of the gage. These oscillations, although undesirable, indicated the shock nature of the forcing function. Most of the smaller irregular variations in the trace arose from characteristic flutter or noise produced by the tape recorders and reproducers.

It will be noted on the plot of peak positive pressures versus distance (Fig. 2.20) that there is an apparent shift in the curve occurring between Stations F-203 and F-204. This is interesting in view of the fact that according to data from the rocket photography of Project 1.5, the Mach stem rose from the ground at about

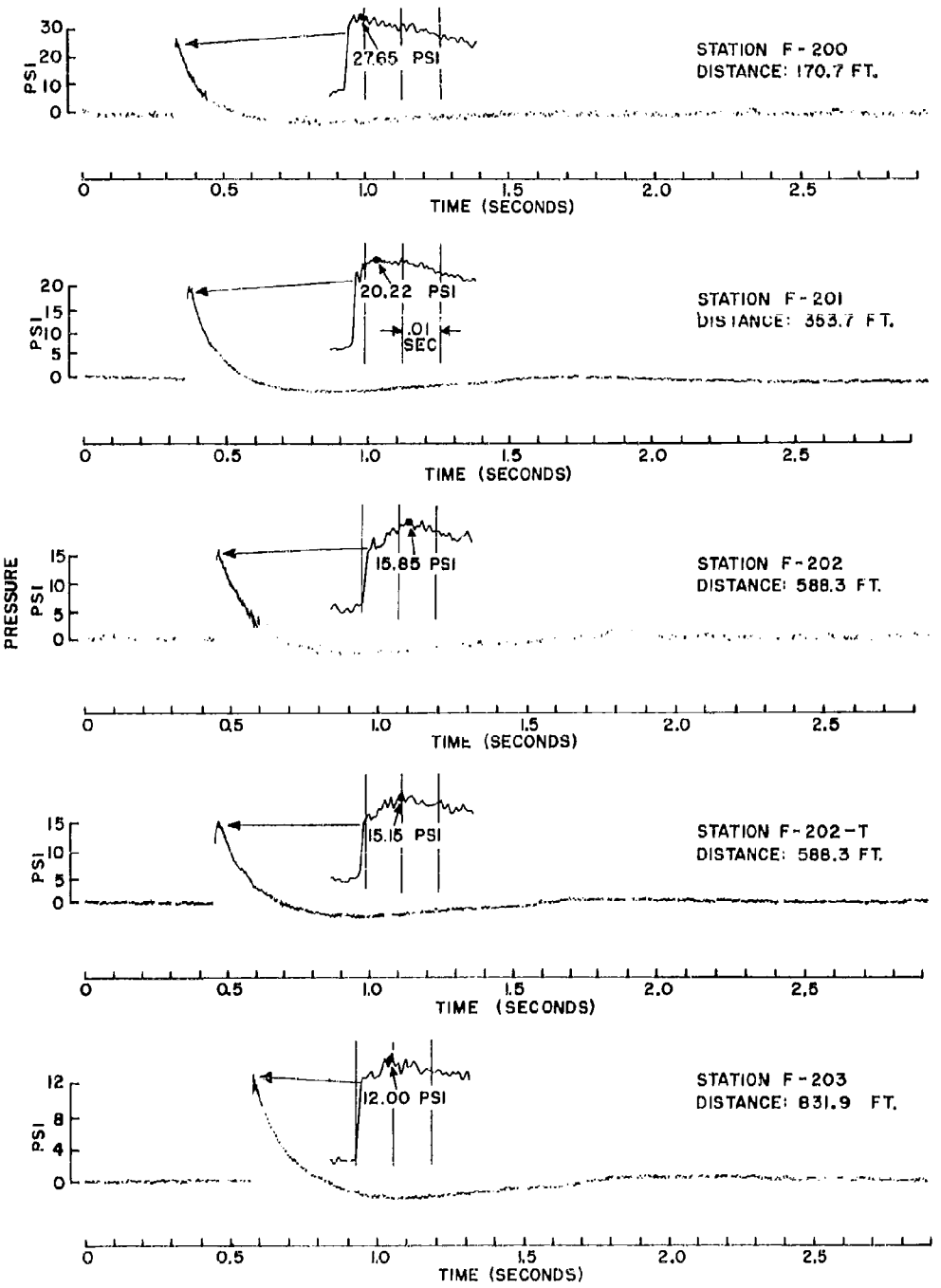

Fig. 2.17 Records, TUMBLER 1, Stations F-200 through F-203

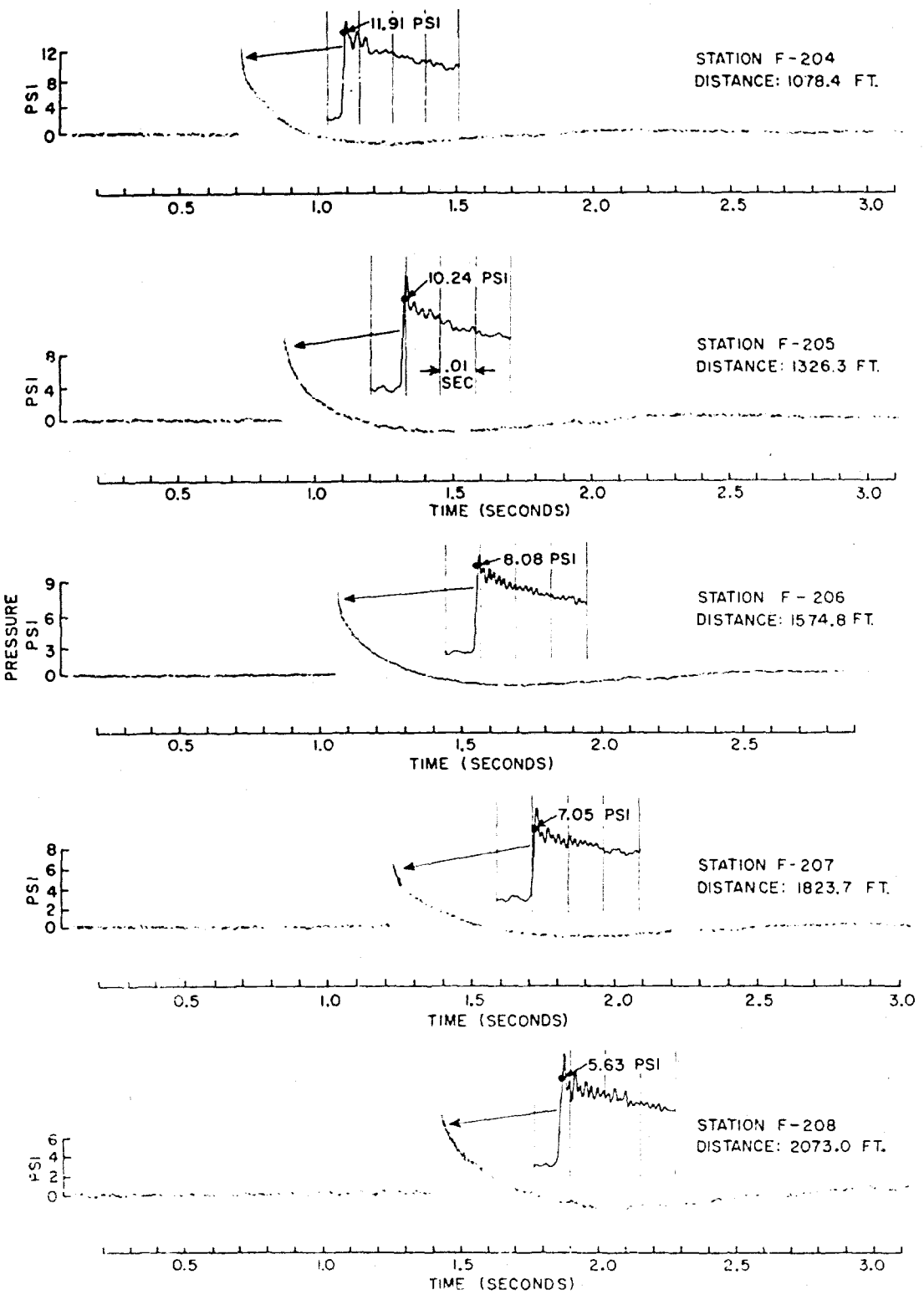

Fig. 2.18 Records, TUMBLER 1, Stations F-204 through F-208

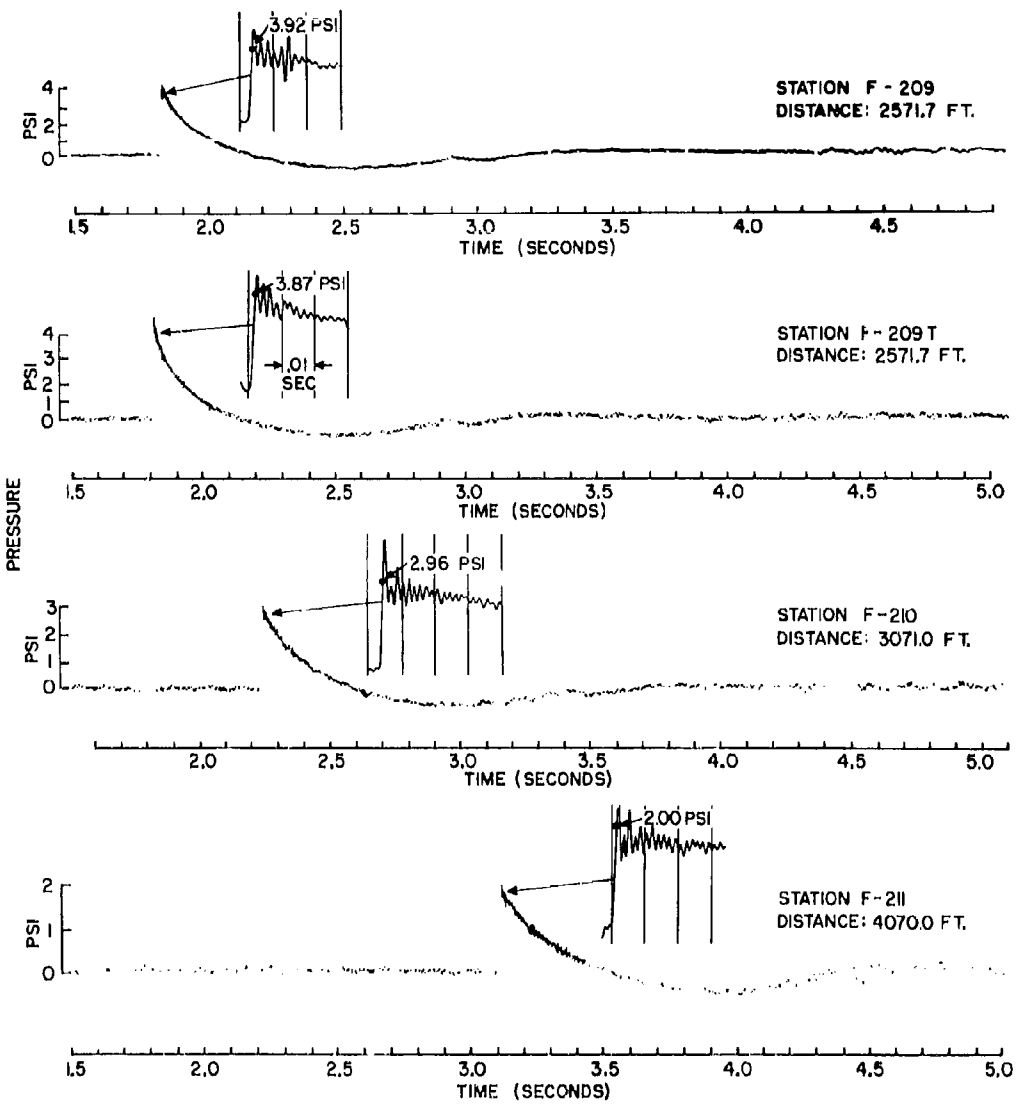

Fig. 2.19 Records, TUMBLER 1, Stations F-209 through F-211

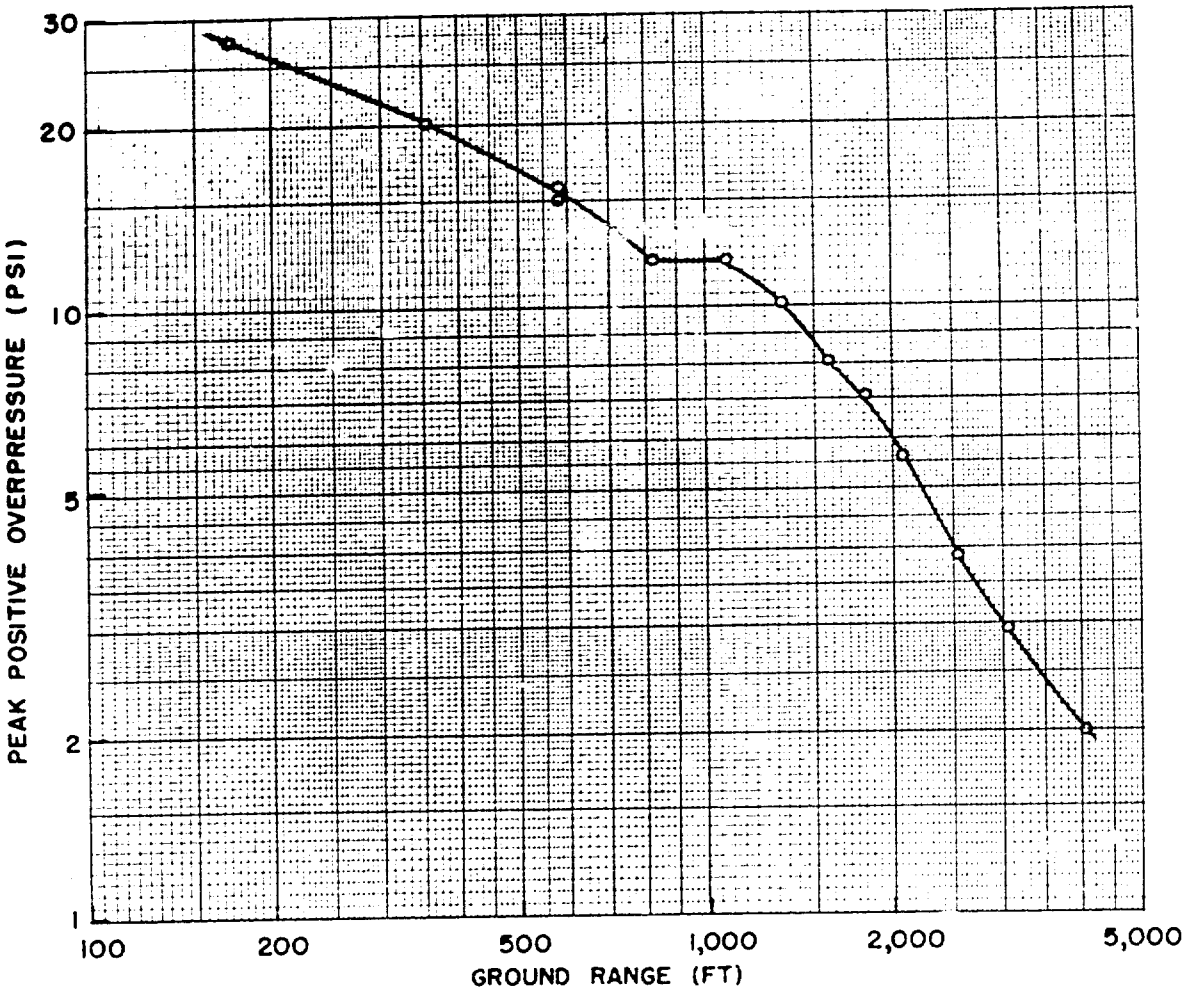

Fig. 2.20 Peak Positive Overpressure, P_c, Ground Level, TUMBLER 1

860 ft, or just beyond Station F-203. The increase of pressure from Mach reflection was evidenced by this curve displacement.

The records of TUMBLER 1 showed an interesting feature not usually mentioned or observed in air blast studies. The negative phase of the shock wave was followed by a second positive phase having a slow rise and small amplitude, approximately 5 per cent of the main shock strength, and of a duration intermediate between the initial positive and negative phases. Movies showing dust displacement on the ground also indicated this second positive phase. Although these char-

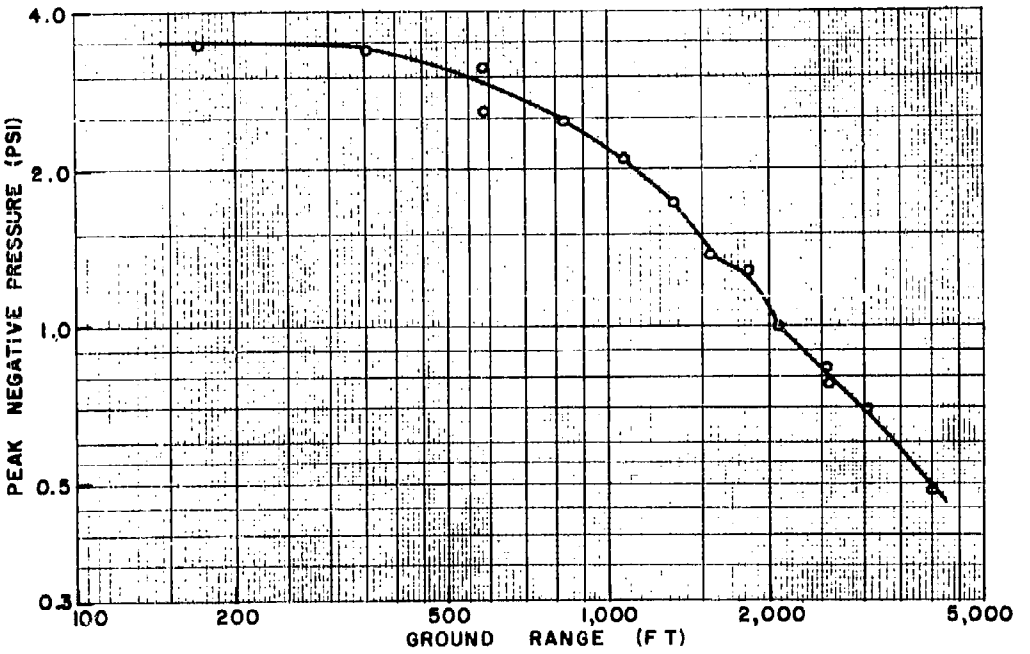

Fig. 2.21 Peak Negative Pressure, P_e, Ground Level, TUMBLER 1

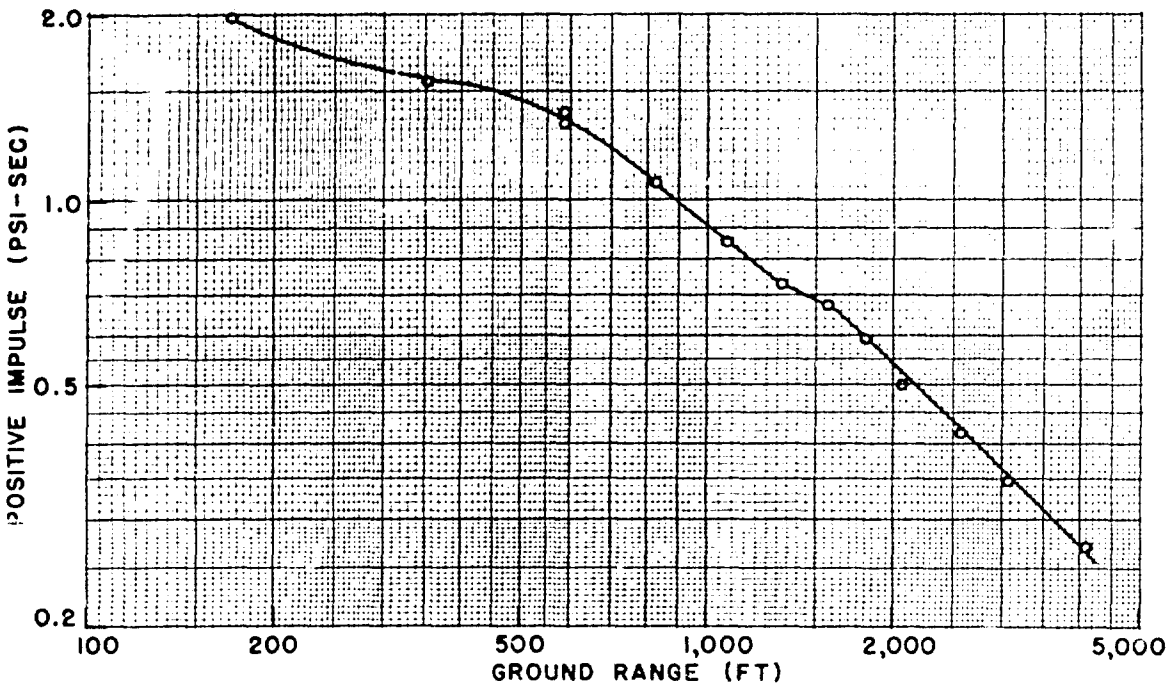

Fig. 2.22 Positive Impulse, Ground Level, TUMBLER 1

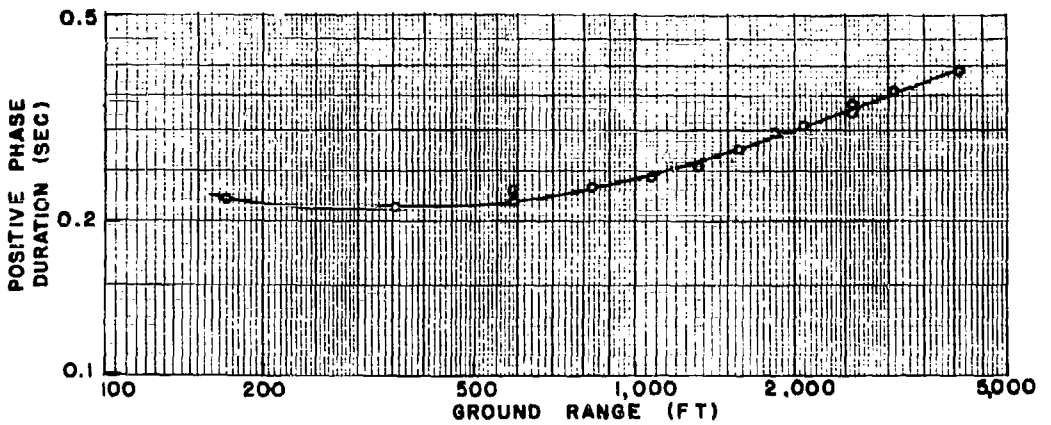

Fig. 2.23 Positive Phase Duration, t_4, Ground Level, TUMBLER 1

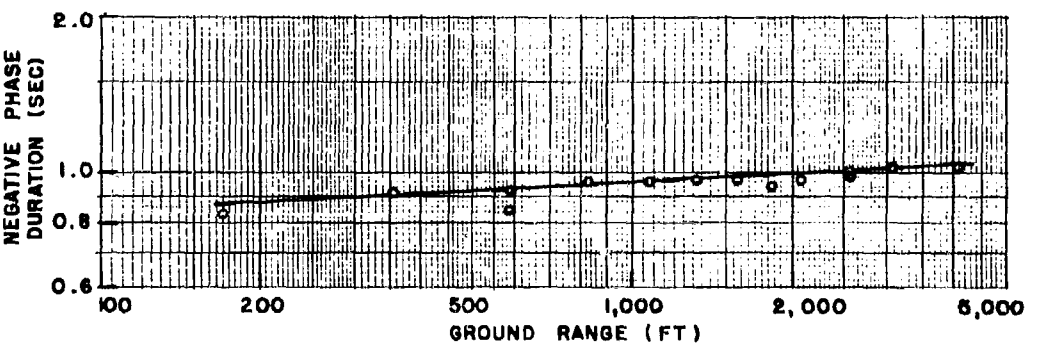

Fig. 2.24 Negative Phase Duration, t_8, Ground Level, TUMBLER 1

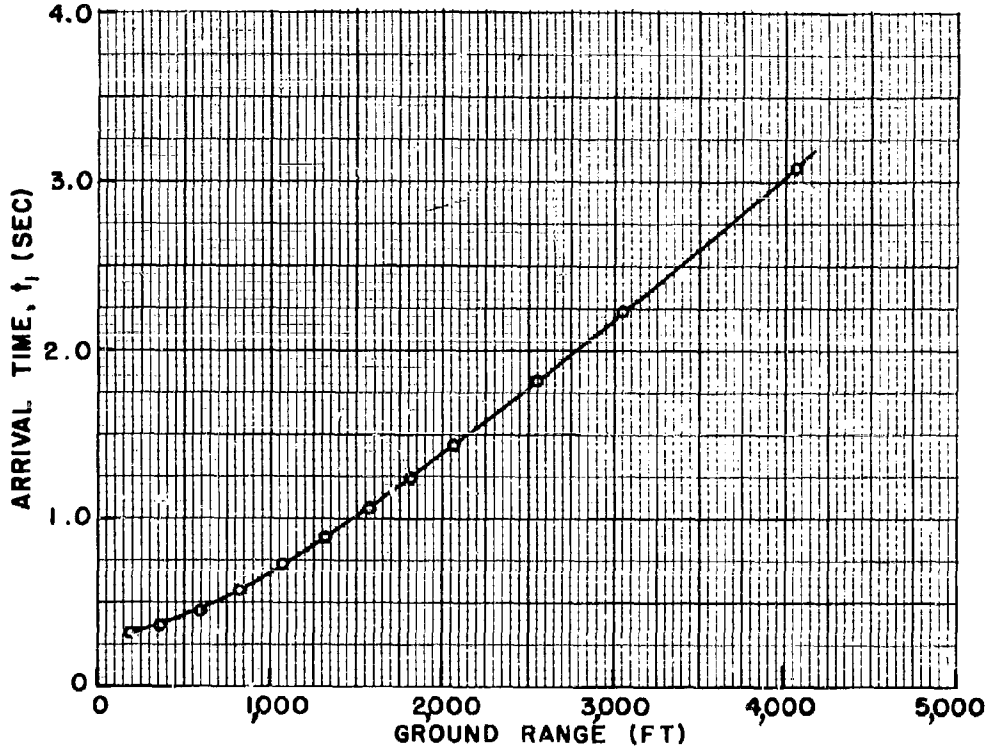

Fig. 2.25 Arrival Time of Initial Disturbance, t_1, Ground Level, TUMBLER 1

acteristics were similar to those associated with the bubble pulse phenomenon in underwater explosions, the origin of this second positive phase is not known and its study may be worthy of consideration.

2.2.2 TUMBLER 2

The high and low-speed record reproductions are shown in Figs. 2.26, 2.27, and 2.28; the results of the data analysis are summarized in Tables 2.4 and 2.5 and graphically presented in Figs. 2.29 through 2.34. The records from this shot were somewhat cleaner, i.e., showed less inherent system noise, than the records obtained from TUMBLER 1. This arose from the fact that the pressures encountered on the second shot were closer to the optimum gage ranges than those on the previous shot. This resulted in large frequency deviations being produced by the pressure signals and minimized the inherent frequency deviations produced by flutter of the recording and playback machines, i.e., a good signal-to-noise ratio was obtained.

The pressure-time records indicated smaller irregularities

in the wave shapes for this shot than for TUMBLER 1. There was some rounding or flattening of the peaks for the stations in the regular reflection region; however, this distortion of the typical shock form was continuous and smooth and unlike the step discontinuities encountered in the TUMBLER 1 records if data taken extremely close to ground zero (Stations F-200 and 7-200) are not considered. If the step discontinuities of TUMBLER 1 arose from a weak precursor, it is reasonable to believe they would not exist on TUMBLER 2 where no precursor was observed, probably because of the higher burst height of the latter shot. In the Mach reflection region, Station 7-203 and beyond, typical shocks were evidenced with their characteristic short rise times to the maximum value. The plot of peak positive overpressure versus distance, Fig. 2.29, showed a slight flattening between Stations 7-202 and 7-203. As in TUMBLER 1, this plateau occurred in the area of the Mach stem formation as determined by Project 1.4 and reported in reference 27.

A second positive phase of small amplitude and averaging 0.3-0.4 sec in duration was also observed on TUMBLER 2.

2.2.3 TUMBLER 3

The reproductions of records for TUMBLER 3 are shown in Figs. 2.35 through 2.38 with summarized data given in Tables 2.6 and 2.7 and plotted in Figs. 2.39 through 2.44. In general, the characteristic features of these records were similar to those on TUMBLER 2. The close-in stations, 7-200 through 7-204, showed a sharp rise with gradual rounding to the peak value; Stations 7-205 and 7-206T exhibited a sharp initial rise with flattened peaks; and Stations 7-207 through 7-211 showed typical shock forms. The plateau in the pressure-distance curve, Fig. 2.39, indicated that the Mach stem formed in the region around Stations 7-206T to 7-208. This was consistent with data from Project 1.23, which showed that the Mach stem was at least 10 ft high at Station 7-209, i.e., that it was formed at a distance closer to ground zero than Station 7-209. As on the previous shots, typical shock-wave features were encountered in the later portion of the pressure distance curve which coincided with the Mach reflection region, and irregular shock characteristics were evident in the regular reflection region or the early part of the pressure-distance curve. Stations 7-205 and 7-206T appeared to be in a transition zone with the shocks changing from a rounded peak through a flattened stage and then to the typical shock form.

Two stations, 7-Q1 and 7-Q2, were added to TUMBLER 3 to investigate the effect of terrain on shock form. These stations were located approximately 800 ft off the right side of the main blast line

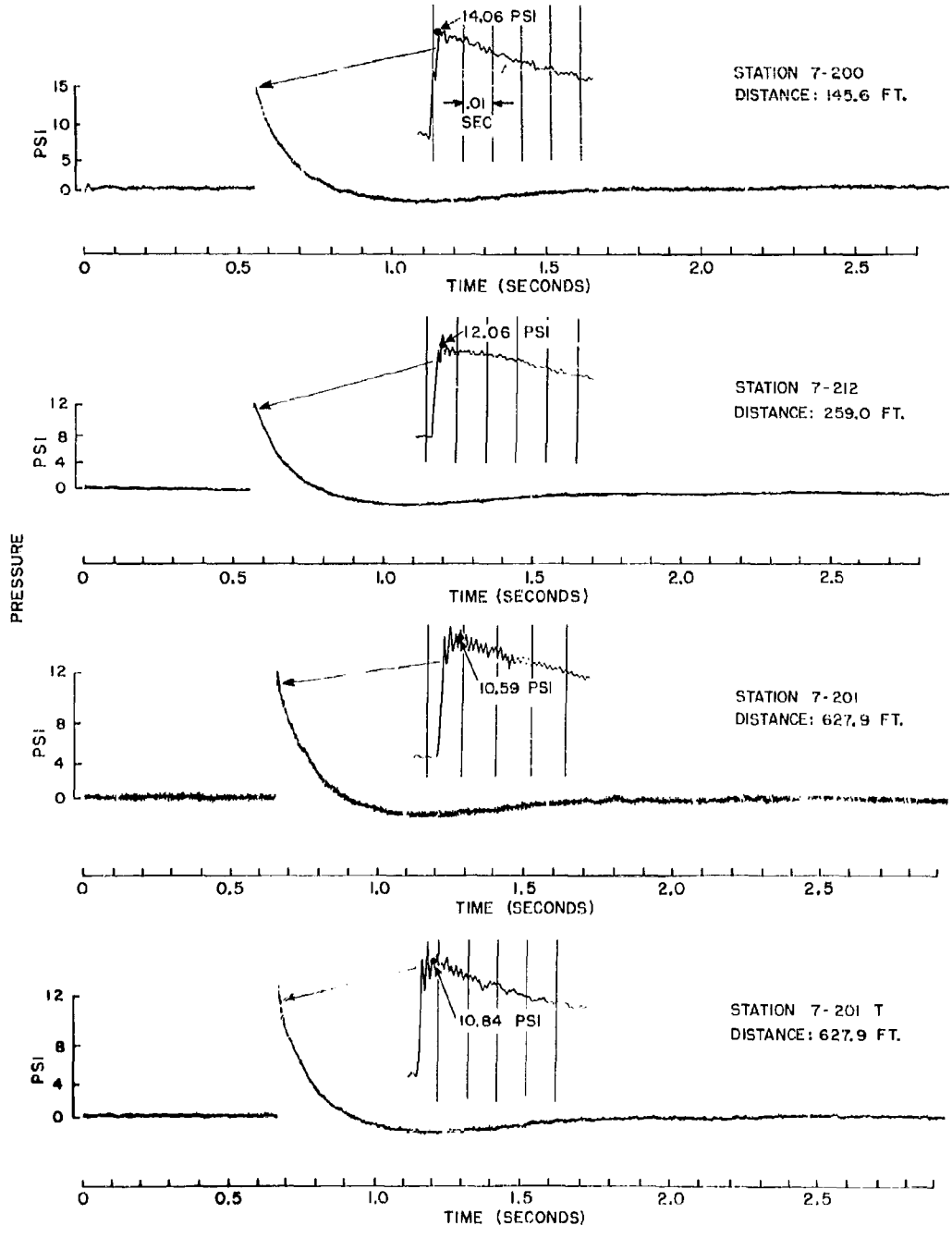

Fig. 2.26 Records, TUMBLER 2, Stations 7-200 through 7-201T

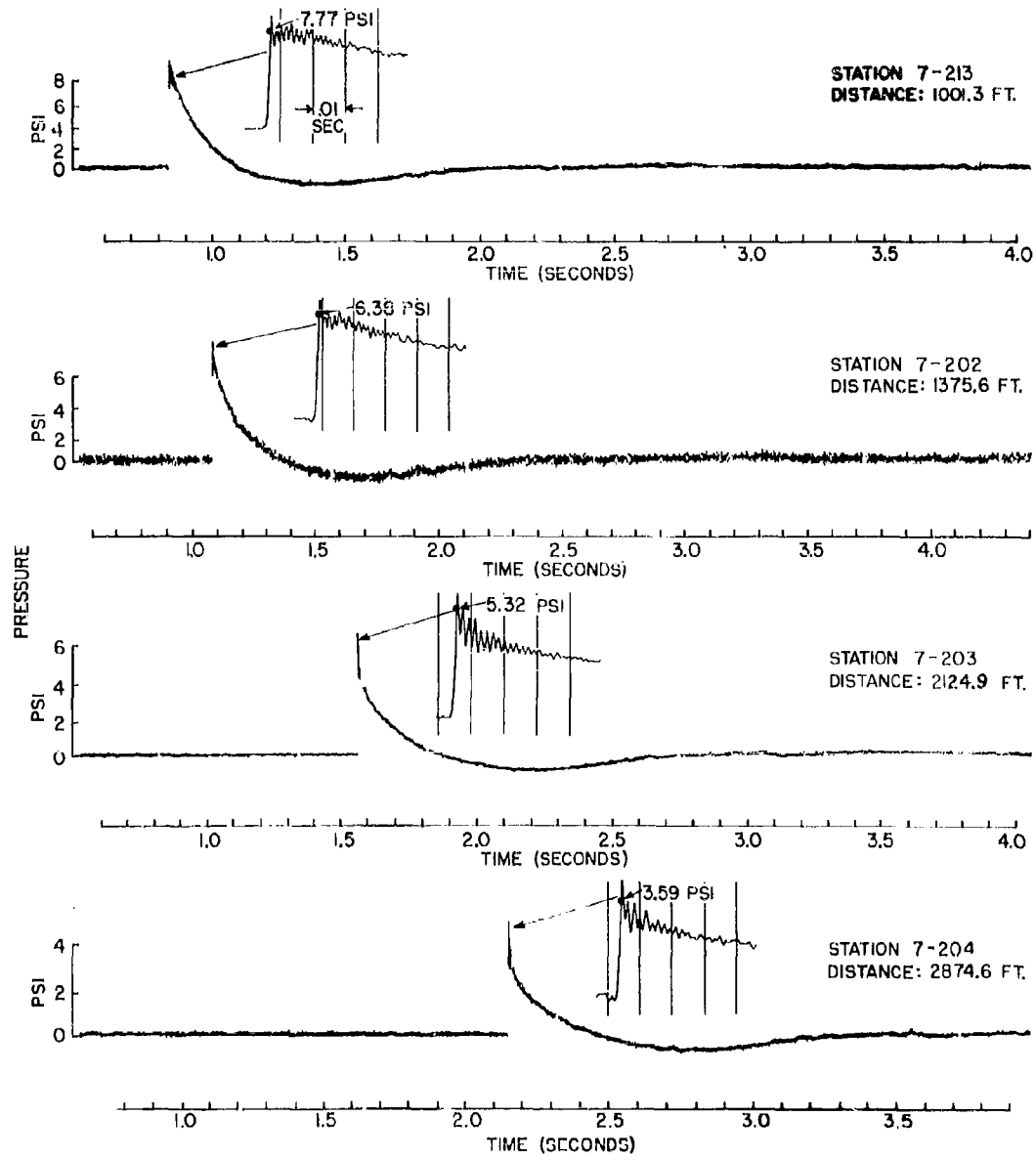

Fig. 2.27 Records, TUMBLER 2, Stations 7-213 through 7-204

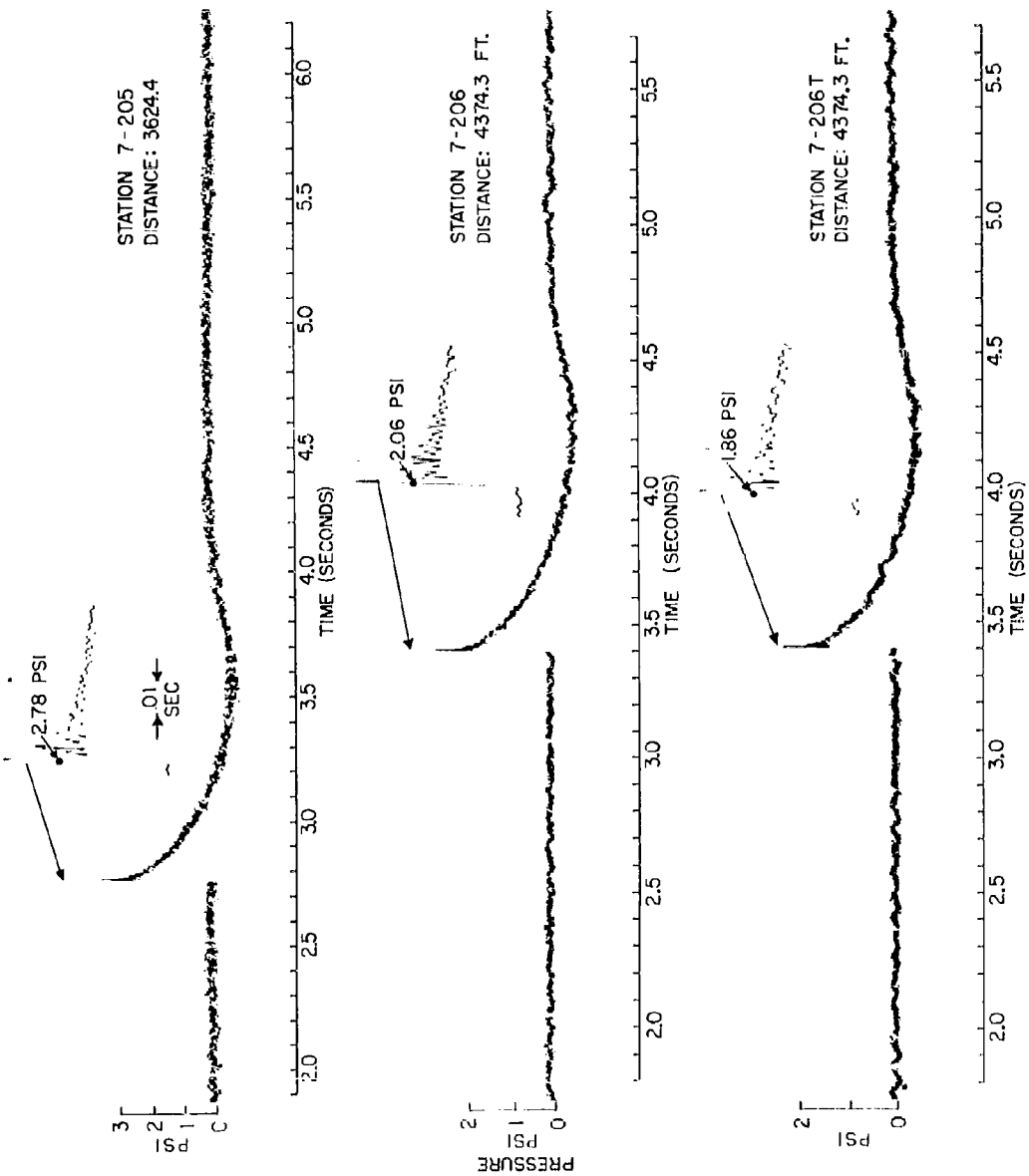

Fig. 2.28 Records, TUMBLER 2, Stations 7-205 through 7-206T

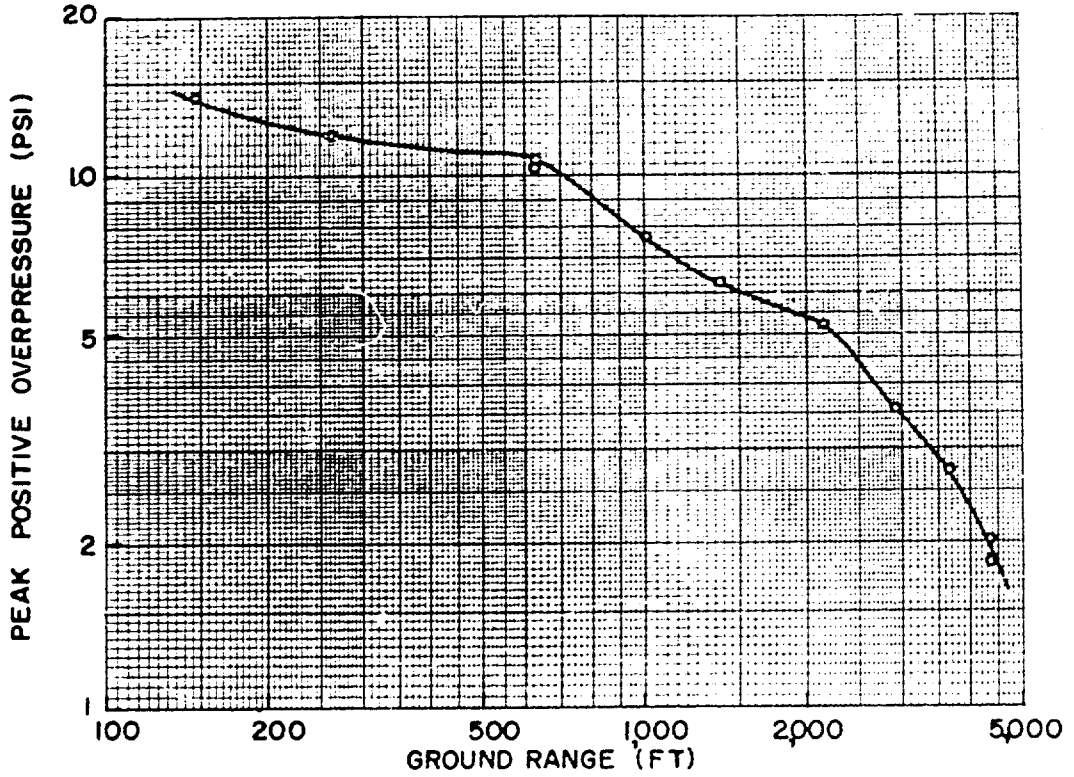

Fig. 2.29 Peak Positive Overpressure, P_c, Ground Level, TUMBLER 2

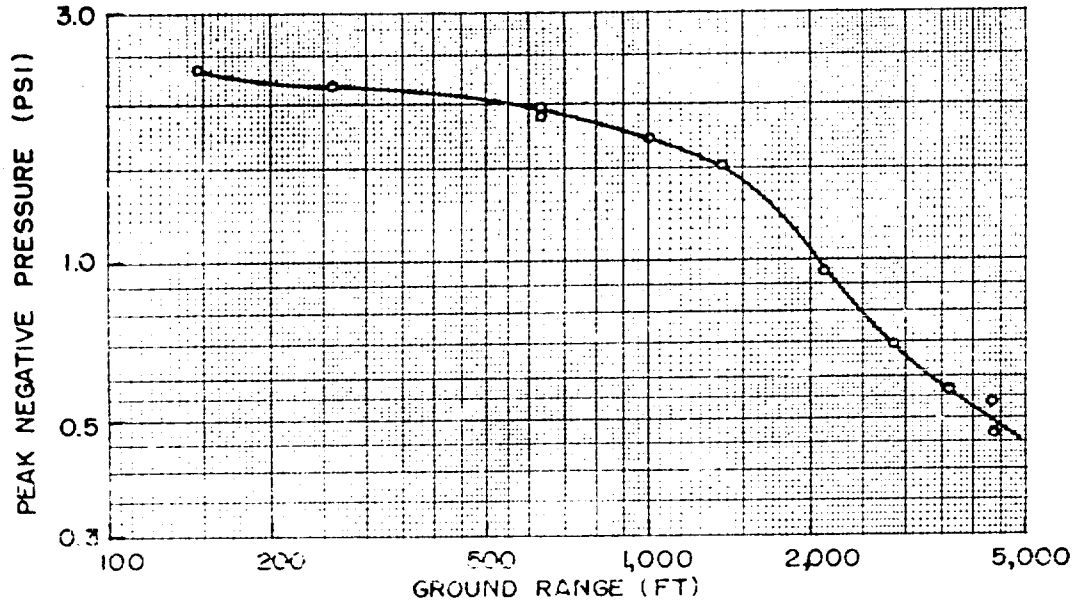

Fig. 2.30 Peak Negative Pressure, P_e, Ground Level, TUMBLER 2

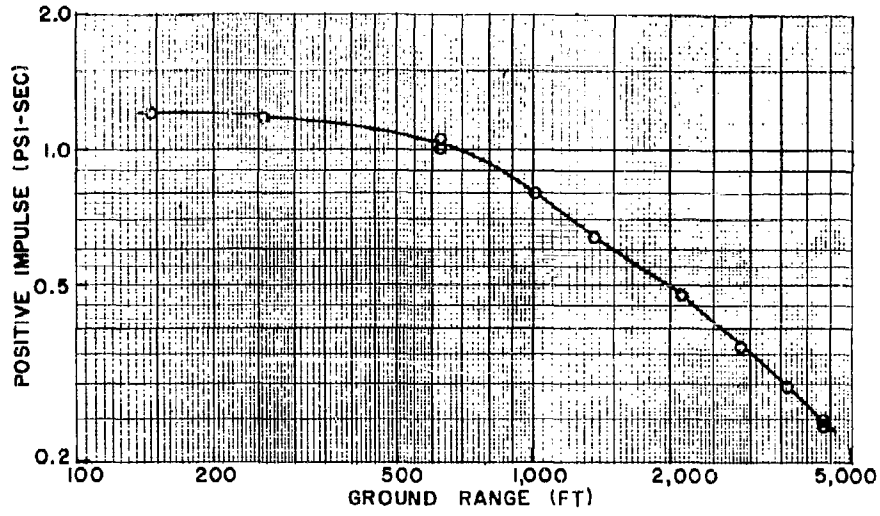

Fig. 2.31 Positive Impulse, Ground Level, TUMBLER 2

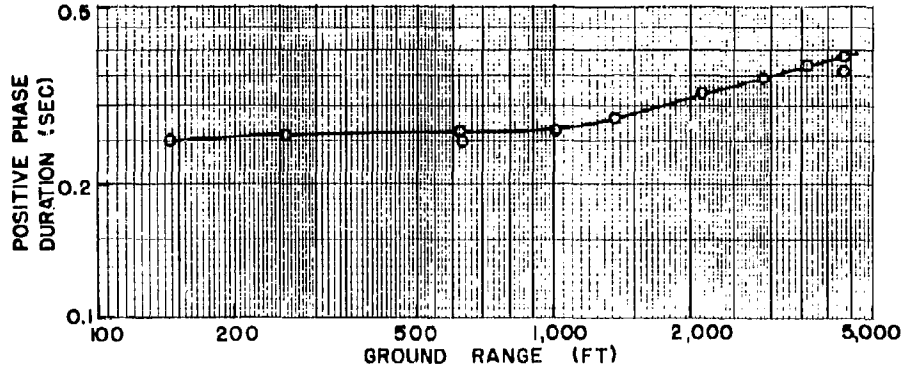

Fig. 2.32 Positive Phase Duration, t_4, Ground Level, TUMBLER 2

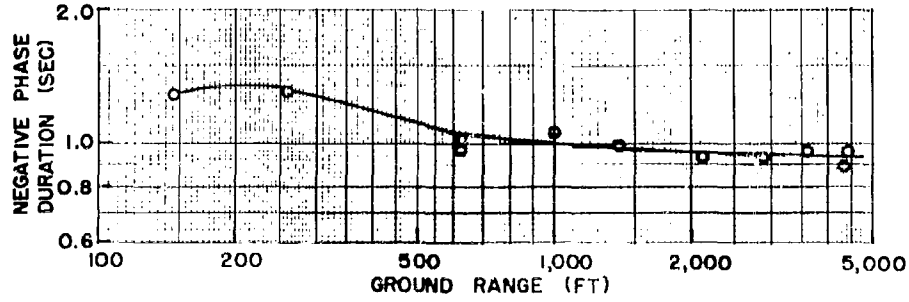

Fig. 2.33 Negative Phase Duration, t_8, Ground Level, TUMBLER 2

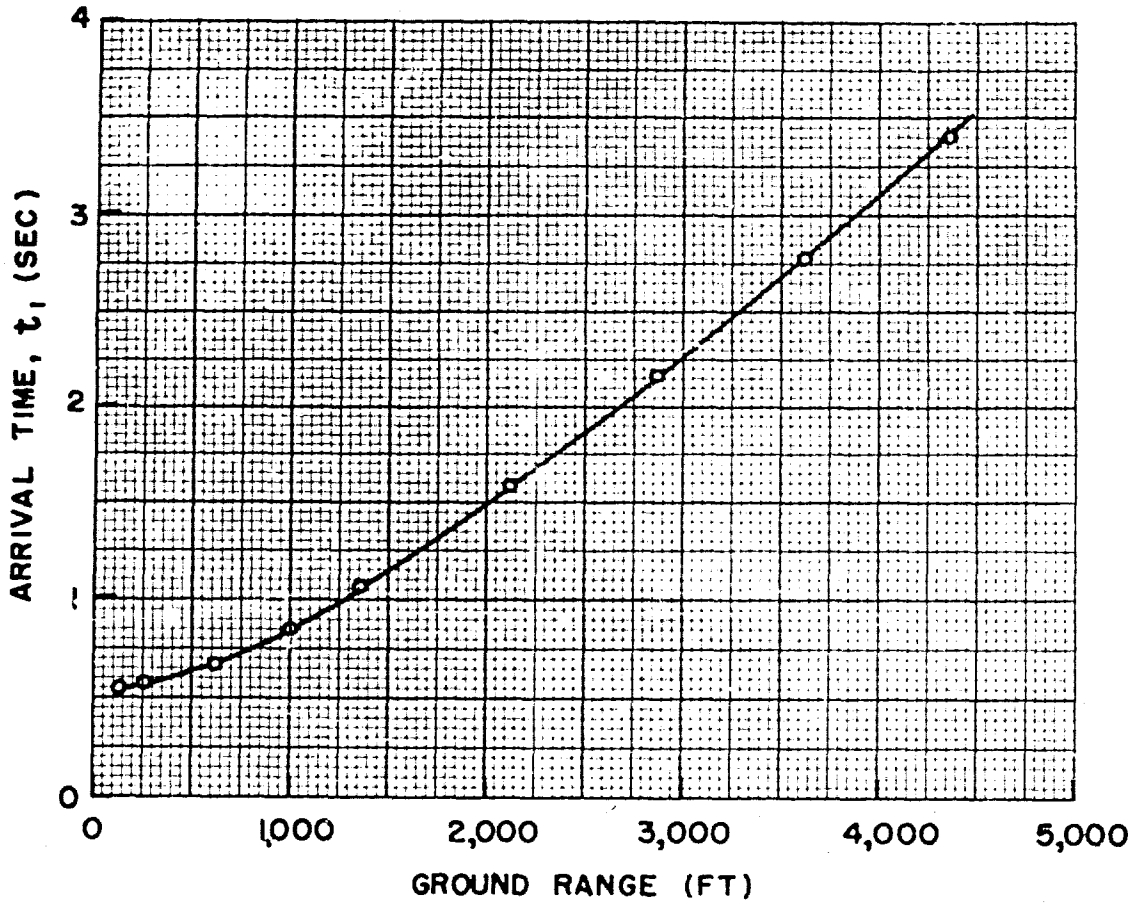

Fig. 2.34 Arrival Time of Initial Disturbance, t_1, Ground Level, TUMBLER 2

(facing zero) and 2917 ft and 3686 ft respectively from Station 7-200 (Fig. 2.1). Here the ground was relatively undisturbed as compared to the main blast line and consequently it was rough, dusty, and covered with a considerable amount of sage brush. The gross characteristics of the records from these stations were very similar to the records from the stations at comparable distances in the transition and Mach reflection regions which showed shock features, i.e., short initial rise times. The first 10-20 milliseconds of the pressure records, however, contained a considerable number of sharp irregularities which, it is believed, were the signals resulting from the combination of gage ringing and irregular, possibly spiked, pressure signals. (It will be noted in Fig. 2.38 that the signal-to-noise ratio for these records was quite high, and therefore few of the irregularities could have been contributed by tape flutter). It has been suggested by Dr. C. W. Lampson of the Ballistic Research Laboratories that these pressure spikes may have been caused by local turbulences induced and abetted by the sage brush, surface discontinu-

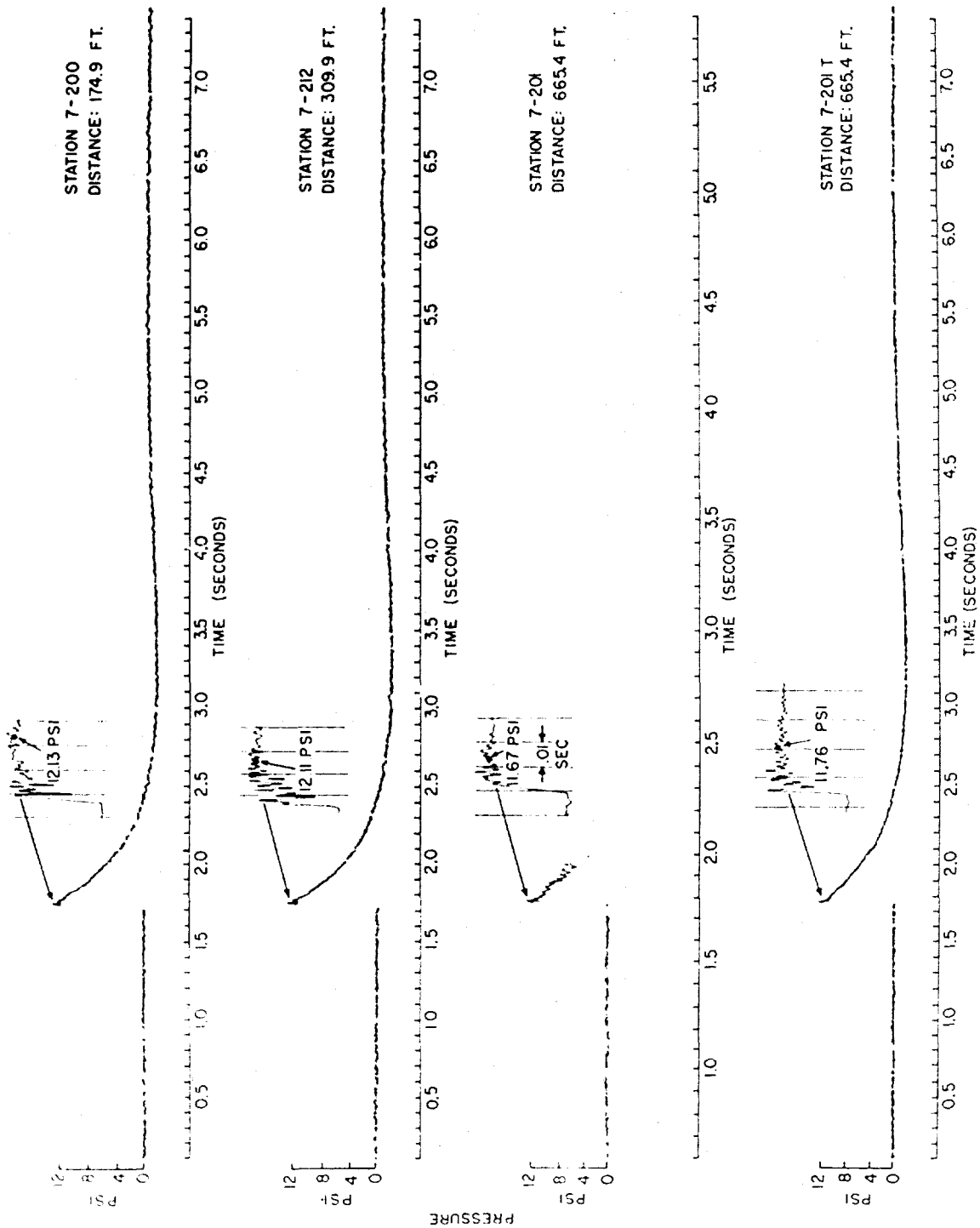

Fig. 2.35 Records, TUMBLER 3, Stations 7-200 through 7-201T

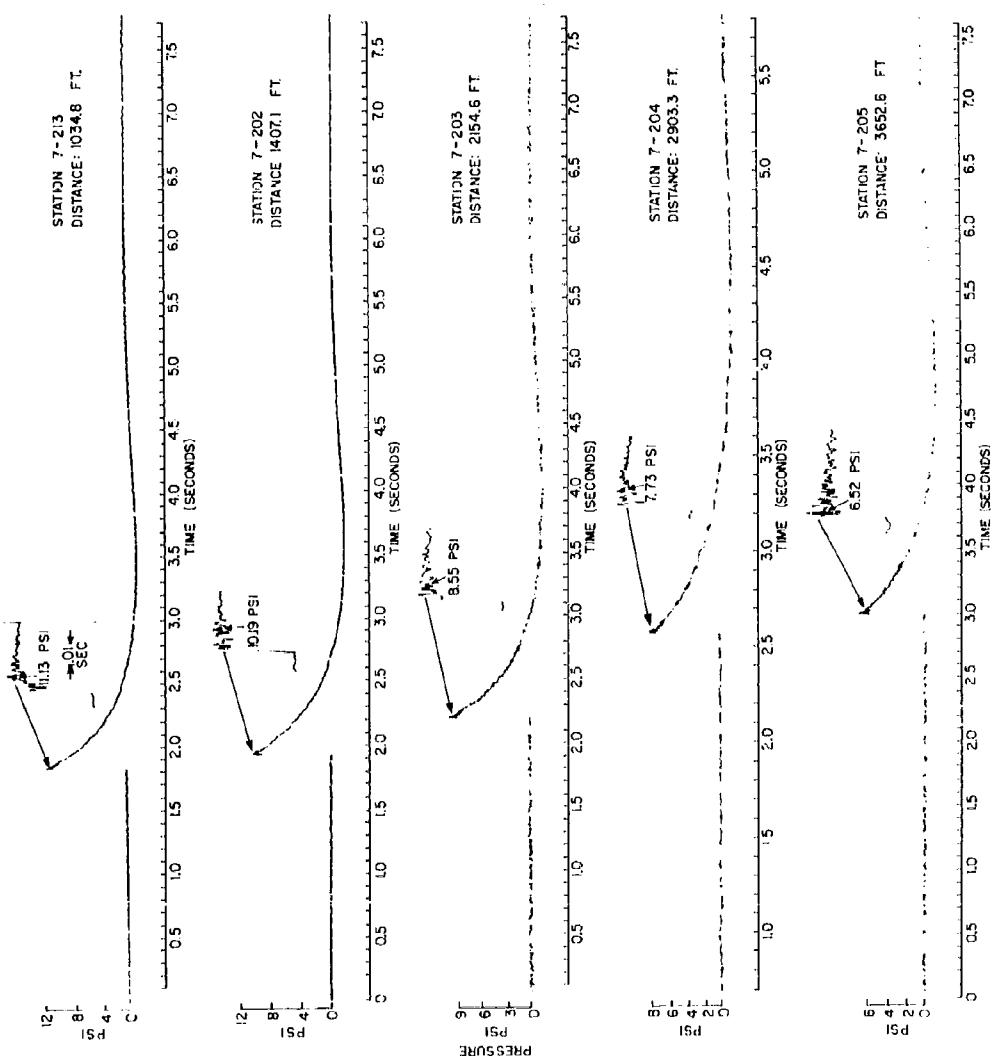

Fig. 2.36 Records, TUMBLER 3, Stations 7-213 through 7-205

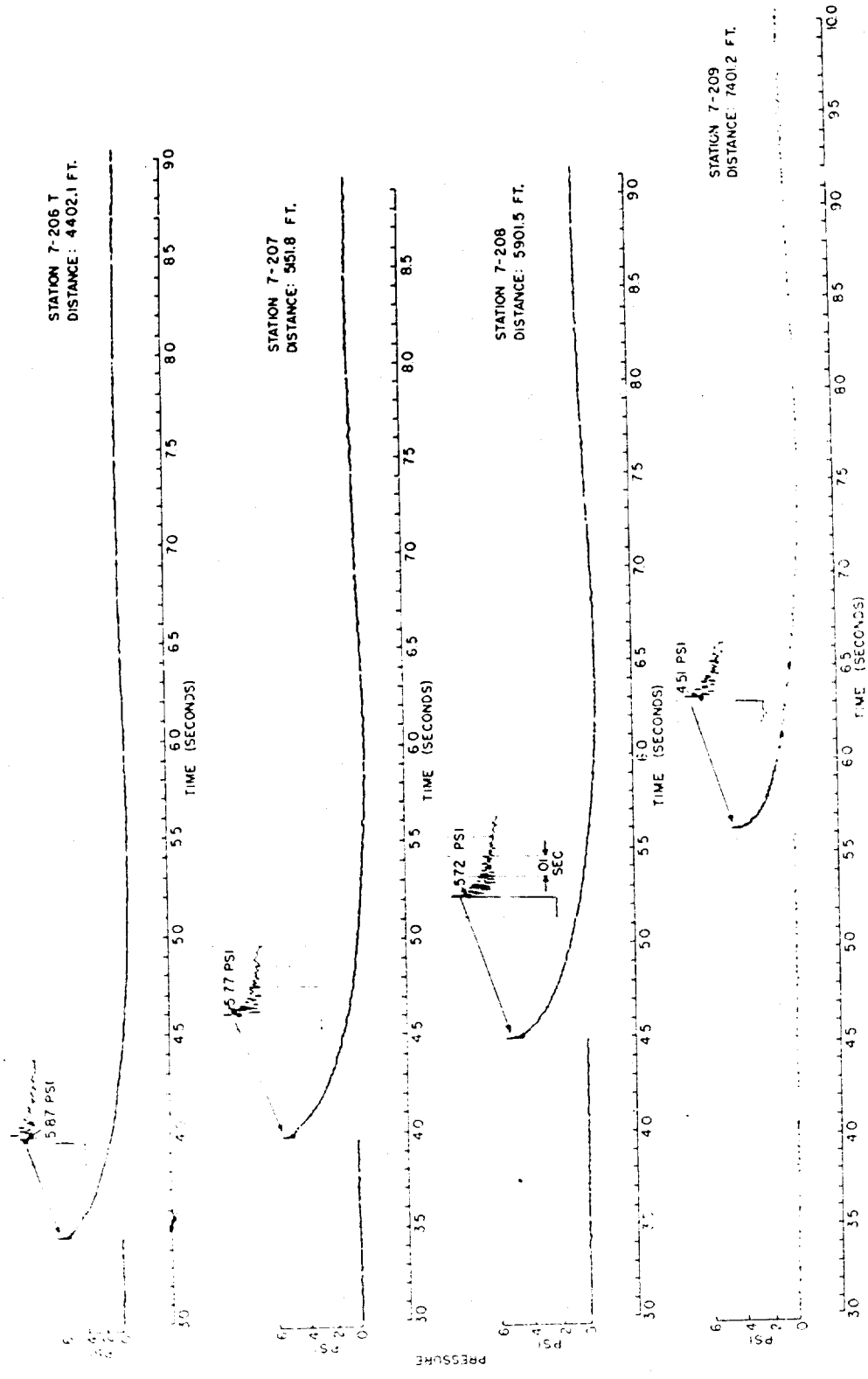

Fig. 2.37 Records, TUMBLER 3, Stations 7-206T through 7-209

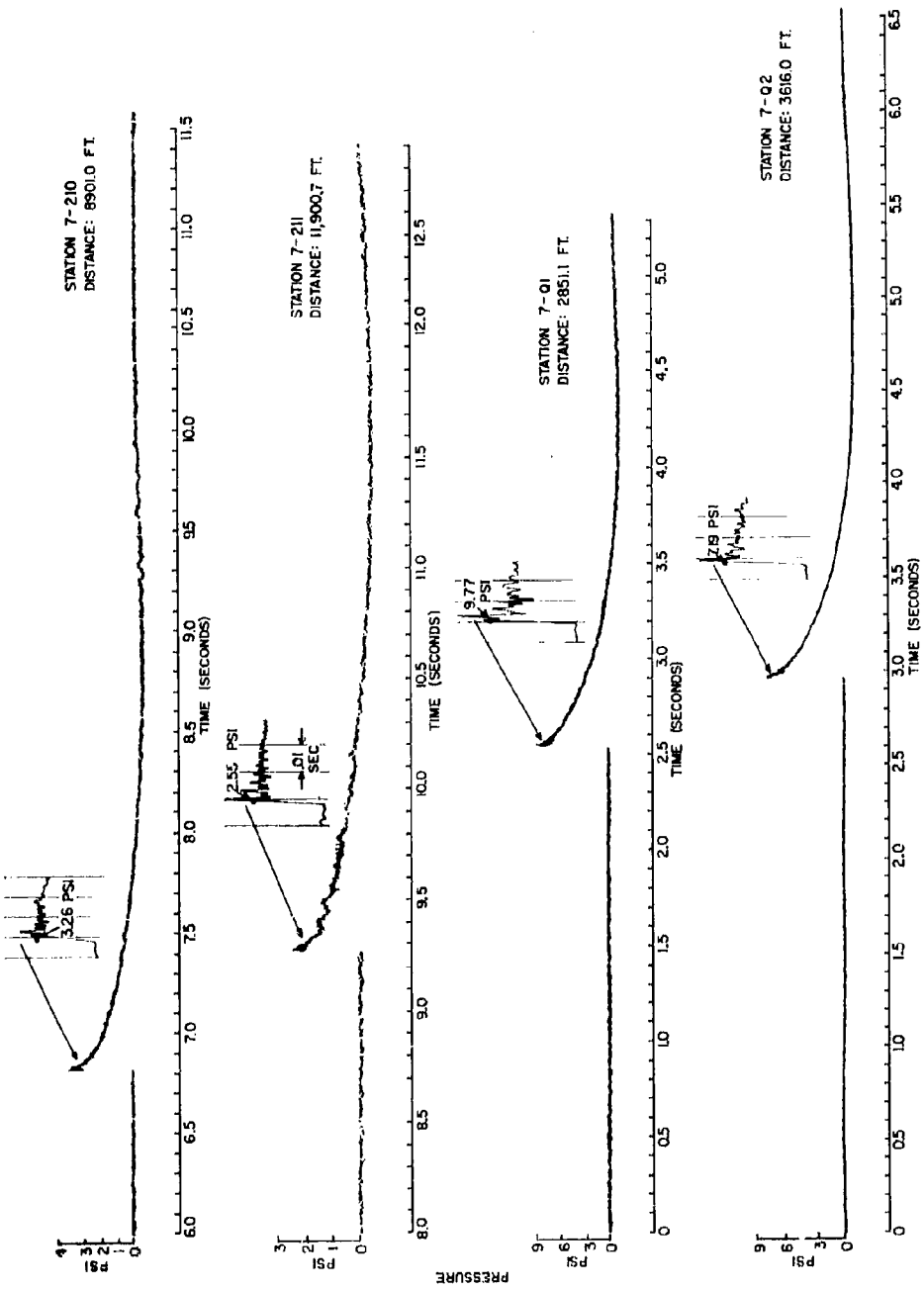

Fig. 2.38 Records, TUMBLER 3, Stations 7-210 through 7-02

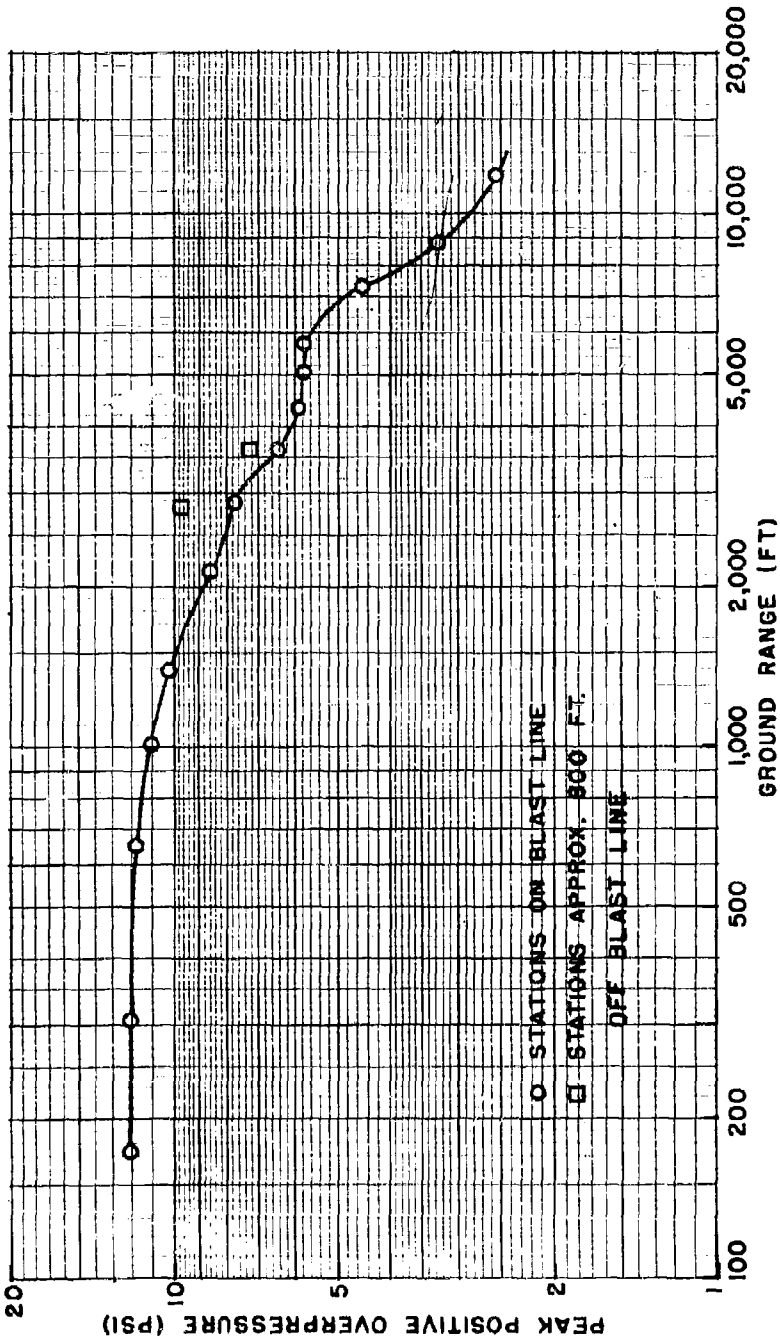

Fig. 2.39 Peak Positive Overpressure, P_c, Ground Level, TUMBLER 3

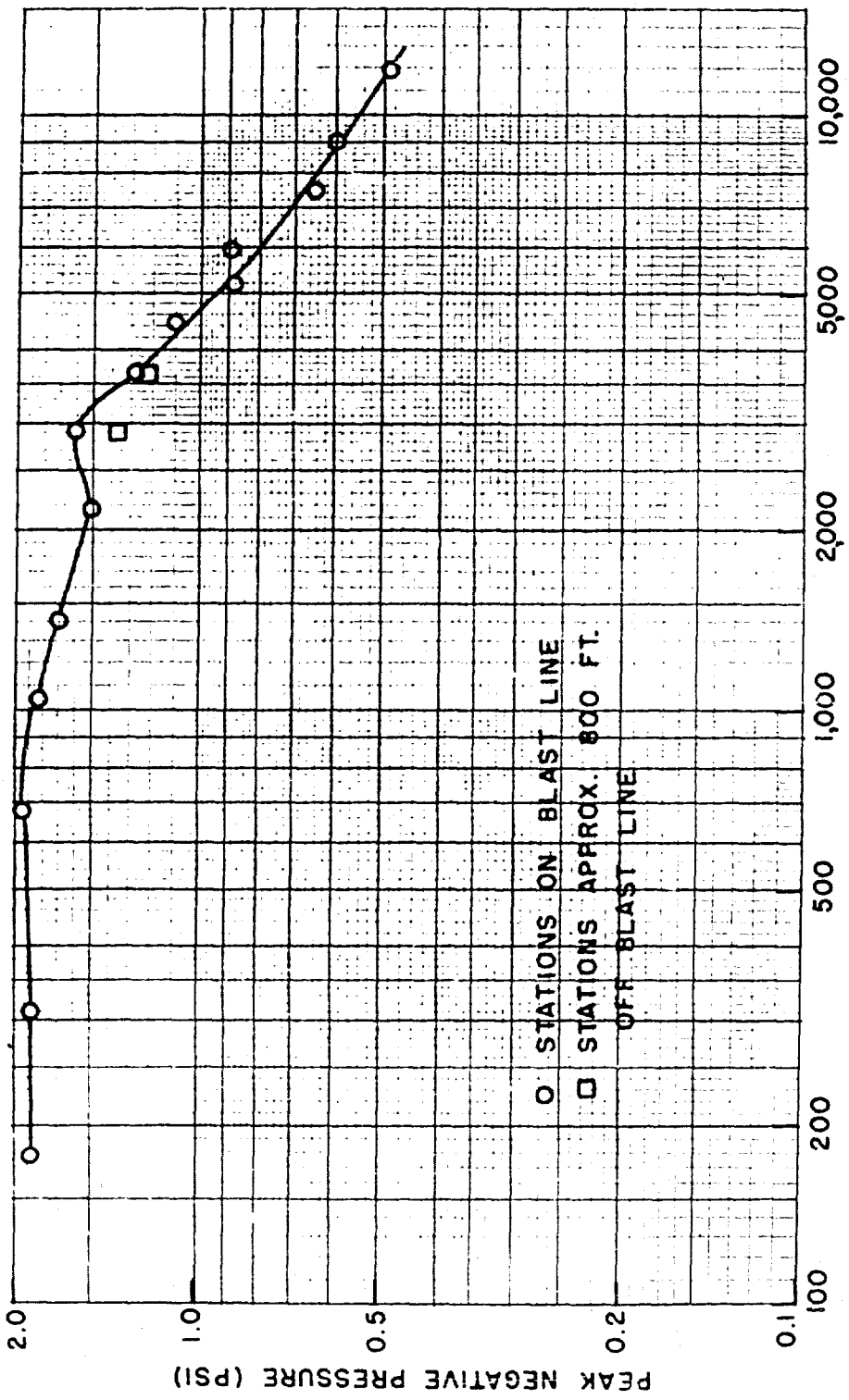

Fig. 2.40 Peak Negative Pressure, P_e, Ground Level, TUMBLER 3

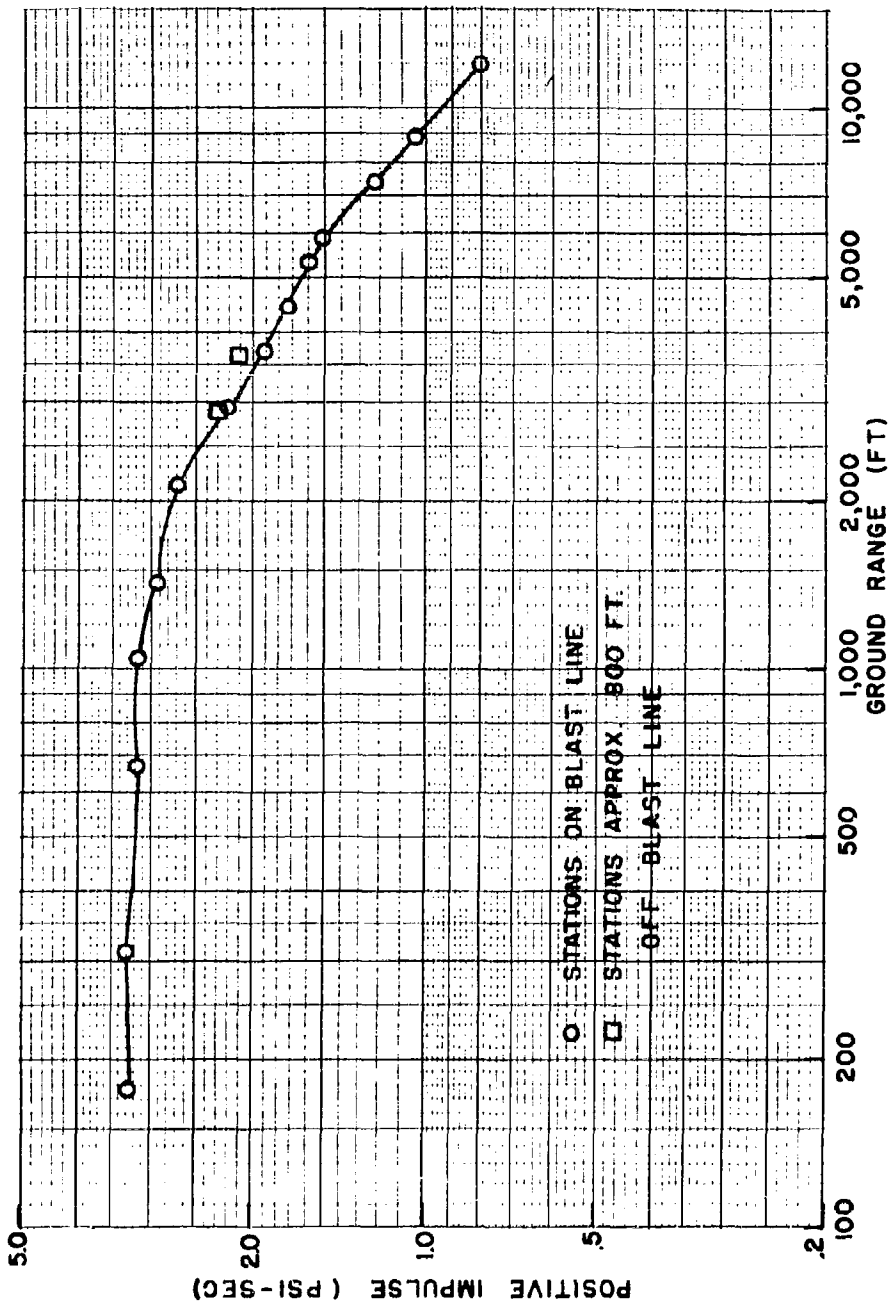

Fig. 2.41 Positive Impulse, Ground Level, TUMBLER 3

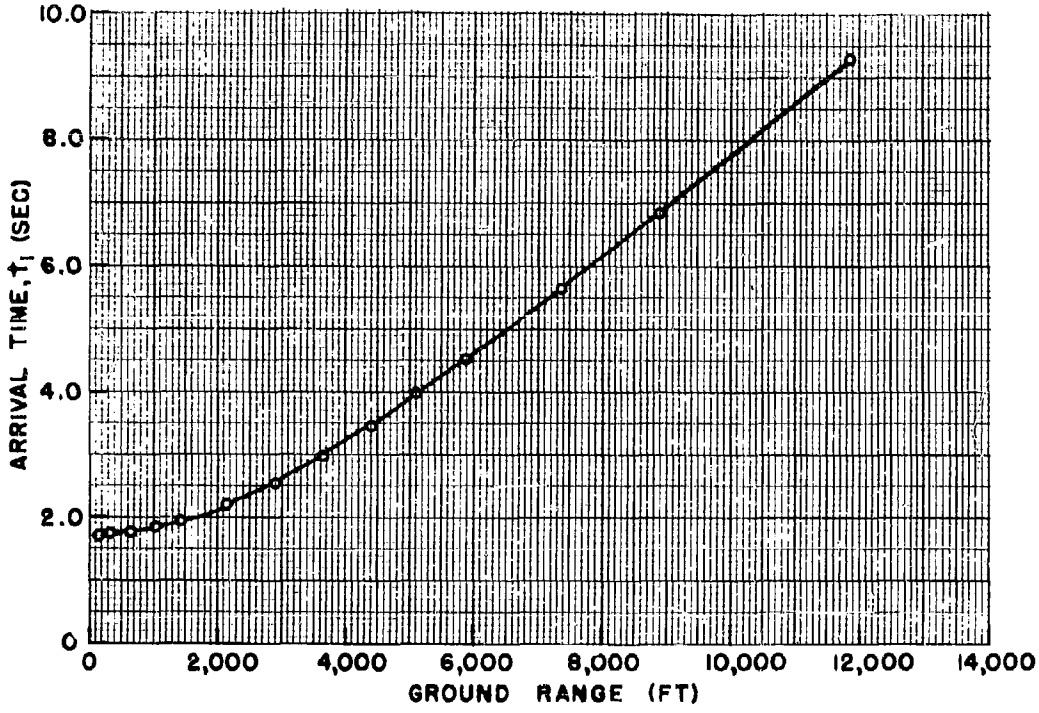

Fig. 2.42 Arrival Time of Initial Disturbance, t_1, Ground Level, TUMBLER 3

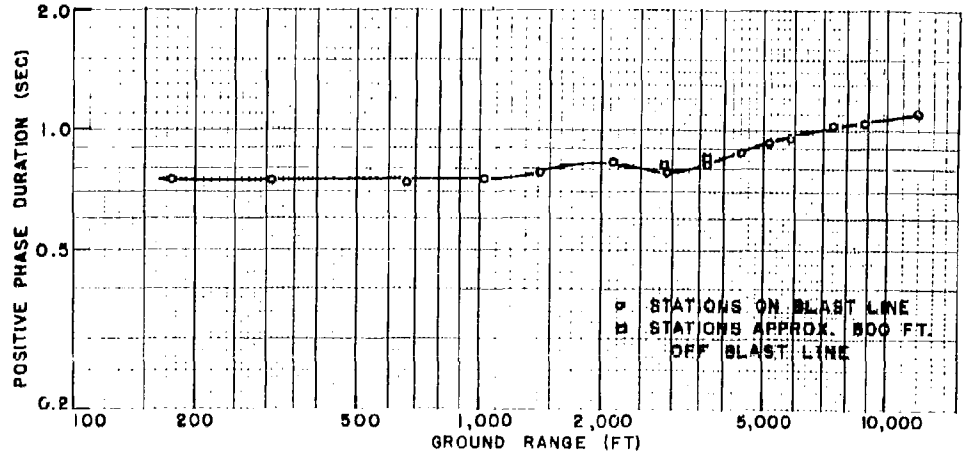

Fig. 2.43 Positive Phase Duration, t_4, Ground Level, TUMBLER 3

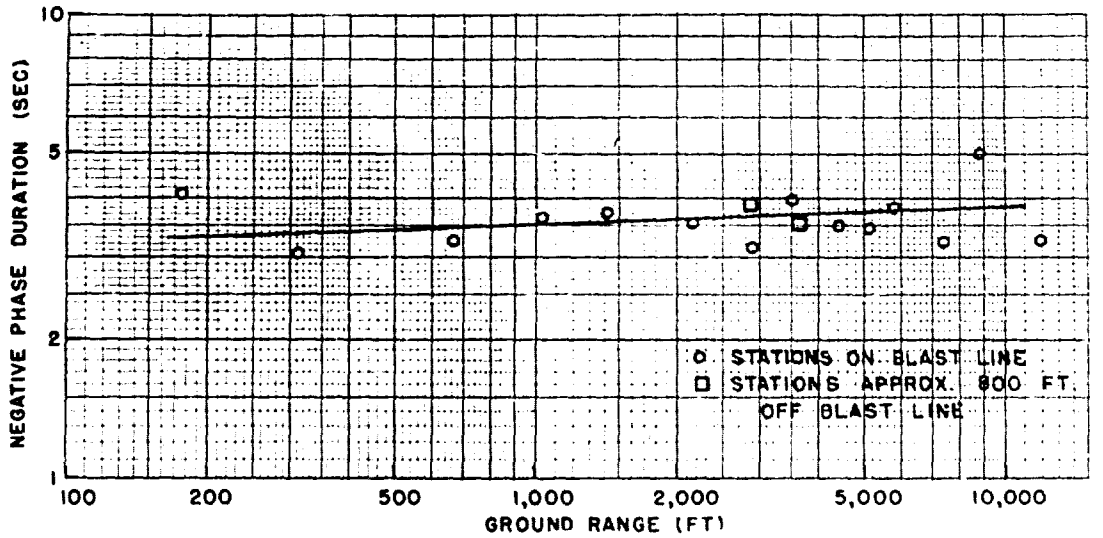

Fig. 2.44 Negative Phase Duration, t_8, Ground Level, TUMBLER 3

ities, and dust peculiar to the immediate vicinity of the gages. It will be noted that the 7-Q stations had higher peak pressure values than the stations on the main blast line which were at comparable distances, 7-204 and 7-205. These high readings were probably due to the influence of the high, sharp spikes occurring in the first 10-20 milliseconds. After this time, however, the pressure levels for Stations 7-Q1 and 7-204, and Stations 7-Q2 and 7-205 were comparable at corresponding times. This indicated that the shocks at the 7-Q stations, regardless of the vastly different terrain, were basically the same as the shocks produced on the main blast line; the spikes and high peak values seem to be extremely local and other stations in the immediate vicinity might well have given quite different results.

A second positive phase did not appear on the records of TUMBLER 3.

2.2.4 TUMBLER 4

The photographic reproductions of the records obtained for TUMBLER 4 are shown in Figs. 2.45 through 2.48; the results of the data analysis are presented in Tables 2.8, 2.9, and 2.10 and plotted in Figs. 2.49 through 2.54.

For the first time in this operation, the instrumentation system at the close-in stations picked up some sort of extraneous signal at zero time. This signal, which appeared on all stations up to and including 7-204, seemed to short-circuit the gage-oscillator

combination for approximately 50 milliseconds, after which time the oscillator recovered and oscillated at a slightly lower frequency. The cause for these signals is unknown. However, it is likely that the intense ionization which occurred at zero time effectively short-circuited the field circuits (gage, oscillator-amplifier, cable) for a short time and also produced changes in the dielectric and/or magnetic properties of the capacitors and inductors of these circuits, which in turn changed the oscillator frequency. As the ionization decreased in intensity, the short circuit ceased, the capacitors and inductors tended to return to their original state, and the frequency of the oscillators shifted towards their pre-zero-time value, or as at some stations, to a new center frequency.

The smooth exponential return of the trace to its final pre-shock arrival position possibly can be interpreted in another way, this time in terms of a pressure signal. The high thermal output of the weapon may have in some way created a high intensity thermal pulse in the air effectively trapped by its own inertia in the immediate vicinity of the surface giving the effect of a pressure pulse. However, with the lack of conclusive evidence to bolster either the ionization or the thermal pressure hypothesis, the signal at zero-time is considered extraneous and discussed only in the interest of presenting a complete picture of the results. Where a permanent base-line shift occurred, the new base line was used for record analysis purposes since it was to this shifted frequency that the oscillator returned when steady atmospheric conditions prevailed after shock passage.

As is evident from the records, even aside from the zero-time disturbance, the gross characteristics for the close-in stations of TUMBLER 4 were markedly different from the corresponding stations of the previous shots (with the possible exceptions of Stations F-200 through F-203 of TUMBLER 1). For Stations 7-200 through 7-203, the pressure increased to its peak value in a double step-wise fashion and in a relatively long time. For Stations 7-212 through 7-202 this stair effect was quite obvious. For Station 7-203, the second step was less prominent; however, it appeared to occur at approximately 50 milliseconds after the initial disturbance. For Station 7-200, the initial step, P_a, was higher than the second step, P_c, and less sharply defined. (Because P_a was of only short duration compared to P_c, the later peak was considered to be the significant one and its value was the one plotted for peak pressure at this station in Fig. 2.49).

It can be seen that at these close-in stations, the first step, P_a, attenuated rapidly and lengthened in duration with distance from ground zero. The pressure pulse associated with P_a has been

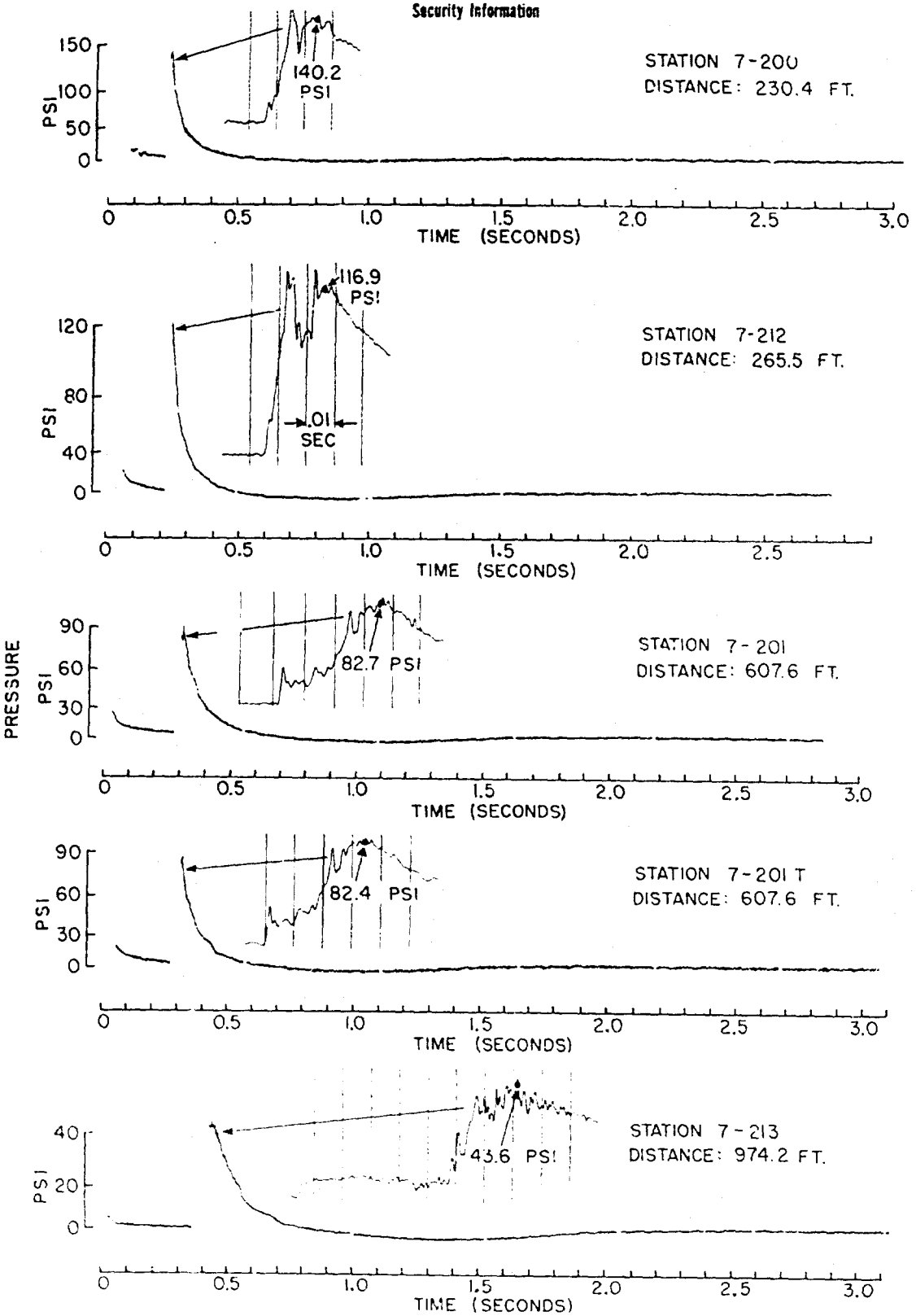

Fig. 2.45 Records, TUMBLER 4, Stations 7-200 through 7-213

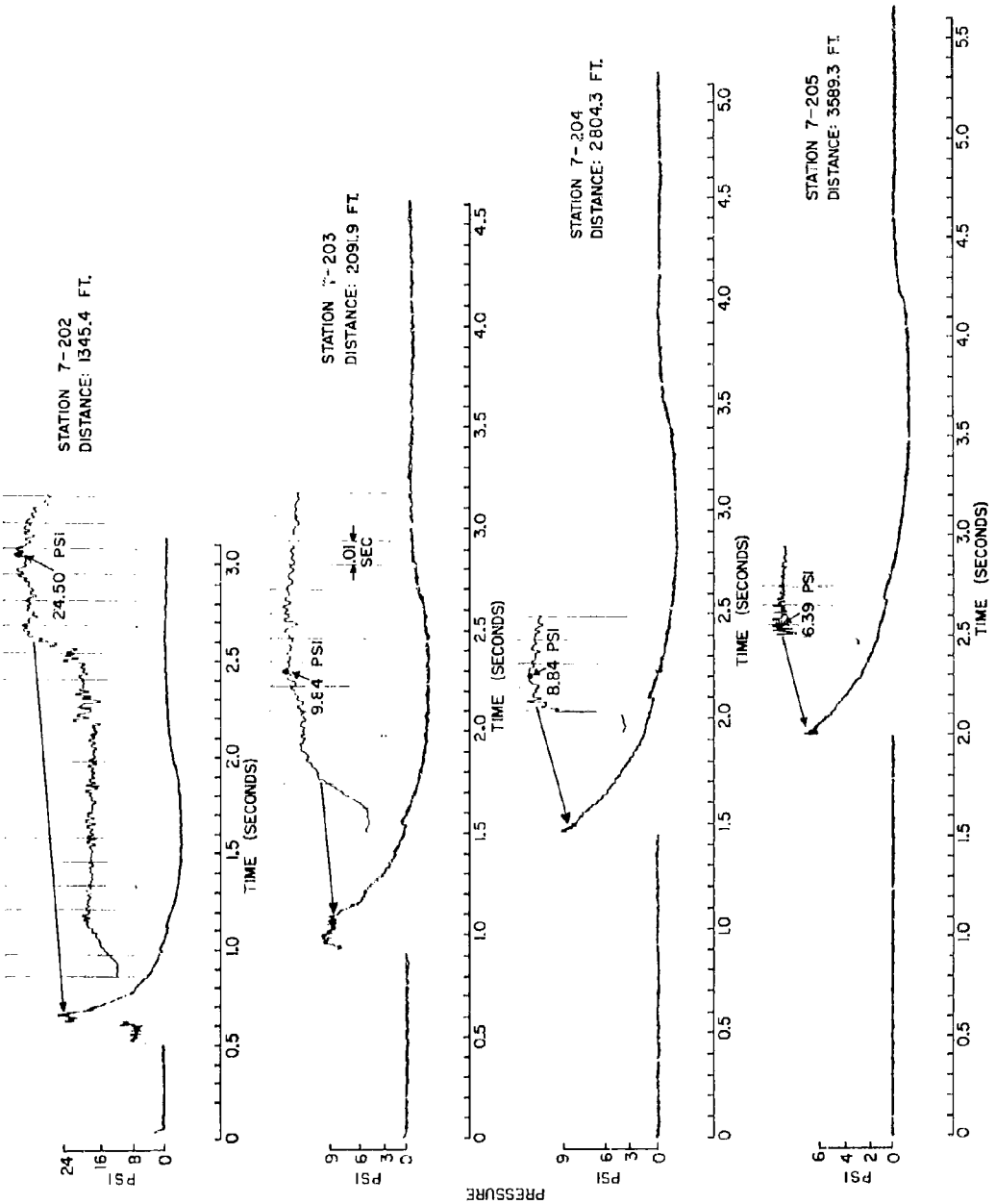

Fig. 2.46 Records, TUMBLER 4, Stations 7-202 through 7-205

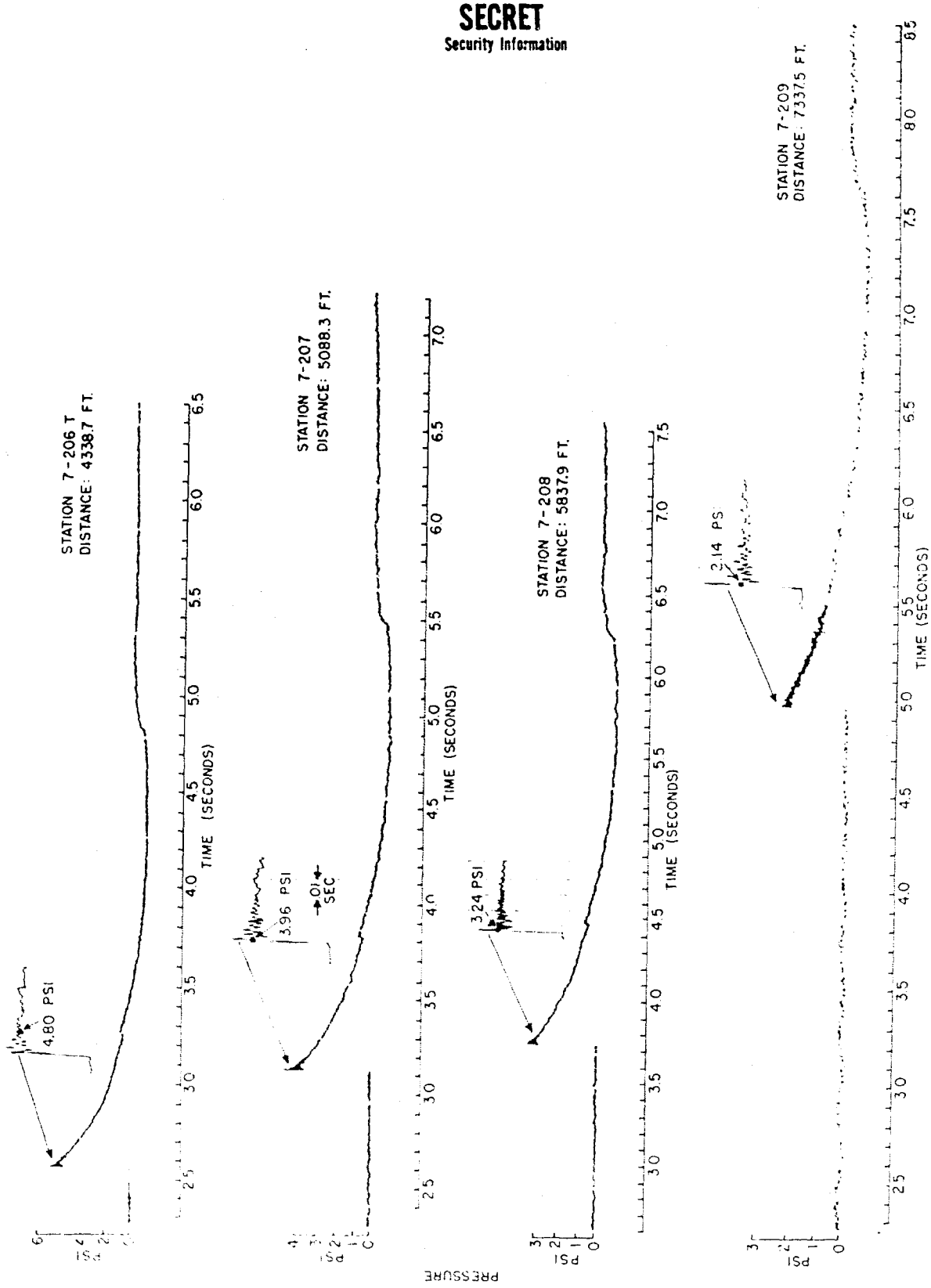

Fig. 2.47 Records, TUMBLER 4, Stations 7-206T through 7-209

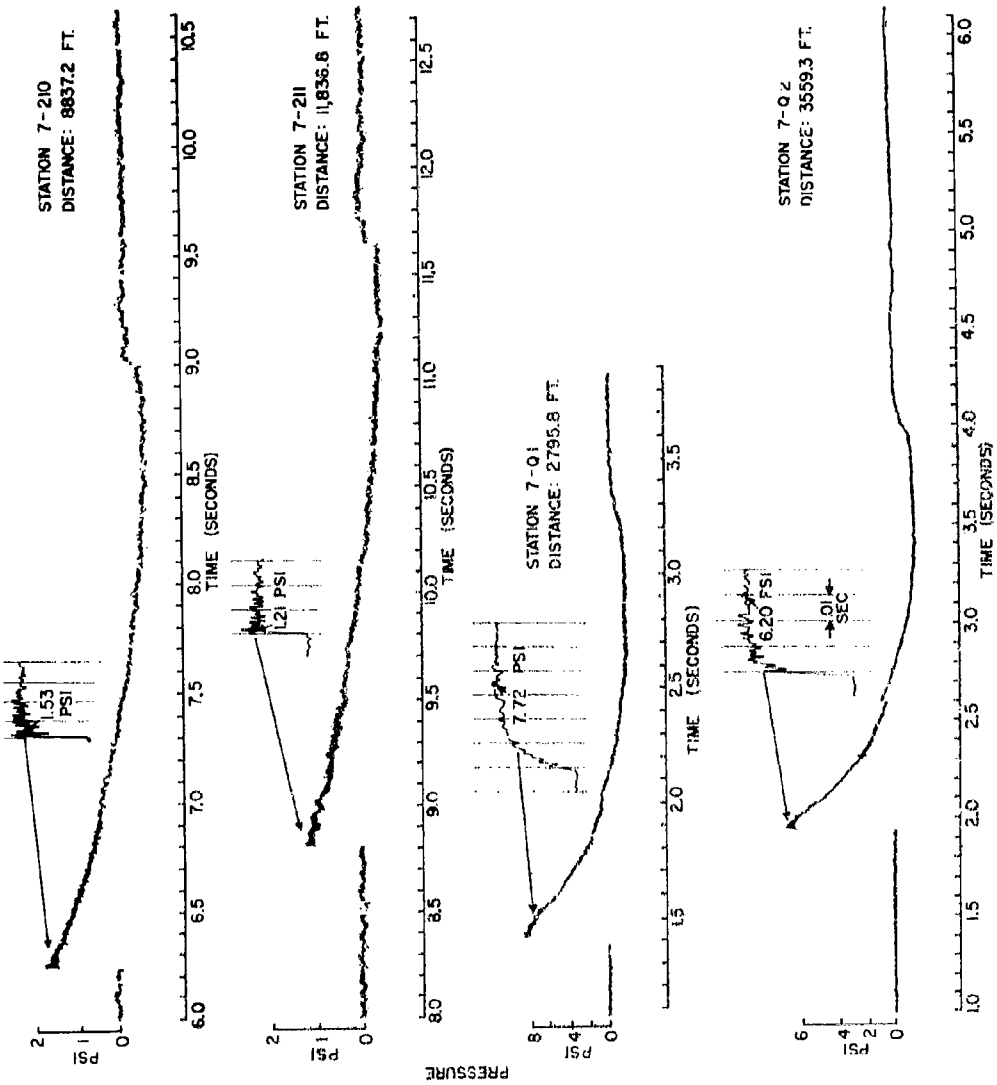

Fig. 2.48 Records, TUNNEL 4, Stations 7-210 through 7-02

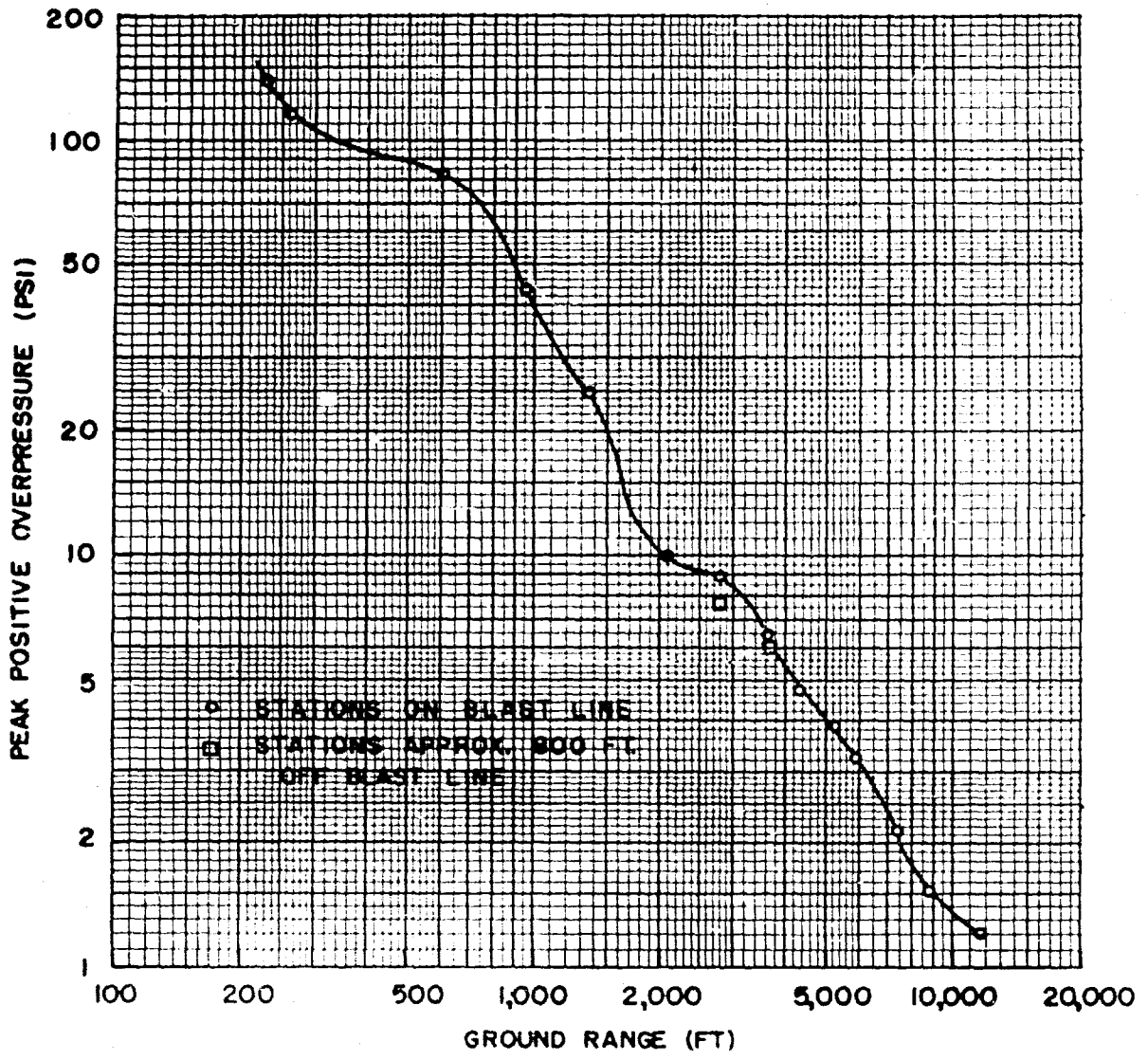

Fig. 2.49 Peak Positive Overpressure, P_c, Ground Level, TUMBLER 4

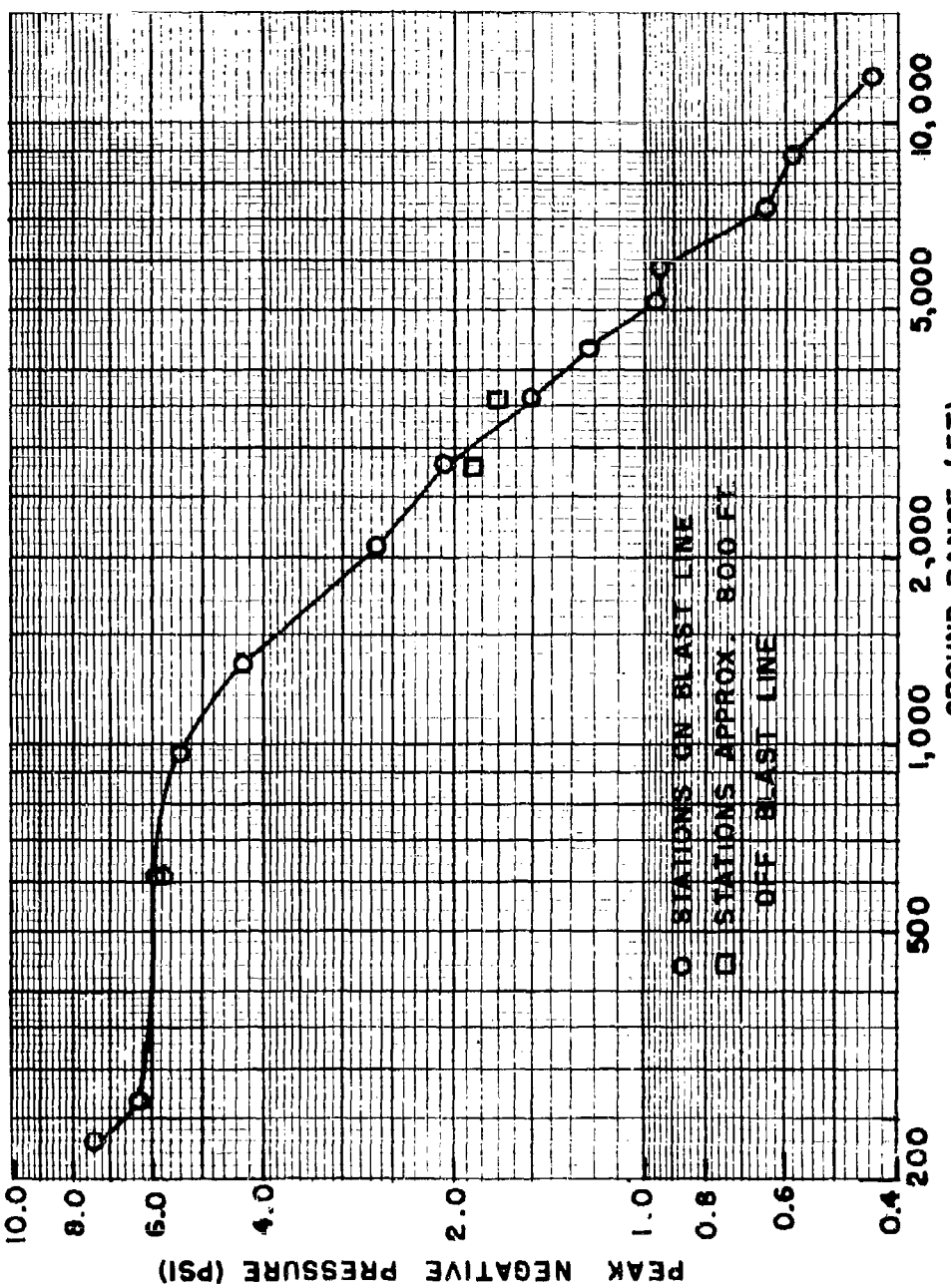

Fig. 2.50 Peak Negative Pressure, P_e, Ground Level, TUMBLER 4

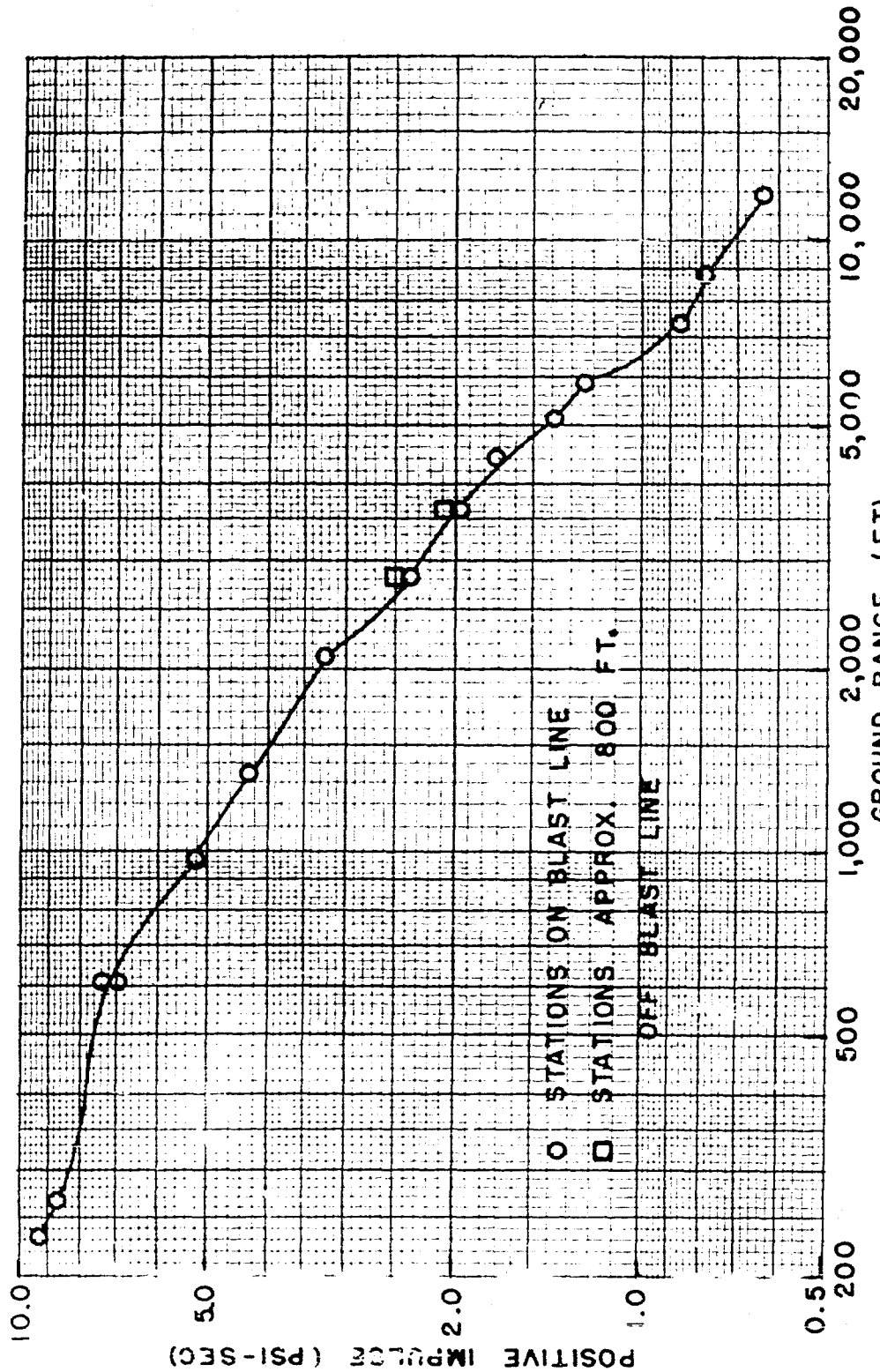

Fig. 2.51 Positive Impulse, Ground Level, TUMBLER 4

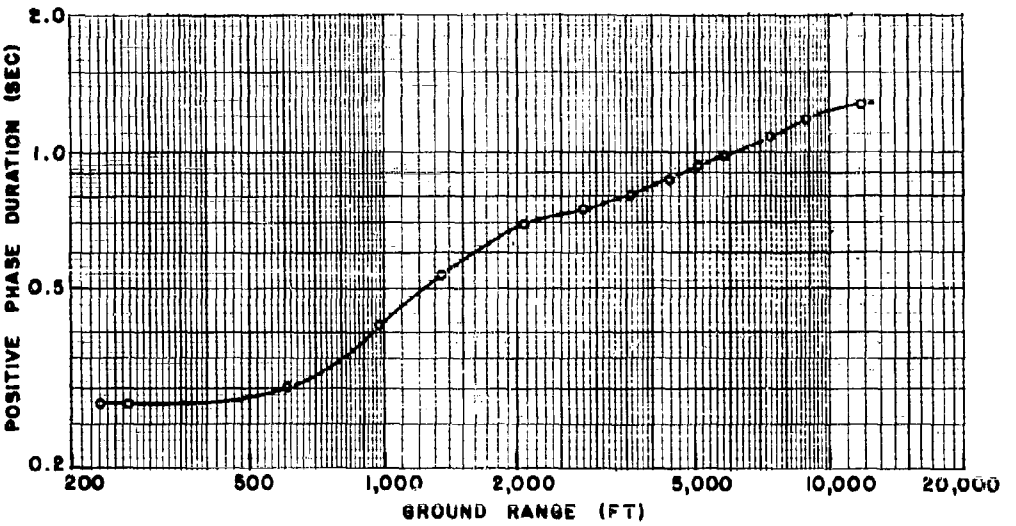

Fig. 2.52 Positive Phase Duration, t_4, Ground Level, TUMBLER 4

identified as a precursor and its origin and significance are discussed in Sec. 5.2. The precursor nature of P_a is evident in the plot of arrival times in Fig. 2.54 with the t_1 curve falling below the t_2 points for the six stations where the precursor was evident. (Before the initial disturbance was recognized as a precursor, the arrival time of all initial disturbances was designated as t_1, and the arrival time of the pressure pulse associated with P_c was designated as t_2. It is for this reason that the arrival time nomenclature for the main shock on TUMBLER 4 is t_2 for Stations 7-200 through 7-203 and t_1 for Stations 7-204 and beyond).

The records from Stations 7-204, 7-205, and 7-206 exhibited the now familiar sharp initial rise with a rounding or flattening to the peak value. Not until Station 7-207 at 5088 ft did a shock form appear; the stations following also showed shocks. Stations 7-Q1 and 7-Q2 showed pressure-time records which were similar to the records obtained from Stations 7-204 and 7-205, the stations on the main blast line located at corresponding distances; however, there was more rounding of the peaks on the 7-Q records and the peak values were somewhat lower. The significance of this is not known; probably it can be attributed to the purely local peculiarities in the terrain in the immediate vicinity of the gages. Certainly, as on TUMBLER 3, the general features of the records for 7-204 and 7-Q1, and 7-205 and 7-Q2 were similar and general terrain conditions seemed to have little

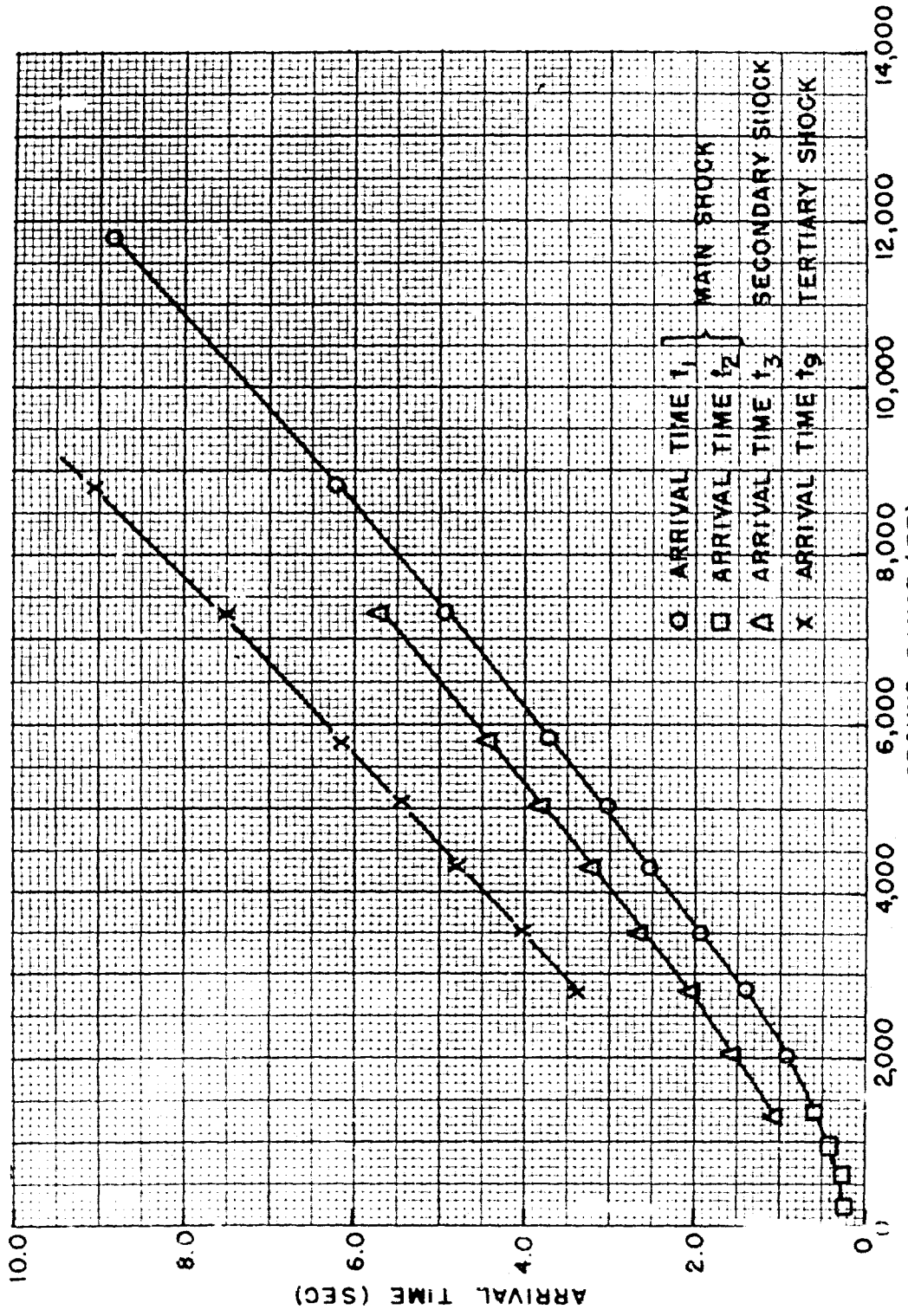

Fig. 2.53 Arrival Times, t_1, t_2, t_3 and t_9, Ground Level, TUMBLER 4

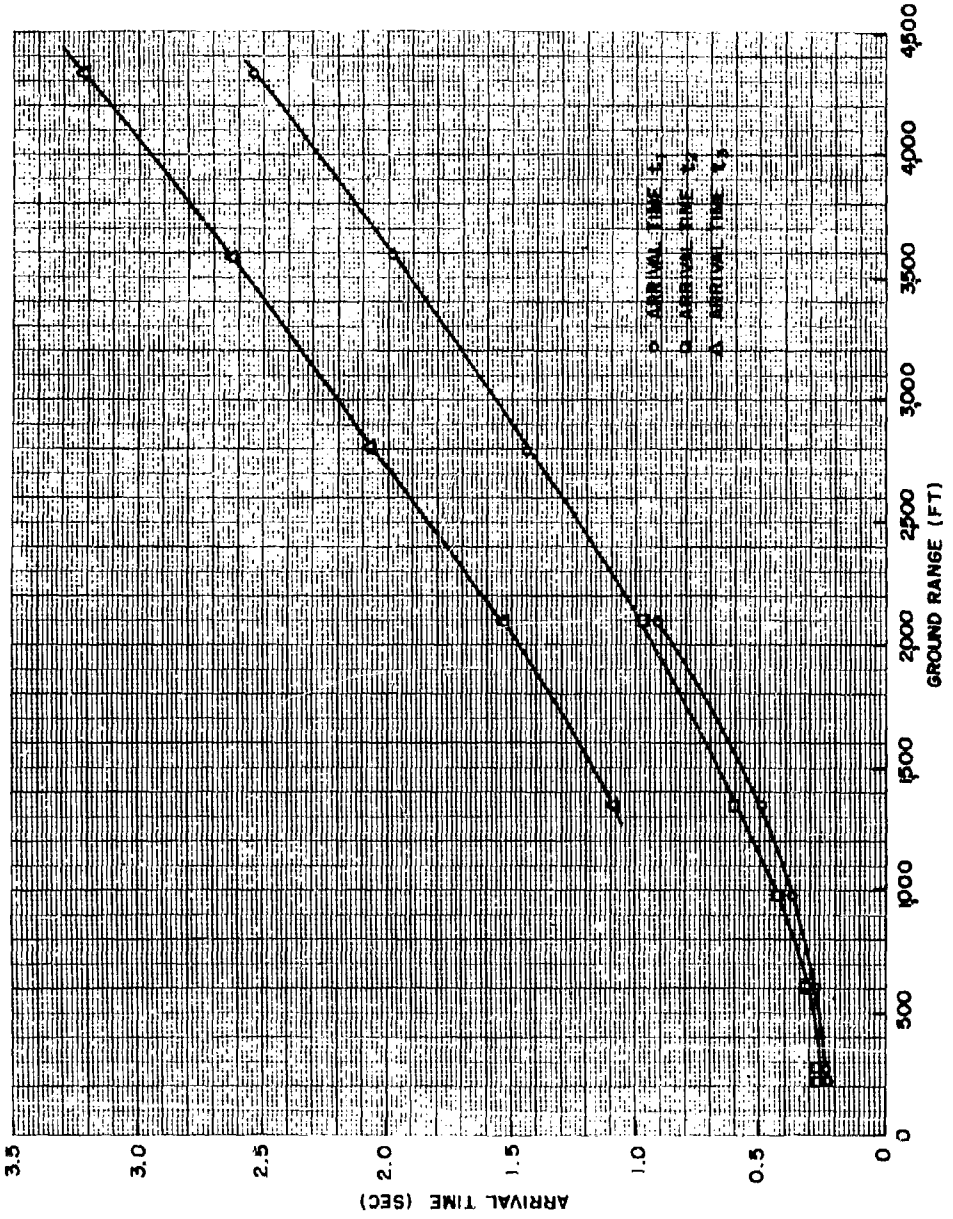

Fig. 2.54 Expanded Scale of Arrival Times, t_1, t_2, and t_3, Ground Level, TUMBLER 4

effect on either wave form or peak pressure values.

The peak positive overpressure versus distance curve, Fig. 2.49, has a plateau at Stations 7-203 to 7-204. Indications from other sources indicated that the Mach reflection region started before Station 7-203; therefore, for TUMBLER 4 there appeared to be no correlation between Mach stem formation and plateau in the curve. Further, whereas in the previous shots only shocks occurred in the Mach region, on this shot slow rise times and rounded peaks also appeared in this region.

TUMBLER 4 gave rise to other interesting results besides the aforementioned ones. Two additional pressure pulses were apparent on the records: one occurring usually during the positive phase, (designated P_d with arrival time of t_3) and the other occurring during the negative phase (designated P_f with corresponding arrival time of t_9). The appearance of P_d was that of a shock wave with short rise time while P_f showed a longer rise time. Both pulses had an amplitude approximately 1/10 to 1/20 of the main shock, P_c. A plot of the arrival times t_3 and t_9, Fig. 2.53, shows the orderly fashion of propagation for P_d and P_f indicating the common origin of all P_d pulses and the common origin of all P_f pulses. It is not known what this source is.

The presence of P_f had the effect of considerably shortening the duration and diminishing the impulse of the negative phase associated with P_e. This effectively distorted the true nature of the negative phase associated with the main shock and made the application of scaling laws inapplicable to this feature of the main shock. In addition this distortion made even the reasonable determination of negative time duration very questionable because of the gradual return of the pressure trace to the base line. For these reasons, only limited quantitative data are provided for negative phase duration and no data for negative impulse for TUMBLER 4.

As on TUMBLER 3, no second positive phase was apparent on the records after the completion of the negative phase. It might be noted that this second positive phase occurred only on the small (approximately 1 KT) bombs used on TUMBLER 1 and 2.

2.2.5 Comparison of Data

A comparison was made between the final NOL ground station data for Operation TUMBLER and the preliminary data presented in references 13, 23, and 28. (It was realized that this comparison may be somewhat premature since the data presented in aforementioned refer-

ences are preliminary and subject to change. However, it was assumed that these changes, if any, would be small, and comparisons and conclusions arrived at herein would hold true for final figures too.) It should be noted that both Stanford Research Institute and Sandia Corporation used similar instrumentation - basically the Wiancko gage circuit - while the NOL utilized the Bendix gage - FM system described in this report and the David Taylor Model Basin used a capacitance gage circuit. The overall response of the Wiancko and Bendix-FM systems was such as to indicate rise times of 1-2 milliseconds for applied step pulses; the response of the David Taylor Model Basin capacitance gage was considerably better, requiring approximately 5 microseconds to rise to full amplitude.

The NOL data for peak pressures for all stations on all shots averaged 7 per cent higher than both the Stanford Research Institute data (Project 1.2) and the Sandia Corporation data (Project 19.1). The NOL data averaged 1 per cent lower than the David Taylor Model Basin data (Project 1.13).

The agreement between NOL and DTMB results was good but only three readings could be compared. However, the indications are that extremely high frequency response is not required for A-weapon tests if high frequency detail such as provided by the DTMB capacitance system can be sacrificed. For effects tests this seems to be a reasonable sacrifice especially if simplified field instrumentation and installation result. The 7 per cent discrepancy between NOL and SRI - Sandia, although probably not significant in terms of military effects, was perplexing particularly since the NOL figures were consistently higher than both the SRI and Sandia values. A random difference could be accounted for by the approximate stated errors of each system. The consistently higher difference would be accounted for only in terms of a constant common factor such as gage calibration or choice of points read on the record.

A comparison of the positive durations reported by the various activities also showed a consistent difference. Here, the NOL final values were consistently lower than the preliminary values of SRI, Sandia and DTMB by approximately 7, 4, and 8 per cent respectively. (It may be of interest to note that although TUMBLER 4 produced the greatest distortions of shock form and disturbances in instrumentation, this shot produced data which showed best overall agreement between SRI and NOL. The NOL pressures were only 3 per cent higher, on the average, than SRI's, and the NOL positive durations were only 4 per cent less). Final values from these other activities may resolve the problem; certainly, additional data on impulse and negative peaks may provide some information which could intelligently compromise the differences.

CHAPTER 3

PHOTO-OPTICAL PRESSURE MEASUREMENTS (PROJECT 1.5)

3.1 BACKGROUND AND BASIC THEORY

3.1.1 The Shock Velocity Method of Peak Pressure Determination

The photo-optical technique and smoke rocket grids employed in Operation TUMBLER to obtain measurements of shock velocity leading to determinations of peak shock pressure as a function of distance in free air have been fully described in reports on Operations GREENHOUSE[2] and JANGLE[3]. Briefly, the method consists of establishing a smoke rocket trail grid behind the air burst and taking high speed motion picture photographs which show the locus of the shock front as a function of time. The shock front is rendered visible as the result of light refraction phenomena caused by the shock wave which intercepts the light from the grid and scattered light on its way to the camera. Time of arrival of the shock at measured distances from the explosion center can thus be found. One or more equations representing curves fitting these data are calculated using the method of least squares. The fitted equations describing the curves are of the form

$$t = A_0 + A_1R + A_2R^2 + A_3R^3 \qquad (3.1)$$

where t is the time at which the shock wave has reached a distance R from the explosion center or some other fixed point. Differentiation of equation 3.1 gives

$$\frac{dt}{dR} = A_1 + 2A_2R + 3A_3R^2 = \frac{1}{U} \qquad (3.2)$$

where U is the instantaneous shock velocity. The peak pressure in the shock wave is shown to be a function of the instantaneous shock velocity by the Rankine-Hugoniot relation:

$$P_s = \frac{2\gamma P_o}{\gamma + 1}\left[\left(\frac{U}{C_o}\right)^2 - 1\right] \qquad (3.3)$$

where P_s is the peak shock overpressure
P_o is the absolute atmospheric pressure ahead of the shock
γ is the ratio of specific heats for air = 1.403
C_o is the velocity of sound in the medium ahead of the shock.

P_o and the temperature, T_o, can be measured directly, and

$$C_o = 1089\sqrt{1 + T_o/273}, \quad T_o \text{ in } {}^oC, \quad C_o \text{ in ft/sec} \qquad (3.4)$$

3.1.2 The Particle Displacement Method of Pressure-Time Determination

In the shock velocity method described above it will be recalled that in obtaining the desired measurements the shock wave is not called upon to do any work other than to refract rays of light. The particle displacement method to be described depends upon the shock wave to move mass, however small. Measurements of the displacement of minute particles of fuming sulfuric and hydrochloric acids comprising the rocket smoke trails provide data which, when properly treated, lead to values of the pressure existing within the shock wave as a function of time as observed at a fixed point.

To obtain particle displacement data the smoke trail grid was located in a nearly vertical plane passing through the burst. Motion picture photographs of the radial motion of the trails, after being struck by the shock wave, provided a record of the time history of the forces acting on the particles of smoke. Figures 3.29 and 3.30 show the trail nearest the burst before and after being struck by the shock wave on TUMBLER 1.

The procedure for translating the measurements of particle displacement into a pressure-time history of the shock wave that would be observed at a fixed distance from the burst was ably developed by Dr. F. Theilheimer of the Naval Ordnance Laboratory and is presented in detail in Appendix B. In this analysis no attempt is made to obtain a peak shock pressure. The peak pressure is taken from the shock velocity data. (These pressures can be determined with a degree of accuracy significantly higher than that for corresponding peak pressure values based on measurements of particle velocity as recorded with the particular instrumentation employed which was designed to provide sufficient space-time resolution to obtain reliable data for the particle displacement method. The resolution would have had to be better if it were desired to measure particle velocity with a sufficient degree of accuracy. See Sec. 3.3.8.) The lower pressures following the peak of the wave are obtained using the particle displacement data. They are determined as functions of the peak pressure and density as shown in Appendix B, and do not rely on a knowledge of the particle velocity.

The principal advantages of the particle displacement

pressure-time method are its simplicity and its relatively low cost, since it circumvents the problem of placing a gage in free air to record directly the pressure-time curve. When the system is used in conjunction with the smoke rocket shock velocity system a nearly complete analysis of the free-air blast phenomena should be possible. The two experiments can be coordinated well in the field and the necessary apparatus for both systems is interchangeable.

A prime disadvantage of the technique is that all data must be graphically fitted with smooth continuous curves and any discontinuity or irregularity, unless its magnitude is large, is lost in this smoothing process. No such large irregularities occurred during the present experiment (see Fig. 3.20 and Fig. 3.21) in the free-air region and the pressure-time curves are probably very representative of the actual shock wave in free air.

3.2 INSTRUMENTATION

3.2.1 The Smoke Rocket Detection Grid

The rocket smoke trails established in the form of a vertical line grid just prior to the time of burst were produced using 5"0 spin-stabilized rockets. For a complete description and details concerning the rockets and the method of launching, the reader is referred to references 2 and 3.

Two innovations introduced on this Operation to establish the smoke trail grids were (1) the use of a different, more powerful rocket motor (5"0 Spin-Stabilized Motor MK3) and (2) an increase in the angle of launching the rocket. See Figs. 3.1 and 3.2. Both measures increased the overall height of the grid from 6000 to about 13,000 ft and permitted a decrease in the time interval between firing the rockets and the time of burst. The latter is especially advantageous, for if the wind is strong it is capable of destroying the continuity of the trails before they have served their purpose.

The spacing of trails, location of grid planes and camera positions, and other data pertinent to the experimental layout are given in Figs. 1.1 and 1.2.

Due to the dissipation of the smoke trails at the closer particle displacement stations after passage of the shock wave and the inaccuracies at the lower pressure levels, it is recommended that in future tests the trails be placed between the 10 and 50 psi levels only and at closer intervals than used on Operation TUMBLER. Inter-

vals of approximately 50 ft would be desirable to obtain more reliable data.

3.2.2 Photographic Instrumentation

The photographic records were obtained by Edgerton, Germeshausen, and Grier, Inc. and submitted to the NOL for analysis within three days of the shot, together with pertinent space and time calibrations. Four Mitchell high-speed cameras were used to obtain the desired records for each test. Throughout the operation, "Eastman Experimental Microfile" film was used with excellent results. Table 3.1 gives a complete listing of cameras, exposures, frame rate, and other photographic details.

Fiducial markers were placed in the field of view of the cameras to provide for horizontal space calibration. The markers were spherical gazing globes mounted on poles at a given height so as to lie in a true horizontal line, as seen from the camera station.

In addition to the space fiducial markers, an accurate space calibration rose was put on each film so that no matter how the film might shrink or expand during processing or storage the calibration would not change. The calibration rose, together with an accurate measure of the focal length of the lens used, is sufficient information with which to calculate a vertical and horizontal scale in any given object plane in the field of view.

Timing marks for calibrating the record were placed on the edge of each film at the rate of 100 marks per sec. A master oscillator controlled these marks to $\pm$ 50 μ sec.

3.3 RESULTS

To avoid confusion, the pressure-distance results based on the shock velocity method are presented first for all four shots. Following this, the pressure-time results based on particle displacement analyses are given for Shots 1 and 4. Only two shots were analyzed because the time required to reduce the remaining data would unduly delay publication of this report. Shots 1 and 4 were chosen so that a comparison of the results could be made to indicate the usefulness of the technique under the most favorable conditions. Shot 4, in particular, was of interest because it was desired to know if the disparity between the results of Shot 4 and the other shots at the ground level could have been predicted from the free-air pressure-time curve.

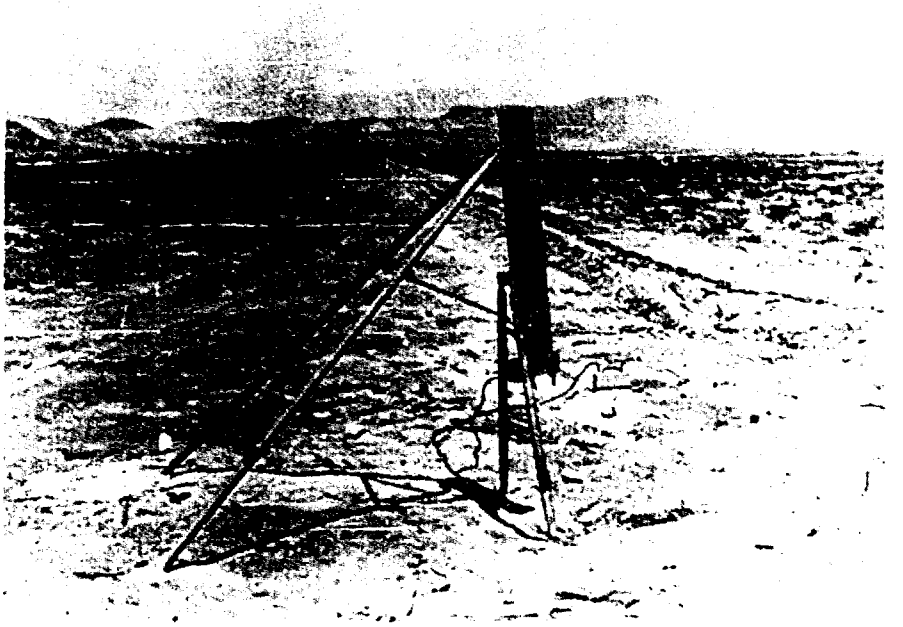

Fig. 3.1 Rocket Launcher with 85° Firing Angle

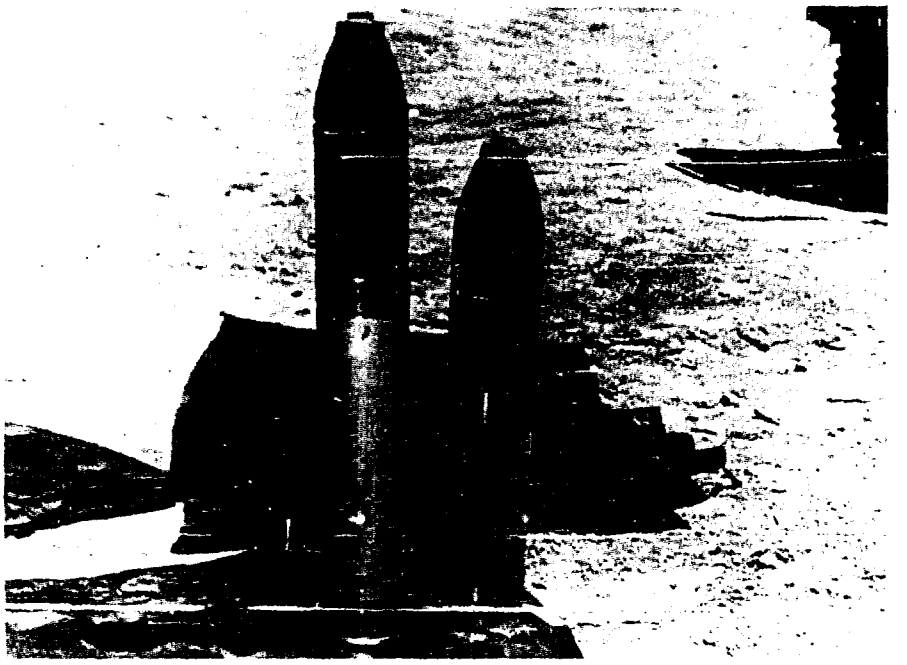

Fig. 3.2 Assembled Smoke Rockets, with MK 3 Motor (Left), MK 4 Motor (Right), TUMBLER 1-4

Only the motion of one trail on each of Shots 1 and 4 was analyzed. Some of the reasons why this was done are: (1) some trails were too close to the burst and disappeared for a considerable time during the period of interest, (2) some trails were in regions of low pressure where no corresponding data from the shock velocity experiment were available, and (3) most of the remaining trails were distorted by the arrival of the reflected wave too soon after the arrival of the incident wave, as shown in Fig. 3.28.

3.3.1 Pressure-Distance Results - TUMBLER 1

The free-air shock wave time-of-arrival data for TUMBLER 1 were taken from film No. 13082. On the enlarged image, distances could be measured accurately to ± 1.0 ft in the plane of measurement (see Fig. 3.3).* From the timing marks on the film it was evident that the camera was in the process of slowing down slightly during the period of interest. At zero time the frame rate was 110.005 frames per sec while at 0.9 sec the frame rate dropped to 108.215 frames per sec. The small corrections dictated by this unusual circumstance have been included in the time-of-arrival data given in Table 3.2. The time values listed in this table and in similar tables for subsequent shots are given in absolute time after zero time of burst. Absolute time was determined on all shots by fitting the early time-of-arrival data to highly accurate fireball growth data.

On this particular shot it was found possible to measure shock times-of-arrival along the ground extending into the Mach region. These data are included in Table 3.2.

Graphs of the data appearing in Table 3.2 are given in Figs. 3.4 and 3.5. Included in these graphs are calculated points based on the equations fitted to the data by the method of least squares. For the shock wave in free air the time-of-arrival curve is represented by

$$t = 0.0158 - 0.1513R + 0.9354R^2 - 0.3426R^3 \quad (200 \text{ ft to } 800 \text{ ft}) \quad (3.5)$$

$$t = -0.1919 + 0.5955R + 0.0446R^2 + 0.0120R^3 \quad (800 \text{ ft to } 1200 \text{ ft}) \quad (3.6)$$

where t is in seconds and R is in thousands of ft from the explosion center.

Along the ground the time-of-arrival curve is represented by

$$t = 0.2966 + 0.1446R + 0.2204R^2 + 0.0079R^3 \quad (200 \text{ ft to } 1200 \text{ ft}) \quad (3.7)$$

*Data were tabulated to higher precision for computational purposes.

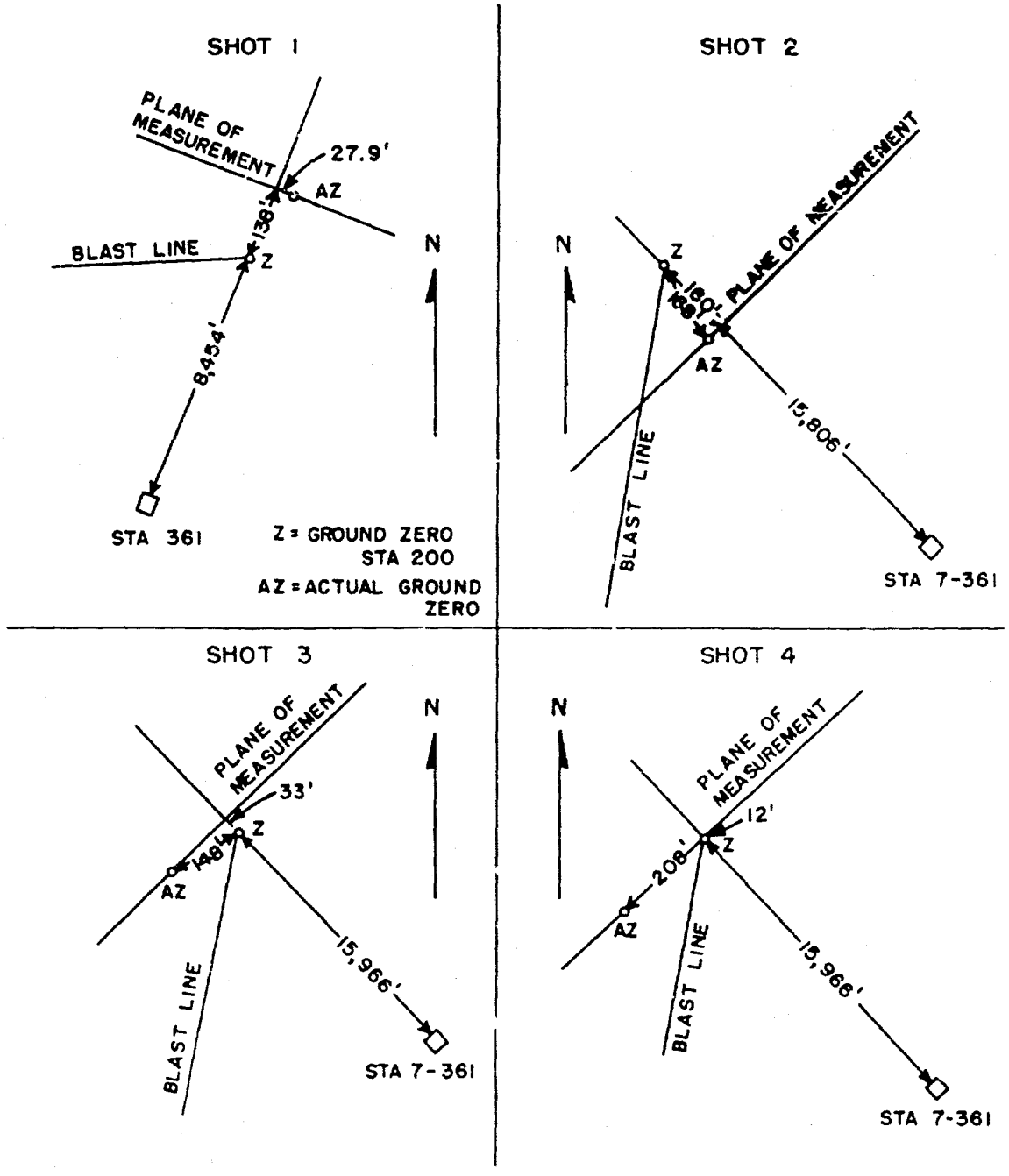

Fig. 3.3 Planes or Measurement used in Free-air Pressure-Distance Analysis, TUMBLER 1-4

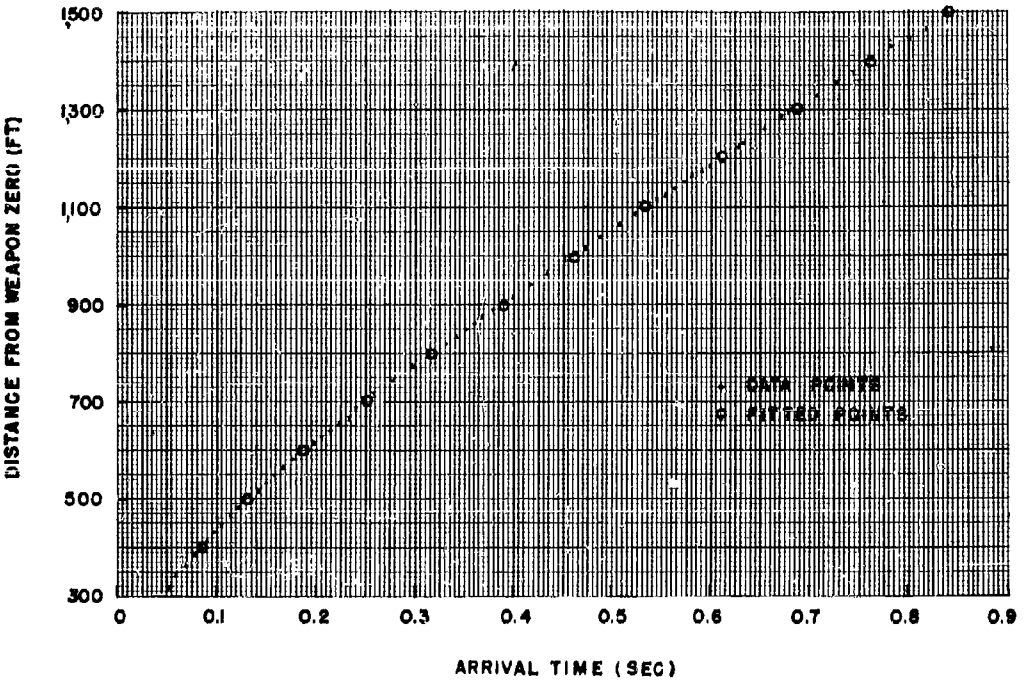

Fig. 3.4 Free-air Shock Wave Time-of-Arrival Curve, TUMBLER 1

where t and R are given in the same units as above.

Film No. 13082 yielded unexpected data concerning the formation and height of the Mach stem. The height of the Mach stem as a function of distance from ground zero (GZ) directly beneath the burst point is given in Fig. 3.6. The point at 10 ft stem height was taken from preliminary results reported by the Stanford Research Institute (SRI).[13] A straight line drawn through the seven data points indicates that the Mach stem began to form at about 860 ft from GZ.

The values of atmospheric pressure, P_o, and temperature, T_o, were measured on the ground and at burst height just prior to shot time. These values are given in Table 1.1 for all shots. Values of the sound velocity, C_o, were computed using Eq. 3.4.

The variations of P_o and C_o with altitude above ground were assumed to be linear for lack of more complete data. See Fig. 3.7. The values read from these curves were used in calculating

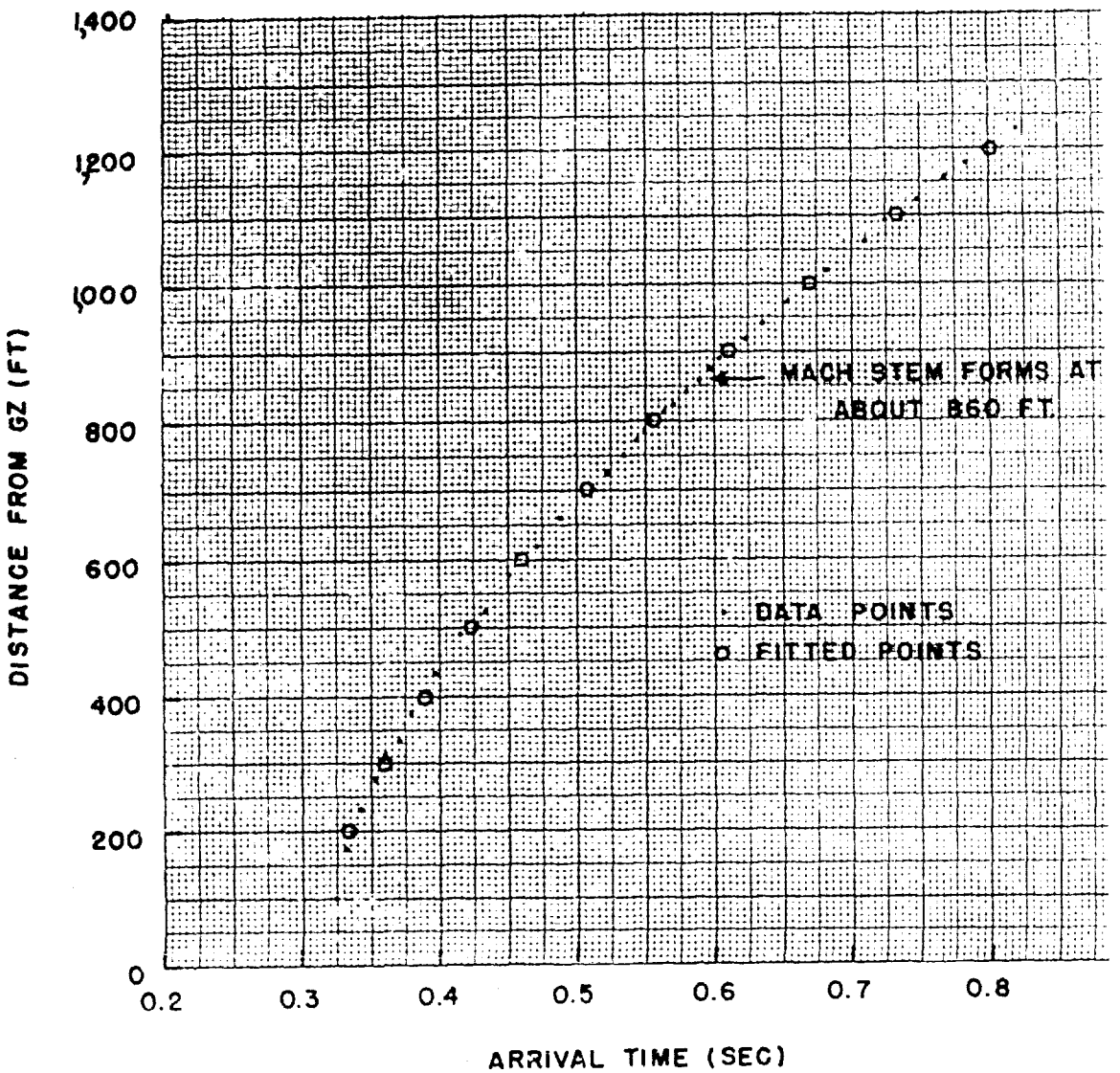

Fig. 3.5 Shock Wave Time-of-Arrival Curve Along the Ground, TUMBLER 1

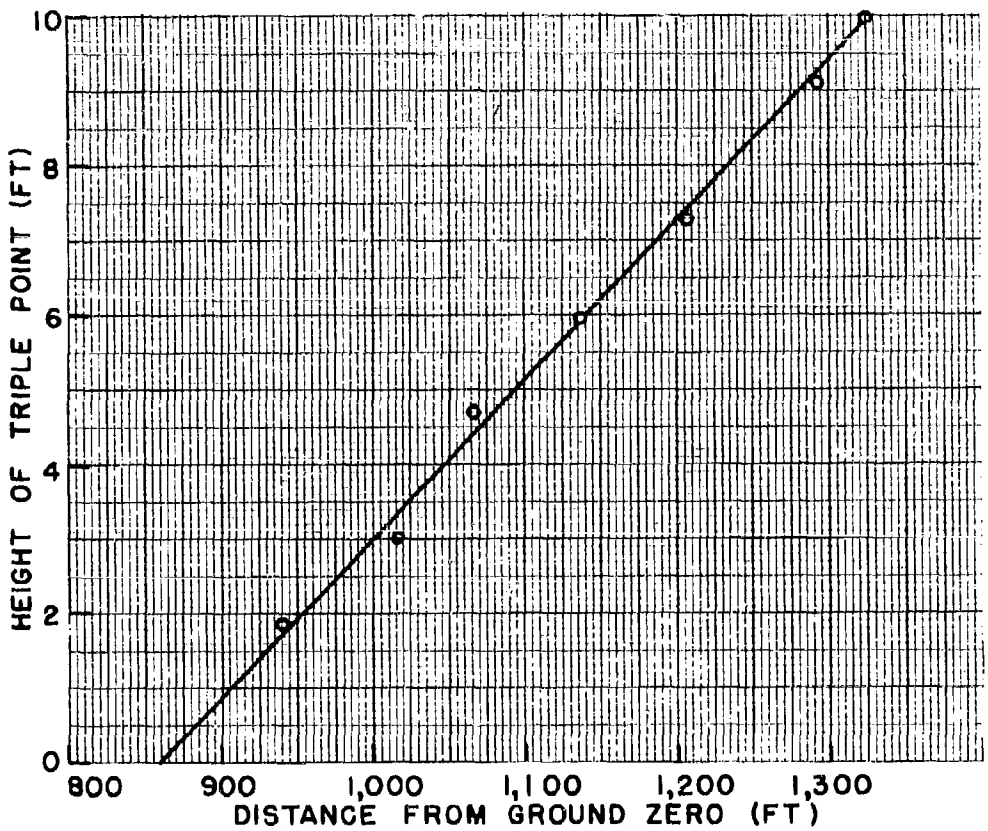

Fig. 3.6 Height of Mach Stem vs Distance from Ground Zero, TUMBLER 1

peak shock overpressures in free air as a function of distance from the burst point.

Of the variety of ways one might use the values of P_o and C_o as functions of altitude, the following was chosen so that comparison with measurements on the ground might be made. Values were chosen at intervals along the vertical line from the burst to GZ. For distances exceeding the burst height, the values of P_o and C_o at an altitude of 100 ft were chosen arbitrarily. If values of P_o and C_o were chosen at burst height and maintained constant throughout the calculations the decay of the pressure-distance curve would be slightly greater than indicated in the graphs shown below. No definite quantitative value can be given for this greater decay because it varies with each shot and the existing meteorological conditions. A careful check which included a proper correction for the geometry involved

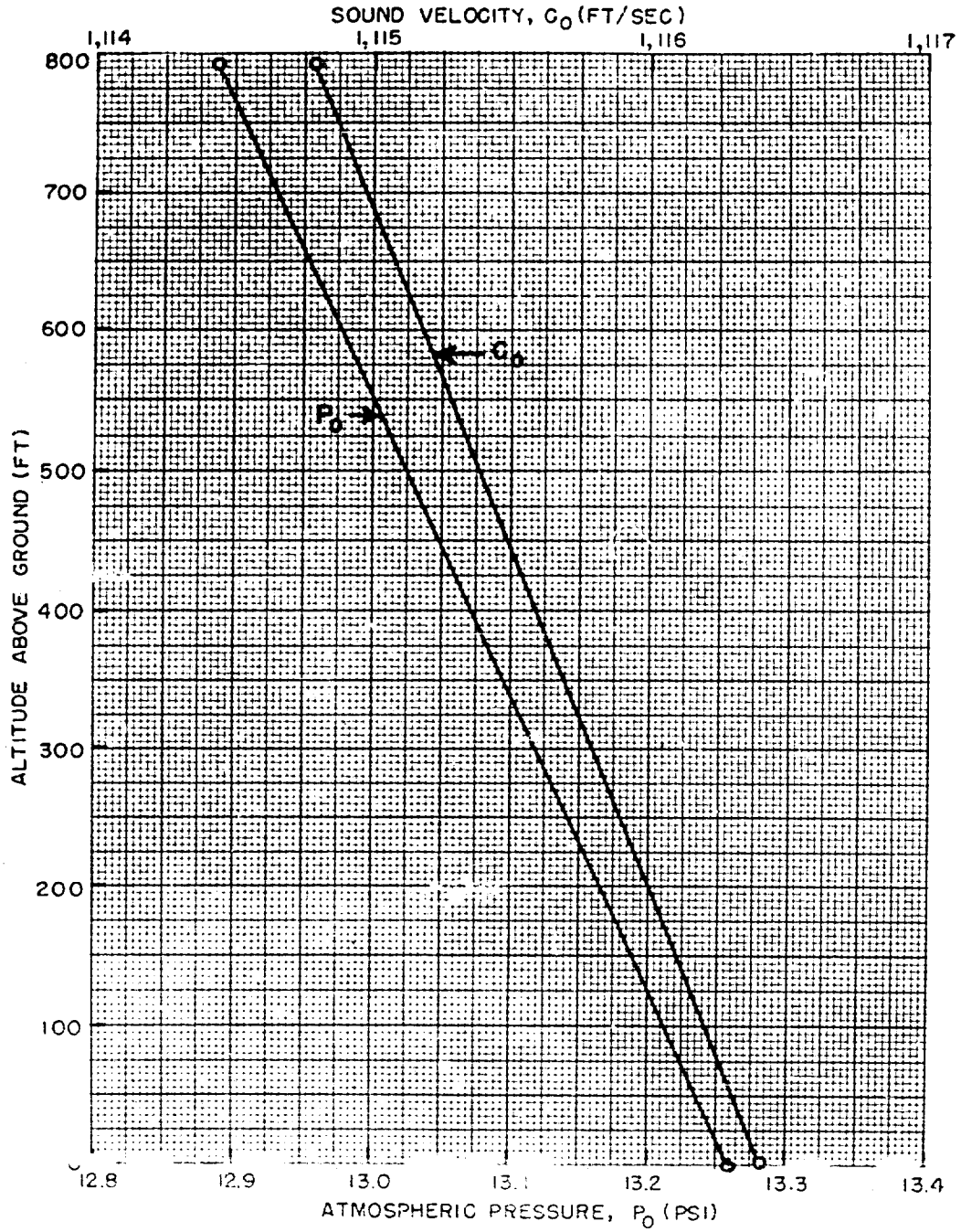

Fig. 3.7 Atmospheric Pressure, P_O, and Sound Velocity, C_O, vs Altitude - TUMBLER 1

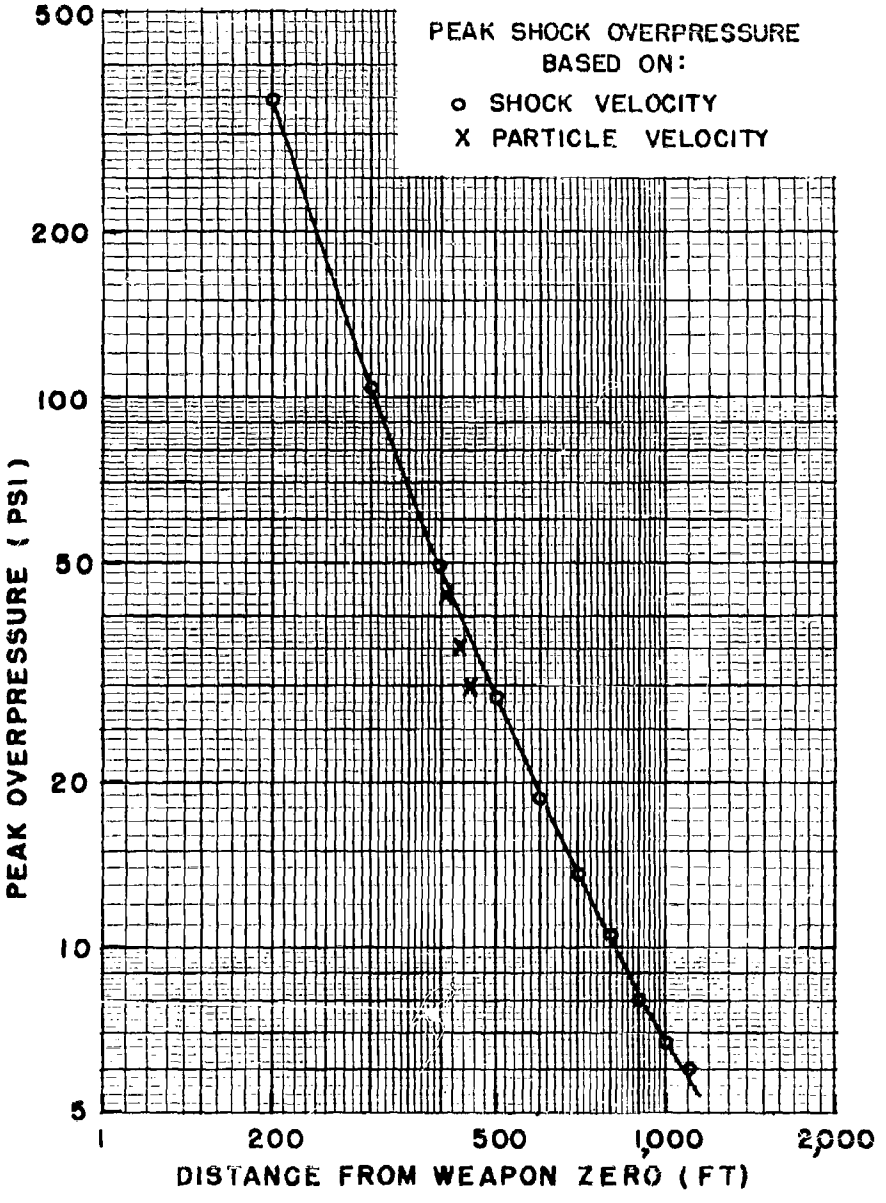

Fig. 3.8 Peak Shock Overpressure in Free Air vs Distance, TUMBLER 1

showed that within the precision of measurement of the films, all initial shock waves were symmetrical around the burst point.

The peak shock overpressures in free air at various distances from weapon zero were calculated using shock velocities, as obtained from the differentiation of the time-of-arrival equations, substituted in Eq. 3.3. Values for shock velocity and peak overpressure at various distances from weapon zero are given in Table 3.3. The pressures are plotted as a function of distance in Fig. 3.8.

As mentioned above, shock arrival times at distances along the ground ranging from 105 to 1231 ft from GZ were obtained. The validity of the shock pressures calculated from these data via the shock velocity method (Eq. 3.3) depends significantly on the values of sound velocity, C_o, (or temperature, T_o) in the medium ahead of the shock. On TUMBLER 1, T_o was measured as a function of time at several distances from GZ. No measurements were obtained, however, between GZ and 1024 ft. The authors are of the opinion that an extrapolation of the temperature data based on a few widely separated points beyond 1024 ft in an attempt to obtain reliable values of sound velocity, C_o, at distances closer to GZ is unjustified. Shock pressures in the limited portion of the Mach region for which time-of-arrival data were obtained have, therefore, not been calculated.

3.3.2 Pressure-Distance Results - TUMBLER 2

The free air, shock wave, time-of-arrival data for TUMBLER 2 were taken from film No. 13182. The vertical plane through zero in which measurements were made is shown in Fig. 3.3. Timing marks on the film showed the camera to be running at constant speed throughout the region of interest. The frame rate was 75.586 frames per sec corresponding to a time per frame of 0.01323005 sec. (The last three decimal places are held for computational purposes only.) On the enlarged image, distance could be measured accurately to ± 1.0 ft. The absolute times of arrival of the shock wave in free air are given in Table 3.4. In Fig. 3.9 the tabular values are plotted together with calculated points based on the equations fitted to the data by the method of least squares. For the shock wave in free air the time-of-arrival curve is represented by

$$t = -0.0142 + 0.0157R + 0.6314R^2 - 0.1708R^3 \quad (400 \text{ ft to } 700 \text{ ft}) \quad (3.8)$$

$$t = -0.0651 + 0.1970R + 0.4316R^2 - 0.1075R^3 \quad (600 \text{ ft to } 1200 \text{ ft}) \quad (3.9)$$

where t is in seconds and R is in thousands of feet from the burst point.

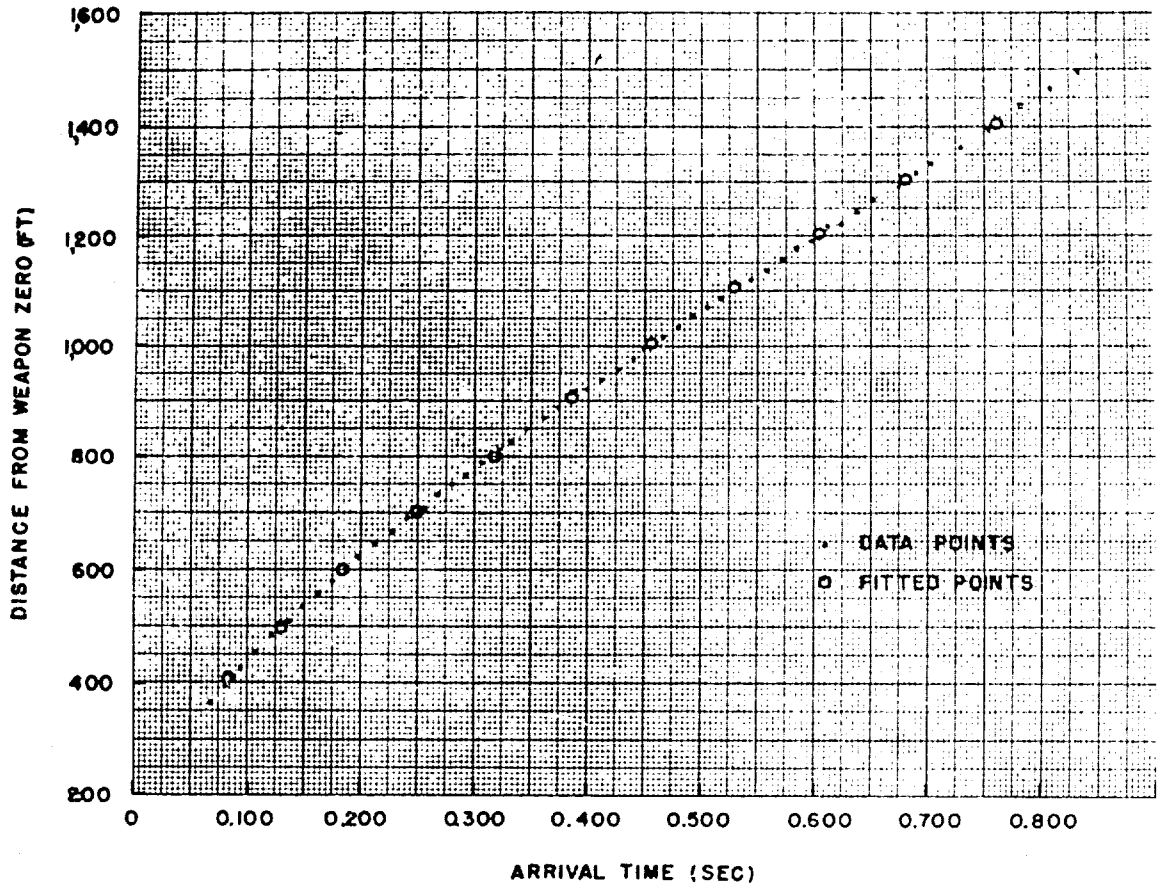

Fig. 3.9 Free-air Shock Wave Time-of-Arrival Curve, TUMBLER 2

No Mach region data were obtained for this nor subsequent shots because of a rise in the T-7 area terrain between the camera station and ground level in the plane of measurement. It is estimated that the lowest point which could be seen in this and later films was 20 to 30 ft above the ground in the planes of the measurement.

The variations of P_o and C_o with altitude above ground are shown in Fig. 3.10. Values taken from these curves were used in calculating peak [illegible] overpressures in free air as a function of distance from the burst point.

Shock velocities and corresponding peak overpressures are tabulated for various distances from weapon zero in Table 3.5. Overpressure vs distance is plotted in Fig. 3.11.

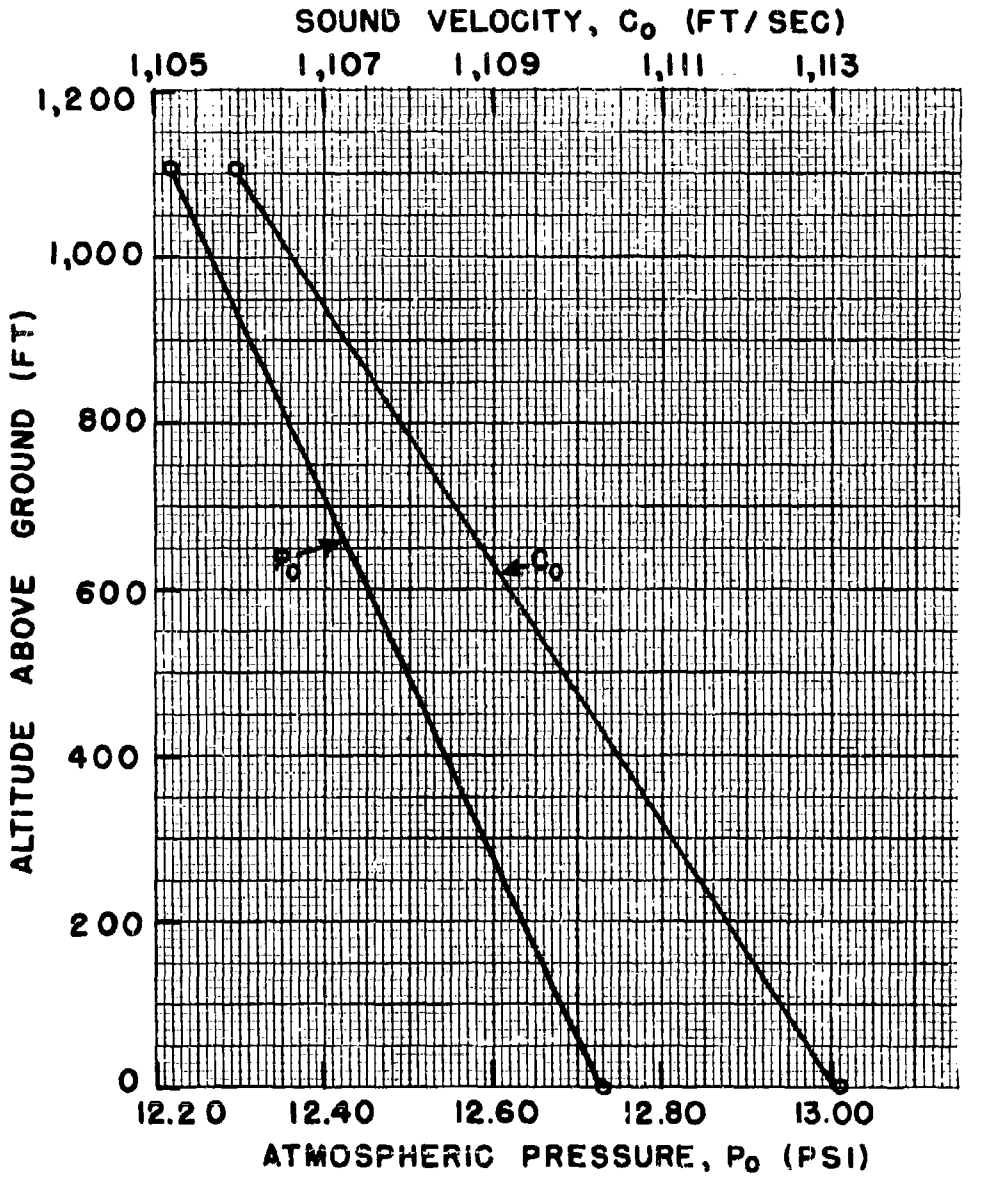

Fig. 3.10 Atmospheric Pressure, P_o, and Sound Velocity, C_o, vs Altitude, TUMBLER 2

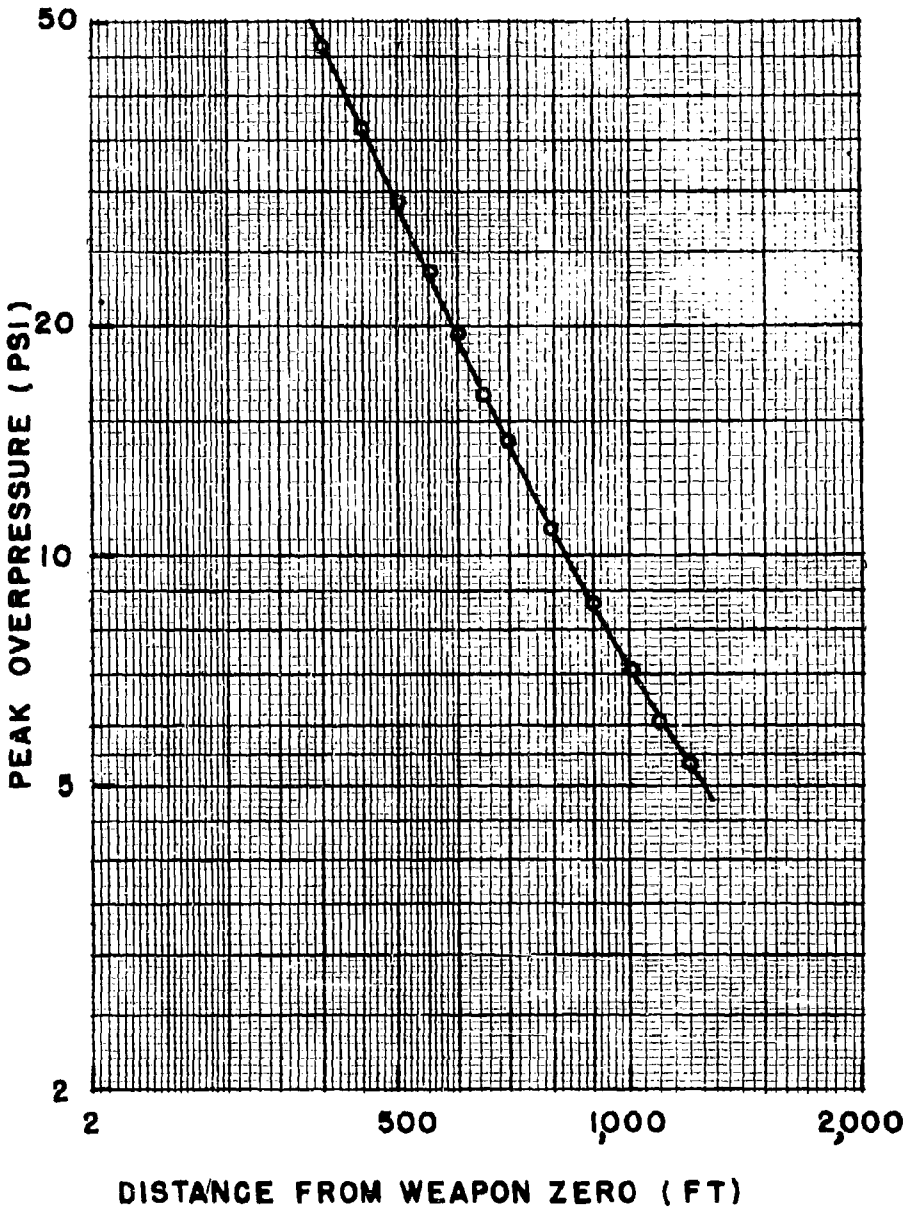

Fig. 3.11 Peak Shock Overpressure in Free Air vs Distance, TUMBLER 2

3.3.3 Pressure-Distance Results - TUMBLER 3

The free air shock wave time-of-arrival data for TUMBLER 3 were taken from film No. 13281. The vertical plane through zero in which measurements were made is shown in Fig. 3.3. Timing marks on the film showed the camera to be running at constant speed throughout the region of interest. The frame rate was 104.644 frames per sec corresponding to a time per frame of 0.0095562 sec. (The last two decimal places are held for computational purposes only.) On the enlarged image, distances could be measured accurately to ± 2.0 ft. The absolute times of arrival of the shock wave in free air are given in Table 3.6. In Fig. 3.12 the tabular values are plotted together with calculated points using the equations fitted to the data by the method of least squares. For the shock wave in free air the time-of-arrival curve is represented by

$$t = -0.1519 + 0.8460R - 1.4614R^2 + 1.0213R^3 \quad (500 \text{ ft to } 650 \text{ ft}) \quad (3.10)$$

$$t = -0.0370 + 0.0861R + 0.0723R^2 + 0.0398R^3 \quad (650 \text{ ft to } 1100 \text{ ft}) \quad (3.11)$$

$$t = -0.1107 + 0.1542R + 0.1101R^2 + 0.0047R^3 \quad (1400 \text{ ft to } 1700 \text{ ft}) \quad (3.12)$$

and

$$t = 0.2286 - 0.4623R + 0.4828R^2 - 0.0701R^3 \quad (1700 \text{ ft to } 2000 \text{ ft}) \quad (3.13)$$

where t is in seconds and R is in thousands of feet from the burst point.

It should be mentioned that the image of the shock wave did not appear symmetrical on the film record, but with the proper geometrical corrections applied it was found to be symmetrical within the accuracy of measurement. The apparent nonsphericity is due only to the geometry involved. The burst occurred at the greatest elevation yet recorded for such a test, (i.e., 3447 ft). The camera was located at ground level and measurements were made in the vertical plane through the burst. A sphere when projected through angles ranging from 5 to 19 degrees into this vertical plane from a point, should not appear spherical. The only true radii appearing on the record, therefore, are those which are measured at the level of burst. The results reported here are based on these shock radii. It will be noted in Fig. 3.12 that a peculiar irregularity appears in the curve near 1250 ft. In this region the shock did not intercept light from the smoke trails at burst height within reasonable limits and the precision of the data declines. Results based on them have been omitted in this

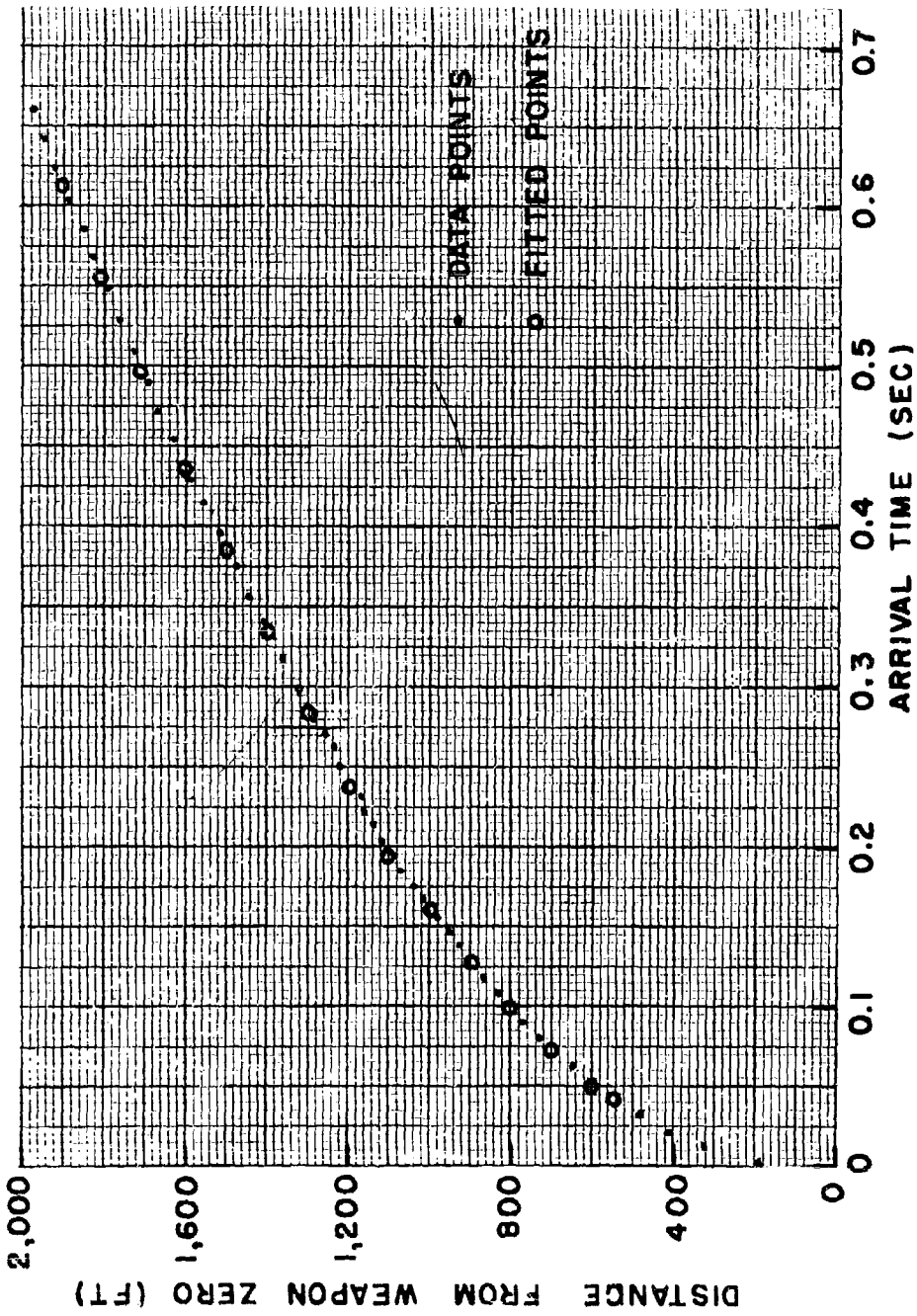

Fig. 3.12 Free-air Shock Wave Time-of-Arrival Curve, TUMBLER 3

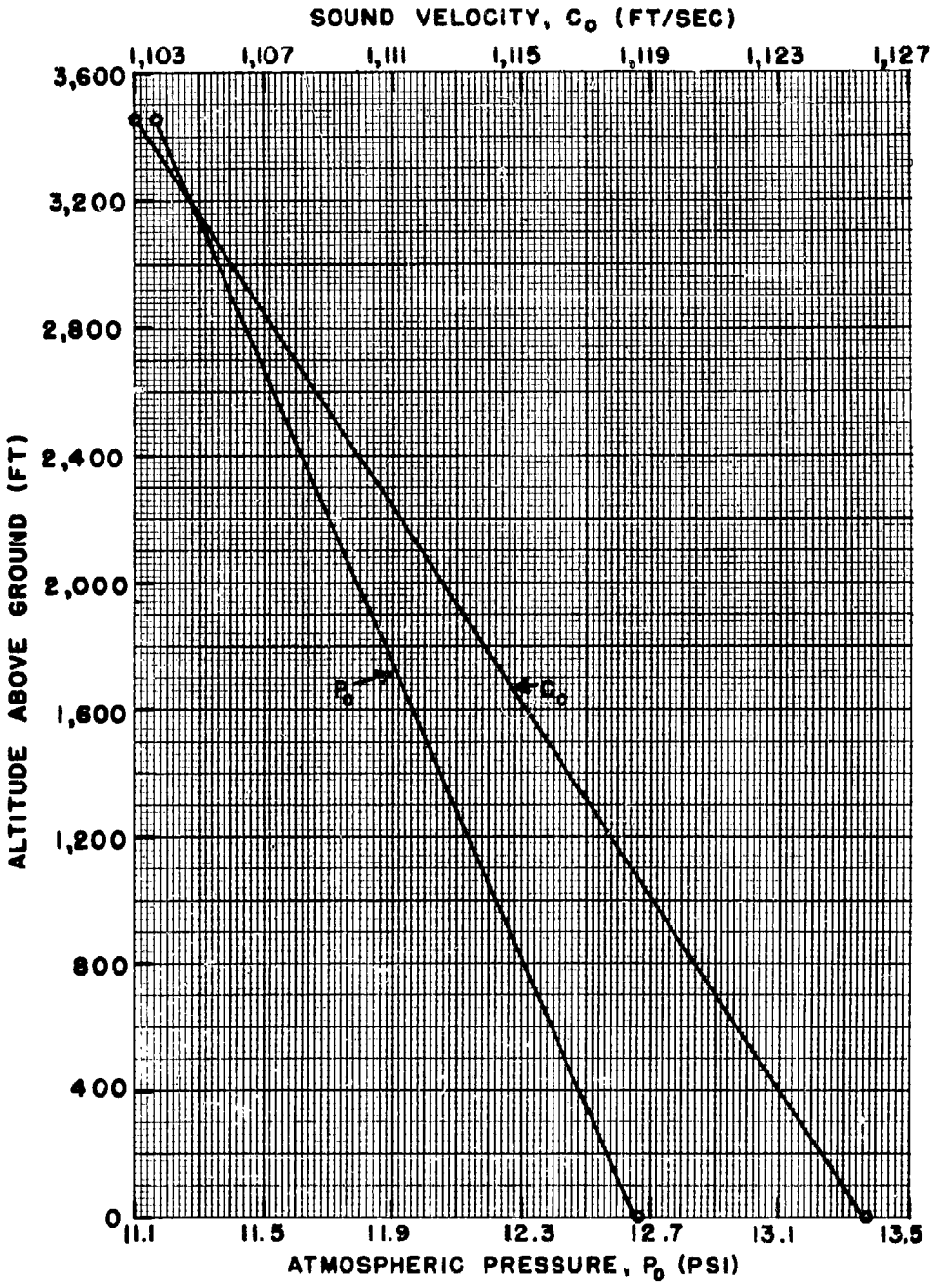

Fig. 3.13 Atmospheric Pressure, P_o, and Sound Velocity, C_o, vs Altitude, TUMBLER 3

region without great loss in the final analysis.

The variations of P_o and C_o with altitude above ground are shown in Fig. 3.13. Values taken from these curves were used in calculating peak shock overpressures in free air as a function of distance from the burst point.

Shock velocities and corresponding peak overpressures are tabulated for various distances from weapon zero in Table 3.7. Overpressure vs distance is plotted in Fig. 3.14. Data points are omitted between 1100-1400 ft for the reasons mentioned above.

3.3.4 Pressure-Distance Results - TUMBLER 4

The free-air shock wave time-of-arrival data for TUMBLER 4 were taken from films No. 13381 and 13382. The vertical plane through zero in which measurements were made is shown in Fig. 3.3. Timing marks on the films showed the cameras to be running at constant speed throughout the region of interest. The respective rates were 101.337 and 102.869 frames per sec corresponding to times per frame of 0.00986800 and 0.00972107 sec. (The last three decimal places are held for computational purposes only.) On the enlarged image, distances could be measured accurately to $\pm$ 1.0 and $\pm$ 1.25 ft respectively. The absolute times of arrival of the shock wave in free air are given in Table 3.8. In Fig. 3.15 the tabular values are plotted together with points calculated using the equations fitted to the data by the method of least squares. For the shock wave in free air the time-of-arrival curve is represented by

$$t = 0.0257 - 0.1584R + 0.4319R^2 - 0.1103R^3 \quad (400 \text{ ft to } 650 \text{ ft}) \quad (3.14)$$

$$t = 0.1891 - 0.7711R + 1.1727R^2 - 0.3966R^3 \quad (650 \text{ ft to } 900 \text{ ft}) \quad (3.15)$$

$$t = 0.0537 - 0.2296R + 0.4523R^2 - 0.0837R^3 \quad (900 \text{ ft to } 1300 \text{ ft}) \quad (3.16)$$

$$t = 0.0419 - 0.1632R + 0.3748R^2 - 0.0581R^3 \quad (1300 \text{ ft to } 1900 \text{ ft}) \quad (3.17)$$

where t is in seconds and R is in thousands of feet from the burst point.

The variations of P_o and C_o with altitude above ground are shown in Fig. 3.16. Values taken from these curves were used in calculating peak shock overpressures in free air as a function of distance from the burst point.

Shock velocities and corresponding peak overpressures are

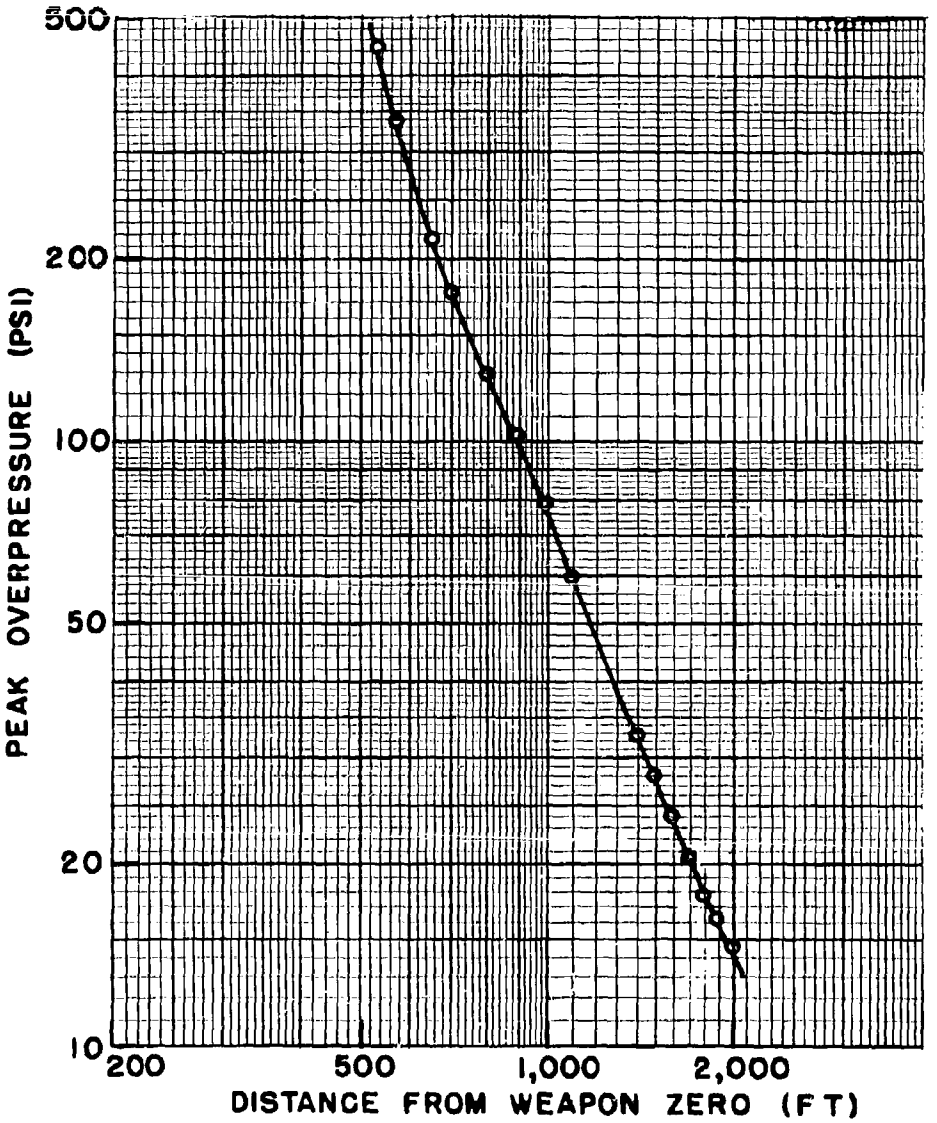

Fig. 3.14 Peak Shock Overpressure in Free Air vs Distance, TUMBLER 3

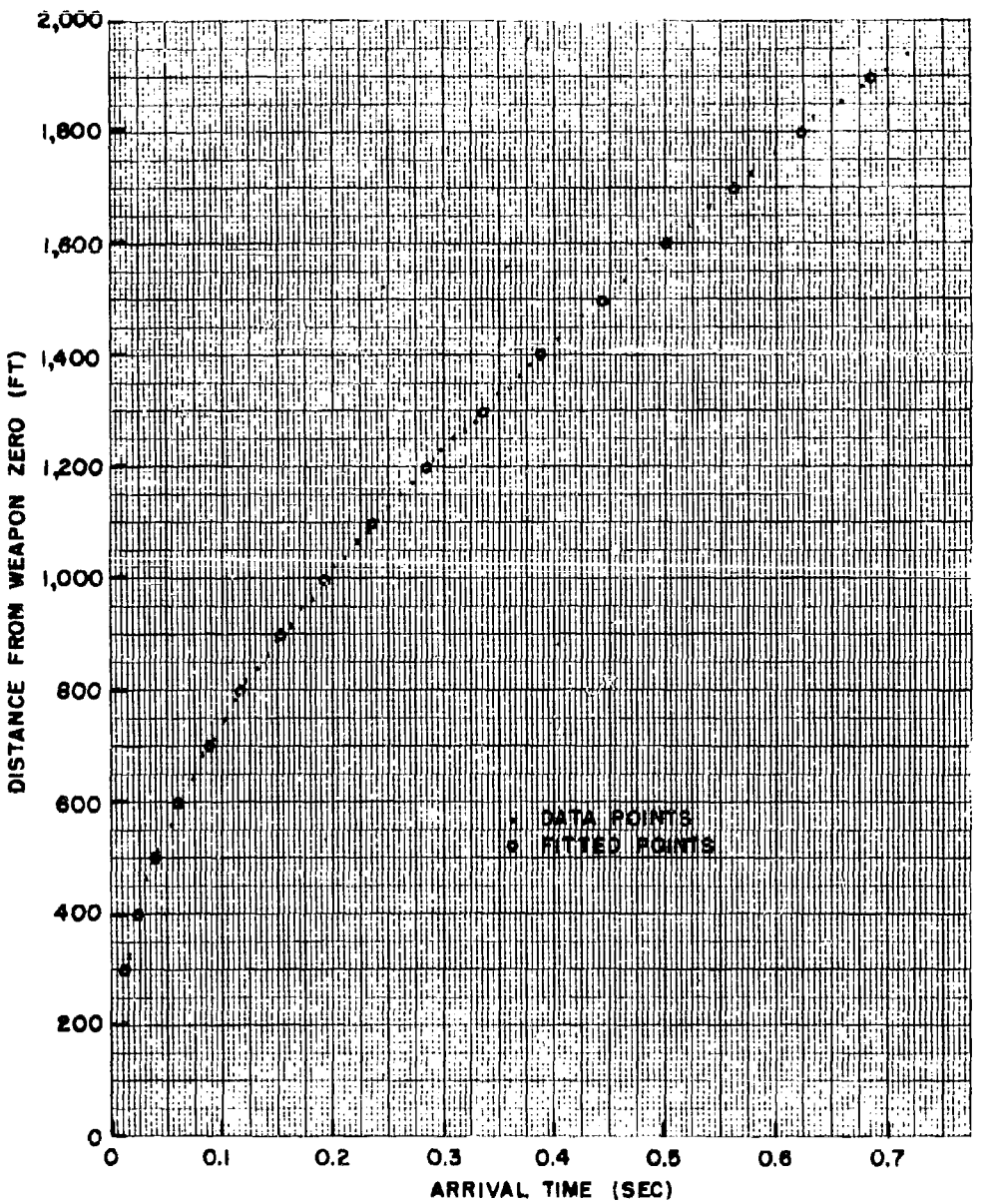

Fig. 3.15 Free-air Shock Wave Time-of-Arrival Curve, TUMBLER 4

tabulated for various distances from weapon zero in Table 3.9. Overpressure vs distance is plotted in Fig. 3.17.

3.3.5 Free-air Pressure-Time Results - TUMBLER 1

The data for Shot 1 were taken from film No. 13083. The frame rate was 93.49 frames per sec, and it was constant over the region of interest. Figure 3.18 shows the vertical plane of measurement through bomb zero. On the enlarged image, distances could be measured to $\pm$ 1.0 ft.

The intersections of the smoke trail as a function of time along different radii (see Fig. B.1) are tabulated in Table 3.10. A plot of these data is shown in Fig. 3.20. From Fig. 3.20, smoothed values of $Z_n - Z_j$, and $X_n - X_j$ were obtained and are given in Table 3.12. (A value Z_n corresponds to the distance from the burst point to a fixed point on the smoke trail chosen before shock arrival. A value X_n represents the distance from the burst to a particle, originally at Z_n, after shock arrival. The values of Z_n, once chosen, remain fixed, while the values of X_n change with time.) The values of K, or $\left(\frac{\partial X}{\partial Z}\right)_t$, required for the solution of P, were calculated by

$$K = \frac{X_n - X_j}{Z_n - Z_j}, \text{ at } Z = \frac{Z_n + Z_j}{2} \qquad \text{(See App. B, Eq. B.2)}$$

and are plotted in Fig. 3.22. These data may be found tabulated in Table 3.14. Values of K were chosen from Fig. 3.22 for several Z's and the pressures as a function of distance at constant times were calculated by

$$P_{n,m} = P_n \left[\frac{6 P_o + P_n}{6 P_n + P_o} \frac{Z_n^2}{X_{n,m}^2} \frac{1}{k} \right]^{1.4} \qquad \text{(See App. B, Eq. B.3)}$$

where P_n is the total peak pressure at the distance Z_n, obtained from the shock velocity data, and P_o is the atmospheric pressure at burst height. These data are given in Table 3.16 and Fig. 3.24.

The pressure-time curves for 590 ft and 690 ft were taken from Fig. 3.24 and are given in Table 3.18 and shown in Fig. 3.26.

The pressure-time curve at 575 ft was reduced to 1 KT(RC)

at sea level and is included in Table 4.17 and Fig. 4.13.

In Sec 3.1.2 it was pointed out that the particle displacement instrumentation, as employed, was not designed to have sufficient space-time resolution to give reliable peak shock overpressure results based on particle velocity measurements. However, since the particle velocity could be determined easily during the course of the pressure-time analysis, a few specific values were found. At 408.7, 430.8, and 449.2 ft the particle velocity was measured to be 1377.2, 1205.1, and 1067.7 ft/sec, respectively. The equation used to convert from particle velocity to peak shock overpressure is

$$\frac{P_o u^2}{C_o^2} = \frac{3.57\, P_s^2}{6\, P_s + 7\, P_o} \qquad (3.18)$$

where u = particle velocity (ft/sec)
C_o = sound velocity ahead of shock wave (ft/sec)
P_o = atmospheric pressure ahead of shock wave (psi)
P_s = peak shock overpressure (psi)

Comparison of these results with those obtained by the more accurate shock velocity method showed that the particle velocity method produced low results in each case:

44.1 psi	vs	46.0 psi
35.7	vs	41.0
29.6	vs	36.5

These values have been plotted in Fig. 3.8. The evident disagreement is discussed further in Sec 3.3.8.

3.3.6 Free-air Pressure-Time Results - TUMBLER 4

The data from Shot 4 were taken from film No. 13383. The frame rate was 82.46 frames per sec and it was constant over the region of interest. Figure 3.19 shows the vertical plane of measurement through bomb zero. On the enlarged image, distances could be measured to ± 1.0 ft.

The intersections of the smoke trail as a function of time along different radii (see Fig. B.1) are tabulated in Table 3.11. A plot of these data is shown in Fig. 3.21. From Fig. 3.21, smoothed

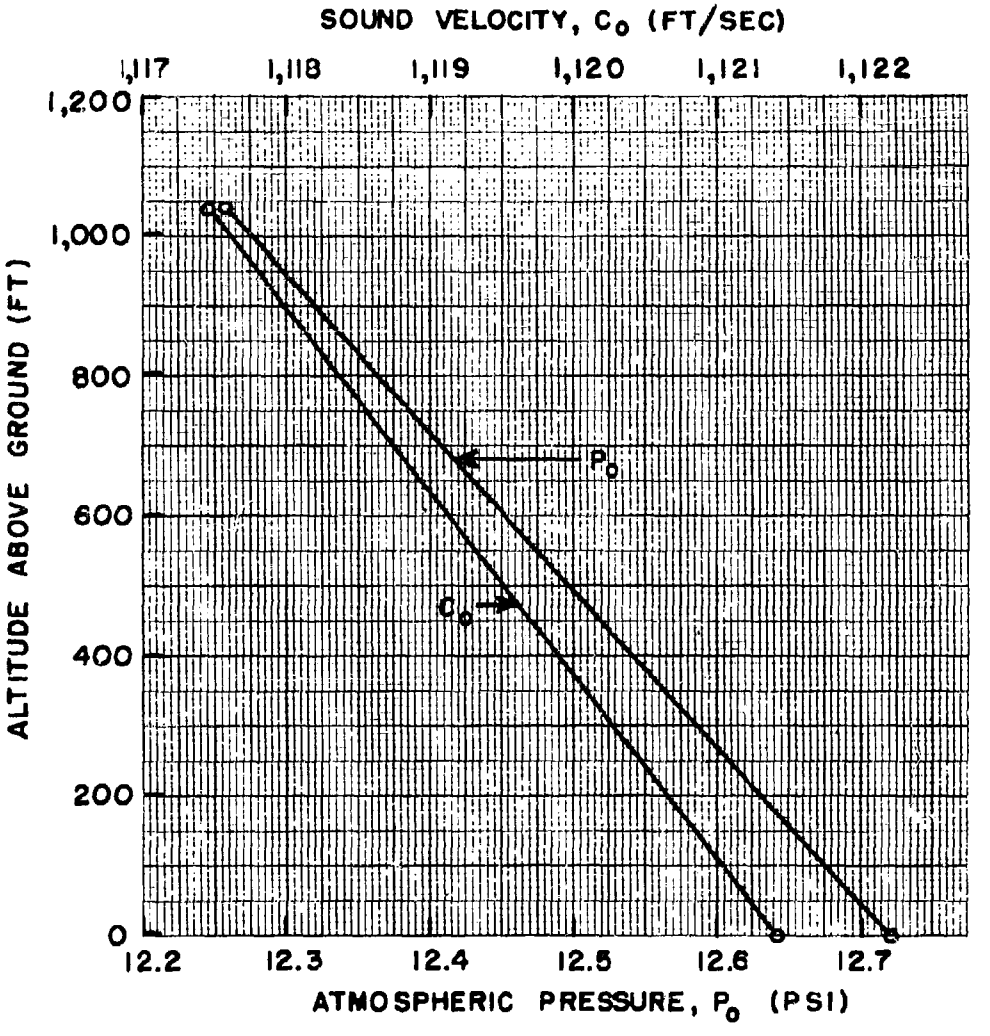

Fig. 3.16 Atmospheric Pressure, P_o, and Sound Velocity, C_o, vs Altitude, TUMBLER 4

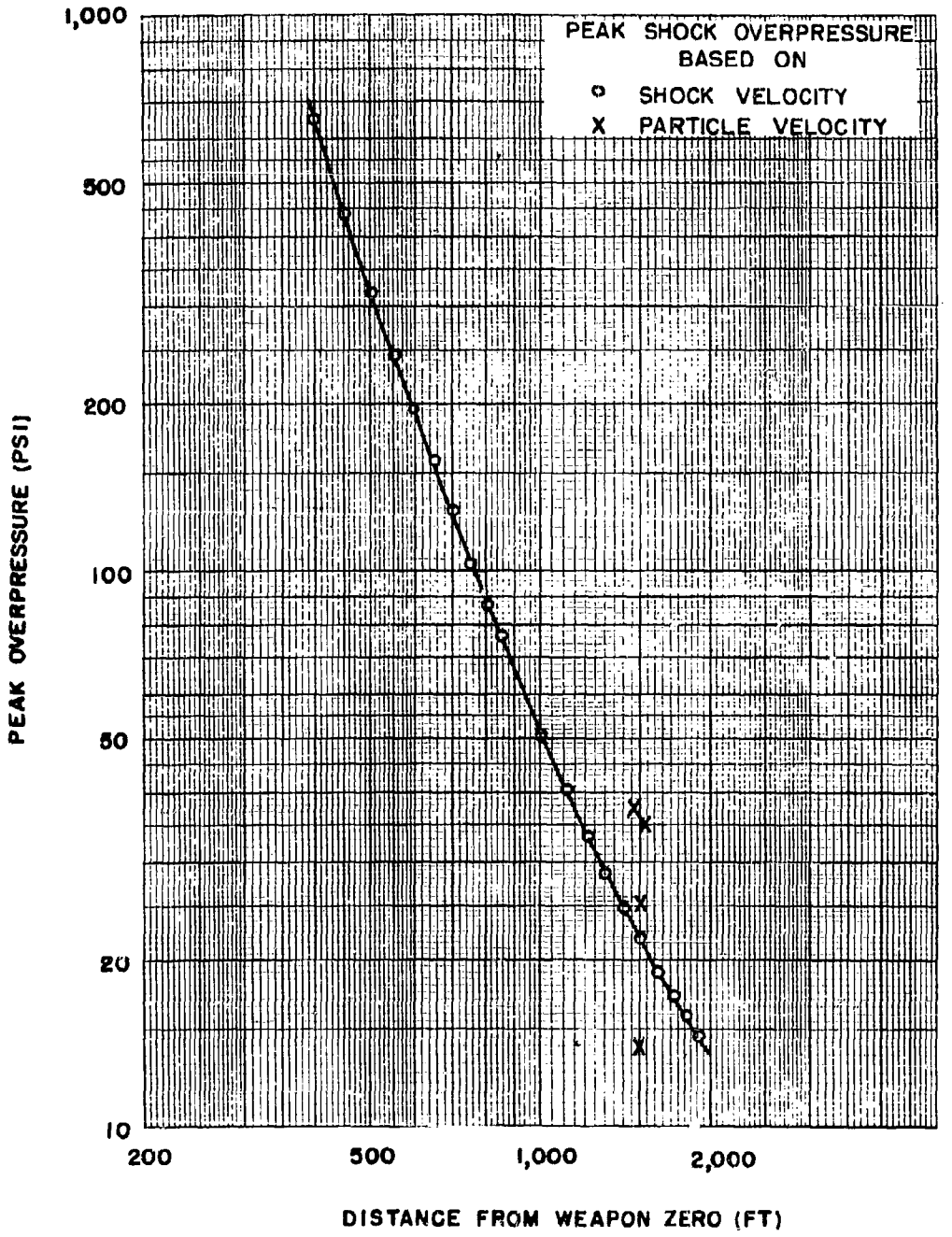

Fig. 3.17 Peak Shock Overpressure in Free Air vs Distance, TUMBLER 4

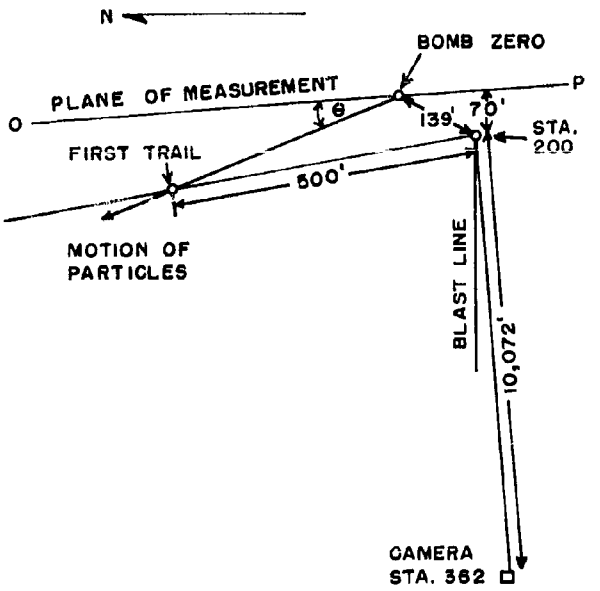

Fig. 3.18 Particle Displacement Layout - TUMBLER 1

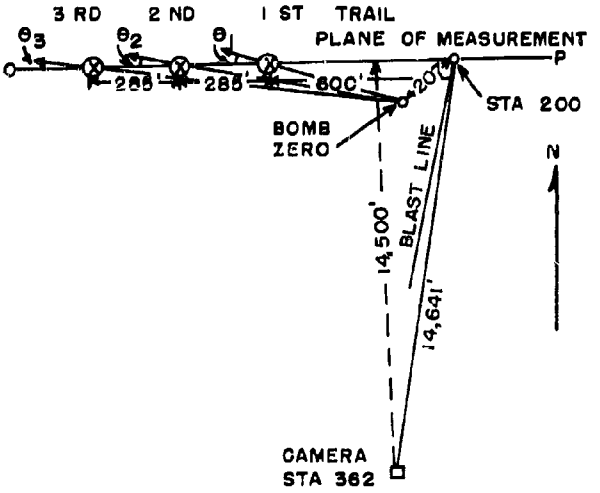

Fig. 3.19 Particle Displacement Layout - TUMBLER 4

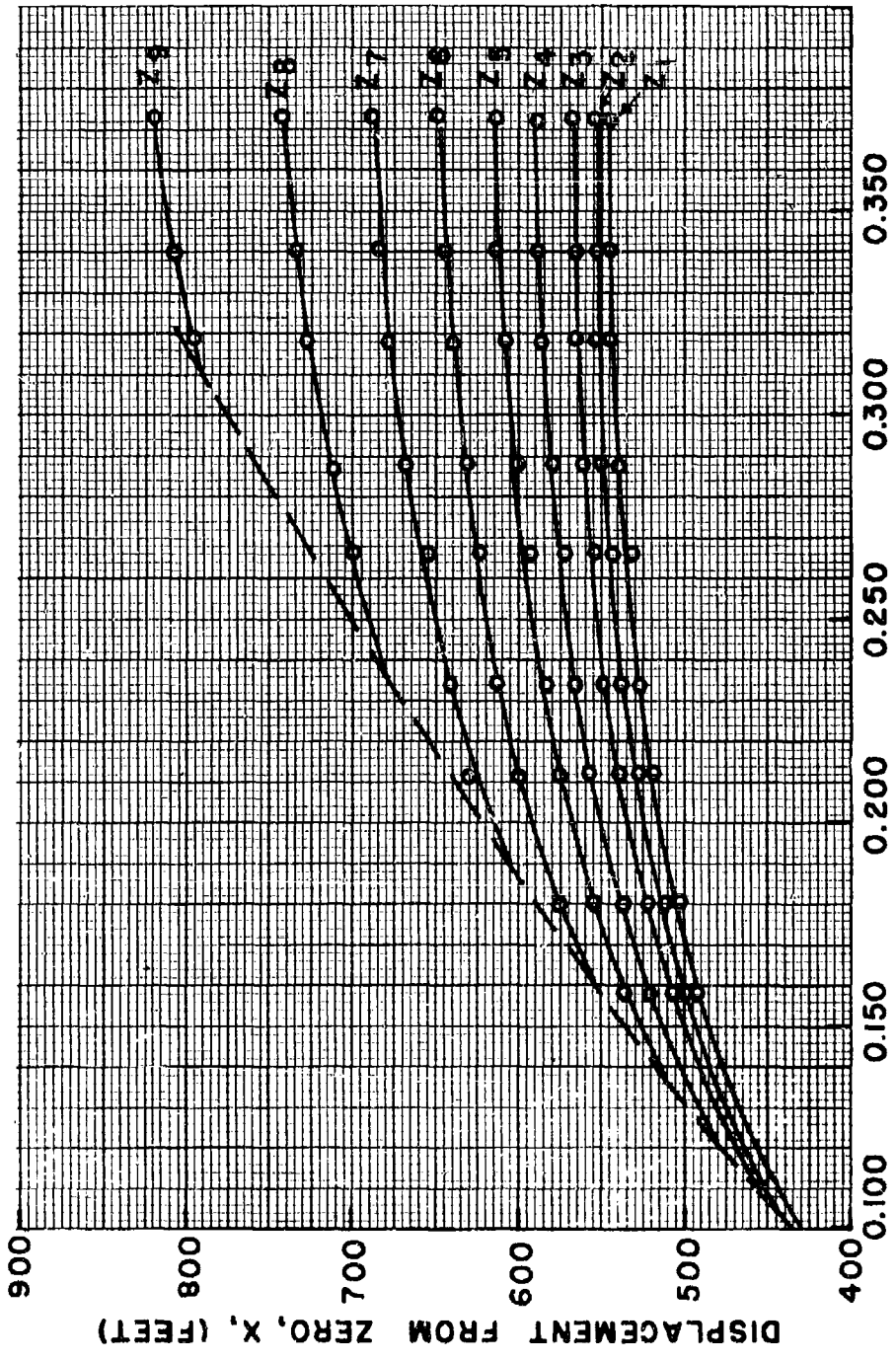

Fig. 3.20 Particle Displacement vs Time, TUMBLER 1

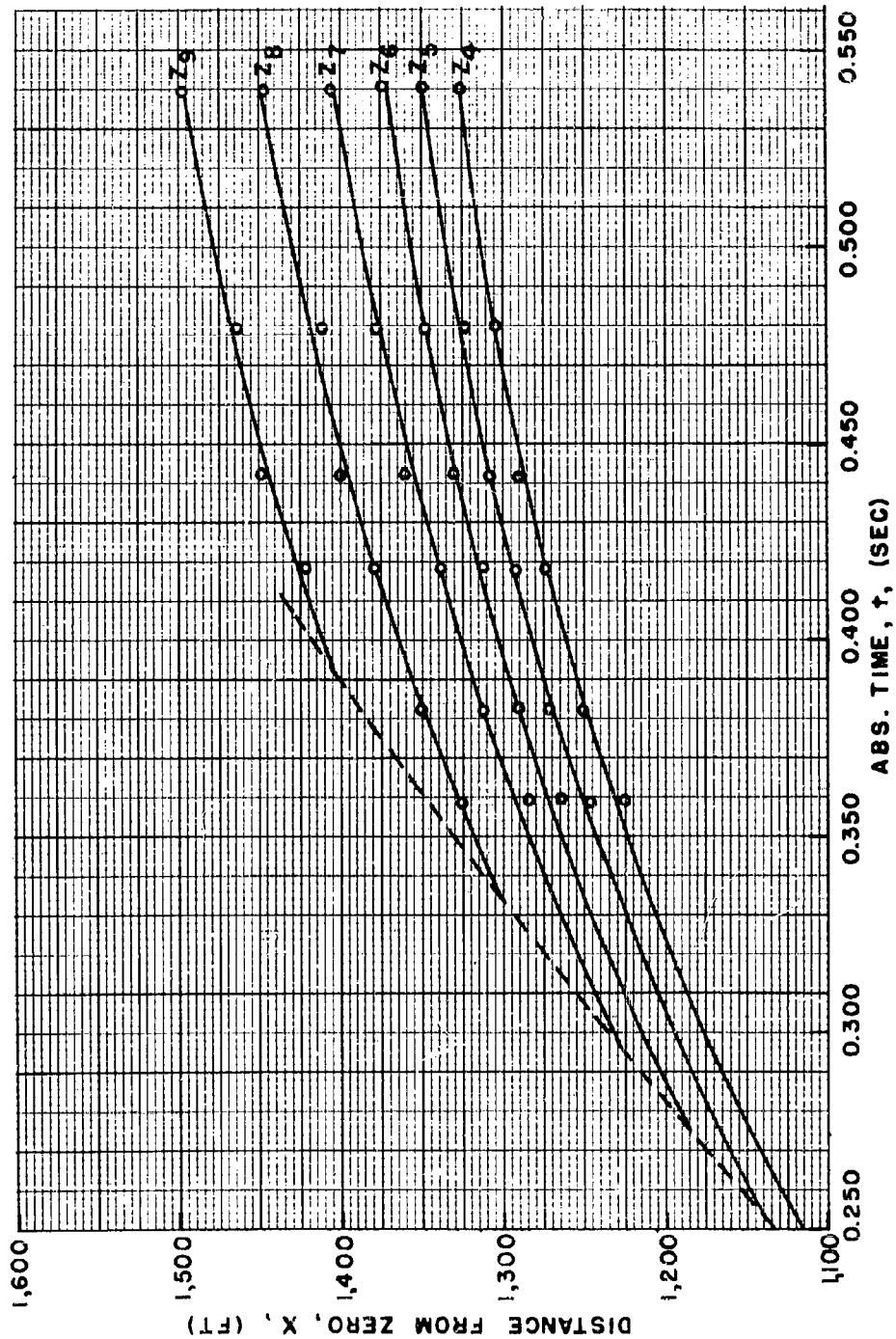

Fig. 3.21 Particle Displacement vs Time, TUMBLER 4

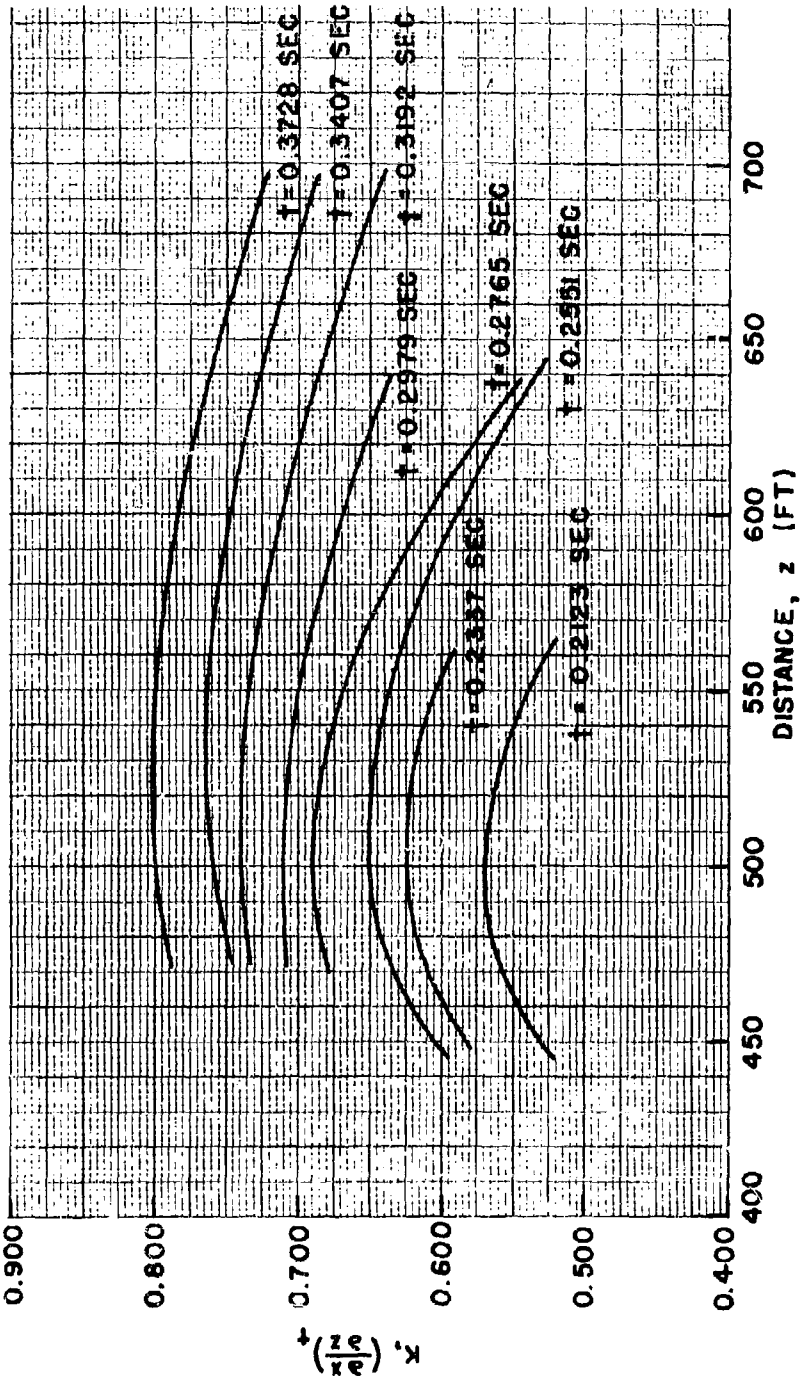

Fig. 3.22 K and Z at Constant Times, TUMBLER 1

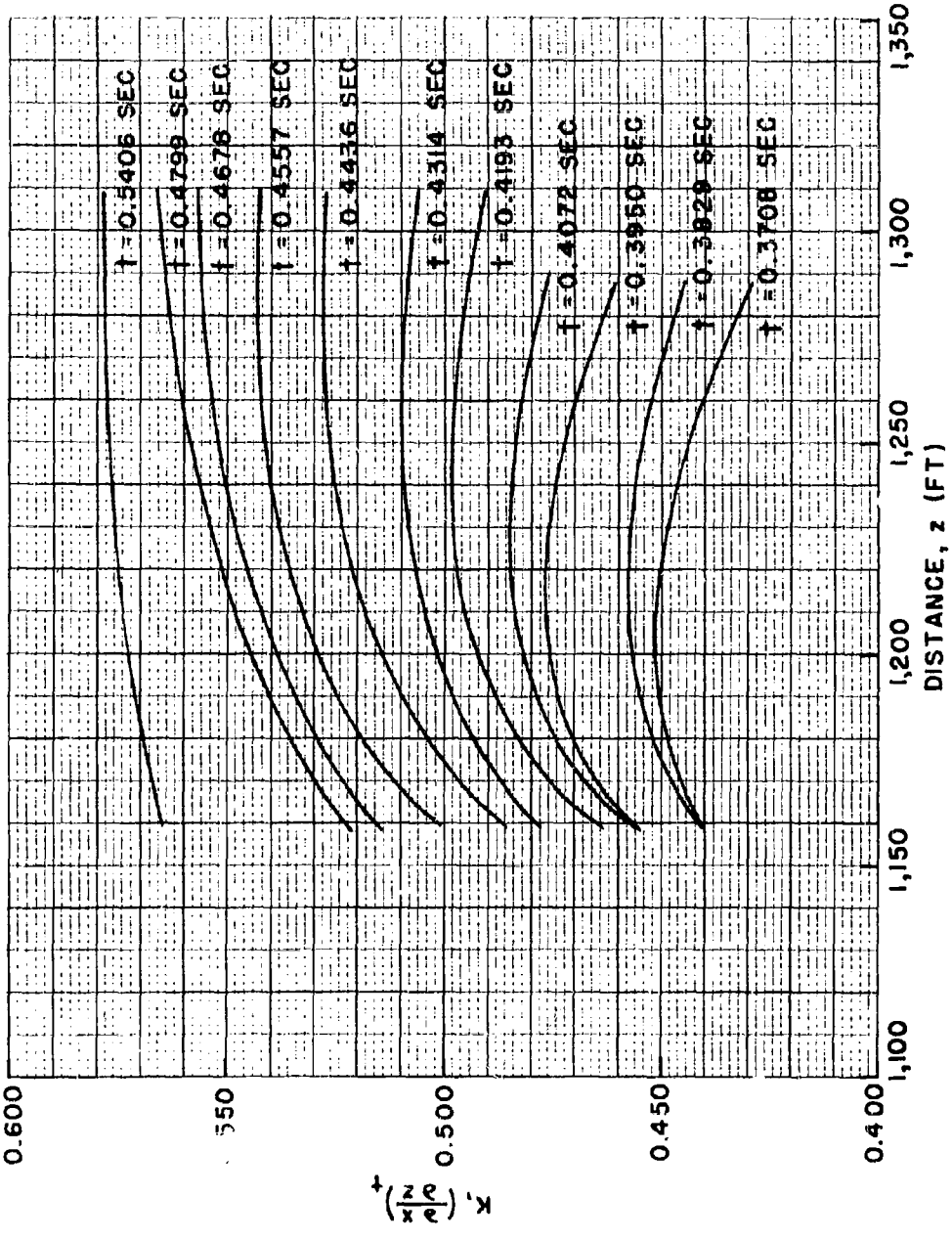

Fig. 3.23 K and Z at Constant Times, TUMBLER 4

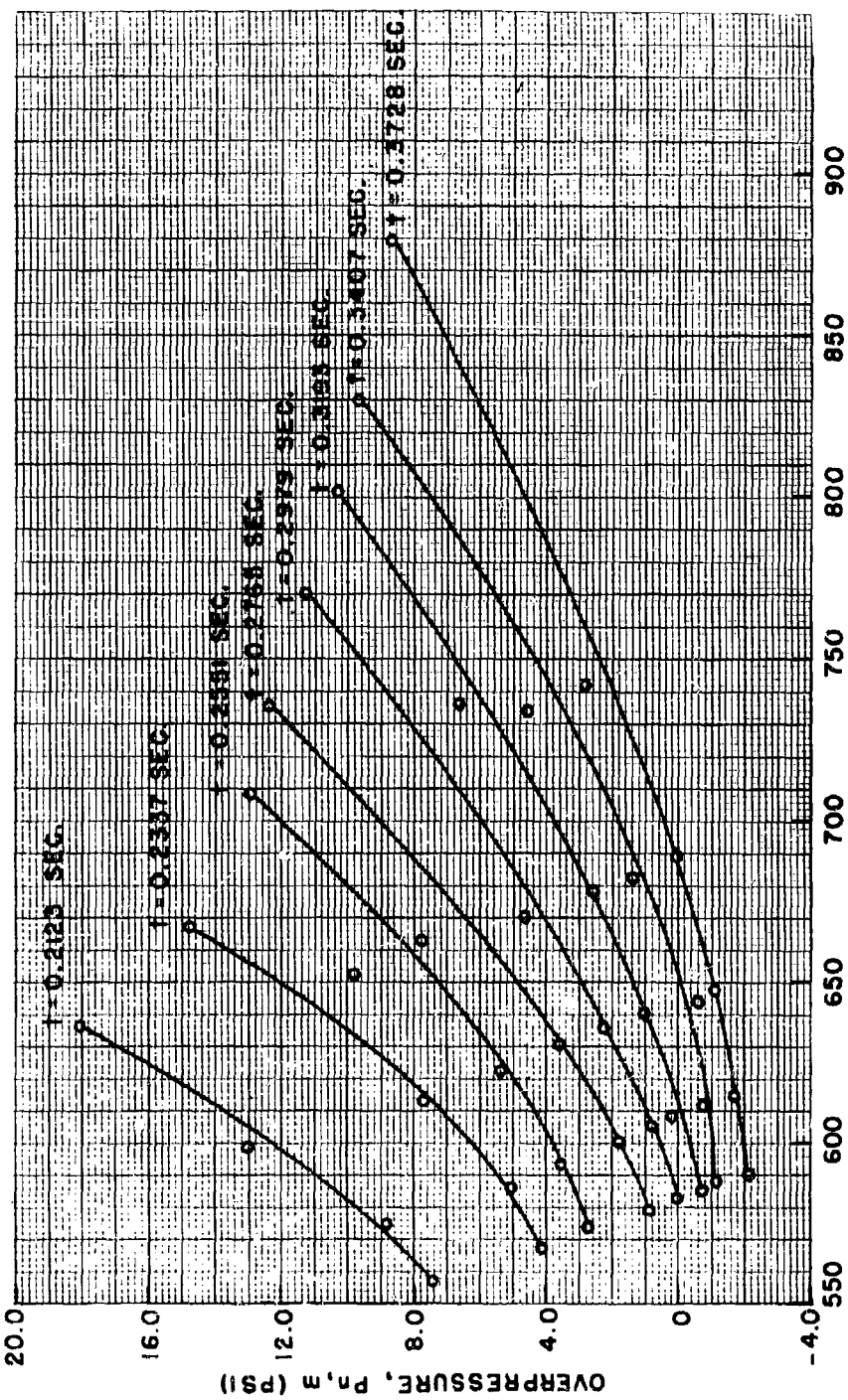

Fig. 3.24 $P_{n,m}$ vs X, TUMBLER 1

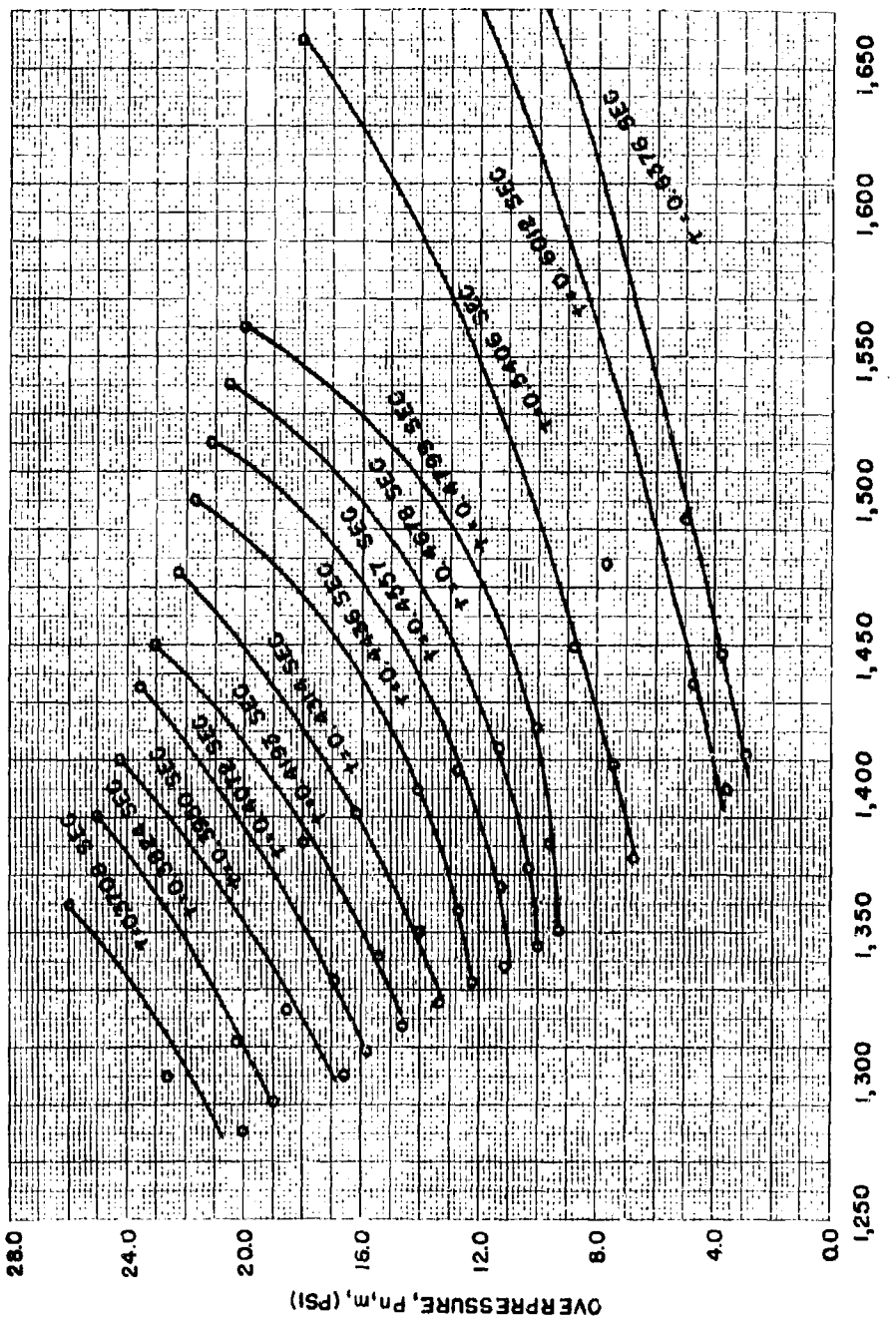

Fig. 3.25 $P_{n,m}$ vs X, TUMBLER 4

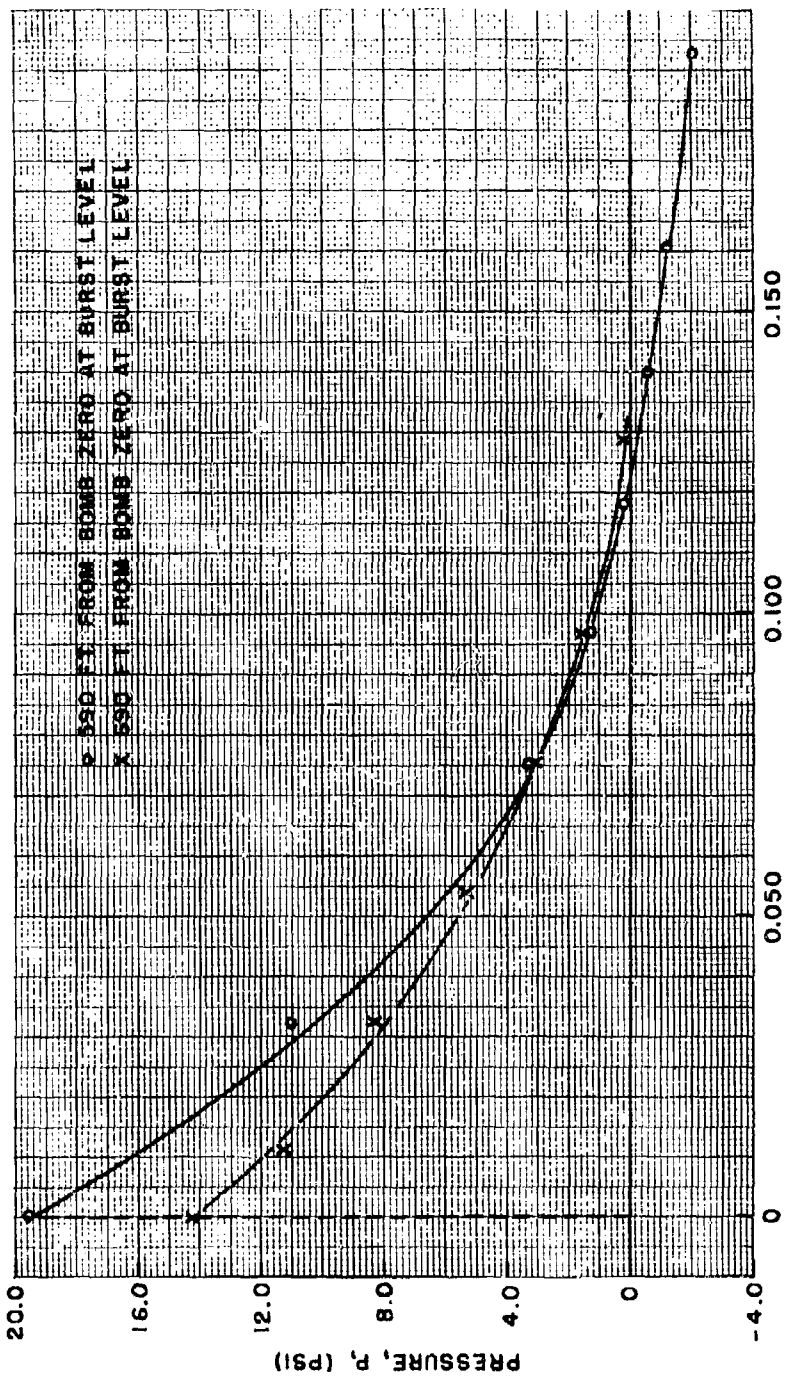

Fig. 3.26 Pressure-Time in Free Air, TUMBLER 1

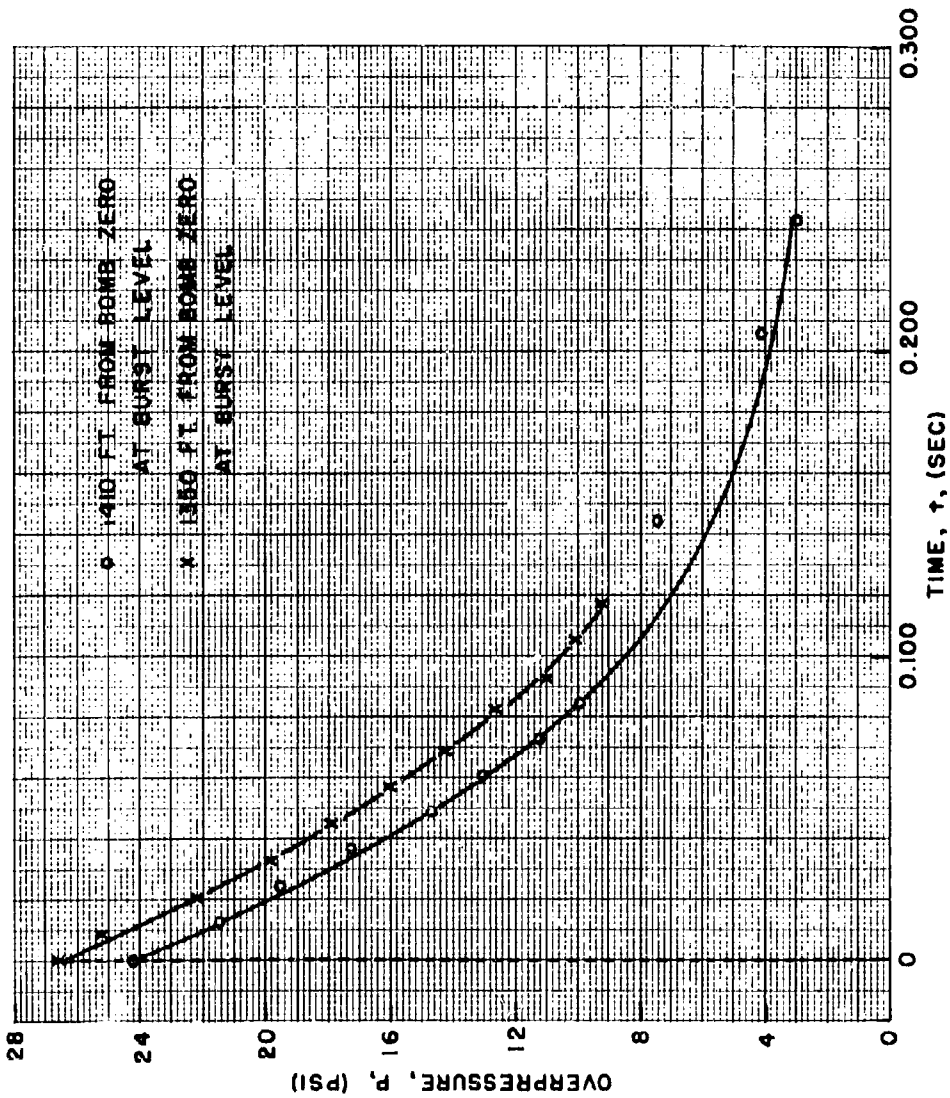

Fig. 3.27 Pressure-Time in Free Air, TUMBLER 4

values of $Z_n - Z_j$, and $X_n - X_j$ were obtained and are given in Table 3.13. The values of K are plotted in Fig. 3.23. These data may be found in Table 3.15. Values of K were chosen from Fig. 3.23 for several Z's and the pressures as a function of distance at constant times were calculated. These data are given in Table 3.17 and Fig. 3.25.

The pressure-time curves for 1350 ft and 1410 ft were taken from Fig. 3.25 and are given in Table 3.19 and shown in Fig. 3.27.

The pressure-time curve at 1550 ft was reduced to 1 KT(RC) at sea level and is included in Table 4.17 and Fig. 4.13.

As in Sec 3.3.5 for Shot 1, a few measurements of the particle velocity were also recorded for Shot 4. At 1464.0, 1488.3, 1500.2, and 1520.3 ft from the burst point the particle velocity was measured to be 1279.7, 981.1, 639.8, and 1237.0 ft/sec, respectively. Equation 3.18 was used to convert these values to the corresponding peak shock overpressures. Comparison of these results with those obtained by the more accurate shock velocity method showed that the particle velocity method produced high results in three of the four cases:

37.5 psi	vs	23.0 psi
25.1	vs	22.2
13.8	vs	21.7
35.6	vs	21.3

These values have been plotted in Fig. 3.17. The evident disagreement is discussed further in Sec 3.3.8.

3.3.7 Determination of the Decay Parameter, θ

In reference 24 an equation is given which was developed by Theilheimer and modified by Hartmann correlating the decay parameter, θ, of the pressure-time curve with the pressure-distance curve. Rearrangement of this equation leads to the form

$$\theta = \frac{\pi}{\pi+1}\left[C_o\sqrt{\frac{6\pi}{7}+1}\left(-\frac{1}{\pi}\frac{d\pi}{dR}\left\{\frac{11}{2}-\frac{5}{6(\pi+1)}-\frac{49}{3(\pi+7)}\right\}-\frac{7}{3R}\right)\right]^{-1} \qquad (3.19)$$

where $\pi = \frac{P-P_o}{P_o}$, C_o is the ambient velocity of sound in ft/sec, R is the distance in ft, and $\theta = \frac{-(P-P_o)}{\frac{\partial (P-P_o)}{\partial t}}$ evaluated at the shock's peak.

Since $\frac{P-P_o}{P_o} = \pi = 1.167 \left[\left(\frac{U(R)}{C_o} \right)^2 - 1 \right]$, from Eq. 3.3,

then $\frac{d\pi}{dR} = \frac{2.334\ U^3\ (2A_2 + 6A_3R)}{C_o^2}$, where the A's are the coefficients of the polynomial fitted to the arrival time data as in Eqs. 3.1 and 3.2.

Assuming the theory leading to Eq. 3.19 to be correct, it can be used as a check on the pressure-time curves determined by the particle displacement technique. Values of θ were determined as above, based on the shock velocity pressure-distance curves. These values were compared with time values at $\frac{(P-P_o)_{max}}{2.718}$ as read from the pressure-time curves given in Figs. 3.26 and 3.27. (If one assumes the pressure-time curve to be of the form $P-P_o = (P-P_o)_{max}\ e^{-t/\theta}$, then $t = \theta$ when $(P-P_o) = \frac{(P-P_o)_{max}}{e}$). The results are given in Table 3.20. The average discrepancy between θ_{sv} (based on shock velocity) and θ_{pd} (based on particle displacement) for TUMBLER 1 is found to be 14.7 per cent while for TUMBLER 4 the average discrepancy is 1.5 per cent. If the sensitivity of these results to such things as small errors in the measurement of slopes is considered, it appears that the correlation is reasonably good and hence the pressure-time curves obtained by the particle displacement measurement are satisfactory.

3.3.8 Accuracy of Results

The sources of possible errors and the procedures for computing their magnitudes in the methods employed to find pressure as a function of distance by the smoke rocket shock velocity technique have been covered extensively in references (2) and (24). The six major sources of error stem (1) from the static and dynamic resolution uncertainties associated with film measurements under optimum conditions, (2) from failing to correct for foreshortening in the image plane, (3) from improper scaling of distance on the film, (4) from improper time calibration, (5) from improper curve fitting, and (6) from use of improper values of the atmospheric pressure, P_o, and sound velocity, C_o, for the region in front of the shock in pressure computations.

The value of γ, the ratio of specific heats for air, is a function of the shock strength. At overpressures above 75 psi, where

the variation in γ starts to become significant, the correct value for γ has been used in the calculations by referring to the Hirschfelder and Curtiss Tables[29]. In these tables, values of P/P_o are listed for values of U/C_o. The desired values include corrections for variation in γ and for changes in the equation of state.

Throughout the analyses of the data presented in Sec 3.3.1 through 3.3.4 care was taken to hold the above-listed errors to a minimum. In all cases the distance measurements were found to fall within a maximum uncertainty of $\pm$ 2.0 ft and measurements of time per frame to within a maximum uncertainty of $\pm$ 0.00005 sec. In most cases these values were $\pm$ 1.0 ft and $\pm$ 0.00001 sec, respectively. Fitting the measured time-distance data with a polynomial by the method of least squares has been shown to be a reliable method of smoothing experimental data to obtain the most probable values[22]. Since the data points form quite a smooth curve when plotted directly, each point having a maximum deviation from the mean of less than 5 per cent, the fitted polynomial is estimated to be accurate to $\pm$ 1 per cent in the region of best fit. The errors in calculated pressures, therefore, are considered to be accurate to 4 per cent at the 5 psi level, 2.5 per cent at the 10 psi level, and decreasingly less than 2.5 per cent at all higher pressure levels within the range of pressures determined[24].

The determination of the free-air pressure-time curve by means of the particle displacement method is at best a compromise. The procedure of differentiation by difference methods is in itself an approximation containing certain inherent errors. Moreover, the differences, $(X_n - X_j)$ and $(Z_n - Z_j)$, must be taken greater than a predetermined value in order to assure pressure errors less than 10 per cent. The minimum value can be found by differentiating Eq. B.2 which gives a maximum percentage error in K of

$$\frac{\Delta K}{K} = 2\ \Delta R \left[\frac{1}{X_n - X_j} + \frac{1}{Z_n - Z_j} \right] , \qquad (3.20)$$

and similarly from Eq. B.3, $\frac{1.4\ (\Delta K)}{K} = \frac{\Delta P}{P}$. Hence the maximum percentage error in $P_{n,m}$ is

$$\frac{\Delta P}{P} \simeq 2.8\ \Delta R \left[\frac{1}{X_n - X_j} + \frac{1}{Z_n - Z_j} \right] \qquad (3.21)$$

where ΔR is the error in reading on the enlarged image.

Now if $\frac{\Delta P}{P} = 0.1$ and $\Delta R = 0.1$ mm on the enlarged film image

then $0.1 = 0.28 \left[\frac{1}{X_n - X_j} + \frac{1}{Z_n - Z_j} \right]$.

Then since $X_n - X_j \geq 2.9$ mm is of the order of magnitude for $X_n - X_j$ at the earlier times, $Z_n - Z_j$ must be greater than 10 mm. On the two shots analyzed to obtain $Z_n - Z_j \geq 10$ mm, α had to be greater than 10 degrees. On the other hand, α was kept less than 20 degrees to keep the ΔX and ΔZ intervals used in the differentiation by differences process reasonably small.

Determination of the projected position of the particle for each frame was accurate to $\pm$ 1 ft. The maximum correction factor for distance due to the displacement of the bomb from the plane of measurement (Fig. 3.18 and Fig. 3.19) was 6 per cent for Shot 1 (first trail) and 1 per cent for Shot 4 (third trail).

Finally, to obtain the pressure-distance curve at constant times the system depended upon the peak pressure-distance measurements from the shock velocity data. Thus, the error in this data, although it is small, is carried over and will add to an uncertainty in the pressure-time results.

The pressures obtained using this particle displacement technique have a maximum error of approximately 10 per cent. Since the highest pressure on each curve in Fig. 3.24 and Fig. 3.25 was taken from the shock velocity data, the first part of any of the pressure-time curves determined is much more accurate than the 10 per cent figure quoted and is accurate to 2-3 per cent.

Although there are no other free-air pressure-time measurements with which to check the particle displacement data, the pressure-time curves of Shots 1 and 4 have been scaled and compared to give some indication of their overall validity. Figure 4.13 shows that the agreement between the curves for the two shots is quite good.

The disagreement between the peak shock overpressure results based on measured particle velocities as compared with those based on shock velocity measurements (see Secs 3.3.5 and 3.3.6) can be readily understood in view of the facts that the measurement of distance from the burst to a point contained a maximum uncertainty of very nearly 2 ft and that the speed of the camera system used was too

slow to obtain an adequate number of measurements to permit statistical smoothing of random errors in the particle velocity determination. In the shock velocity method random errors are minimized by the smoothing process involved in fitting a polynomial to the data. The time resolution of the system has been found adequate for the shock velocity measurements.

On the other hand, Eq. 3.18, correlating particle velocity with pressure, is based on the Rankine-Hugoniot shock conditions and applies only to the peak, instantaneous particle velocity immediately behind the shock front. A system having better time resolution, therefore, would be necessary to obtain adequate data in a sufficiently short period of time so that a smoothing technique could be applied. Without smoothing, as in the case at hand, the maximum uncertainty of 2 ft in the distance moved by a particle in the time elapsed between two successive frames of the film leads to a maximum uncertainty in the measured particle velocity of 10 per cent. An error of this magnitude in turn could lead to an error in calculated peak overpressure of as much as 70 per cent.

A film exposure rate of 1000 frames per second with a space resolution of $\pm$ 1 ft is estimated to be just adequate to obtain reasonably reliable peak shock overpressures based on particle velocity measurements. The term "reasonably reliable" is used because with the high space-time resolution afforded by the system proposed, it is believed that it would be possible to discern the effect on acceleration which would arise from the mass of the smoke particles being greater than that of air molecules, to which Eq. 3.18 applies. Only a "reasonably reliable" measure of the desired particle velocity could, therefore, be obtained.

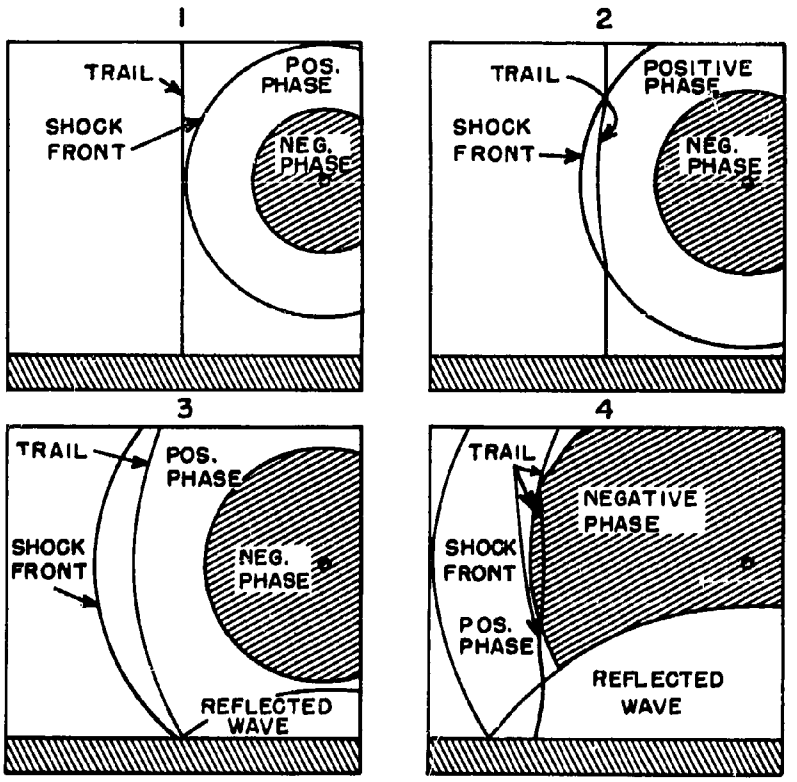

1: TRAIL JUST BEFORE ARRIVAL OF SHOCK
2: TRAIL JUST AFTER ARRIVAL OF SHOCK
3: BEGINNING OF REFLECTED WAVE
4: NEG. PHASE ARRIVAL AT TRAIL AND INTERFERENCE OF REFLECTED SHOCK AT BOTTOM OF TRAIL

Fig. 3.28 Effect of a Nearby Surface on Smoke Trail Particle Motion

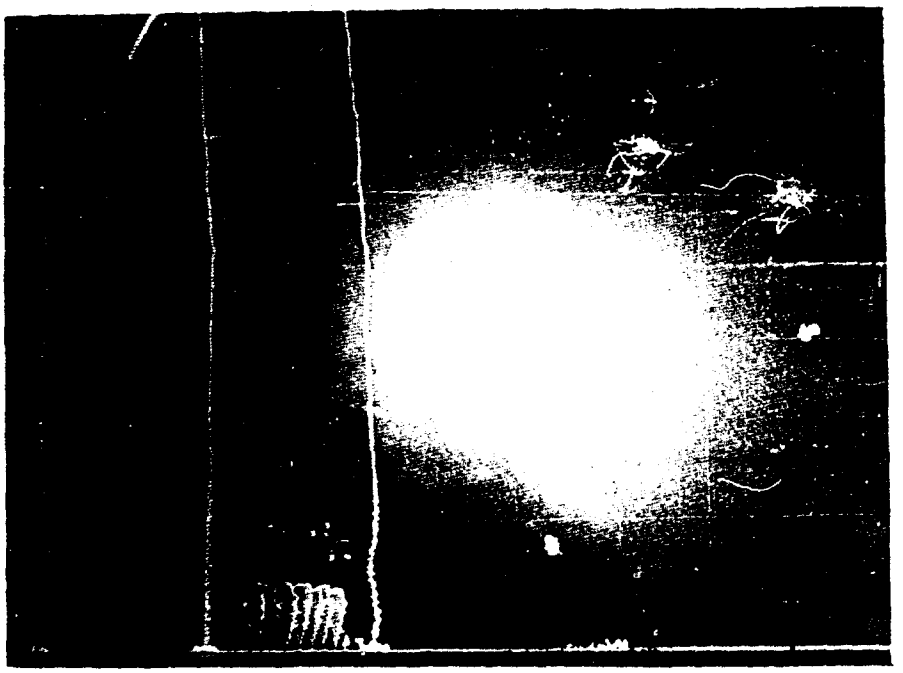

Fig. 3.29 Particle Displacement Smoke Trails Before Shock Arrival, TUMBLER 1

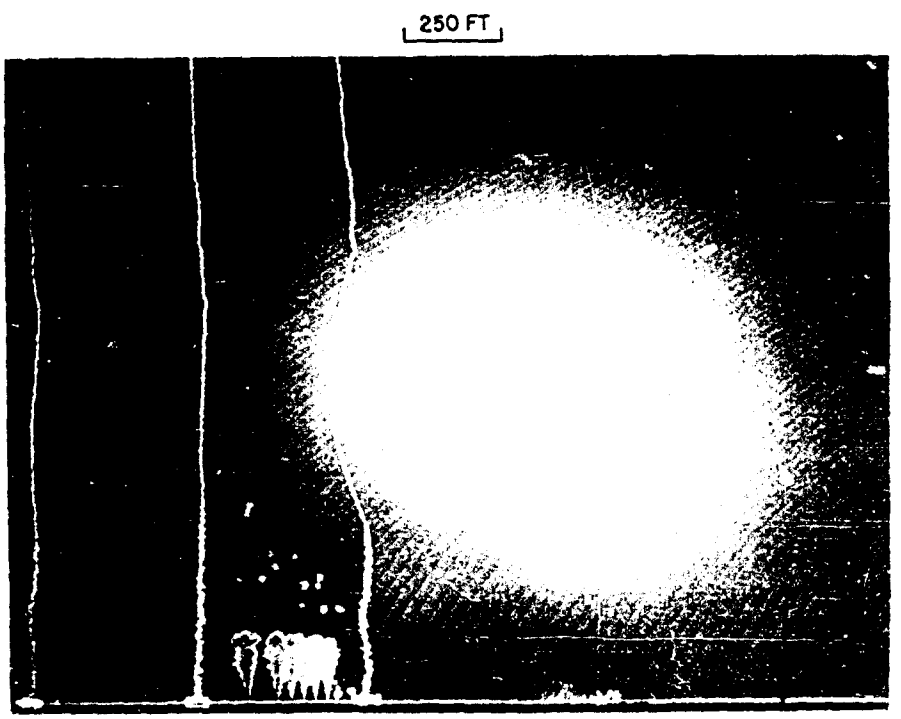

Fig. 3.30 Particle Displacement Smoke Trails After Shock Arrival, TUMBLER 1

CHAPTER 4

REDUCED RESULTS

To get an overall picture of the results obtained on this operation and to facilitate the comparison of these results with those obtained on other nuclear weapon operations, the significant data for all TUMBLER shots were normalized to 1 KT(RC) at sea level. The normalizing factors, weapon yields, and other pertinent test data are given in Table 1.1 and discussed in Sec 1.6.

4.1 GROUND LEVEL DATA

The normalized data obtained from the ground level measurements of Project 1.3 are presented in Tables 4.1 through 4.4 and shown in graphical form in Figs. 4.1 through 4.10. The blast phenomena were plotted against reduced ground range in Figs. 4.1 through 4.5 and against reduced slant range in Figs. 4.6 through 4.10.

It will be observed that in many of these figures a single curve was drawn through the data points of TUMBLER 2 and 3; this curve was the best fit that could be made by eye for both sets of data for the phenomena plotted. The identity of the normalized data for these two shots indicates the similarity of TUMBLER 2 and 3. It also confirms the validity of the model law since these two shots were fired under conditions designed to check directly the applicability of normal cube-root blast scaling laws to nuclear explosions, i.e., both TUMBLER 2 and 3 were fired in the same test area under similar ground conditions and at nearly the same scaled height, 995 and 1012 ft for 1 KT(RC). In Fig. 4.4 where reduced arrival times were plotted against reduced ground ranges the percentage accuracy in measuring time was sufficient to resolve the differences in times of arrival of the shocks because of the slight difference in heights of burst for TUMBLER 2 and 3; hence in this and some other figures, the general spread in the data resulted in separate curves being drawn for TUMBLER 2 and 3.

Inspection of Figs. 4.1, 4.2 and 4.3, in which no account of the heights of burst has been taken, shows that the TUMBLER 1 scaled data yield higher pressures and impulses than TUMBLER 2 and 3 except in the far Mach region where they all agree reasonably well. The curve for TUMBLER 4, as would be expected from its low height and high yield, falls well above the curves of the other shots at the high pressure and impulse levels and below the others at the far distances. Figure 4.4 shows the differences in shock-arrival times as measured from detonation with the shot at the lowest normalized height of burst, TUMBLER 4, showing the shortest times of arrival, and the highest burst shot, TUMBLER 3, giving the longest times. The relative heights

of the four shots again are indicated in Fig. 4.5, where TUMBLER 4 has the shortest reduced positive durations at the close-in distances and the longest durations in the far region.

In Figs. 4.6 through 4.10 heights of burst for the four TUMBLER shots were taken into account to some extent by plotting the blast phenomena against reduced slant range (i.e., reduced radial distance from the bomb) instead of ground range. The results are interesting in that on all plots except that of arrival time (Fig. 4.9), the data points for the first three shots tend to group themselves around a single curve while the points for TUMBLER 4 form a separate curve. The pressures and impulses for TUMBLER 4 are definitely lower than for TUMBLER 1, 2, and 3 indicating that if the given weapon yields are correct, TUMBLER 4 produced blast effects of lower magnitude than the preceding three shots. This decrease probably can be attributed to the influence of the low burst height with its attendant greater ground and thermal effects.

It is not clear why the reduced positive durations, Fig. 4.10, for TUMBLER 4 were greater than for the other three shots at corresponding reduced slant ranges. The time contribution of neither the precursor at the early stations nor the secondary peak, P_d, at the later stations could account entirely for the longer durations. In Fig. 4.9 it is interesting to note that although reduced arrival times were plotted against reduced radial distances, four curves resulted; the curves once again so positioned, one with respect to the other, as to indicate the differences in burst heights for TUMBLER 1, 2, 3, and 4. It is obvious from these curves that ground measurements, even when presented in the same manner as free-air measurements, are different from free-air results throughout the whole range of measurements from regular reflection region through Mach reflection region. In addition to effects which might be predicted from ideal reflection theory the presence of the ground influences the blast by such effects as energy absorption of the ground, thermal and dust effects, and localized effects from small peculiarities in the terrain.

4.2 PHOTO-OPTICAL DATA IN FREE AIR

The data obtained in free air have been reduced using the same scaling factors given in Table 1.1 that were used to reduce the ground level data of Sec. 4.1 to 1 KT(RC) at sea level.

4.2.1 Arrival Time of the Shock Wave in Free Air

The arrival time data tabulated in Tables 3.2, 3.4, 3.6,

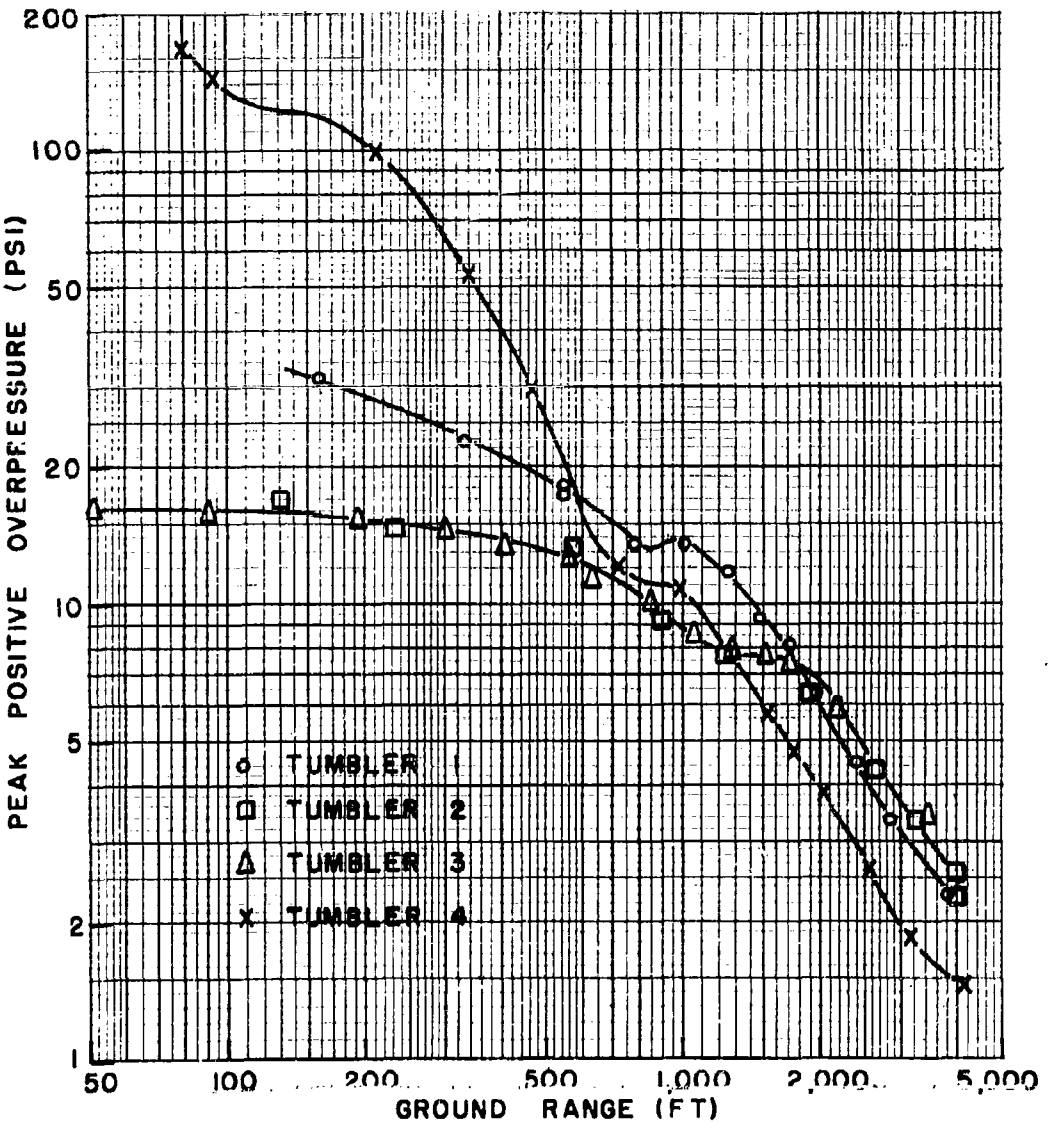

Fig. 4.1 Peak Positive Overpressure vs Ground Range, Data Reduced to 1 KT at Sea Level

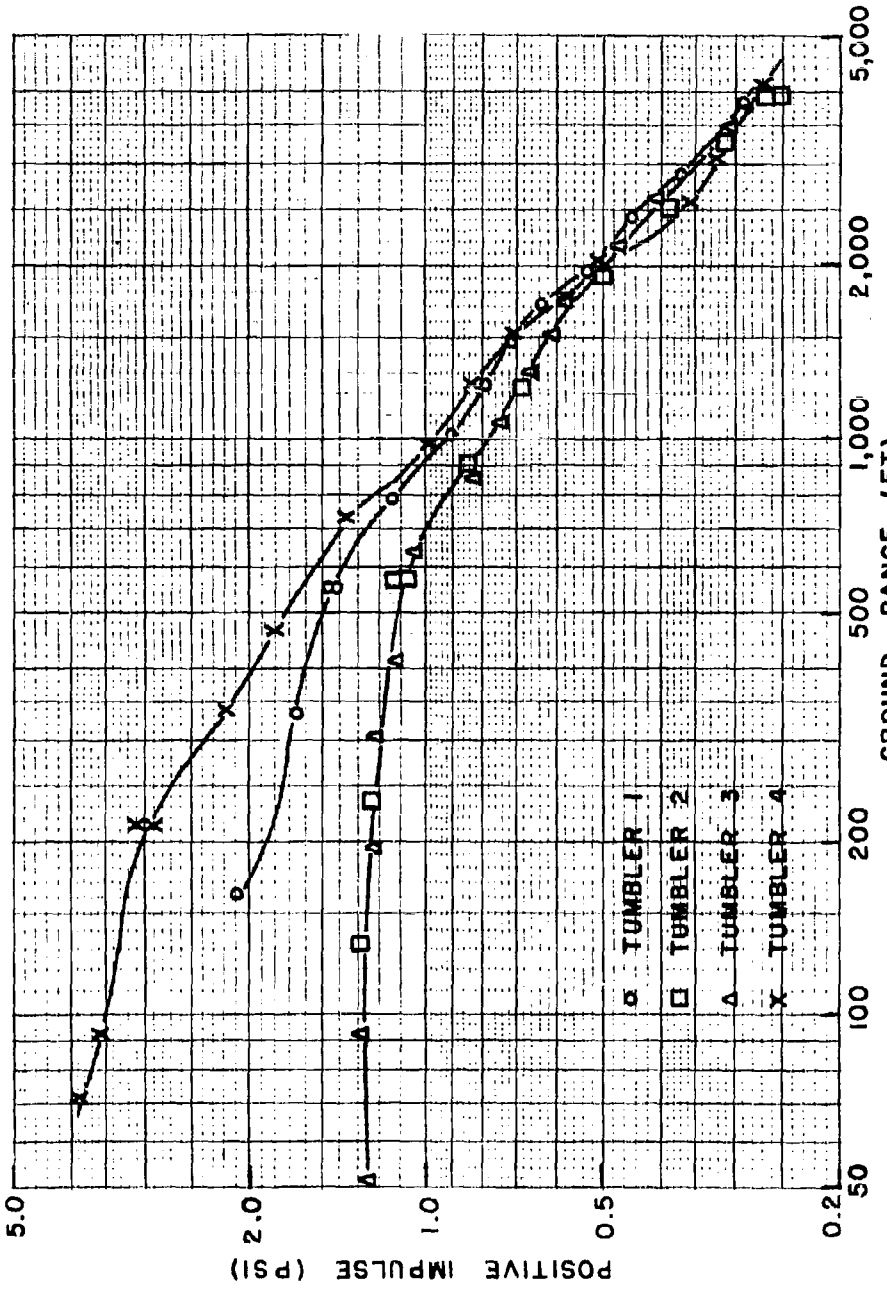

Fig. 4.2 Positive Impulse vs Ground Range, Data Reduced to 1 KT at Sea Level

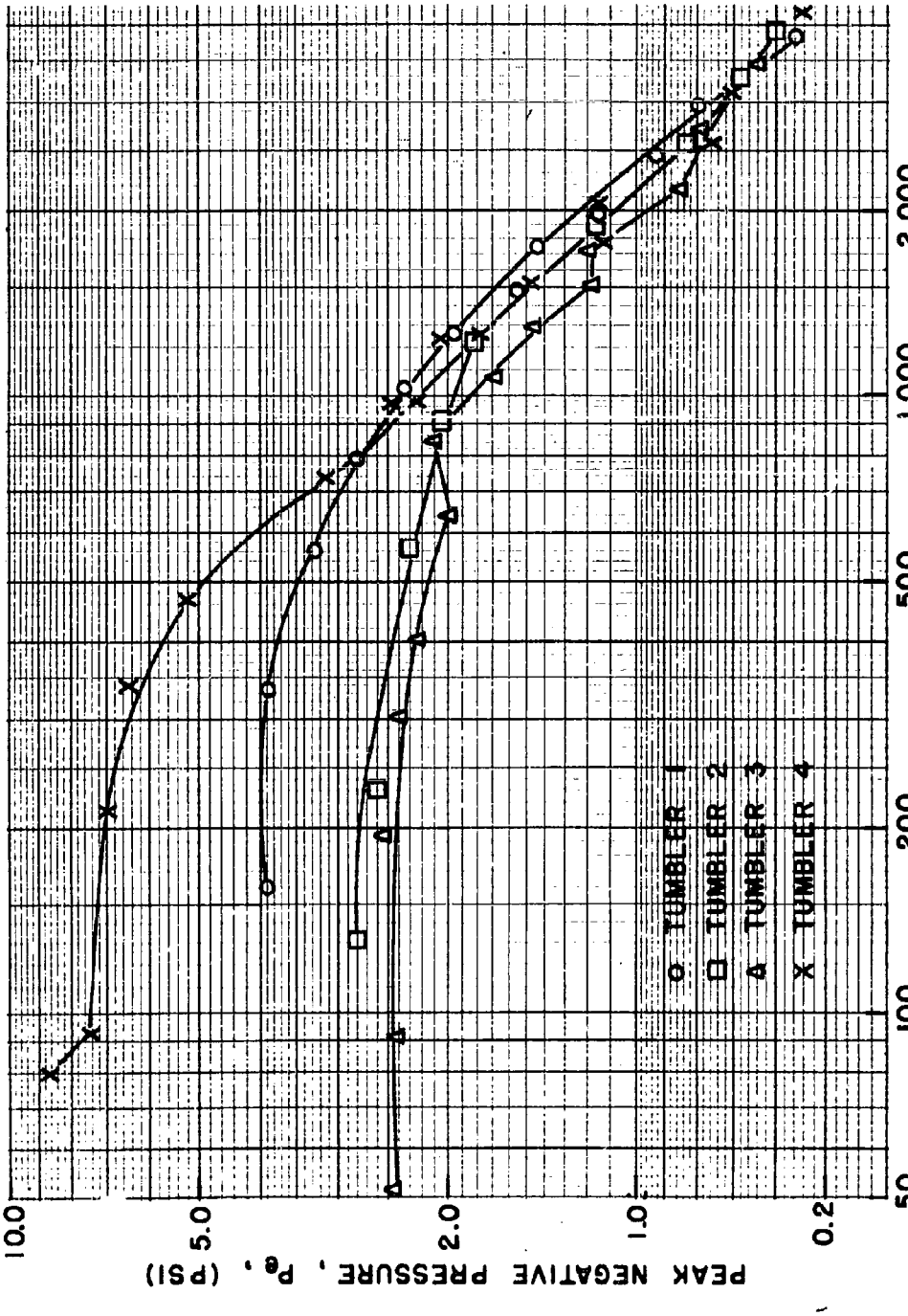

Fig. 4.3 Peak Negative Pressure vs Ground Range, Data Reduced to 1 KT at Sea Level

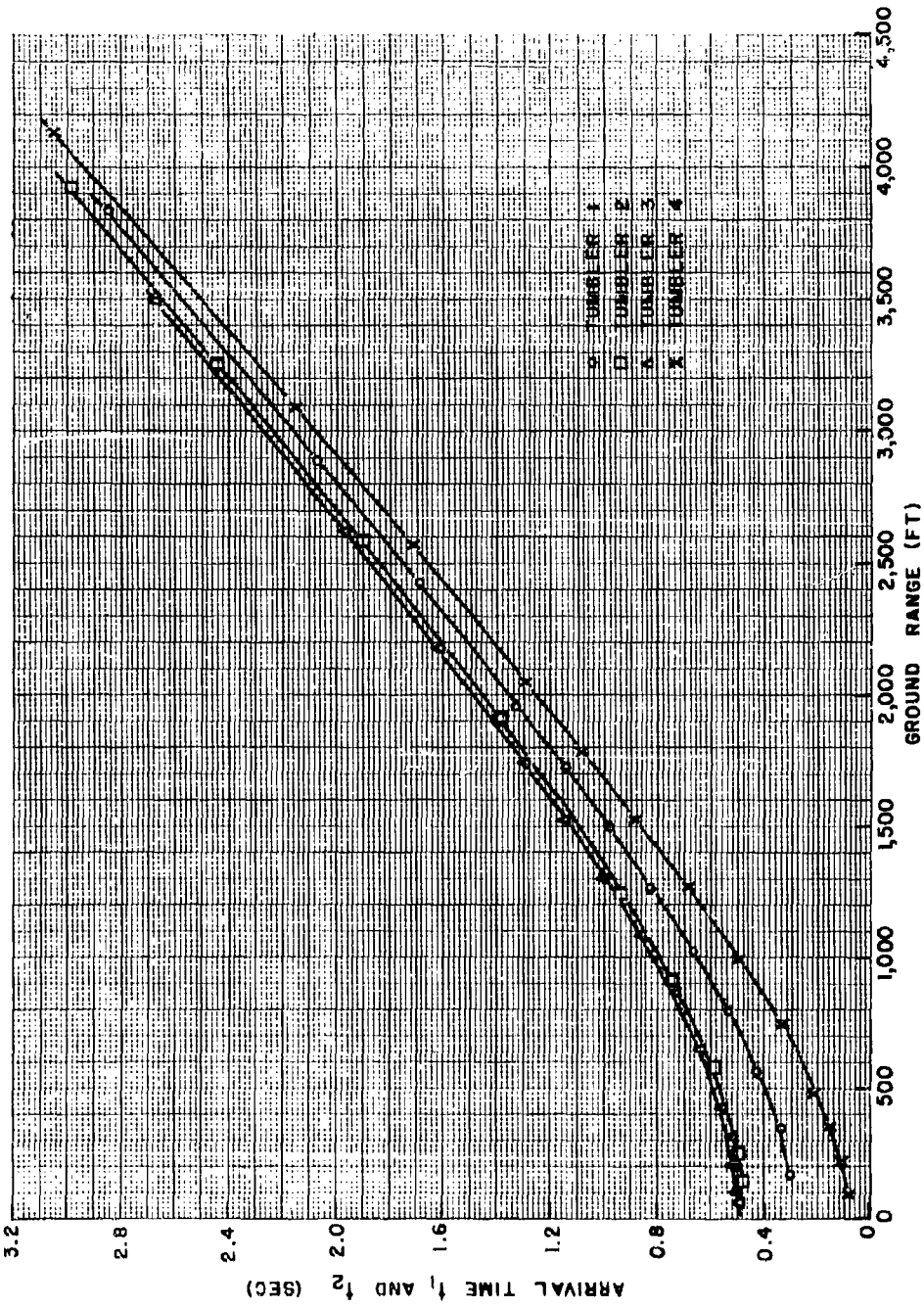

Fig. 4.4 Arrival Times, t_1 and t_2 vs Ground Range, Data Reduced to 1 KT at Sea Level

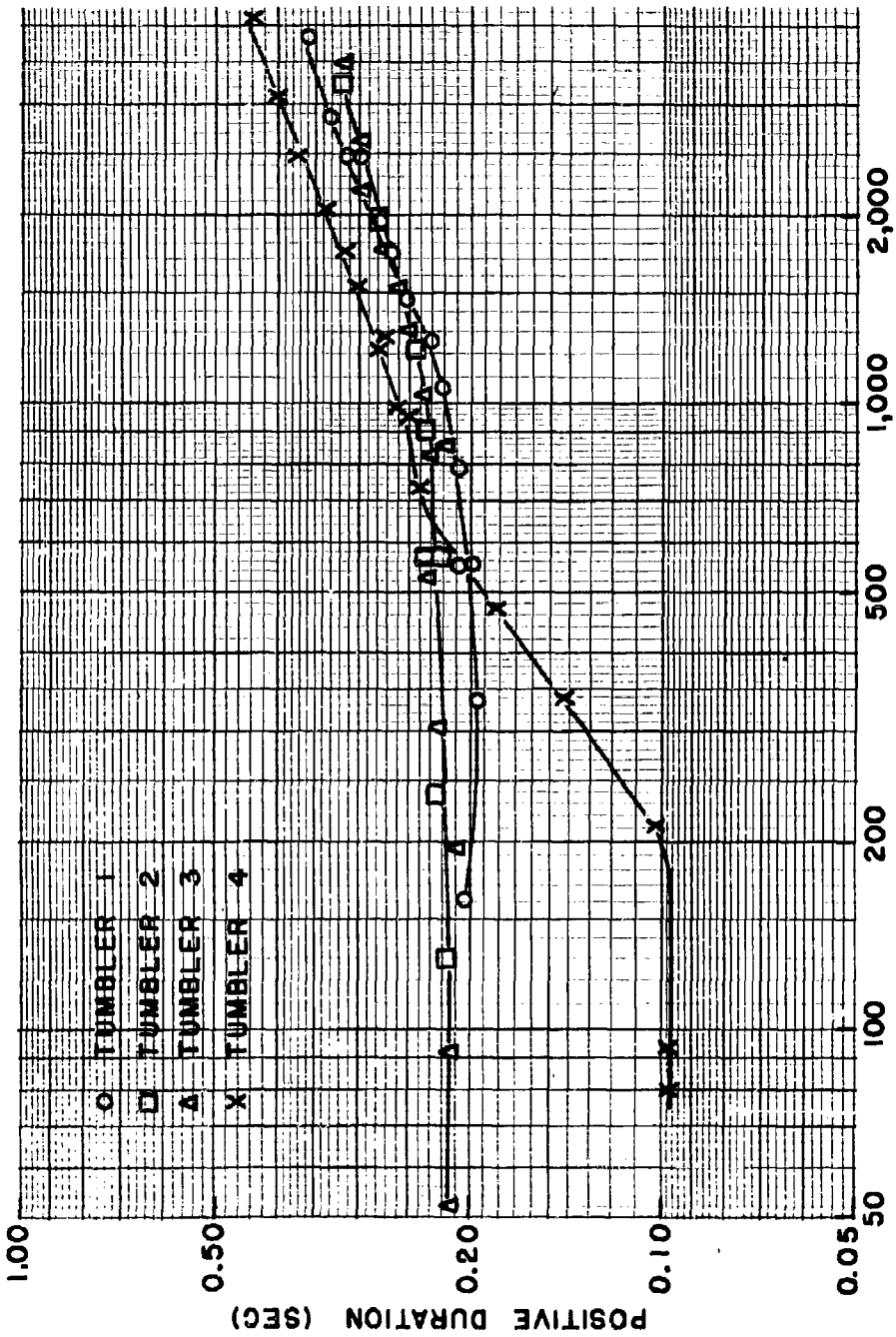

Fig. 4.5 Positive Duration vs Ground Range, Data Reduced to 1 KT at Sea Level

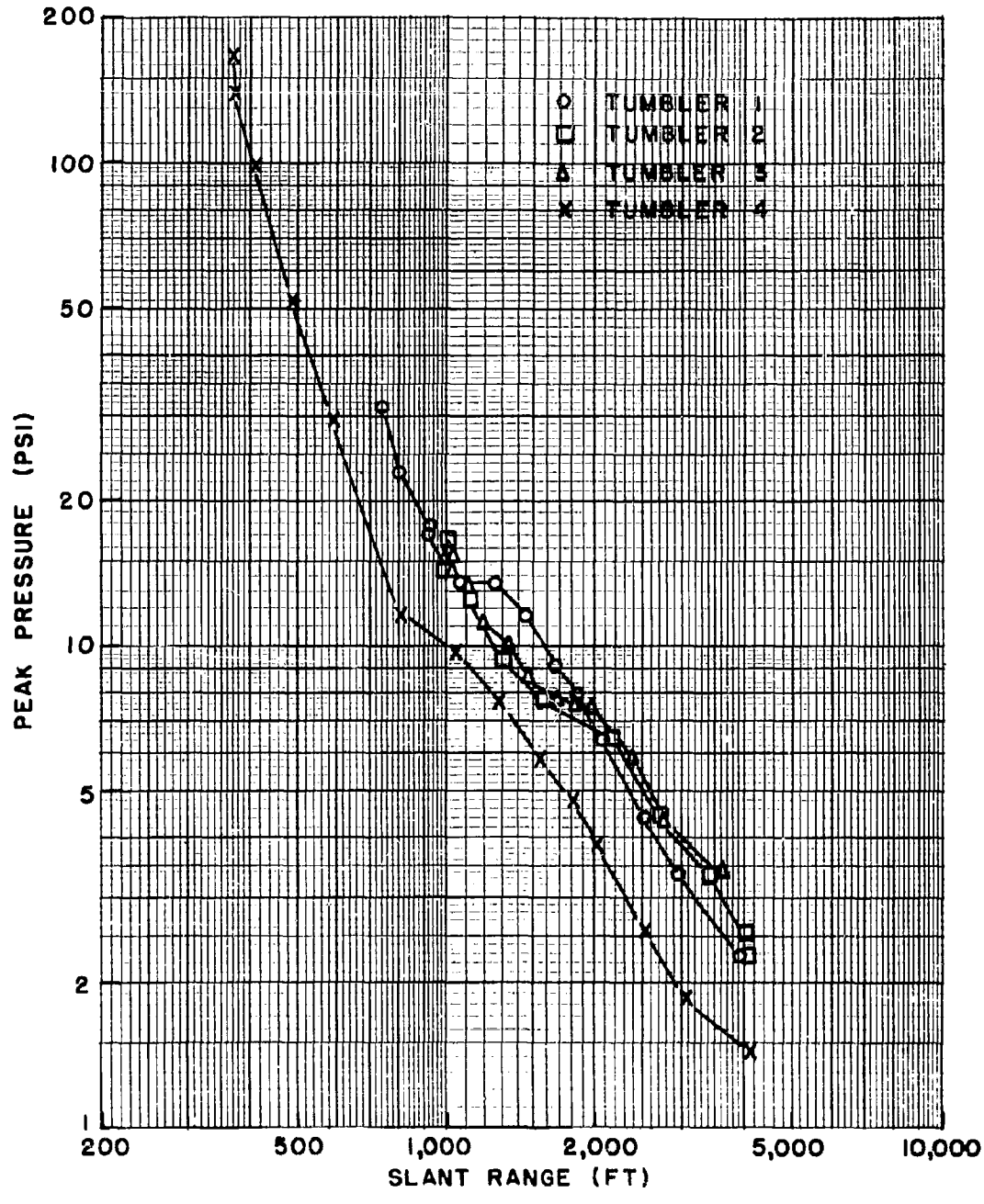

Fig. 4.6 Peak Positive Overpressure vs Slant Range, Data Reduced to 1 KT at Sea Level

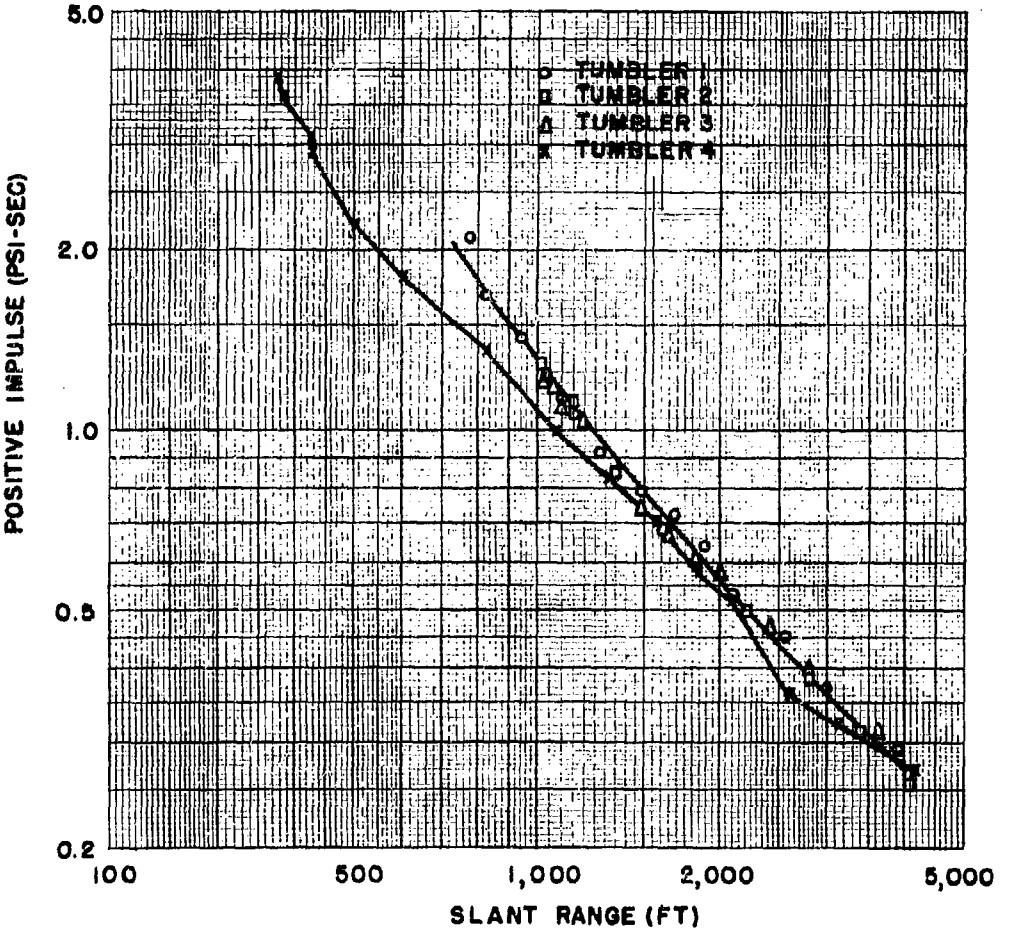

Fig. 4.7 Positive Impulse vs Slant Range, Data Reduced to 1 KT at Sea Level

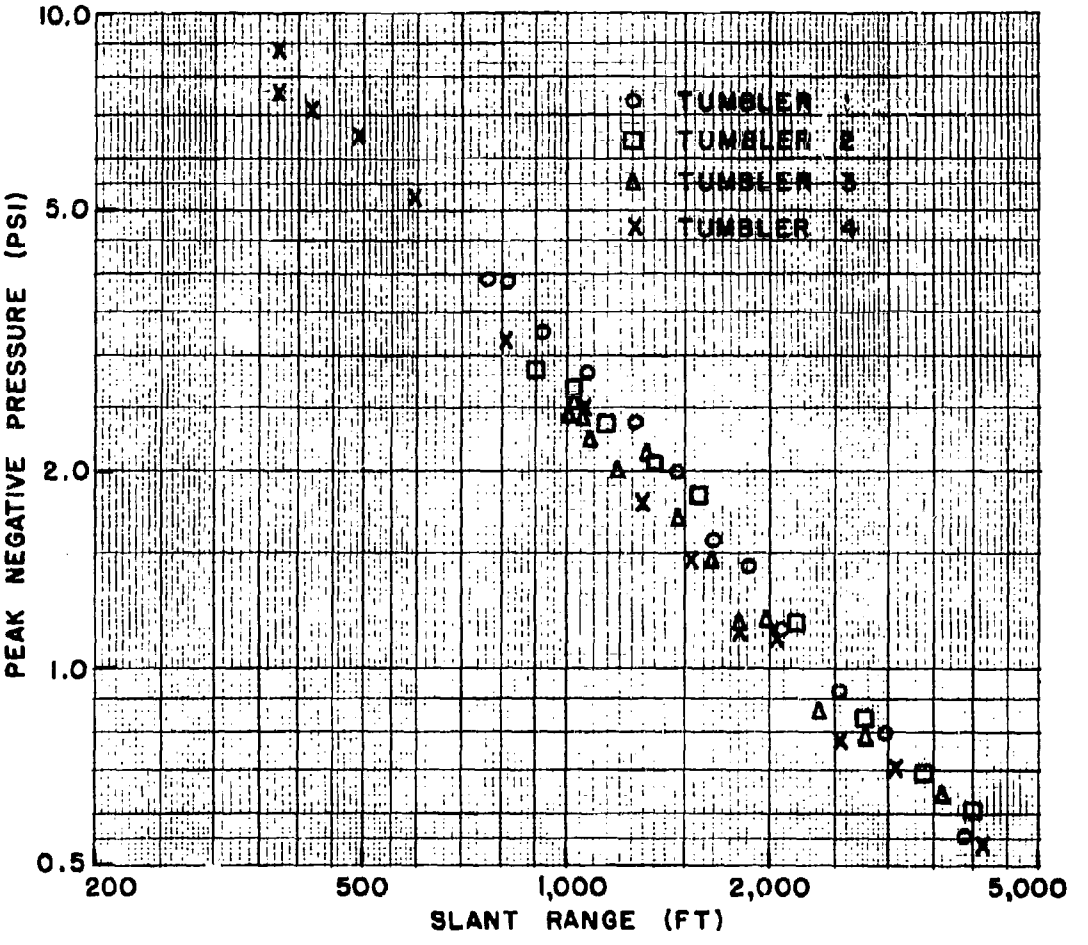

Fig. 4.8 Peak Negative Pressure vs Slant Range, Data Reduced to 1 KT at Sea Level

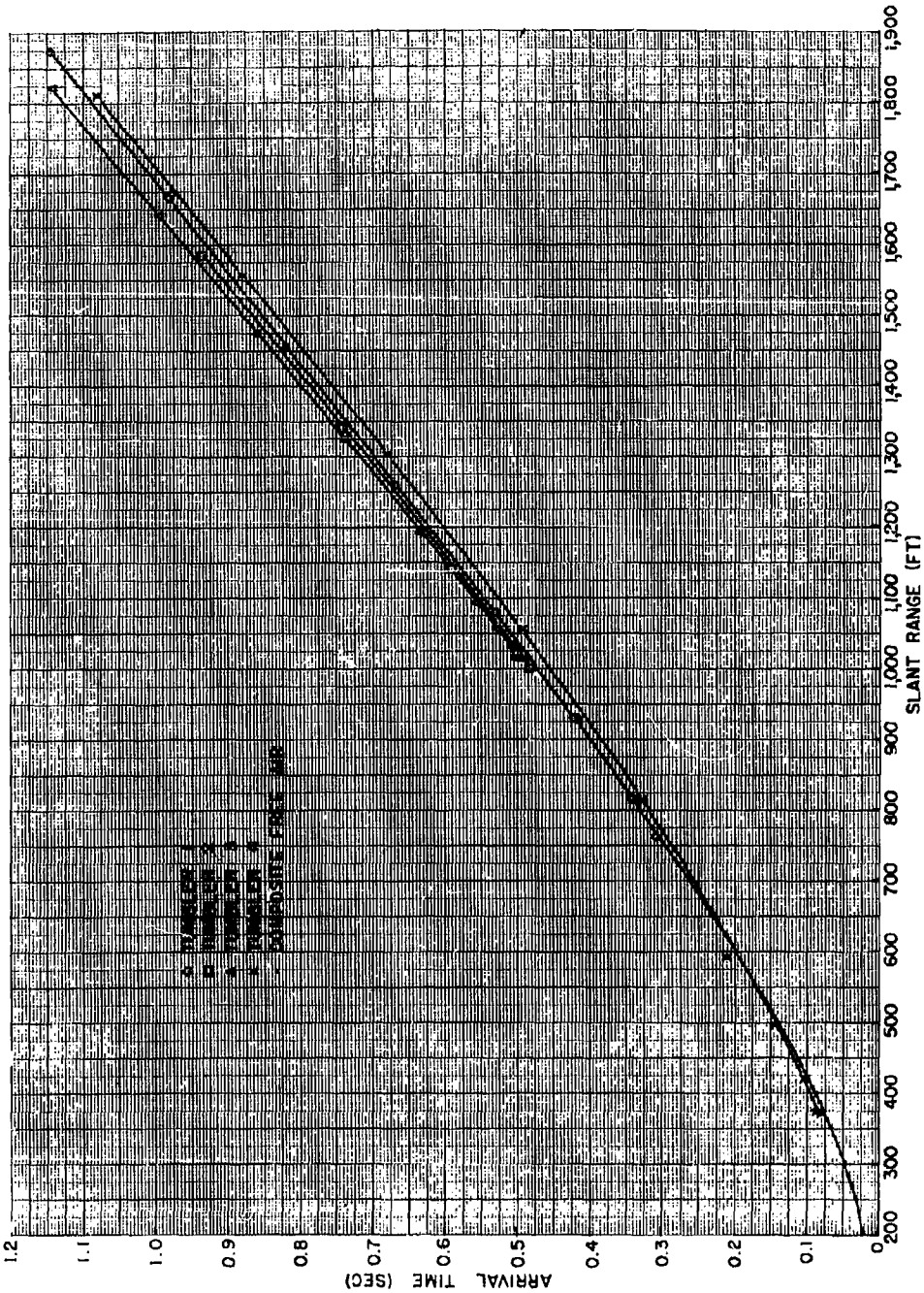

Fig. 4.9 Arrival Times, t_1 and t_2, vs Slant Range, Data Reduced to 1 KT at Sea Level

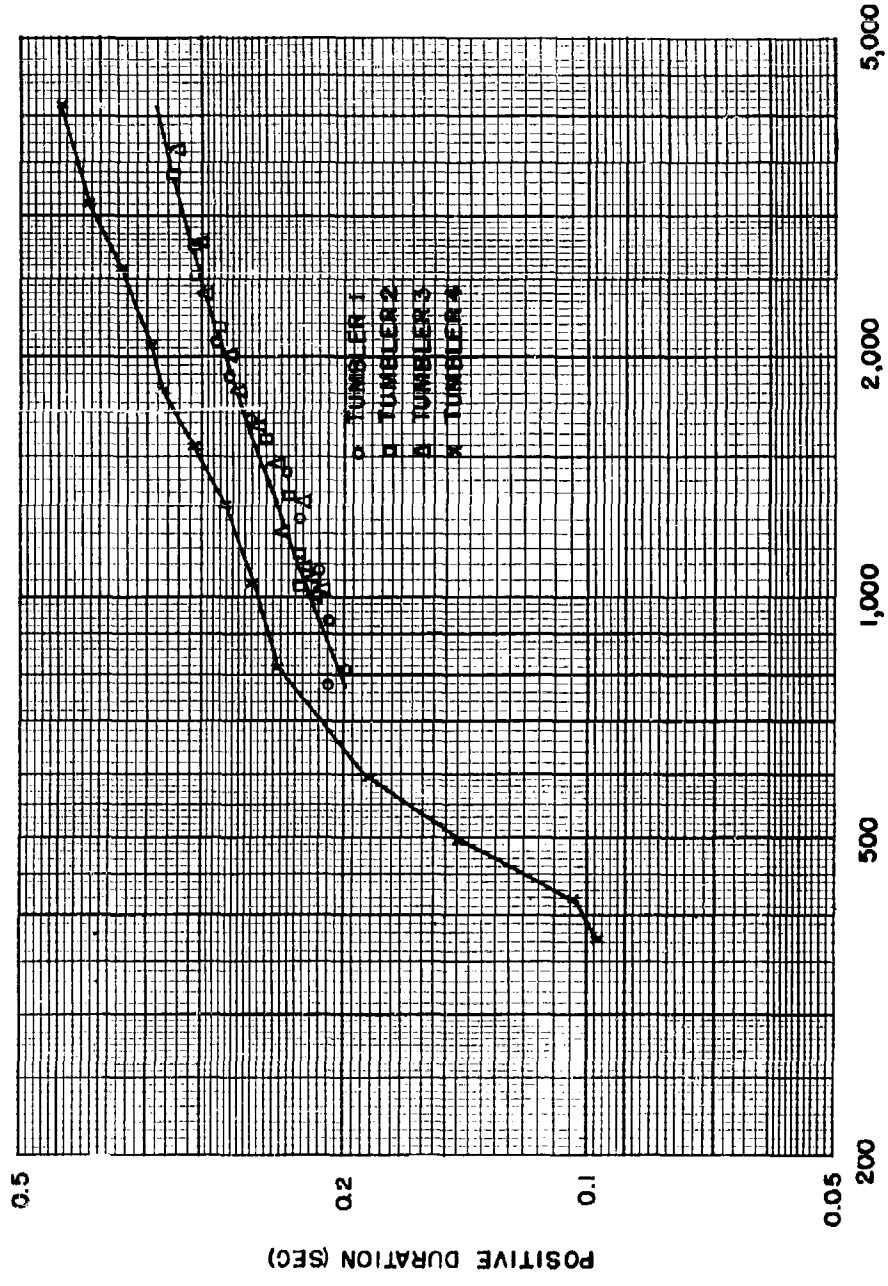

Fig. 4.10 Positive Duration vs Slant Range, Data Reduced to 1 KT at Sea Level

and 3.8 have been reduced to correspond to values that would be obtained using a weapon of 1 KT(RC) at sea level. The reduced values are given in Tables 4.5, 4.6, 4.7, and 4.8 for TUMBLER 1, 2, 3, and 4, respectively.

If it were assumed that all of the original data were equally accurate and that the radiochemical equivalents were correct, then one would expect to find that the original data, after reduction or normalization, would all fit a single smooth curve perhaps representing from henceforth the arrival time of the shock wave in free air for an air burst atomic weapon.

The reduced data appearing in the tables mentioned above have been plotted in Fig. 4.11, no attempt being made to identify any point as to shot number. Also plotted in this graph are calculated points taken from polynomials fitted to all these data. The polynomials fitting the data over the ranges indicated are:

$$t = 0.0079 - 0.1303R + 1.0153R^2 - 0.4461R^3 \text{ (From 100 to 550 ft)} \quad (4.1)$$

$$t = -0.0504 + 0.1745R + 0.4804R^2 - 0.1314R^3 \text{ (From 550 to 1200 ft)} \quad (4.2)$$

where t is in seconds for a 1 KT bomb and R is in thousands of feet for a 1 KT bomb at sea level (see Table 1.1).

As can be seen from Fig. 4.11 all four TUMBLER shots scale rather well. The maximum uncertainty exists at the larger distances and later times - as would be expected since timing errors are accumulative in the representation of the data in this form. The maximum uncertainty in time was found to be 1 per cent while that for distance is slightly less than 0.1 per cent. Out to a reduced distance of about 582 ft (i.e. for 1 KT(RC) at sea level) all four shots are represented and the very small uncertainty existing is not evident. Beyond a reduced distance of 735 ft only TUMBLER 1 and 2 are represented and the uncertainty is observable in this region. It is interesting to note that although all the data of TUMBLER 2 consistently fall below those of TUMBLER 1, they agree within the range of uncertainty given above. These uncertainties are much smaller than the uncertainty of 10 per cent (2.15 per cent reduced) which was given to the assigned radiochemical kilotonnages.

It should be emphasized that the error or uncertainty pointed out above is not a simple error in fitting to absolute time or zero distance. It is a compound error caused by errors in time calibration, space calibration, and reduction factors. Fortunately they are small (see Sec 3.3.8).

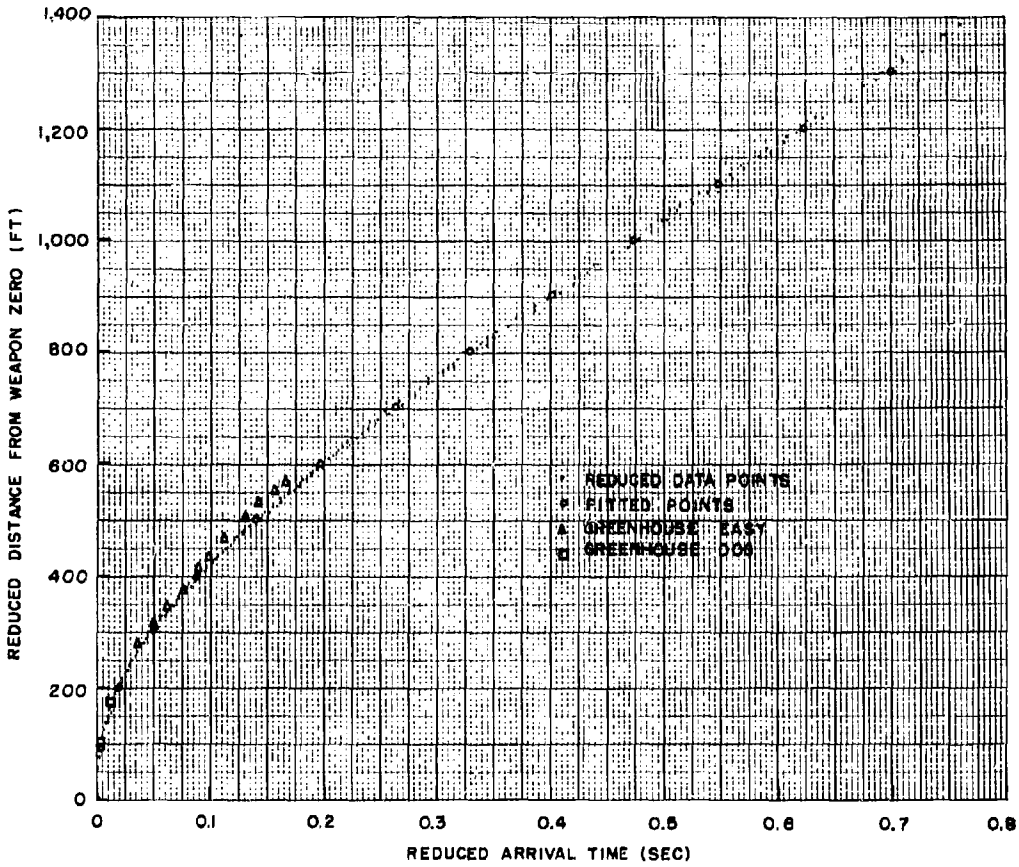

Fig. 4.11 Composite Reduced Free-Air Arrival-Time Curves, TUMBLER 1-4

Several data points picked at random from Shots Dog and Easy of Operation GREENHOUSE have been tabulated in Tables 4.9 and 4.10 and are also plotted in Fig. 4.11 for comparison.

It is clearly evident that Shot Easy arrival time data do not fit the TUMBLER data. If the kilotonnage equivalent (46.7 KT(RC)) and arrival time data for this shot be assumed correct, then a distinct difference appears to exist between a low tower burst and a free air burst, or the scaling laws correcting for altitude are inadequate, or the weapons were substantially different. Other reasons such as the effect of the additional mass of the tower and the existence of ar

additional adiabatic pulse as an explanation of GREENHOUSE have been discussed to some extent in references (24) and (2). The authors are of the opinion that the Easy arrival time data are nearly as reliable as those obtained on Operation TUMBLER. They feel that the scaling laws are trustworthy, especially in view of the TUMBLER results, and fail to understand how the proximity of the burst to the ground might have such a significant effect on the arrival time data in the free-air region.

4.2.2 Pressure-Distance in Free Air

The pressures and corresponding distances found in Tables 3.3, 3.5, 3.7, and 3.9 have been scaled to 1 KT(RC) at sea level and are presented in Tables 4.11, 4.12, 4.13, and 4.14. Pressure vs distance reduced to 1 KT at sea level is plotted for all four TUMBLER shots in Fig. 4.12.

On the same graph, pressures calculated from the composite free-air arrival time equations (Sec 4.2.1) are plotted as given in Table 4.15. This pressure-distance curve may be considered as a standard for air dropped weapons representing the best available measurements to date for the free-air region down to the 10 psi pressure level. Uncertainties in the data upon which the curve is based were minimized in all respects and a figure of accuracy of 2 per cent is judiciously assigned. This figure contains a "safety factor" of approximately 1/3 and is considered by the authors to be highly reliable. Values of pressure below 10 psi are considered to be less reliable and should be used with caution.

In agreement with the trend shown in the composite arrival time curve, Fig. 4.11, the GREENHOUSE pressure data given in Table 4.16 and plotted in Fig. 4.12 diverge from TUMBLER data towards the low pressure end of the curve. Reasons for this divergence are not readily forthcoming, as was discussed in Sec 4.2.1.

In the region between 300 and 600 psi on the reduced composite pressure-distance curve it was found that the overpressure, P, is related to the radial distance from the burst, R, by $P \propto R^{-3.11}$ in terms of psi and thousands of feet. The values of the exponent for GREENHOUSE, Shots Dog and Easy, were -2.82 (1,500 -150 psi) and -3.15 (10,000 -1,500 psi), respectively[24]. Thus at high pressures the slopes agree fairly well, as shown in Fig. 4.12.

4.2.3 Pressure-Time in Free Air

Pressure-time measurements based on the particle displace-

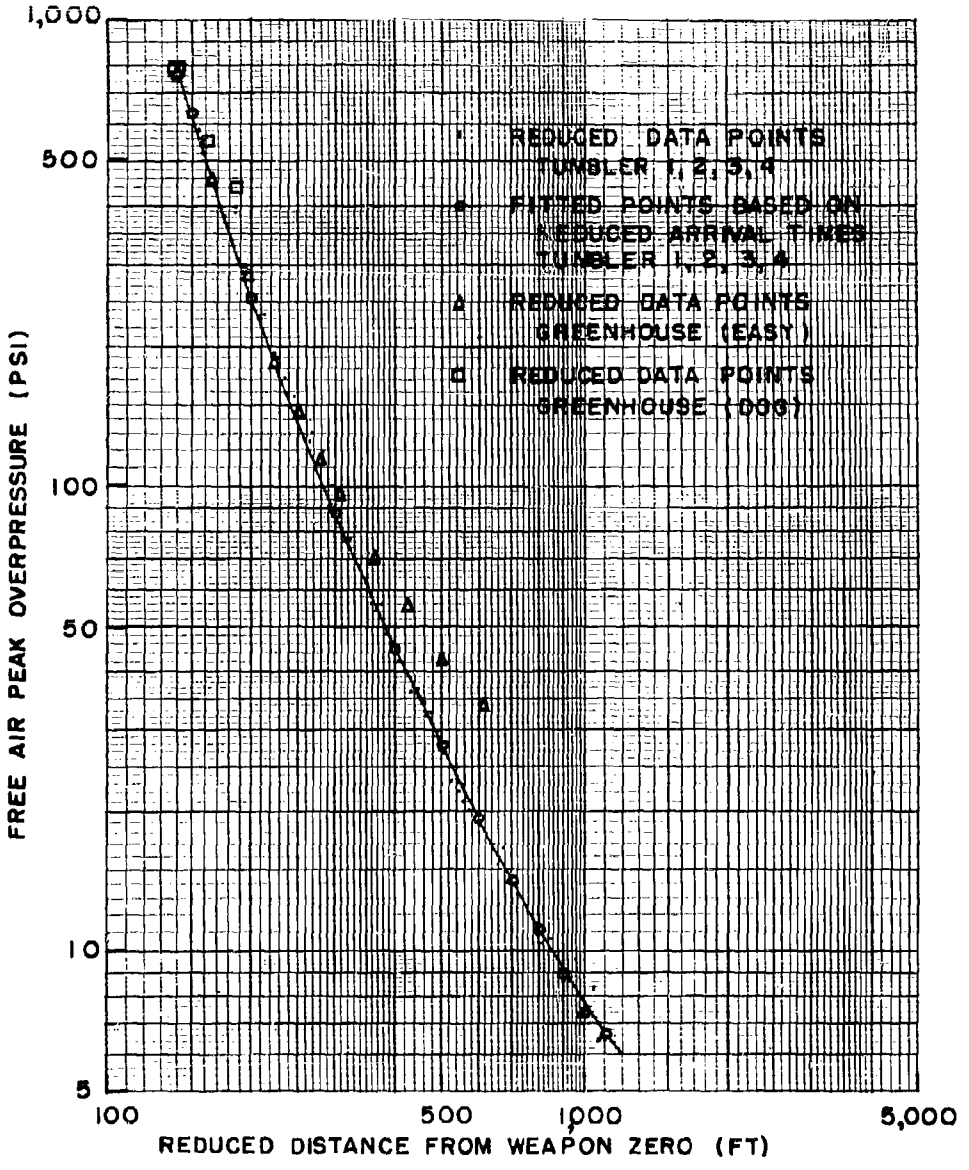

Fig. 4.12 Composite Reduced (1 KT(RC) at Sea Level) Free-air Pressure-Distance Curve, TUMBLER 1-4

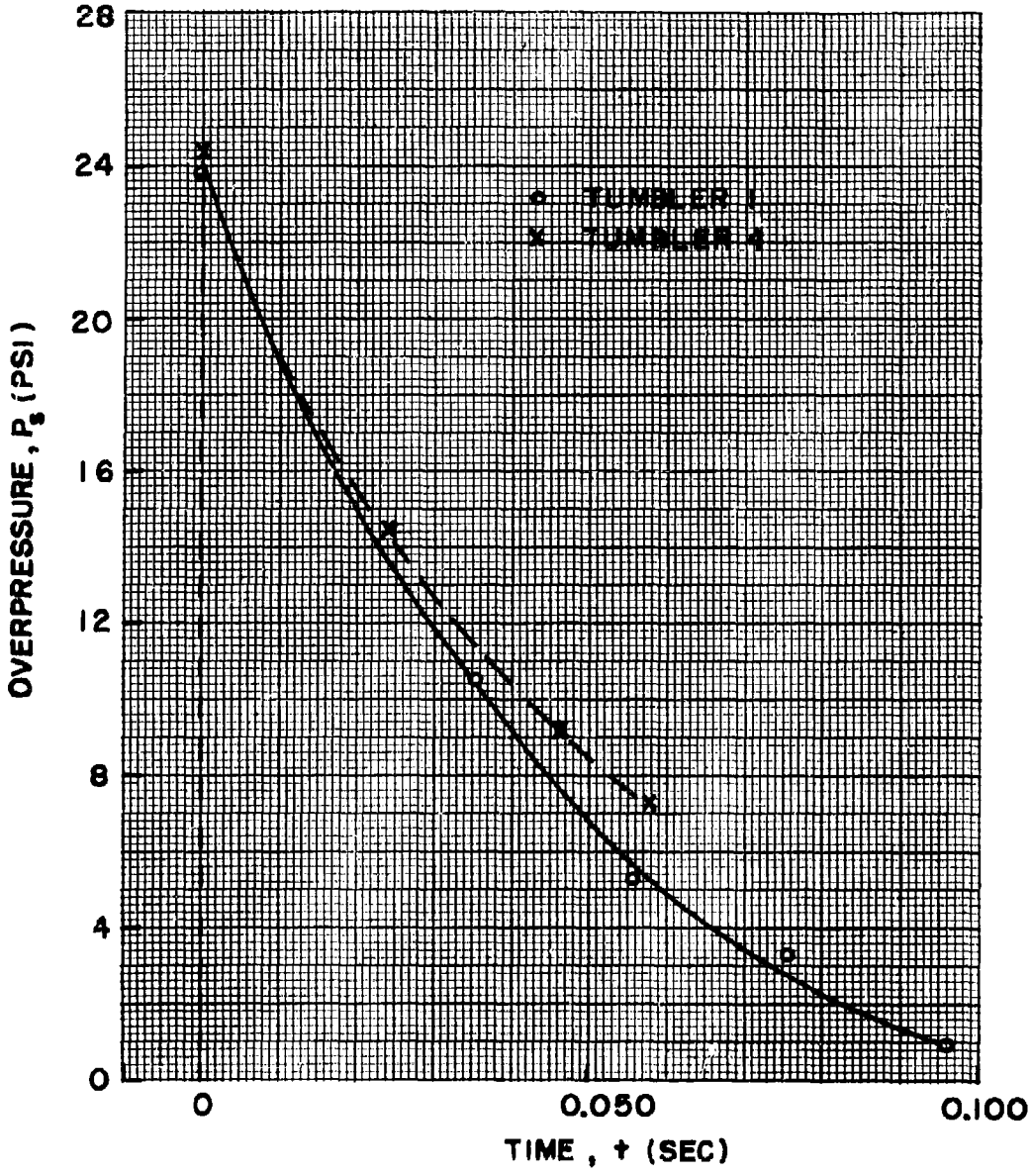

Fig. 4.13 Reduced p vs t for TUMBLER 1 and 4 at a Reduced Distance of 541 ft for 1 KT(RC) at Sea Level.

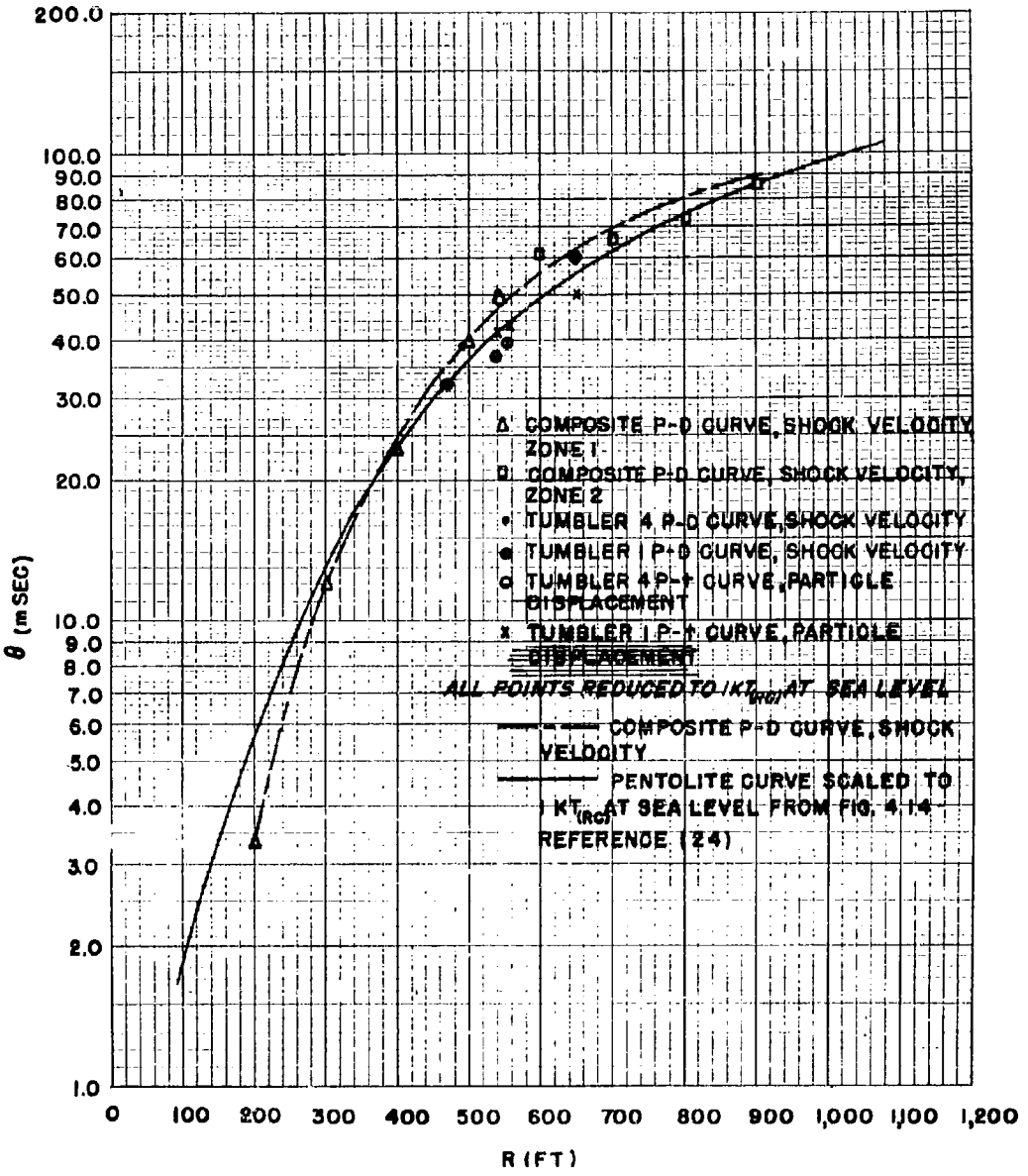

Fig. 4.14 θ vs Distance Reduced to 1 KT(RC) at Sea Level (Free Air)

ment method were obtained in particular at 575 ft on Shot 1 and at 1550 ft on Shot 4 so that when reduced to 1 KT(RC) at sea level, a comparison between the two might be made. On the reduced scale, both the above distances correspond to a distance of 541.1 ft. The pressures for corresponding reduced times for Shots 1 and 4 are given in Table 4.17. Data from both tables are plotted in Fig. 4.13 for comparison purposes.

The superposed curves shown in Fig. 4.13 can be used as a means for determining a qualitative estimate of the accuracy of the particle displacement method. It is encouraging to note the agreement with regard to reduced decay parameter (41.5 vs 46.5 msec) and the general similarities of the curves. It should be pointed out, nevertheless, that the uncertainties (not necessarily errors) must for the present remain of the order of 10 per cent, as indicated in Sec 3.3.8. The agreement observed in Fig. 4.13 is not accepted by the authors as proof that the accuracy of the method is equivalent to, say, that of the smoke rocket shock velocity method. More experience using the particle displacement method may change this opinion.

An additional note of interest which may or may not affect the argument in the preceding paragraph is that in Fig. 4.13 the curve for Shot 4 indicates a longer reduced positive duration than for that of Shot 1. Similar indications were observed in the ground level measurements (Sec 4.1, Fig. 4.10) and may be significant.

4.2.4 Reduced Decay Parameter, θ

The values of θ have been computed by use of the method outlined in Sec 3.3.7 as applied to the composite reduced pressure-distance data from all four TUMBLER shots as given in Table 4.15. These values of θ are given in Table 4.18 and are plotted as a function of reduced distance in Fig. 4.14. The pentolite curve in Fig. 4.14 was taken from the GREENHOUSE Summary Report (Fig. 4.14, reference (24)) as scaled to 1 KT(RC) at sea level. The curve, as calculated by the method in Sec 3.3.7, is in good agreement with the pentolite curve considering that the method involves the second derivative of the shock arrival time curve, which leads to large errors in θ for small discrepancies in peak pressure.

Also given in Table 4.18 and Fig. 4.14 are the values of θ reduced to 1 KT at sea level for TUMBLER 1 and 4 as obtained from the free-air pressure-time curve by the particle displacement method and from the individual pressure-distance curves obtained by the shock velocity method. (See Sec 3.3.7). These points are in good agreement with the pentolite curve considering the limits of accuracy.

CHAPTER 5

DISCUSSION OF RESULTS

5.1 HEIGHT-OF-BURST COMPARISONS

Height-of-burst data for TUMBLER were obtained from Fig. 4.1, as tabulated in Table 5.1. From such data height-of-burst charts, i.e., plots showing the distance along the ground at which certain pressure levels occurred, can be presented in several ways, three of which are given in this report:

(a) Drawing height-of-burst curves based principally on the data obtained on TUMBLER plus data obtained from a surface shot (Operation JANGLE). (Fig. 5.1),

(b) Plotting TUMBLER data on curves calculated from recent high explosive (small-charge) experiments[15] (Fig. 5.2), and

(c) Plotting TUMBLER data on curves traced from reference (16) which gave the official values up to the time of this operation (Figs. 5.3 through 5.7).

5.1.1 Height-of-Burst, TUMBLER and High Explosive

Figure 5.1, which is based almost entirely on TUMBLER data as extended by JANGLE data[12], shows that down to the 12 psi pressure level the optimum height of burst over the Nevada Proving Grounds is zero (ground level) if the effect of shadowing by structures and irregular terrain is ignored. As the pressure level decreases, the empirical optimum height of burst for 1 KT(RC) sea level, H'_{op}, can be characterized by the relation

$$H'_{op} = \frac{19,890}{14.7 + p}, \qquad (5.1)$$

where $3 < p < 12$ if H'_{op} is in reduced feet and p is the desired overpressure level in pounds per square inch. For comparison, this relation and another, based on one given by Hartmann and Kalavski[15] for the optimum height of burst of pentolite over concrete, are also plotted on Fig. 5.1 and tabulated in Table 5.2. Although casual inspection of these two optimum height-of-burst relations, as superposed on the conventional height-of-burst curves, shows a higher optimum height of burst for nuclear weapons, this difference is likely to be misleading. To see this more clearly, Fig. 5.2, which gives height-of-burst curves

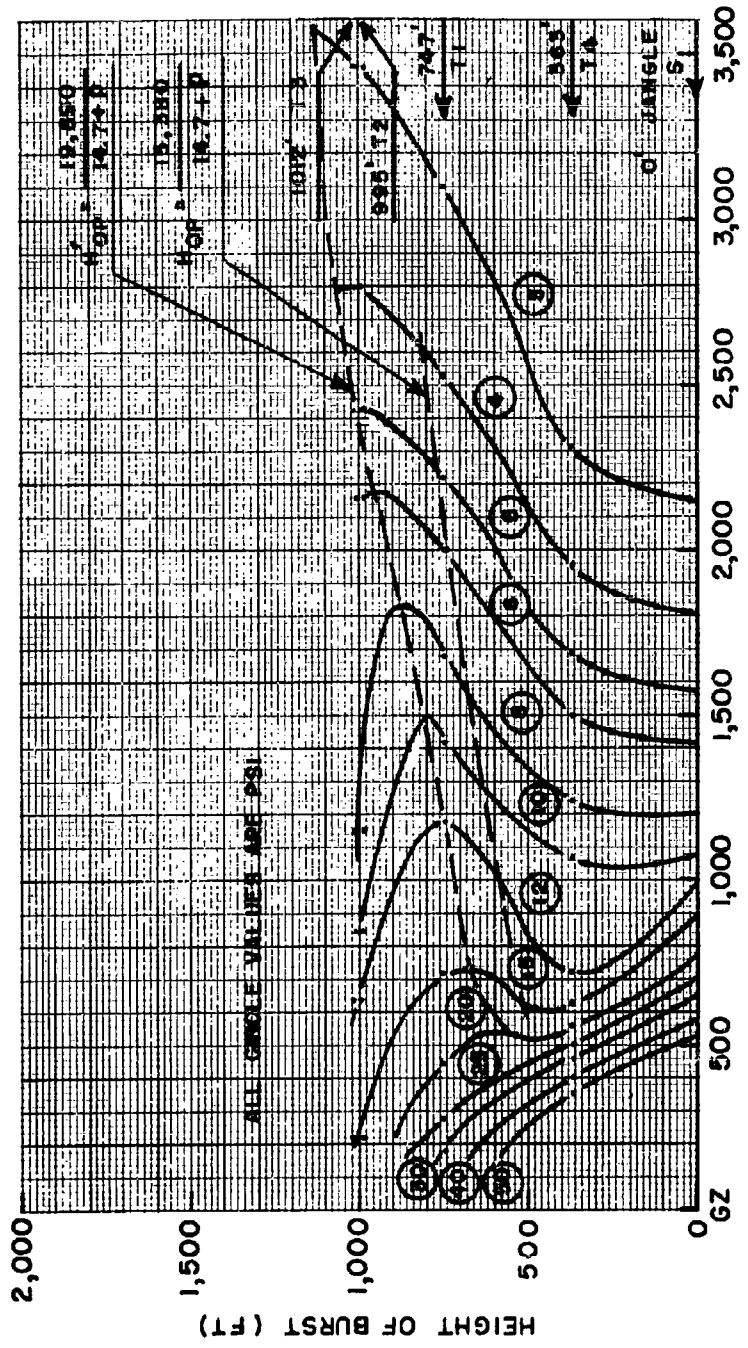

Fig. 5.1 Height of Burst vs Horizontal Distance for 1 KT(RC) Bomb.
Curves based on TUMBLER Data.

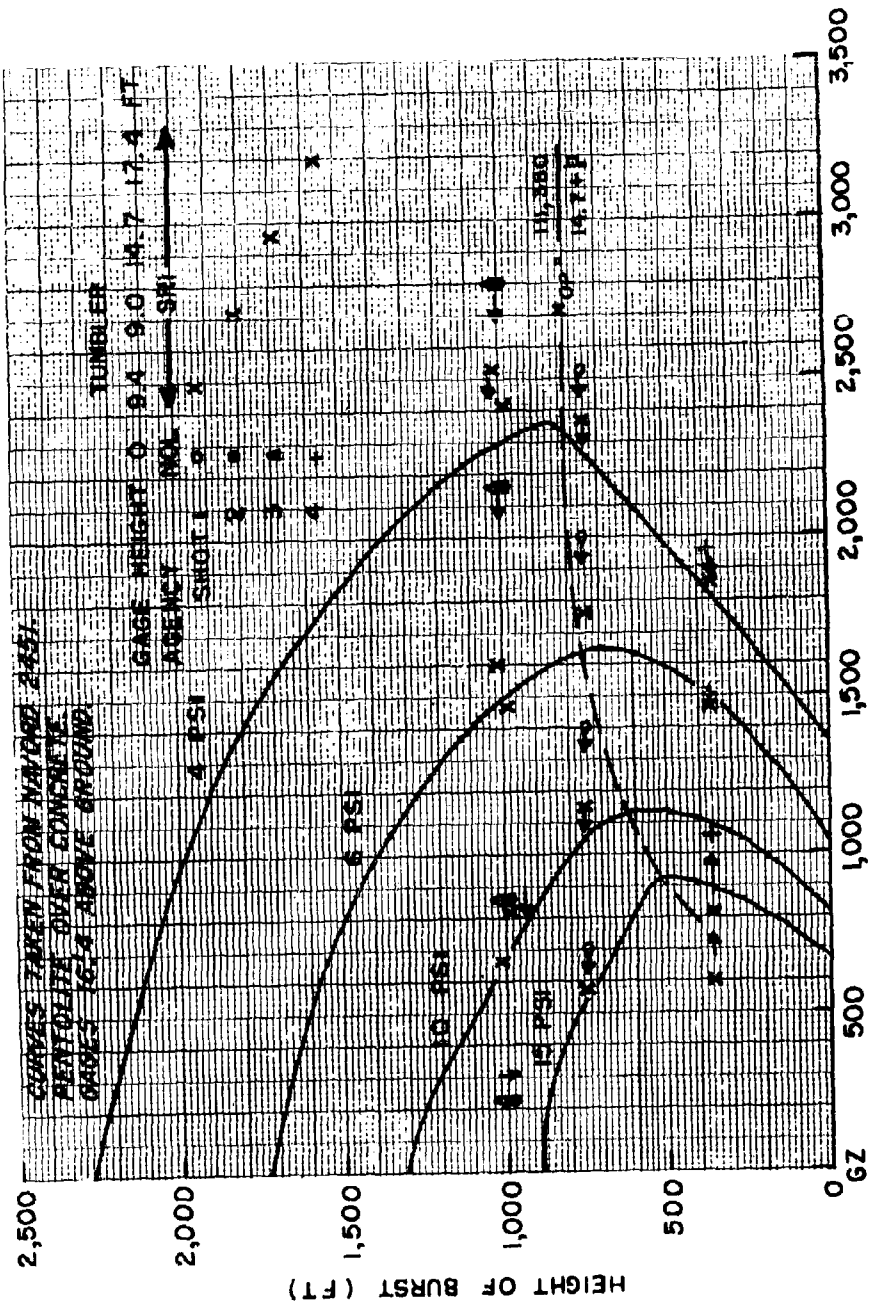

Fig. 5.2 Height of Burst vs Horizontal Distance for 1 KT(RC) Bomb - Comparison with High Explosives and Effect of Gage Height

for pentolite[15], should be consulted. On these high explosive height-of-burst curves are plotted the TUMBLER data collected at ground level by the NOL (Project 1.3) and the TUMBLER preliminary data collected on towers by the SRI (Project 1.2)[13] (See also Table 5.3). As was pointed out in reference (15), the high explosive data were measured with gages close-to but not flush-with the ground. When the mean height of the sensitive area of these gages is scaled to 1 KT(RC), it indicates that the resulting HE data should be compared with measurements made 16.4 ft above the ground. The SRI data used for comparison were measured at 10 ft above the ground on Shots 1 and 2, which scaled to 9.4 and 9.0 ft, and at 50 ft on Shots 3 and 4, which scaled to 14.7 and 17.4 ft. It can be seen from this figure that the appropriate tower data* check the HE data much more closely than the ground level data, except on Shot 4 where they are similar or where the ground level checks a little closer, such as at the 10 psi level. The conclusion, therefore, is that the two relations for H_{op} plotted on Fig. 5.1 represent the optimum height-of-burst in one case for gages flush with the ground (Eq. 5.1) and the other for gages at a reduced height of 16.4 ft. Furthermore it indicates that, except under the conditions of Shot 4 where the precursor disturbed the blast appreciably, the HE and nuclear height-of-burst data scale satisfactorily.

One serious difference in the shapes of the high explosive and nuclear height-of-burst charts arises from the tie-in points used for the zero height-of-burst. It can be seen from the Operation

---

* The reader may justifiably object to using NOL ground data with SRI tower data, since as is mentioned elsewhere in this report, the SRI data differed from the NOL data on the ground by about 7 per cent. However, the SRI data available at this writing were only preliminary, and it was desired to use as much final data as possible in this presentation. As a check, SRI preliminary data on the ground level reduced in the same manner as the other data on Fig. 5.2, were also plotted but not published. These data also indicated that pressures on the ground level occurred farther away from ground zero than the same pressures measured on the towers. The differences, however, were not so striking. It is suggested that when final SRI data become available, Fig. 5.2 be revised using only SRI and high explosive data.

JANGLE air blast results[12] that the blast efficiency of nuclear weapons fired on the ground is nearer 80 per cent than the 45 per cent which was used to convert the remaining HE data. Therefore if high explosive height-of-burst data are used for nuclear prediction, this fact should be taken into account. (To scale the blast effect of one-pound charges of pentolite to 1 kiloton of TNT(RC), it was assumed that 45 per cent of the radiochemical energy (weight) went into blast and that 1.2 pounds of TNT were necessary to equal one pound of pentolite. Hence distances for the one pound pentolite charges, were multiplied by $\left(\frac{2 \times 10^6 \times 0.45}{1.2}\right)^{1/3} = 91$. Additional discussion of nuclear blast compared with that from high explosives blast is in Sec 5.4.)

5.1.2 Height-of-Burst, TUMBLER vs Previous Operational Instructions

As an additional way to view the height-of-burst data, the TUMBLER results from the ground level gages were plotted on curves traced from the guide to be used in firing nuclear weapons[16]. This reference, which was based on all height-of-burst data previous to Operation TUMBLER, gave for each pressure level three curves designated as Good, Fair, or Poor. Which curve should be used in each instance was to depend on the nature of the target surface. Inspection of this information as shown on Figs. 5.3 through 5.7 shows that the TUMBLER points fall on the Good-Fair-Poor curves as follows:

Pressure PSI	TUMBLER 1	TUMBLER 2	TUMBLER 3	TUMBLER 4
50	-	-	-	F-P
40	-	-	-	F-P
30	G-F	-	-	F
25	F	-	-	F-P
20	F	-	-	P
15	F	F	F	P
12	G	F	F	P
10	G+	F	F	F
8	G+	F	F	F
6	G+	G+	G+	F
5	G+	G+	G+	F
4	G+	G+	G+	G-P
3	G+	G+	G+	G-P

The above list shows that, in general, Shots 1, 2, and 3 can be considered to be between Good and Fair and Shot 4 is between Fair and Poor. Inspection of the pressure-time records reveals them to be consistent

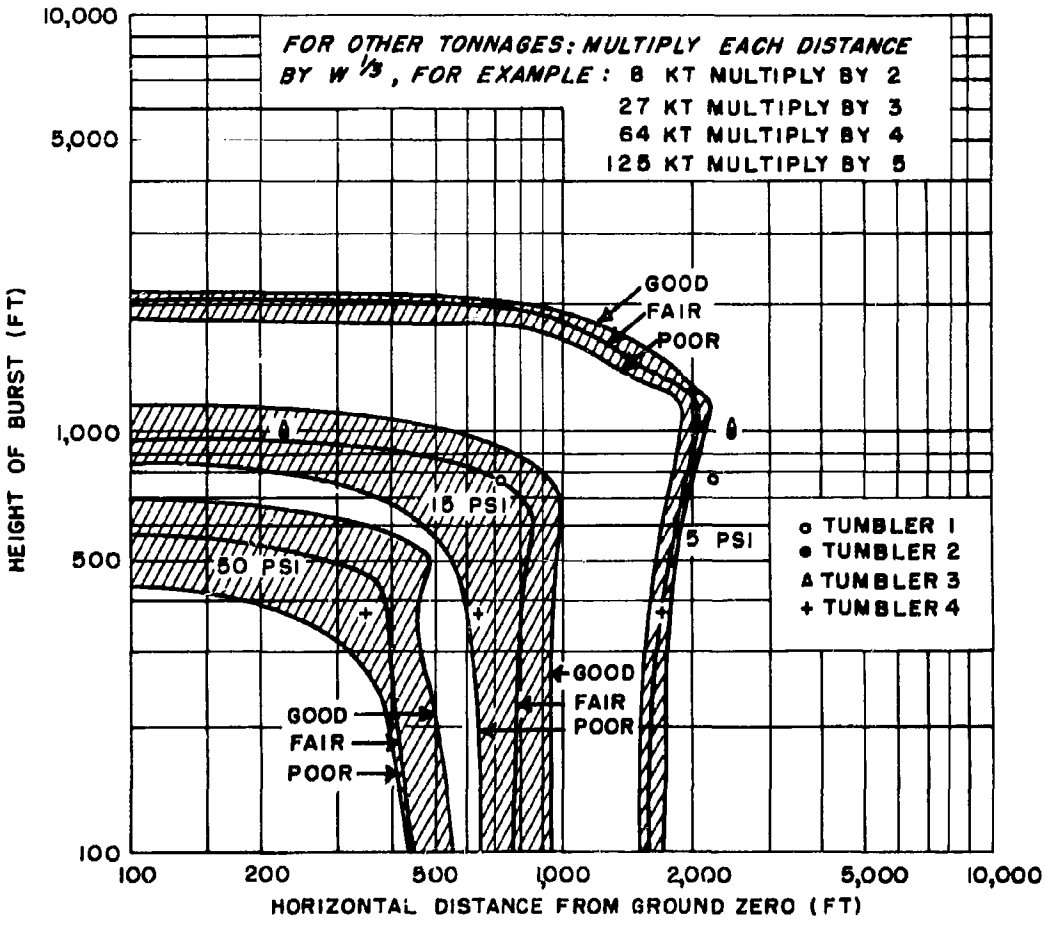

Fig. 5.3 Height of Burst vs Horizontal Distance for 1 KT(RC) at Sea Level for 50, 15, and 5 psi
Shaded Curves from Supp. 1 TM 23-200, 8 Feb 1952

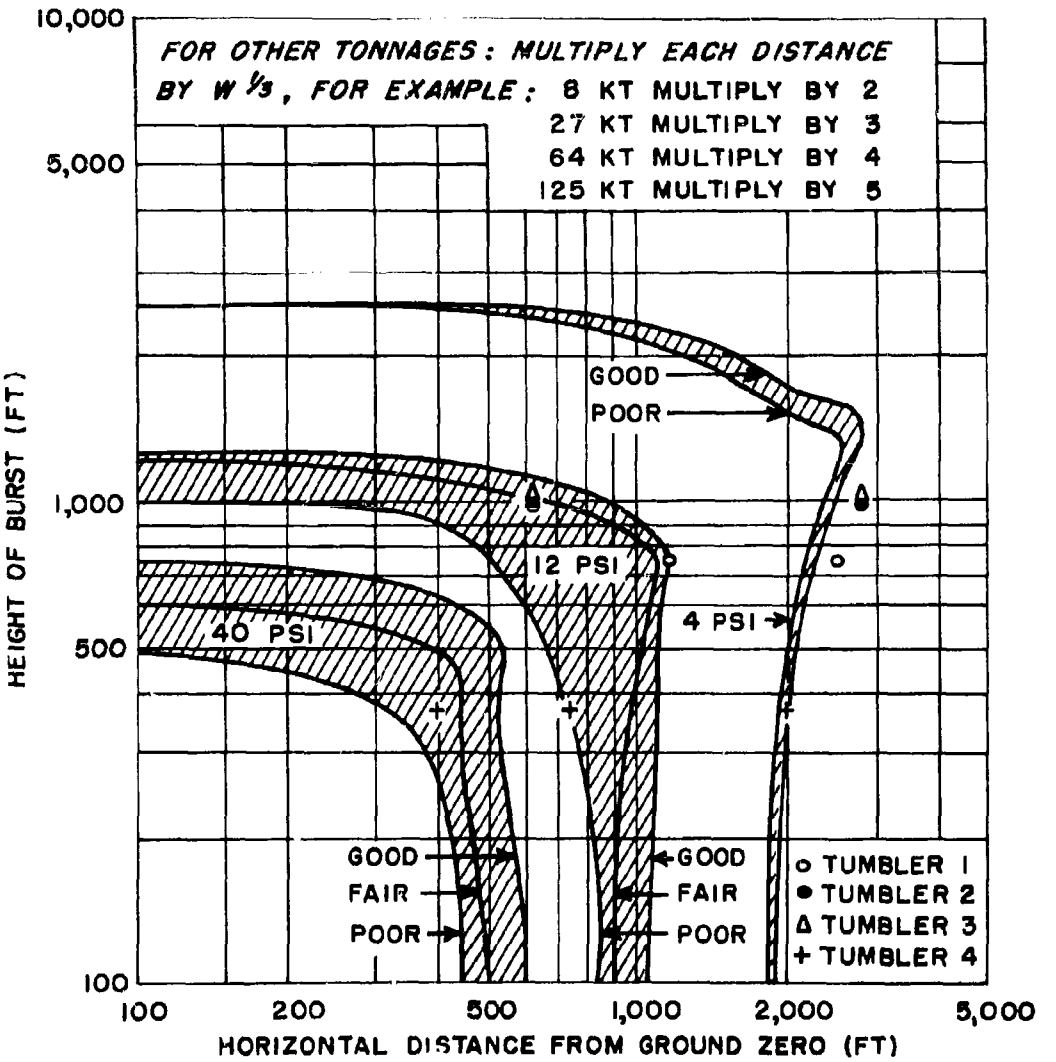

Fig. 5.4 Height of Burst vs Horizontal Distance for 1 KT(RC) at Sea Level for 40, 12, and 4 psi
Shaded Curves from Supp. 1 TM-23-200, 8 Feb 1952

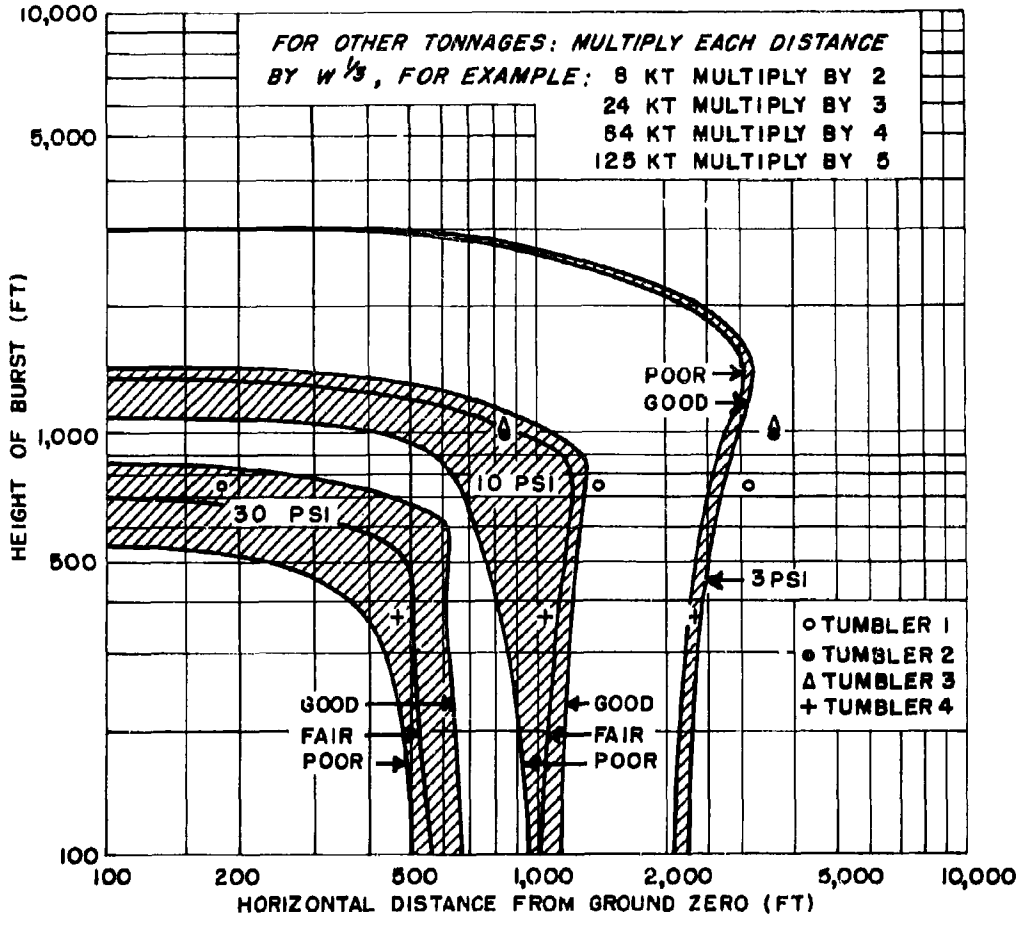

Fig. 5.5 Height of Burst vs Horizontal Distance for 1 KT(RC) at Sea Level for 30, 10, and 3 psi Shaded Curves from Supp. 1 TM-23-200, 8 February 1952

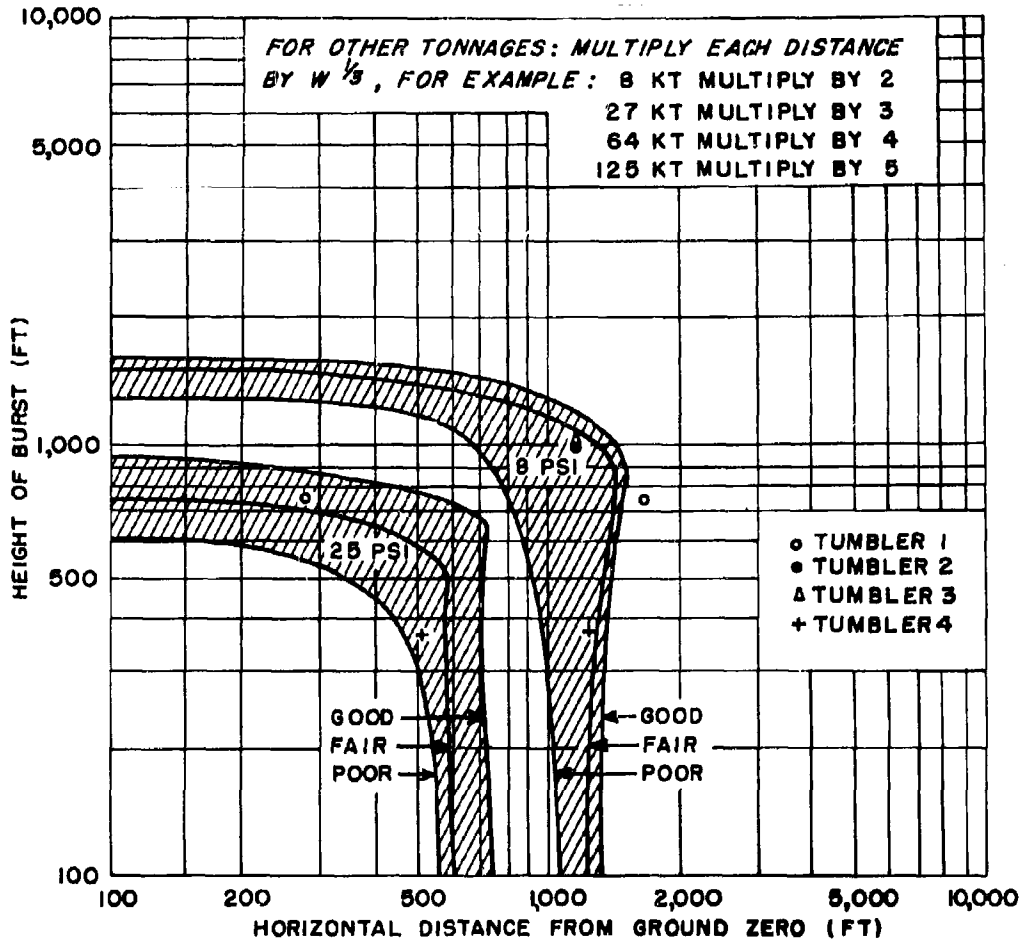

Fig. 5.6 Height of Burst vs Horizontal Distance for 1 KT(RC) at Sea Level for 25 and 8 psi Shaded Curves from Supp. 1 TM-23-200, 8 February 1952

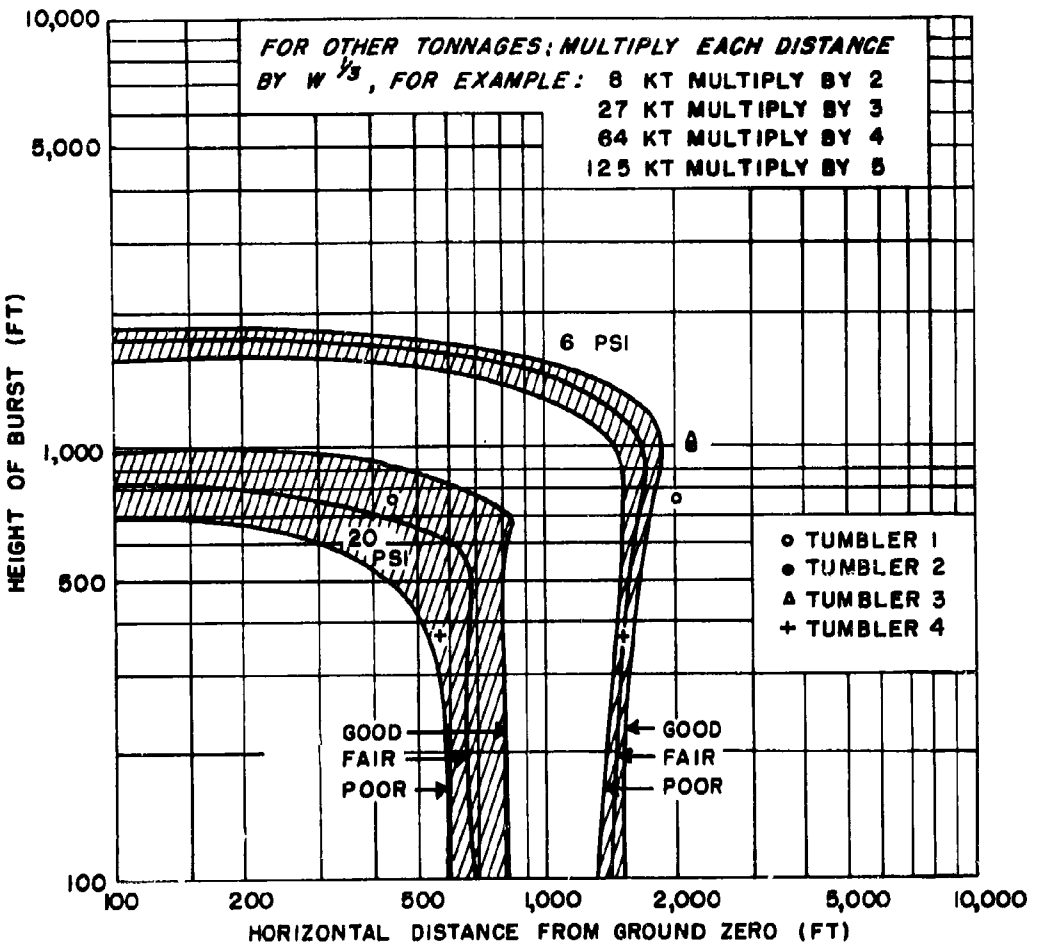

Fig. 5.7 Height of Burst vs Horizontal Distance for 1 KT(RC) at Sea Level for 20 and 6 psi - Shaded Curves from Supp. 1 TM-23-200, 8 February 1952

with this conclusion. The traces on the first three shots show sharp initial rises at all distances, though traces in the regular region show a rounding off or break at the peak. On Shot 4, however, there were several stations where no sharp rise was visible at all; and the stations on this shot which had sharp rises with rounded peaks were located as far as 4339 ft from ground zero, i.e., beyond the theoretical regular region.

5.2 THE PRECURSOR OF TUMBLER 4

5.2.1 Description of the Phenomenon

In addition to the usual incident and reflected shock waves intersecting at the ground level on TUMBLER 4, there was also a third wave visible which appeared to extend from the ground ahead of the incident and reflected waves back through the incident wave to connect nearly tangentially with the reflected wave. This third wave, or "precursor," is shown in Figs. 5.8, 5.9, 5.10, and 5.11 taken from photographs (EGG 13381) in time sequence. This is believed to be the first time that such a phenomenon was observed and analyzed; though after attention was called to it, others have noted its presence in photographs taken of BUSTER Shots Charlie, Dog, and Easy. There is even some slight indication that a meager precursor was formed on TUMBLER 1.

The precursor was formed a short, but undetermined time after the incident wave struck the ground at 210 msec after burst, as best as could be determined from the photographs of TUMBLER 4. It was visible in the films out to their limit of view of 1765 ft in the plane of measurement containing GZ. Close-up photographs exposed primarily for mortar and Jato particle motion studies (Project 19.2a) showed the precursor passing Station 7-202 (1345 ft from GZ), while at Station 7-203 it was no longer visible. (At Station 7-203, 2092 ft from GZ, the NOL pressure-time records gave a small barely perceptible indication of a precursor; none was evident at Station 7-204 at 2804 ft (See Sec 2.2.4).

Especially in the close-up mortar and Jato photographs of Station 7-202, it was observed that ahead of the precursor the ground was clearly visible and the air above it was not dust-laden. Immediately behind the precursor the dust rose rapidly. After the arrival of the precursor but before the arrival of the incident and reflected waves this dust appeared to be rolling outward radially from GZ in great billows.

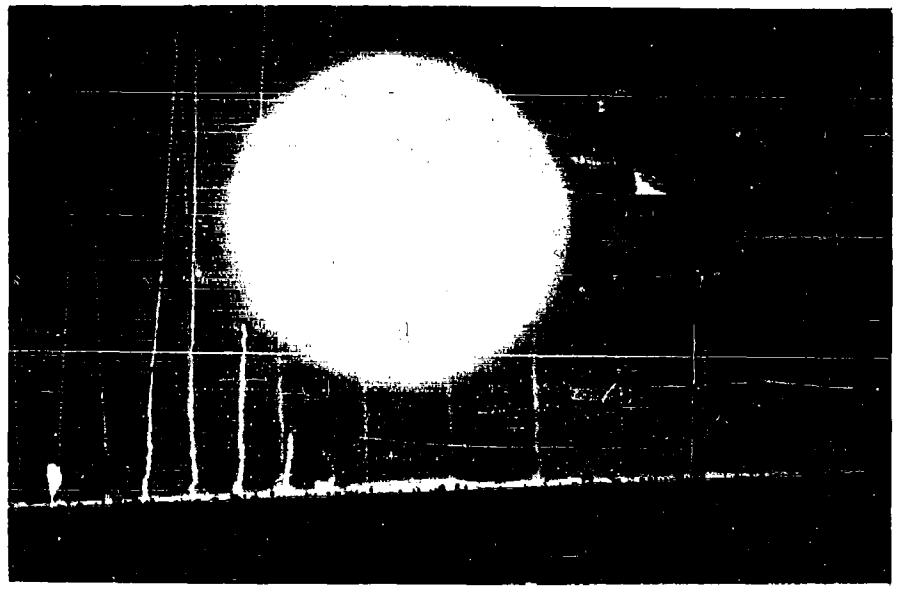

Fig. 5.8 Precursor Sequence, 0.2512 sec, TUMBLER 4

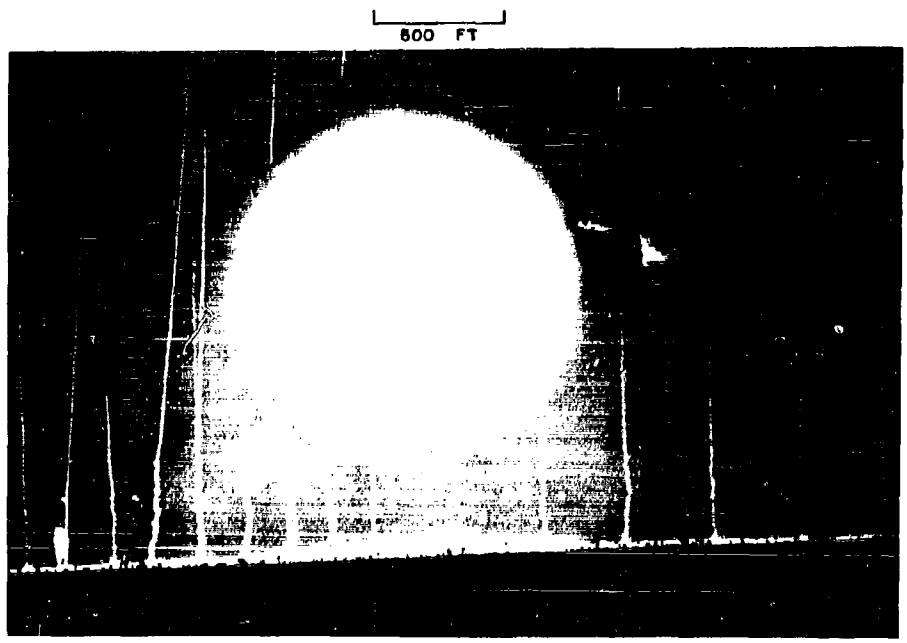

Fig. 5.9 Precursor Sequence, 0.2906 sec, TUMBLER 4

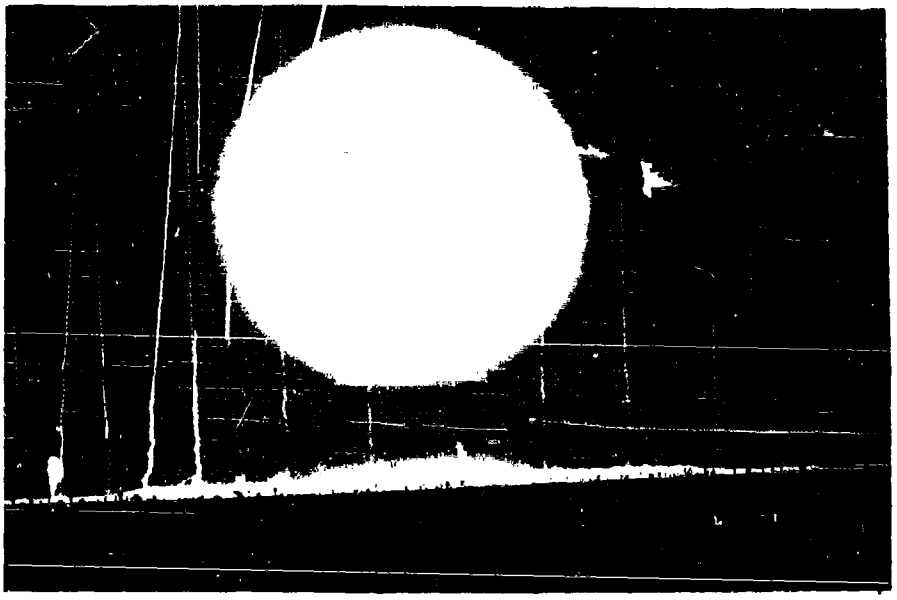

Fig. 5.10 Precursor Sequence, 0.4189 sec, TUMBLER 4

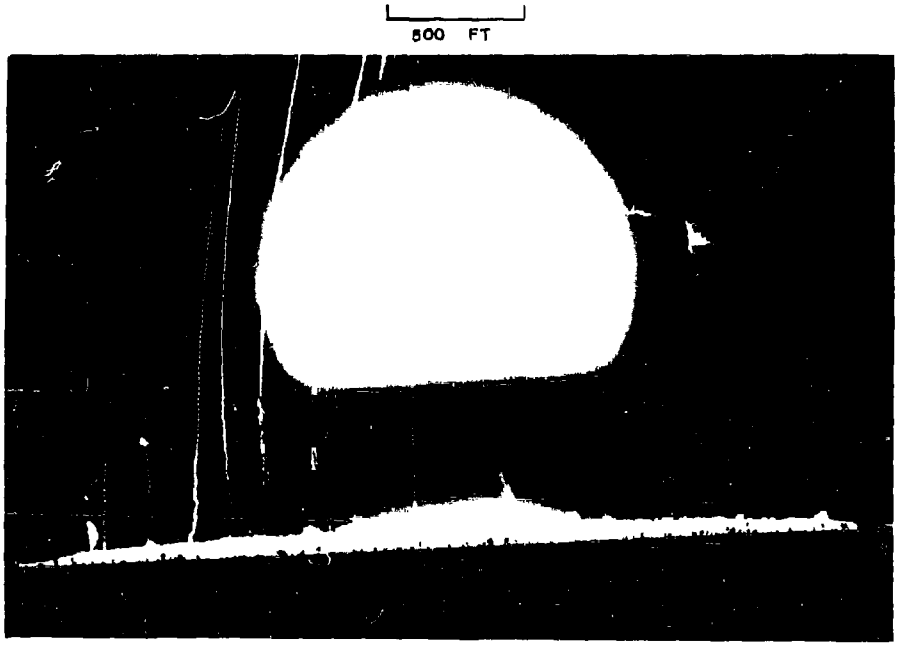

Fig. 5.11 Precursor Sequence, 0.5867 sec, TUMBLER 4

At the ground in the vicinity of Station 7-202 the precursor appeared nearly vertical but in less than 20 ft above the ground it slanted sharply forming an angle of roughly 45° with the horizontal. It curved gradually back until it joined with the reflected wave, at which point it made an angle with the horizontal of about 20°. Also, as the wave progressed outwardly there was some indication of a sudden change of slope, although very slight, at approximately 150 ft above the ground.

Measurements of the mortar and Jato photographs of Station 7-202 revealed that smoke particles originating at the top of the 50 ft instrument tower were first struck by the precursor and moved away from the pole at an angle of approximately 45°, i.e., in a path normal to the front of the precursor. Following the arrival of the incident wave, which was nearly normal to the precursor, the smoke particles changed their course to follow in the direction of motion of the incident wave. An attempt to determine with certainty the direction in which dust left the ground was fruitless, because the dust appeared as a cloud not as small groups of particles which could be identified from frame to frame.

The mortar puff appearing in these photographs was first struck by the incident wave causing the smoke particles to move toward the ground radially from zero. The puff was struck soon thereafter by the reflected wave and the direction of motion of the particles changed to that of the reflected wave. The mortar puff was sufficiently high so that at no time was it observed to be struck by the precursor.

5.2.2 Arrival Time of the Precursor Along the Ground

On TUMBLER 4 the pressure-time gages mounted at the ground surface and on towers indicated that possibly a low pressure wave arrived at the station before one of higher pressure, i.e., the pressure-time curves, as far out as Station 7-202, exhibited a long flat step between arrival of the initial disturbance and the peak (see Fig. 2.46). To determine whether or not this effect was associated with the precursor, the times of arrival of the precursor and the reflected wave at points along the ground were measured and compared with shock arrival times taken from the NOL pressure-time records.

A small rise in the level of the ground between the camera and ground zero made it impossible to see the ground level near GZ in the rocket trail photographs. In the analysis, therefore, it was nec-

essary to establish some frame of reference in order to establish the position of the precursor and the reflected shock wave. This was done as follows:

From rocket smoke trail data (Sec 3.3.4) the incident shock wave was observed to be spherical, and the locus of the center, O, and the shock radius, R, (Fig. 5.12) were known. The reflected shock wave was assumed to be spherical for a short time after its formation, and furthermore its radius was assumed to be the same as that of the incident wave. This latter assumption was checked in the first few frames after the formation of the reflected wave and was found to be reasonable. (The frame of reference was established in these frames. In later frames the reflected wave became distorted at the center from heating in the region immediately below the burst). The reflected shock wave's center, O', was found by using the visible ends of the reflected wave, points S_E and S_W, as base points and striking arcs of radius R from these points. The point at which these arcs intersect is the center (O'). With this center as the base, an arc of radius R intersected the incident wave at two points, C and D. A straight line through these points forms a datum level the slope of which approximates that of the terrain behind the rise. A perpendicular was dropped from bomb zero (O) to the line (CD) in order to establish a zero position, m, at this level. Perpendiculars were dropped from the visible ends of the precursor, P_E and P_W, and the reflected wave, S_E and S_W, to datum level. The points of intersection were then measured. This method of establishing a frame of reference was proved to be internally consistant as follows:

The position of the datum zero (m), which was transferred after its initial establishment from frame-to-frame by use of the fiducial markers, was checked in some of the later frames by using the ends of the reflected wave as reference points. Within the precision of the measurements both methods agreed well.

The plane of measurement is shown in Fig. 3.3 (Shot 4) and was roughly at an angle of 30° with the blast line. The results of the analysis are given in Table 5.4 and are shown graphically in Fig. 5.13. The scatter in the points is due to the method of determining their radial distances and cannot be improved under the circumstances.

5.2.3 Analysis of Results

The data, as presented, show primarily the qualitative difference in arrival times of the precursor and incident shock at a point. As can be seen, the precursor advanced with a velocity along the ground exceeding that of the reflected wave. (The slope of the curve for the precursor, Fig. 5.13, is always greater than that for the reflected wave within the range of measurements.) A glance at the photographs.

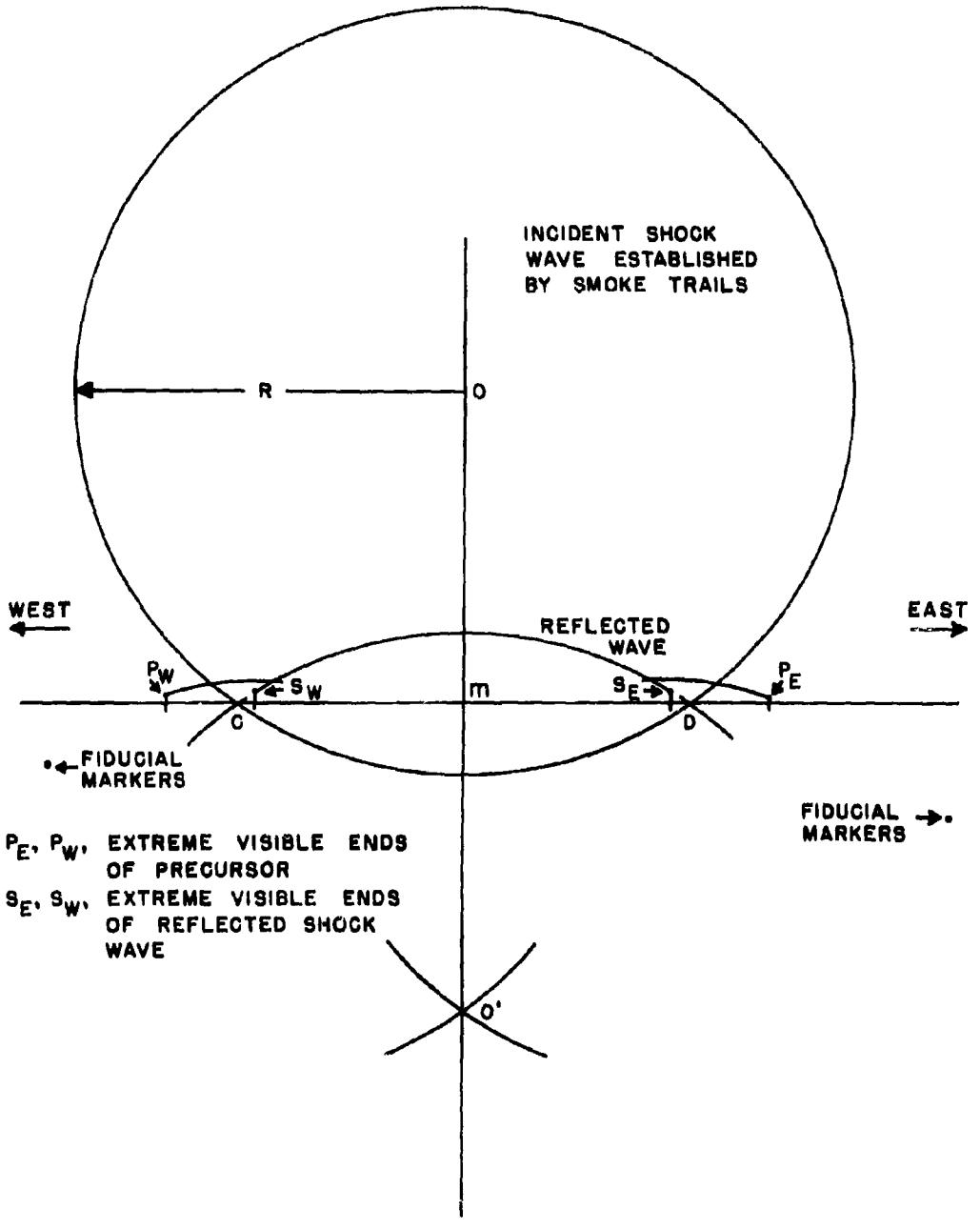

Fig. 5.12 Sketch Showing Construction of Reference Frame for Precursor Measurements

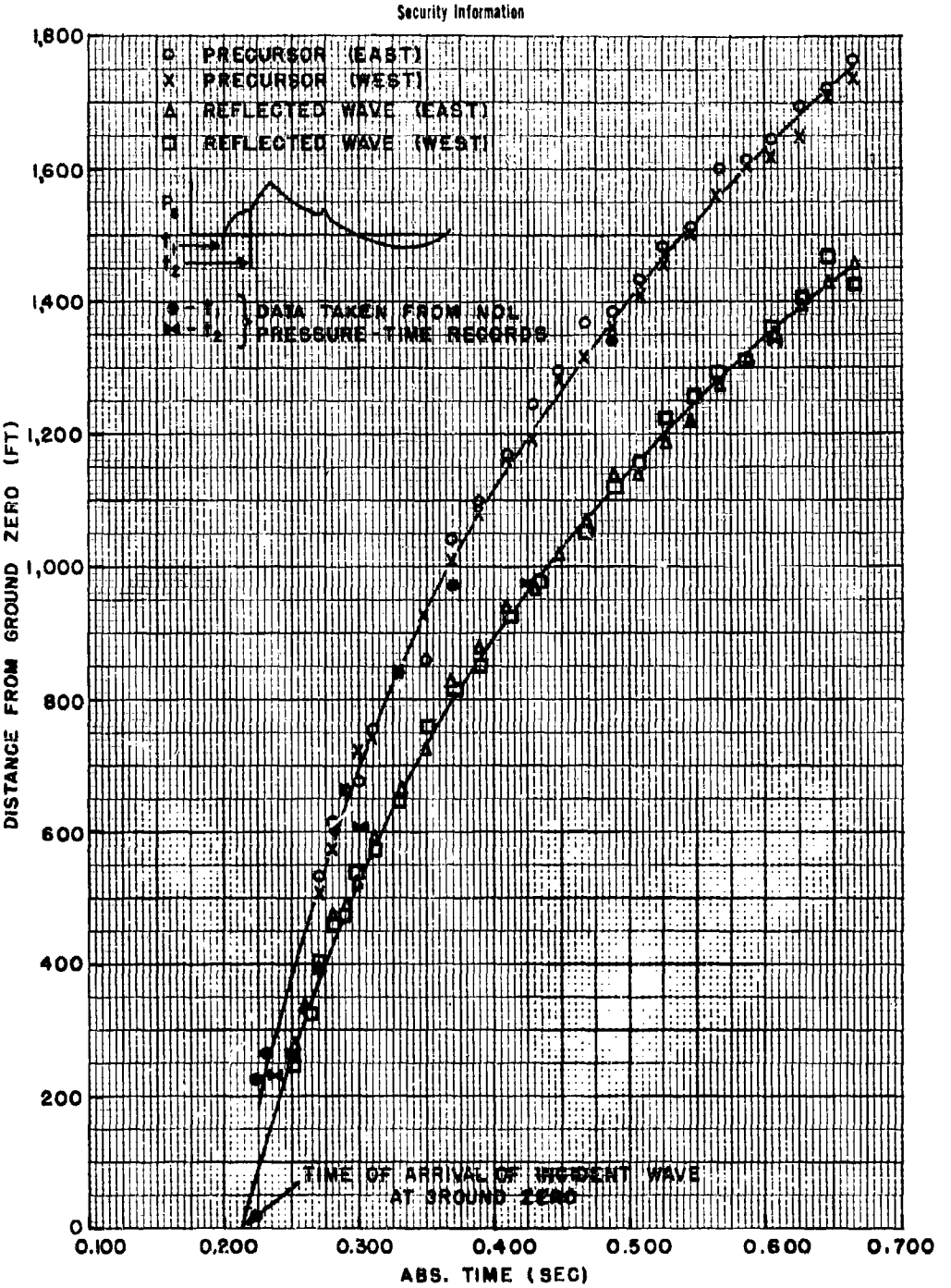

Fig. 5.13 Time-of-Arrival of Precursor and Reflected Shock Wave - TUMBLER 4

Figs. 5.8 through 5.11, can leave no doubt that at a given instant the reflected wave lags behind the precursor. The incident wave, made apparent by the breaks and hooks in the rocket smoke trails, clearly passes through the upper portion of the precursor apparently to join with the reflected wave at the ground (when extended through the dust layer).

The curves drawn through the data points in Fig. 5.13 do not represent a least squares fit to the data but were simply drawn in by eye. The time-of-arrival of the incident wave at ground zero is plotted in the same figure to show that the formation of the precursor was nearly coincident with that of the reflected wave.

Also shown in Fig. 5.13 are the arrival-time data recorded by NOL inductance gages. The sketch in the upper left corner of the graph shows the points on the pressure-time curves for which arrival times were plotted. All possible errors considered, it is difficult to deny that the precursor was responsible for the "front porch" effect on the pressure-time curves, as it has been aptly named by E. B. Doll of the Stanford Research Institute. The gages responded upon the arrival of the precursor, indicating an increase in pressure. Upon the arrival of the reflected wave the pressure jumped to a higher value. At Station 7-204 and beyond, the NOL pressure-time gages indicated that the precursor had completely dissipated itself or that it coincided with the Mach wave which had apparently formed before reaching this station. The mortar and Jato photographs showed no dust billows and only a single shock at this station.

5.2.4 Discussion and Conclusions

Acoustic theory has predicted that a sound wave can form a "precursor" having similar characteristics to the one formed from the shock wave on TUMBLER 4. The basic theory from which its origin can be deduced was presented by Rayleigh[32], and has since been applied to similar problems met in the study of underwater explosion phenomena[31, 36]. It is also interesting to note that shadow photographs of this phenomenon were recently displayed by Dr. H. Schardin at the International Symposium on High-Speed Photography. Dr. Schardin attributed the work to a German investigator at about the turn of the century.

The attention of the authors was called by Dr. G. K. Hartmann to a David Taylor Model Basin summary report[25]. This reference from which Fig. 5.14 has been taken, clearly states how a precursor is formed at the critical angle, θ_c, when a spherical

acoustic wave, having its origin at O, is reflected and refracted at an interface separating two media of different sound wave velocities, C_1 and C_2, where in the present instance, the medium containing the source of the wave is one of lower sound velocity, C_1.

From reference (25): "When a symmetrical spherical wave falls on a plane interface of infinite lateral extent, the angle of incidence increases progressively from 0° to 90° as the wave spreads outward. According to analytical results, each part of the wave is reflected nearly like a plane wave incident at the same angle. As illustrated in Fig. (5.14), the reflected wave is spherical in form but centered at a point O' which is the mirror image in the interface of the center O of the incident wave. The ratio of the reflected pressure to the incident pressure is least at the point P which is reflected first. The refracted wave is likewise variable in strength but its form is spherical only if $C_2 = C_1$.

"If $C_2 > C_1$, a remarkable change occurs as the angle of incidence of the enlarging incident wave passes the critical angle[33]. At the critical angle itself, the refracted wave stands perpendicularly on the surface, as at C in Fig. (5.14), in which the various waves are shown at three successive times. Beyond C, the refracted wave remains perpendicular to the surface but runs ahead of the common intersection of the incident and reflected waves with the interface; it is connected with the reflected wave by a fourth wave AB which is conical in form, tangent to the reflected wave at A, and inclined to the interface at the constant critical angle θ_c. This connecting wave (precursor) draws its energy from the refracted wave, which rapidly diminishes in intensity. The intensity of the connecting wave (precursor) decreases from A to B. At a point in space such as Q the connecting wave (precursor) will arrive ahead of the incident wave.

"The curves drawn in the figure may represent the front of a pulse of pressure together with the associated reflected and refracted fronts. They may also be taken to represent related fronts in a prolonged train of waves, but in this case the train of connecting waves is superposed upon the ordinary reflected train and may not be distinguishable as separate waves."

Jacobs and Liddiard[36], of NOL, conducted some experiments in which very small charges were immersed and fired in water suspended above a layer of carbon tetrachloride. The velocity of sound for the two media were sufficiently different so that some excellent pictures resembling the precursor on TUMBLER 4 were obtained.

On TUMBLER 4, energy coupling considerations make it dif-

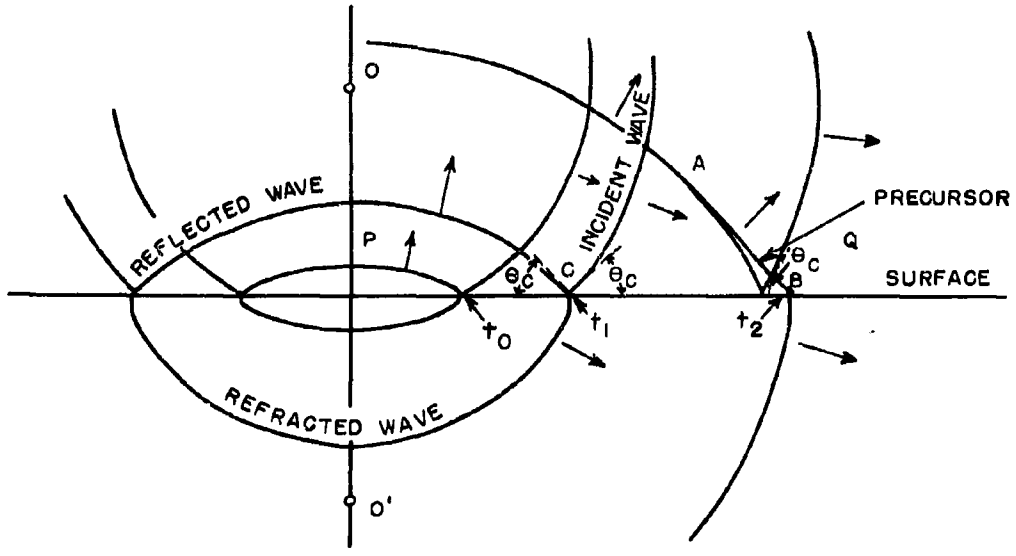

Fig. 5.14 Reflection of a Spherical Wave by a Medium of Higher Wave Velocity (Reference (25))

ficult to accept the theory that ground shock, or upward surface displacement, as has been proposed, could have given rise to such high pressures as were measured before the arrival of the reflected wave. As stated above, the precursor draws its energy from the refracted wave, so another explanation must be sought if the acoustic theory applies.

The thermal layer hypothesis appears as though it might satisfy all the basic requirements for an adequate explanation of the origin of the precursor. Furthermore, it is supported somewhat by observations made on the photographs. If it can be assumed that up to some level above the ground the air was sufficiently heated and in which the velocity of sound was sufficiently greater than that in the undisturbed air above it, then the interface separating the sufficiently heated layer from the air above it could serve as the surface layer shown in Fig. 5.14. Energy would be fed to the precursor from the refracted wave in the heated layer rather than from the ground, and the obstacle encountered in the ground shock theory would be overcome.

In Sec 5.2.1 it was stated that in the mortar and Jato photographs the front of the precursor was nearly vertical up to some

20 ft above the ground at Station 7-202. Assuming this to be in the sufficiently heated layer, the vertical portion of the precursor as observed would correspond to the vertical portion of the refracted wave shown in Fig. 5.14. In that figure the precursor above the interface, or surface as it is marked, is shown as a straight line. Now it is known from temperature measurements that the air was heated significantly as high as 50 ft above the ground. Some measurements at Station 7-202 indicated a rise of as much as 600°C above ambient air temperature before shock arrival[34]. Measurements at this station at grade level indicated a rise of as high as 1350°C. The temperature gradient and resultant gradient in sound velocity in the medium could account for the observed curvature of the precursor almost without question. Closer to ground zero the temperatures must have been even greater but no suitable measurements were obtained. At more distant stations such as 7-204 the temperature increase at the 50 ft level was only 5°C before shock arrival. As mentioned above, the precursor dissipated itself somewhere in the vicinity of Station 7-203 in which region the Mach stem apparently began to form.

The theory for the origin and formation of the precursor might well be applied in considerations of the formation of jets from the fireball along guy cables as has been observed on tower shots. It should be considered also in connection with the slow rise times in pressure-time measurements made on past tower shots on Operations SANDSTONE, GREENHOUSE, and others.

5.3 COMPARISON WITH REGULAR REFLECTION THEORY

5.3.1 Method

It was thought that there might be some interest in seeing how much the pressure values on the ground differed from values calculated from ideal reflection theory, as given by Polachek and Seeger[18]. As a basis for such a calculation, the appropriate free-air curve as measured by smoke-rocket photography was used with Fig. 5(b) of reference (18) which plots ξ' vs ξ for various angles of incidence, α, for an ideal gas of $\gamma = 1.4$. In references (18) and (15) these terms are defined so that:

$$P_s = P_o\left[\frac{1}{\xi} - 1\right] \quad \text{and} \tag{5.2}$$

$$P_f = P_o\left[\frac{\xi'}{\xi} - 1\right] \tag{5.3}$$

where P_s equals excess pressure behind the incident shock, P_f equals

excess pressure behind the reflected shock, and p_o equals the ambient pressure. The quantity γ is the usual ratio of specific heats and α is the angle between the normal to the wave front and the normal to the ground.

It was not possible to make these calculations over a wide range of values since the ground-level gages could be no closer to the burst than the height of burst and the rocket smoke-trail measurements could not be made farther away than the limitation of motion picture frame size and illumination level permitted. A summary of these conditions is given in Table 5.5.

Further inspection showed that even the entire range of overlap given in this table cannot be investigated in this manner because it extends beyond the theoretical origin of the Mach stem.

Tables 5.6, 5.7, and 5.8 show a comparison between the calculated and measured values of P_f on Shots 1, 2, and 4.

To arrive at these comparisons the calculations indicated in Tables 5.9, 5.10, and 5.11 were necessary to determine the proper ranges of β in terms of P_s and p_o. With these tables and Fig. 5(b) of reference (18) various values of P_f can be found for each value of α and p_o. These are given in Tables 5.12, 5.13, and 5.14; a sample plot of such data is given in Fig. 5.15. (All sixteen of the P_f vs P_s graphs required for this evaluation are not reproduced in this report as it was the opinion of the authors that publication of such detail was not warranted. If other members of this family of graphs are desired they may be plotted from the tables.) These plots of P_f vs P_s were used with the measured values of P_s from the rocket smoke-trail experiment to find the ideal reflected pressures. Plots of these results are given in Fig. 5.16 together with the values measured by the ground-mounted gages of the NOL, SRI[13], and Sandia Corporation[23].

5.3.2 Results in Regular Region

Inspection of Fig. 5.16 reveals that Shot 1 gave pressures in the regular region which were substantially those predicted by theory. Shot 2 pressures were about 12 per cent lower at one point and about as predicted at the other point where comparison could be made. As might be expected from inspection of the pressure-time records, Shot 4 gave results which were 25 to 30 per cent lower than predicted from free-air measurements and regular reflection theory. It is interesting to see that the scatter of experimental results is about the same as the scatter from theory, though it is necessary to

remember that the SRI and Sandia values were from their preliminary reports.

5.4 TNT EFFICIENCIES OF TUMBLER WEAPONS

5.4.1 Comparison of Free-air Data with TNT

A curve, Fig. 5.17, representing pressure-distance from 1 KT of TNT in free air, was constructed from information given by Hartmann[19] and Kirkwood-Brinkley[21]. TUMBLER pressure-distance curves corrected to sea level were made up from Tables 3.3, 3.5, 3.7, and 3.9 by adjusting the appropriate values for pressure and distance by the scaling factors of Table 1.1. These were plotted, the values of particular pressure levels were read off, and are presented together with Kirkwood-Brinkley values in the left side of Table 5.15. The ratios of these distances to the distance at which the TNT curve gave the same pressure were then obtained and cubed to give KT(TNT) equivalents at each pressure level from 200 to 7 psi. These KT(TNT) values and their averages for each shot are tabulated on the left side of Table 5.16. On the right side of Table 5.16 the TUMBLER values of KT(TNT) have been multiplied by 100 and divided by the KT(RC) value to obtain blast efficiencies at each pressure level. In addition averages for each shot and each pressure level are presented. On the right side of Table 5.15 the sea level distances for TUMBLER have been divided by the average $(KT(TNT))^{1/3}$ and the results are plotted on Fig. 5.17.

It can be seen from this figure that the average KT(TNT) values used represent the data best over the range from 30 to 200 psi and give an efficiency of about 44 per cent under these conditions. Elsewhere in this report the value of 45 per cent was used to scale to high explosives, but it is believed this difference is insignificant depending somewhat on how averages are taken. The variation of efficiency with pressure level was observed on GREENHOUSE[24], where it was suggested that a second wave added to blast effectiveness in the lower pressure regions.

5.4.2 TNT Efficiencies at Ground Level

A simple direct measure of the TNT efficiency as measured at ground level is harder to achieve than in the free-air region; however, an estimate of it can be made by a series of approximations or by at least two graphical methods. The difficulty in these processes lies in the lack of good reflection factor data from TNT under the exact conditions that the TUMBLER shots were fired; therefore, this estimate was based on the height-of-burst curves presented by Hartmann

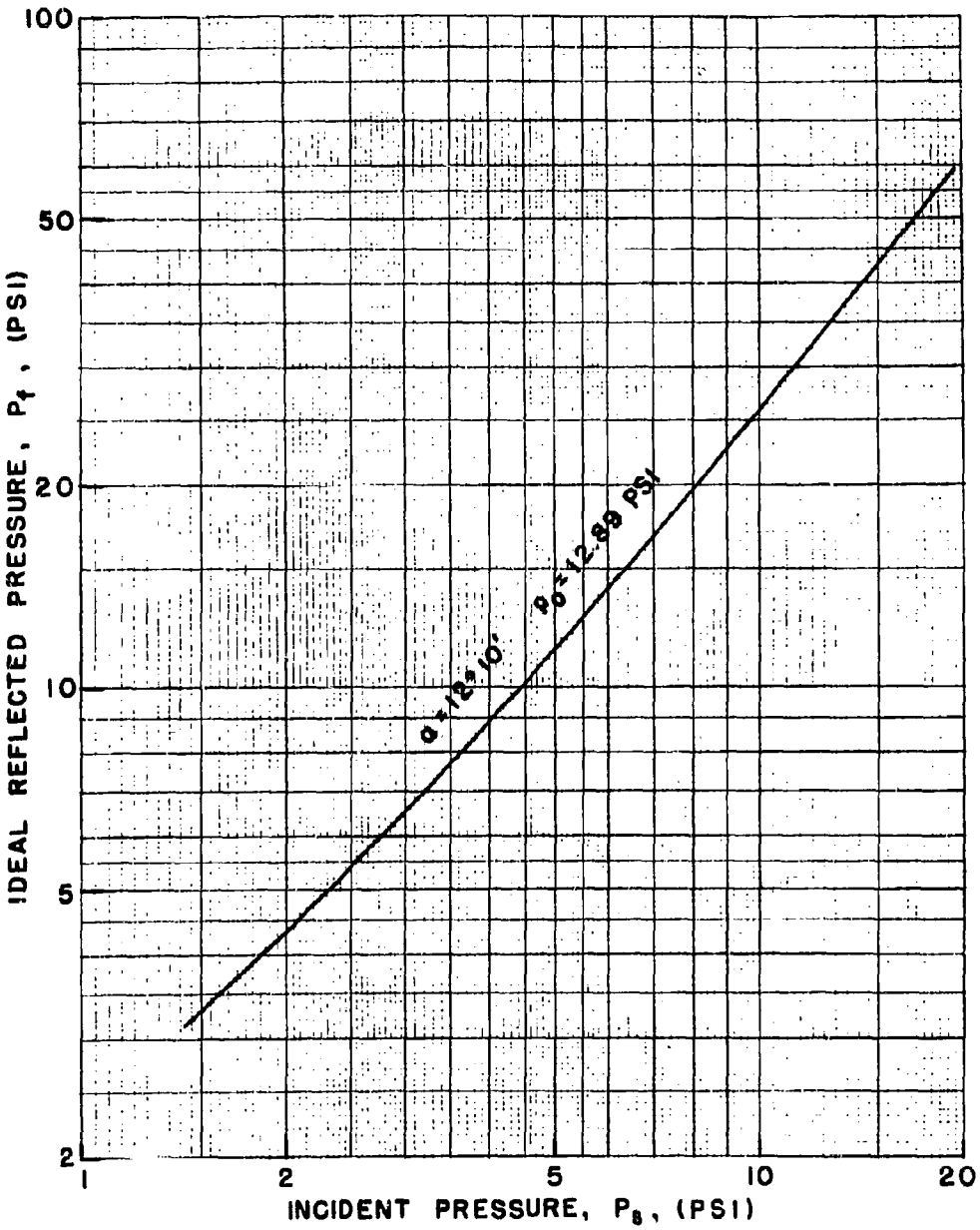

Fig. 5.15 One of the Family of Curves Showing P_r vs P_s for Ideal Reflection of Shocks from a Rigid Surface - Changes in α or P_o will generate Other Curves of This Family

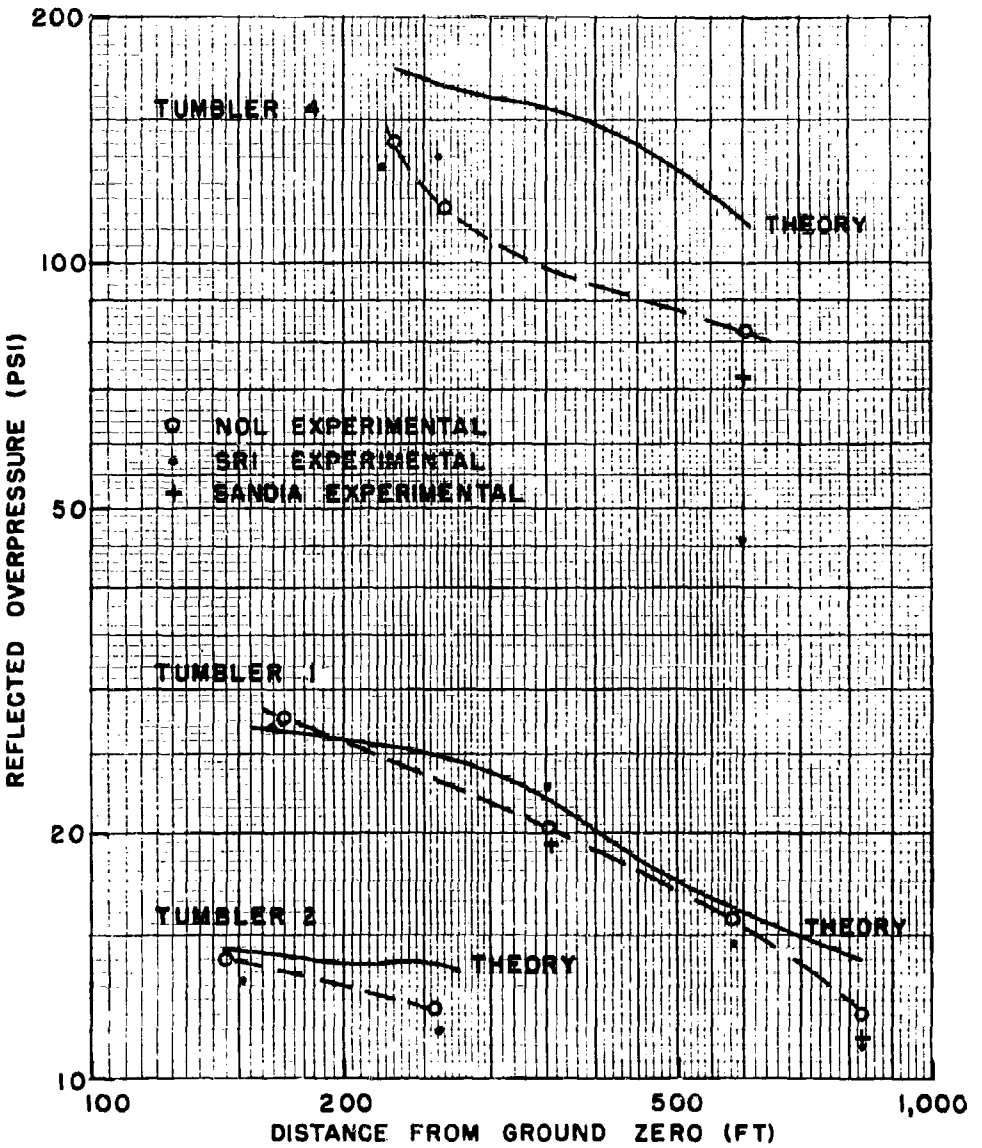

Fig. 5.16 Pressures in the Regular Reflection Region - TUMBLER 1, 2 and 4

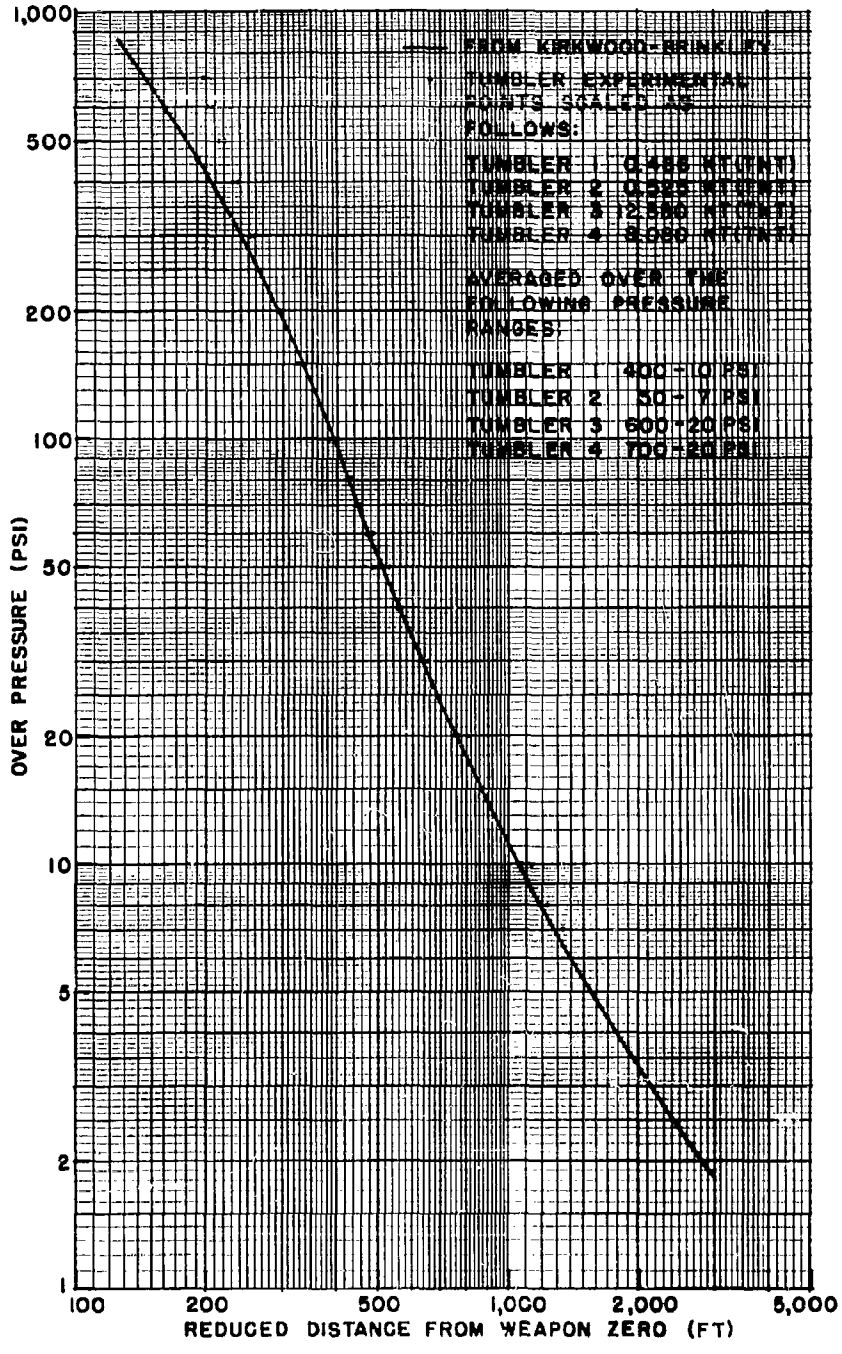

Fig. 5.17 Free-air Pressure Reduced to 1 KT of TNT at Sea Level

and Kalavski[15]. It is realized, as discussed in Sec 5.1, that these curves represent gages well above ground level and that pentolite (taken as 1.2 times as effective as TNT), not TNT, charges were used. Since no adjustment was made in this estimate for the error introduced by the higher gage position, the resulting efficiencies will be somewhat in error. The methods used were as follows:

The first method is applied by assuming an efficiency and calculating from this a reduced height, μ. This reduced height is then used with Fig. 19 of reference (15)* to get a reduced distance, λ, which can then be scaled up using the same efficiency factor. A plot of these scaled distances is made vs the assumed efficiency and the proper efficiency is read off where this curve crosses the measured distance. A sample calculation for an assumed efficiency of 50 per cent on Shot 2 at the 10 psi level is as follows:

$$\mu = \frac{h}{W^{1/3}} \frac{(Ft)}{(Lbs)^{1/3}} = \frac{995}{\left(\frac{0.50}{1.2} \times 2 \times 10^6\right)^{1/3}} = \frac{995}{94.1} = 10.57$$

where h and W are the values of height-of-burst and charge weight reduced to 1 KT(RC). This gives a $\lambda = 7.9 \frac{Ft}{(Lbs)^{1/3}}$ or a distance of $7.9 \times 94.1 = 743$ ft which can be compared with the measured value of 850 ft. By assuming other values of efficiency and plotting the results, one arrives at an efficiency of 57.1 per cent for this method. The second approach, which is somewhat simpler, is also based on the idea that the μ/λ of the height-of-burst curves for high explosives will scale to atomic weapons. This method is shown by the sample calculation given below for the 10 psi level on Shot 2:

$\frac{h}{R} = \frac{995}{850} = 1.171$ where h and R are the height-of-burst and distance from ground zero where the 10 psi level occurs - all reduced to 1 KT(RC). A line having this slope, plotted through the origin of Fig. 19 of reference (15), crosses the 10 psi curve at a $\mu = 10.0$. Hence the scale ratio is $\frac{h}{\mu} = \frac{995}{10} = 99.5$ and $\left(\frac{h}{\mu}\right)^3 = 0.985 \times 10^6$ is the equivalent weight of the charge of Shot 2 in pounds of pentolite.

* Data from Fig. 19 of reference 15 is plotted in Fig. 5.2 after correction to 1 KT(RC) by the method shown in Table 5.3 and Sec 5.1.1.

(Shot 2 is still in terms of 1 KT(RC)). To convert 0.985×10^6 to per cent of 1 KT(TNT) it is multiplied by 1.2 (pentolite to TNT), by $\frac{1}{2 \times 10^6}$ (pounds to kilotons), and by 100 to get the percentage value, which in this example is found to be 59.1 per cent.

A third method of determining the efficiencies of the TUMBLER shots in terms of TNT equivalents was also a graphical one. It involved the determination of the weights of TNT which when fired under the same conditions as the TUMBLER shots would give the same pressure results at the same distances. These TNT weights were then compared to RC weights given for the four TUMBLER shots, the resulting ratio being the efficiency of the TUMBLER weapons in terms of the standard TNT. The steps required to do this were as follows:

The height-of-burst curve for pentolite (from Fig. 19 of reference (15)) at the 10 psi level was redrawn on a log-log scale with ordinate and abscissa in terms of actual height-of-burst and ground range for a 1-pound charge. A curve for any different weight of pentolite would be displaced along a 45 degree line from this curve. The normalized values (for 1 KT at sea level) of TUMBLER data for height-of-burst and ground ranges at the 10 psi level were plotted on the same sheet of log-log paper and 45° lines drawn through these points. The points of intersection between the 1-pound pentolite curve and the 45° lines gave values of ground range R_1 which scaled to the reduced TUMBLER equivalent R, and therefore the relationship $\frac{R}{R_1} = \left(\frac{W}{W_1}\right)^{1/3}$ could be used to determine W, the weight of pentolite required to give 10 psi at the distance R when fired at the scaled height (R_1 and W_1 are associated with the 1-pound pentolite charge). These calculated values of W for pentolite were then multiplied by 1.2 to obtain the TNT equivalents. The TNT values were then finally compared to the W(RC) of the TUMBLER shots. As an example for the 10 psi level of TUMBLER 2, the 45° line through R = 850 ft and h = 995 ft (as normalized for 1 KT(RC) at sea level) intersected the 1-pound pentolite curve at $R_1 = 8.5$ ft. Then the ratio $\left(\frac{W}{W_1}\right)^{1/3} = \frac{R}{R_1} = \frac{850}{8.5}$ or $\frac{W}{W_1} = 10^6$, i.e., 10^6 pounds of pentolite or 1.2×10^6 pounds of TNT. This means that 1.2×10^6 pounds of TNT fired at a height of 995 ft would give a pressure of 10 psi at a ground range of 850 ft. These height and distance values are the scaled parameters for the TUMBLER 2 shot scaled to 1 KT(RC) or 2×10^6 pounds RC. Therefore, the TNT efficiency of the shot was

the ratio of these figures, i.e., $\frac{1.2 \times 10^6}{2 \times 10^6}$ or 0.60.

Table 5.17 gives the average results as computed by the first two methods described. The differences which were averaged out were small and can be wholly attributed to the limits of precision with which the height-of-burst curves can be read. The wide variation of efficiencies with pressure level arose from the following sources of error:

(1) The fact that the HE values used as a standard were measured not at ground level but at a height of several feet above the ground. (See Sec 5.1.)

(2) The fact that the pressure-distance curves for pentolite, TNT, and nuclear explosives are not similar, i.e., their slopes vary differently with pressure level.

(3) Small errors of measurement of the nuclear pressure-distance curves occurred particularly at low pressure levels. (Errors are more likely here than in the HE results which are average values from a series of six or more identical shots.)

(4) These calculations of TNT efficiencies are very sensitive to small errors because of the cube law for scaling.

(5) There may be important differences between the reflecting surface at the Nevada Proving Grounds and the concrete slab used at the NOL firing field.

(6) Effects of thermal layers created by radiation from the nuclear explosion are known to be substantial.

As a result the tabular values only indicate the trend which can be seen in the other types of analysis, viz, that TUMBLER 1 was most efficient, TUMBLER 4 least efficient, and TUMBLER 2 and 3 were moderately efficient in the 10 psi region. It is felt that the present best-estimate of TNT efficiency should be obtained from free-air comparison as discussed in Sec 5.4.1 above.

5.5 POSITIVE IMPULSE IN FREE AIR COMPARED WITH TNT

The free-air positive impulse curve shown in Fig. 5.18 was taken from reference (20), plate 7. It is the experimental curve for cast

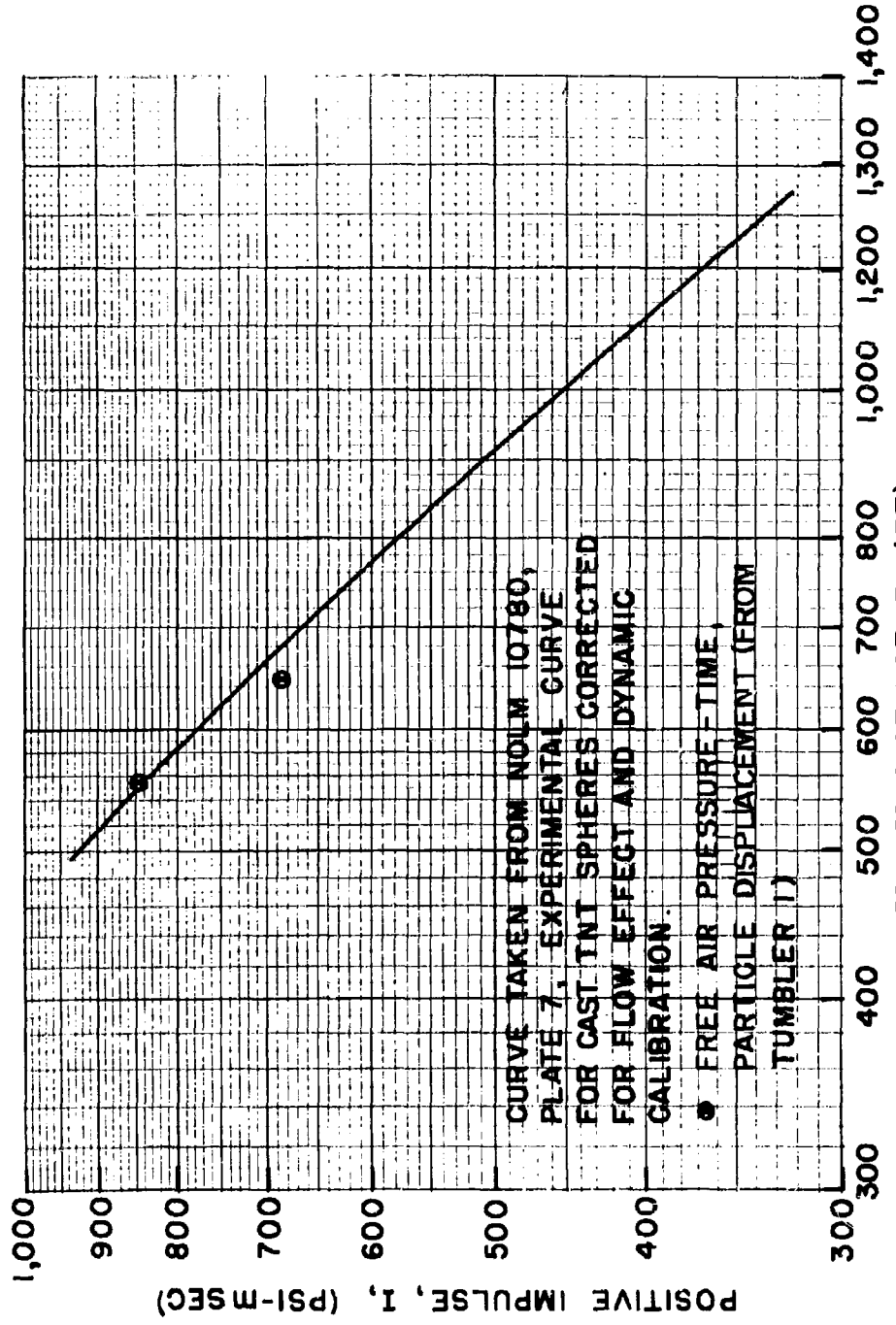

Fig. 5.18 Free-air Positive Impulse Reduced to 1 KT(RC) at Sea Level - Particle Displacement Compared with TNT Results

TNT spheres as corrected for the effect of shock flow past the pressure-time gages and based on the dynamic calibration of these gages. This curve was scaled to 1 KT(RC) at sea level using a blast efficiency of 45 per cent for TUMBLER 1. A comparison of these data and data obtained by the particle displacement method is shown in Fig. 5.18 and given in Table 5.18.

Positive impulse could be measured directly only on TUMBLER 1 at 590 and 690 ft (see Fig. 3.26). No attempt was made to extrapolate the pressure-time curves obtained for TUMBLER 4 because they did not cross the zero axis. The two points measured are in very good agreement with the experimental curve for TNT indicating that the overall free-air p-t curves for TUMBLER 1 scale well and therefore are considered to be reasonably accurate.

CHAPTER 6

CONCLUSIONS AND RECOMMENDATIONS

6.1 CONCLUSIONS ON SYSTEMS USED

6.1.1 Pressure-Time Measurements on the Ground

The frequency-modulation system used to record pressure-time measurements made on the ground was reliable, accurate, and reasonably simple to operate. Furthermore the effects of radiation induced in the system, while noticeable, did not cause any loss of reliability nor of actual results. The Bendix diaphragm gages used as end-instruments with this system were reliable and easy to use; however, they are not perfectly damped so that the resultant ringing makes appreciable judgment and experience in their use necessary to get consistent results in reading the records. Furthermore the sealed reference volume of air in these gages necessitates careful calibration in the field to correct for the proper ambient conditions of pressure and temperature. In spite of these difficulties the results checked those of other systems to within a few per cent.

6.1.2 Peak Pressure Measurements in Free Air by the Shock Velocity Method

This system once again showed itself to be reliable, simple, reproducible, and self-consistent. It suffers from its requiring a long and careful analysis procedure which is subject to human errors; although much of this might be avoided by the use of machine calculators such as the IBM type. The system has the further advantage of showing up asymmetries, if they exist, and special effects such as the precursor on Shot 4 and the rise of the Mach stem on Shot 1.

6.1.3 Pressure-Time Measurements in Free Air by the Particle Displacement Method

This experiment gave pressure-time curves which, when associated with peak-pressures measured by the shock velocity method, gave time-decay rates and impulse values comparable with those from high-explosives. It has the advantages of the shock velocity system as far as simplicity and reliability are concerned and suffers from the same disadvantage of requiring a complicated analysis system. As used for the first time, the system suffers from a low-frequency response which arises from the need to smooth the data, so that small rapid changes in the pressure-time history cannot be detected. It

probably is slow to react, i.e., the shock may be well past the smoke trail before the motion of the particle has approached the velocity of the air with sufficient accuracy. This, it is believed, arises from the fact that the smoke particles have substantially greater mass than the air particles and a relatively low viscosity with the result that there is probably a small delay before their velocity approaches that of the air stream. A result of this is that calculated peak-pressures would probably be in error when particle velocities measured by this method are used in the Rankine-Hugoniot particle velocity equations for air; therefore, it is necessary to use the shock velocity method to obtain the peak pressure for the initial portion of the pressure-time curve. The system at present is also limited to the 10 to 30 psi region because lower pressure shocks do not give sufficient displacements to maintain accuracy requirements, and larger pressure shocks are hot enough to evaporate the trails during the initial part of their motion. Some of these disadvantages would be overcome if the smoke trail were made up of particles more nearly like air particles and if the camera system had a better space-time resolution than the system used on TUMBLER. To sum up, this method can, as a result of fairly lengthy analysis, give pressure-time curves in free-air which have poor time resolution but reasonably accurate initial decay and impulse values.

6.2 CONCLUSIONS ON EXPERIMENTS

The following general conclusions are listed to summarize the main results:

(a) The cube law of scaling in free-air was confirmed for nuclear explosions between 1 and 30 KT(RC). This enabled generalized free-air arrival-time and pressure-distance curves to be determined in terms of 1 KT(RC) at sea level.

(b) Height-of-burst curves for four heights over the Nevada Proving Grounds were determined in terms of 1 KT(RC). In general Shots 1, 2, and 3 fell between the Good and Fair curves of the operational data available before TUMBLER and Shot 4 fell between the Fair and Poor curves.

(c) The optimum height-of-burst for the test conditions was found to be zero for pressures down to 12 psi and to be $H'_{op} = \frac{19,890}{14.7 + p}$ for pressures between 3 and 12 psi where H'_{op} is in ft and p is the overpressure in psi, both quantities reduced to 1 KT(RC) at sea level.

(d) The cube law of scaling for pressures and impulses at the ground level was confirmed for nuclear explosions between 1 and 30 KT(RC) at a height-of-burst equivalent to 1,000 ft for 1 KT(RC) at sea level.

(e) For the first time a detailed analysis was made of the effect on blast of the high radiation produced by a nuclear bomb close to the ground. This effect, called the precursor in this report, had never been so clearly observed and measured both by pressure-time gages and by photography.

(f) Whereas the pressure-time curves seem to be smooth in free air, the effect of the ground (probably because the absorbed heat produces a thermal layer near the surface) seems to cause the ground level pressure-time curves to be altered both during their initial rise and during their decay.

(g) Calculated reflected pressures based on regular reflection theory and the measured free-air pressure-distance curves gave reasonably close agreement with measured values from Shots 1 and 2. Shot 3 could not be compared for lack of data. As might be expected, Shot 4 data fell below the theoretical predictions for an ideal reflecting surface.

(h) The summary of the TNT equivalents for the TUMBLER shots is given in Table 6.1 which indicates that, over the regions measured in free air, these efficiencies fell between 46 and 41 per cent.

(i) The ground level TNT equivalents for the TUMBLER shots at the 10 psi level ranged between 42 and 84 per cent but these values are based on data which may be so inappropriate that the results can not be considered to be meaningful.

(j) A study made with TUMBLER and small charge data indicated that the optimum height-of-burst for a given pressure level is appreciably higher for gages placed on the ground than for gages placed a short height above ground.

(k) There seems to be little difference in the blast reflectivity of the ground at Frenchman Flat and at the T-7 area for fairly high bursts.

(l) Typical shocks seem to have existed in the Mach region except on Shot 4; and even there they existed at low pressure levels.

(m) In the regular region, the shocks were always rounded off, had double-steps, or disappeared completely into slow rise times.

(n) Small secondary and tertiary pressure pulses were observed during the main shock on TUMBLER 4; a small second positive phase occurred on TUMBLER 1 and 2.

(o) The decay parameters and positive impulses of the free-air shock waves compared favorably when scaled to HE data.

6.3 RECOMMENDATIONS

(a) Insofar as possible, all atomic explosions should be instrumented for measurement of free-air peak pressures and ground level pressures vs time so that statistically reliable information can be obtained for free-air and height-of-burst effects.

(b) Pressure measurements at various heights above the ground from this and future operations should be used to determine new height-of-burst curves and some decision should be made, based on further investigations, as to whether such height-of-burst curves are not a better basis for operational action than the present height-of-burst curves which are based on data measured at ground level.

(c) Use of the particle displacement method for measuring pressure-time in free air as described in this report should be limited to experiments where gross irregularities are expected, as the present system does not have high resolution. Use of the particle velocity method to measure peak pressures in free air should probably be limited to experiments where shock velocity measurements are impossible to make.

(d) Photography of blast on future tests should be arranged to provide direct pictures of the precursor, if formed, and the rise of the Mach stem.

(e) The system used on this operation of preparing preliminary reports in the field was highly satisfactory and should be made standard practice for future tests of similar size.

APPENDIX A

MEASUREMENT OF PEAK PRESSURE BY INDENTER GAGES DAMPED WITH SILICONE AND WITH BAFFLE CHAMBER

By: F. J. Oliver

A.1 FIELD EXPERIMENTS

On TUMBLER Shots 3 and 4 some indenter gages [7, 8, 9, 10] were placed in the ground next to the NOL inductance gages at selected stations. The indenter gages were damped to prevent overshoot and were covered with a baffle as shown in Fig. A1. The baffle was provided mainly to shield the rubber air seal from damage from radiation and sand blast. On GREENHOUSE, damage to the air seal prior to the arrival of the peak pressure was the most likely cause of low reading gages in the regions where the pressure was over 20 psi.

For TUMBLER 3, each baffle had a 1/8-in. orifice which allowed a slow rise to maximum pressure. In addition each gage was damped with 100,000 centistoke, DC 200 silicone fluid. All gage mounts were coupled to the ground with a "Calseal" mix.

The results are shown in Fig. A2 and Table A1. All records were too low and there was much scatter.

In the time between TUMBLER 3 and TUMBLER 4 the baffle fill time, as measured with the inductance gage system, was found to be between 20 and 30 msec. It was found that if the rubber spacer (see Fig. A1) was loose and there was no clearance seal, this 20- to 30-msec fill time of the chamber was greatly increased. A clearance seal was added for TUMBLER 4 by increasing the gage diameter with tape and grease to make a tight fit.

For TUMBLER 4, the orifice was increased to 3/8-in. diameter. This gave a fill time of 4 to 6 msec. For comparison the orifice plate was omitted for half the gages, giving a fill time probably around 1/4 msec depending on how tight the steel wool was packed. To obtain some data on the effect of the oil, half the gages were damped with 100,000 centistoke silicone and the rest with 1,000,000 centistoke silicone. The "Calseal" cement was omitted on TUMBLER 4 to avoid the possibility of a heavy blow being transmitted to the ground mount when the shock front passed, which might have caused the gage to bounce.

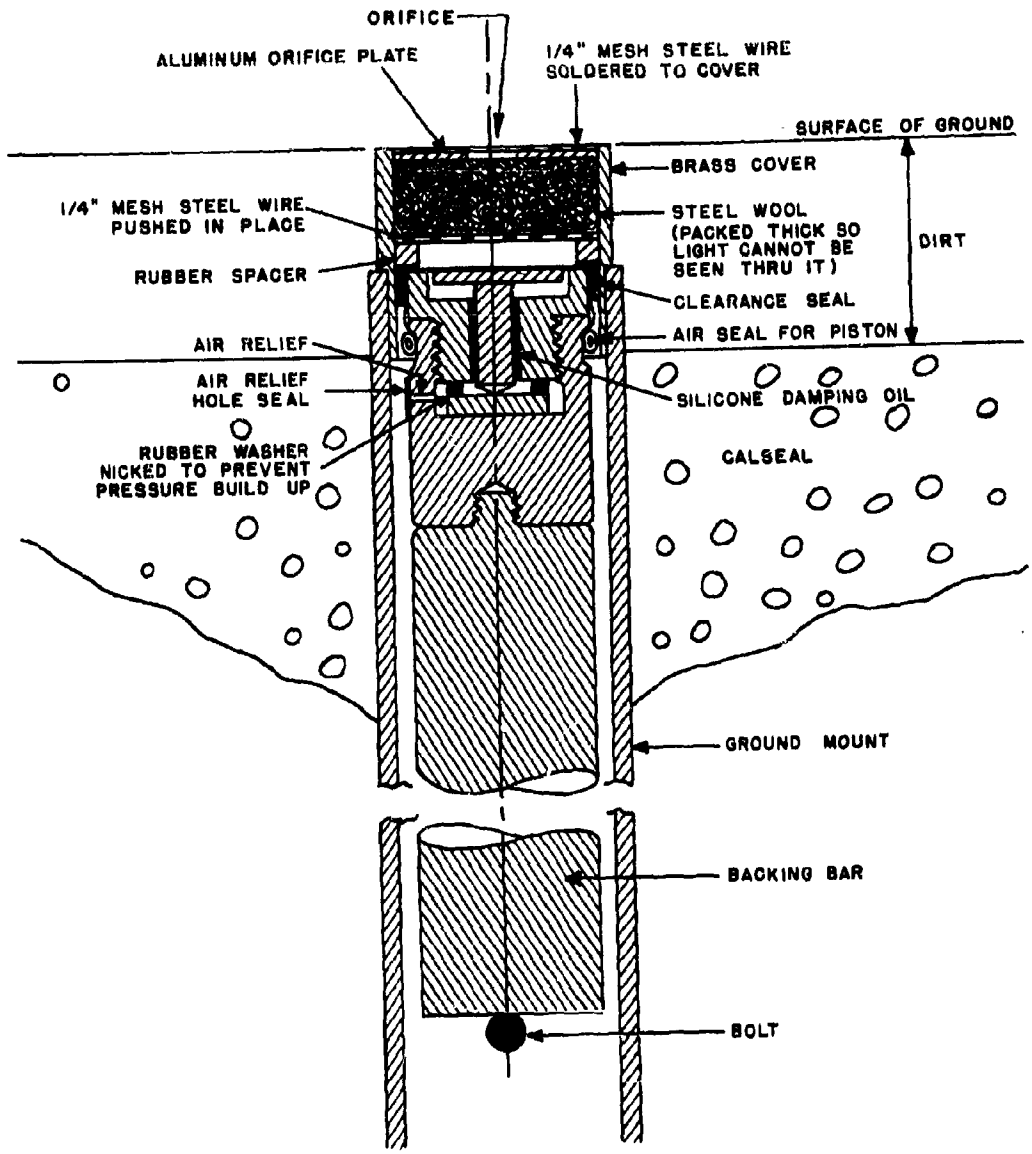

Fig. A1 Arrangement of Indenter Gage with Baffle Chamber

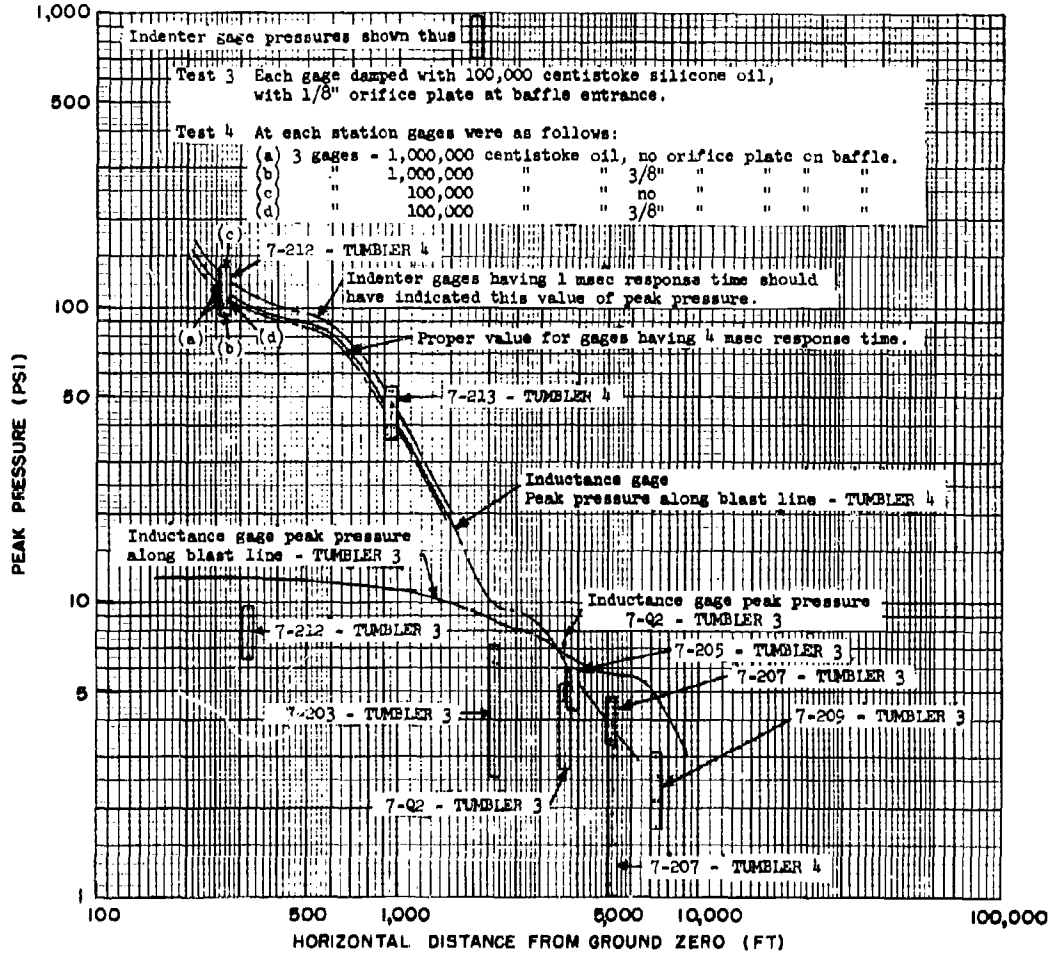

Fig. A2 Comparison of Inductance and Indenter Gages
TUMBLER 3 and 4

A.2 ANALYSIS

Results of indenter gages having no orifice plate on TUMBLER 4 (Fig. A2 and Table A2) showed excellent agreement with inductance gage data in the high pressure region. With the 3/8-in. orifice the results were about 10 per cent low, and the scatter seemed excessive. In the low pressure region results again were too low. All air seals were intact although many baffles showed burning of steel wool down about 1/4-in. There was no apparent effect of sand blast.

After the tests further work was done at the NOL to find an explanation for the scatter and the poor low pressure results. Viscosity tests on the silicone at various rates of shear showed surprising results. The viscosity, instead of being constant, was inversely proportional to some power of the shear rate[30]. For instance the nominal 1,000,000 centistoke oil showed an effective viscosity of around 5,000 centistokes when tested in the laboratory under high shear rates, e.g., a rise to 35 psi in one msec.

A study of the GREENHOUSE damping procedure revealed that the crater compound used for damping had a viscosity of around 10,000 centistokes and tests at high shear rate showed only a slight lowering of viscosity. GREENHOUSE results were about 10 per cent low, indicating that the viscosity should have been less for better correlation with inductance gage results.

These results furnish an explanation for the fact that both shock tube and field results were good at high pressures, but were poor at low pressures. At high pressures, the breakdown of the oil produced erratic damping, resulting in a variation of plus or minus 20 per cent in the peak pressure records as compared to mean inductance gage values. Examination of inductance gage pressure-time records revealed that the response times of the indenter gages were between 1 and 12 msec approximately.

At low pressures, the large scatter indicates great variation in damping, but it is significant that there were no values as high as the inductance gage values. This means that the damping was much too high. Examination of pressure-time records in this region show that a response time of around 100 msec would have caused low values such as recorded.

A.3 CONCLUSION

Although investigation of the behavior of these gages under different loadings is still being conducted, it appears that the best way

to use these gages to measure peak pressures from atomic blasts is as follows:

(a) Use a baffle chamber designed to give protection from thermal radiation and sand blast.

(b) Shape the baffle so that the ratio of volume to orifice area is 40 in. This gives a fill time of 4 msec at about 7 psi. (See page 37 of reference 8).

(c) Damp each gage so that the time of fall of the piston under its own weight, for a distance of 1/2 cm, is approximately 1 sec.

The author is indebted to R. R. Caforek, W. S. Filler, and LT B. M. Loring for their assistance in the laboratory work, to H. P. Feldman for manufacturing, and to J. R. Mitchell for assistance in obtaining material needed in the field.

APPENDIX B

DETERMINATION OF PRESSURE-TIME CURVES FROM OBSERVED PARTICLE MOTION IN BLAST WAVES

By: F. Theilheimer

B.1 INTRODUCTION

The problem to be discussed here deals with the determination of the pressure due to an explosion. It is assumed that it is possible to observe and measure the displacement of certain particles, and from these data the pressure field due to the explosion can be computed.

The explosion is to take place high up in the air. On a horizontal radial line drawn from ground zero a number of smoke-producing rockets are fired upward and the smoke trails thus generated can be photographed by means of a motion picture camera. If these smoke trails are generated immediately before time zero, then the motion of these smoke trails will give information about the motion of the air particles due to the blast wave passing over them. It is assumed here that the difference in velocity between smoke and air particles is negligible soon after the passage of the shock.

The explosion is assumed to be spherically symmetric. Therefore, if two frames were superposed corresponding points in the two frames could be identified by drawing radial lines through the center of the explosion. It is of course understood that in this particular procedure care had been taken that the images of some markers unaffected by the explosion coincide exactly in the two frames.

The method to be discussed here can be used to find pressure-time relations for points that have been passed by the shock wave. The peak shock pressure itself is not to be found by this method. It is assumed that other better methods are available for that purpose and the peak shock pressure can, therefore, be assumed as given.

B.2 ANALYSIS OF PHOTOGRAPHIC RECORDS

The various points whose motion is to be studied can be chosen in the following way: Draw lines through the center of the explosion, say every ten degrees, on a frame that was taken before the shock front touched the nearest trail. (See Fig. B.1). Choose a certain number, say N, of the intersections between the lines drawn and the various

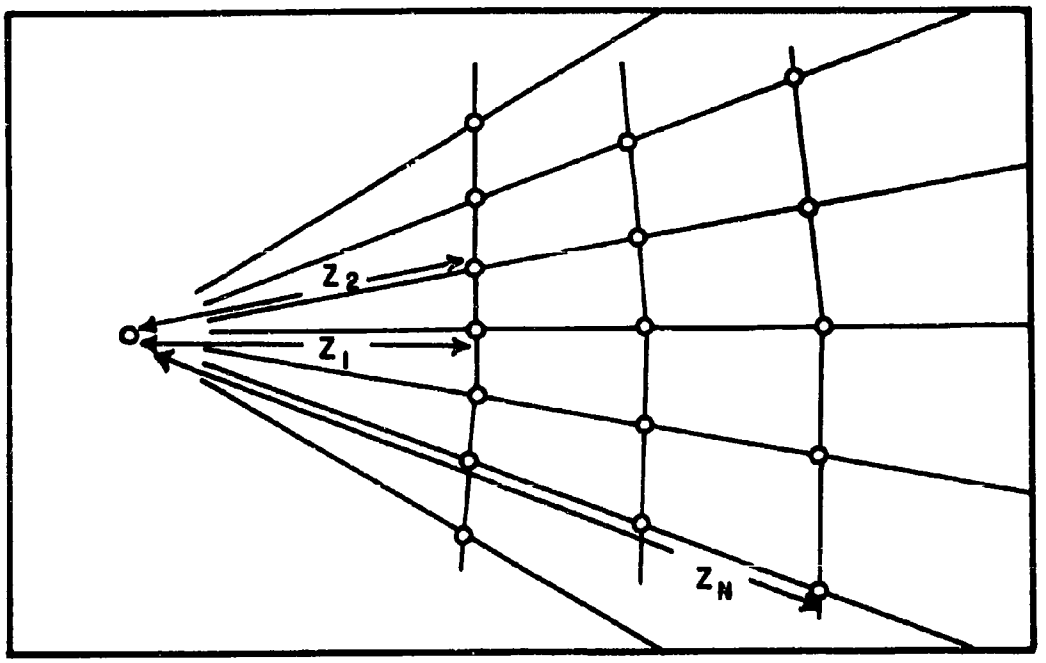

Fig. B.1 Smoke Trails Before Passing of Shock

smoke trails. Measure the distances from the center of the explosion to these N points. For increased accuracy this measurement should be carried out for each point on the last frame before the point is reached by the shock. Then the points should be ordered according to distance and their distances denoted by

$$Z_1, Z_2, Z_3, \ldots, Z_{N-1}, Z_N.$$

Let frame one be the frame in which at least the point Z_1 has changed position; the time when it was taken will be called t_1. Let there be M frames at times

$$t_1, t_2, \ldots, t_M.$$

For each frame again draw lines through the center of the explosion and measure the new distances of each of the points which were originally at distances $Z_1, Z_2, \ldots, Z_N$.

The following notation will be used: $X_{n,m}$ will be the distance at time t_m of the point which was originally at distance Z_n. One can, therefore, set up M tables A_m*, giving X versus Z. It is clear that the tables for the first frames will contain only a few entries, but as soon as the shock has reached Z_N each table A_m will have N entries.

Each table A_m gives X as a function of Z at constant t. For the determination of the pressure it will be necessary to find the derivative of X with respect to Z at constant t. Let us write

$$K = \left(\frac{\partial X}{\partial Z}\right)_t \qquad (B.1)$$

Then K for the midpoint between Z_n and Z_{n+1} can be found as a difference quotient. If we denote by $K_{n+1/2,m}$ the value of K for $Z + 1/2\ (Z_{n+1} + Z_n)$ and $t = t_m$, then

$$K_{n+1/2,m} = \frac{X_{n+1,m} - X_{n,m}}{Z_{n+1} - Z_n} \qquad (B.2)$$

Thus tables B_m can be set up giving K as function of Z at constant t at the midpoint $1/2(Z_{n+1} + Z_n)$. If a graph of K versus Z is drawn for every t_m, then the values of K for Z_n can be read from the graph and tables C_m can be constructed.

B.3 DETERMINATION OF PRESSURE-TIME CURVES

To find the pressure for any point it is necessary to know the peak pressure at the instant when the point was reached by the shock. It is assumed that the peak pressure as a function of distance is available through other observations. Let P_n denote the absolute peak pressure - not the excess pressure - when the point at the distance Z_n is reached by the shock. Thus one can immediately set up a table P giving peak pressure as a function of distance.

The pressure prevailing at time t_m at the point whose original distance was Z_n is denoted by $P_{n,m}$. This pressure is found to be (See Sec B.4):

$$P_{n,m} = P_n \left(\frac{(6\ P_o + P_n)\ \ Z^2_n}{(6\ P_n + P_o)\ \ X^2_{n,m}\ K_{n,m}}\right)^{1.4} \qquad (B.3)$$

* Figure B.2 shows a number of tables useful in carrying out the pressure-time analysis.

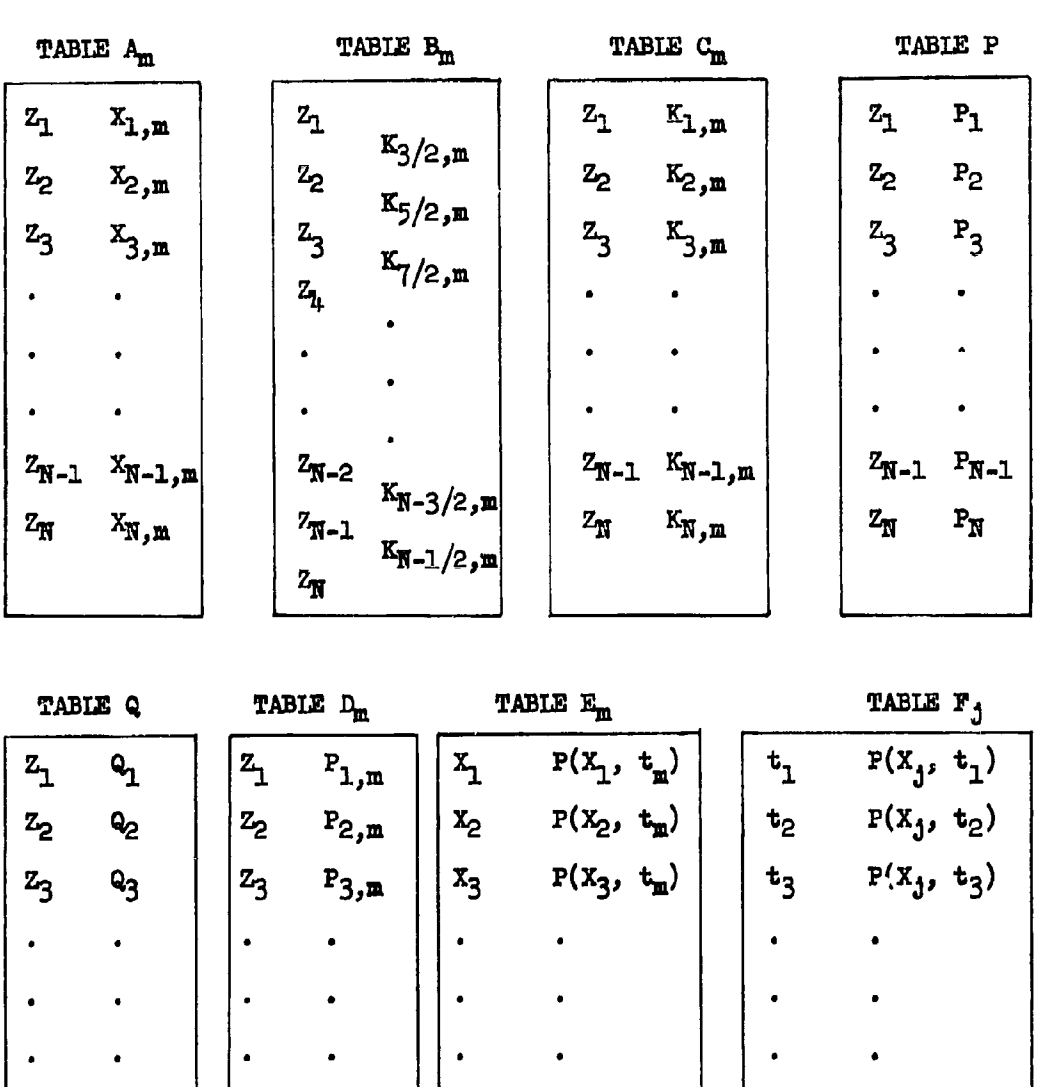

Fig. B.2 Tables Required for Complete Pressure - Time Analysis

where P_o is the pressure of the undisturbed air.

For computational reasons it will be advisable to combine those factors which do not depend on time into

$$Q_n = P_n \left[\frac{(6 P_o + P_n) \quad Z^2_n}{6 P_n + P_o} \right]^{1.4} \tag{B.4}$$

and then

$$P_{n,m} = Q_n \left[\frac{1}{X^2_{n,m} \quad K_{n,m}} \right]^{1.4} \tag{B.5}$$

Now one can construct first a table Q, giving Q in terms of Z, and then tables D_m giving P in terms of Z.

As soon as tables D_m are found, one knows the pressure at any time t_m for all those points whose initial distances were Z_n; that means that at different times one knows the pressure for different distances. This is not what one customarily means by pressure-time relation or pressure-time curve. Then one wants to know the pressure for all times for one or more fixed distances from the explosion.

Suppose we want to know the pressure at the distances

$$X_1, X_2, \ldots, X_J.$$

To find the pressure at these points for time t_m a graph is drawn of pressure P versus distance X at time t_m by taking corresponding values of P and X from Tables A_m and D_m. From the graph one reads the values of P at $X_1, X_2, \ldots, X_J$ and sets up a Table E_m.

As soon as all these Tables E_m are found for all t_m, one can collect all pressure values that occur at the distance X_j at the various times and form J tables F_j which contain the data from which pressure-time curves can be drawn.

Finally one may consult the given peak-pressure data and enter the peak-pressure in each of the pressure-time curves.

B.4 DERIVATION OF EQUATION (B.3)

The distance of a particle from the center of the explosion before the particle was reached by the shock was denoted by Z. The distance of such a particle at any time after passage of the shock

was called X, where X is a function of Z and t. This function X = X(Z,t) is tabulated in the Tables A_m for the various times t_m.

A relationship between Z, the Lagrangian coordinate, and X, the Eulerian coordinate, can be found by observing that a sphere consisting of the same particles does not change its mass as time goes on, even if it changes its volume. Thus if ρ denotes the density at any time and ρ_o the density of the undisturbed medium then

$$\frac{4}{3}\pi Z^3\rho_o = 4\pi\int_o^{X(Z,t)} X^2\rho\, dX \qquad (B.6)$$

Differentiation with respect to Z yields

$$Z^2\rho_o = X^2\rho\left(\frac{\partial X}{\partial Z}\right)_t . \qquad (B.7)$$

If we write as in equation (B.1)

$$K = \left(\frac{\partial X}{\partial Z}\right)_t$$

then a simple formula for the density is found:

$$\rho = \frac{Z^2\rho_o}{X^2 K} \qquad (B.8)$$

To derive a formula for the pressure it now becomes necessary to find a relationship between pressure and density. If the medium studied is an ideal gas with constant ratio of specific heats $\gamma = 1.4$, then pressure and density change in such a way that

$$P\ \rho^{-1.4} = \text{const.} \qquad (B.9)$$

provided that there is no change in entropy. When a particle is passed by a shock it undergoes a change in entropy depending on the strength of the shock; after the passage of the shock, however, no further change in entropy takes place. Therefore, equation (B.9) holds for each particle that has been passed by the shock. The pressure P(Z) at the shock front at the instant when the particle of coordinate Z is reached by the shock is considered a known quantity. If the

corresponding density is called $\rho_s(Z)$, then equation (B.9) yields

$$P(Z,t)\,\rho(Z,t)^{-1.4} = P(Z)\,\rho_s(Z)^{-1.4} \qquad (B.10)$$

Since $\rho(Z,t)$ can be found from equation (B.8) it remains only to express $\rho_s(Z)$ in terms of known quantities. This is done by the Rankine-Hugoniot relation

$$\frac{\rho_s}{\rho_o} = \frac{6P + P_o}{6P_o + P} \qquad (B.11)$$

which is found from the general form of the Rankine-Hugoniot equation by applying it to an ideal gas with $\gamma = 1.4$.

Substituting equations (B.8) and (B.11) in equation (B.10) one finds

$$P(Z,t) = P(Z)\left[\frac{(6P_o + P(Z))\,Z^2}{(6P(Z) + P_o)\;X(Z,t)^{\,2}\,K(Z,t)}\right]^{1.4} \qquad (B.12)$$

which is equivalent to equation (B.3).

B.5 CHECK ON THE ACCURACY OF THE PROCEDURE

A check on the data found here can be based on one of the differential equations of fluid dynamics, the one which expresses the conservation of momentum. Considering that Z is the Langrangian and X the Eulerian coordinate this differential equation assumes the form

$$\frac{\partial^2 X}{\partial t^2} + \left[\frac{X^2}{\rho_o Z^2}\,\frac{\partial P}{\partial Z}\right] = 0. \qquad (B.13)$$

The differential equation can be replaced by the following difference equation:

$$\frac{X_{n,m+1} - 2X_{n,m} + X_{n,m-1}}{\left[1/2\,(t_{m+1} - t_{m-1})\right]^2} + \frac{X^2_{n,m}}{\rho_o Z^2_n}\left(\frac{P_{n+1,m} - P_{n-1,m}}{Z_{n+1} - Z_{n-1}}\right) = 0. \qquad (B.14)$$

Then equation (B.14) provides a check on the accuracy of the procedure by comparing the n-th lines of Tables A_{m-1}, A_m, and A_{m+1} with the (n-1)-st and (n+1)-st lines of Table D_m.

REFERENCES

1. Porzel and Reines, "Height of Burst for Atomic Bombs" LA-743R dated 3 Aug 1949 (Secret-RD)

2. Moulton and Simonds, Annex 1.6, Part II Sec 1 to the Scientific Director's Report - Operation GREENHOUSE, "Peak Pressure vs Distance in the Free Air and Mach Regions Using Smoke Rocket Photography" draft of 14 July 1951 in Publication (Secret-RD)

3. Moulton, Walthall, Hanlon, Project 1.3b Operation JANGLE, "Peak Pressure vs Distance in Free Air Using Smoke Rocket Photography" June, 1952 (AFSWP WT-389) (Secret-RD)

4. Redmond et al "SANDSTONE Blast Telemetering Report" SANDSTONE No. 22 Annex 5, Part III of the Scientific Director's Report, June 1948 (Secret-RD)

5. Price et al Annex 1.6 Part VI Sec 1a to the Scientific Director's Report Operation GREENHOUSE "Pressure-Time Measurements in the Mach Region with Variable Inductance Diaphragm Gauge" draft of 15 July 1951 in Publication (Secret-RD)

6. Morris et al, Project 1.1 Operation JANGLE, "Ground Acceleration Measurement" June, 1952 (AFSWP WT-388) (Secret-RD)

7. Shafer, "A Copper Indenter Gauge for Air Blast Measurement" SANDSTONE No. 21, Annex 5, Part II of the Scientific Director's Report, June, 1948 (Secret-RD)

8. Shafer and Walthall, "A Copper Indenter Gauge for the Measurement of Air Blast Peak Pressure" NavOrd 2192, 10 July 1951 (Unclassified)

9. Shafer, Annex 1.6, Part III, Sec 3 of the Scientific Director's Report - "Positive Peak Pressure Measurements in the Mach Stem Region by Means of Copper Indenter Gages" draft of July, 1951 in Publication (Secret-RD)

10. Caforek, "Evaluation of Copper-Disc Indenter Gage in Measurement of Peak Pressure and Pressure Ratios of Small Charges" NavOrd Report 2170, 16 September 1951 (Confidential SI)

11. Operation TUMBLER Preliminary Report (Parts One and Two) AFSWP 15 May 1952 (Secret-RD)

REFERENCES (CONT.)

12. Eberhard et al, Project 1.2a-1, Operation JANGLE, "Peak Air Blast Pressure from Shock Velocity Measurements along the Ground" (AFSWP WT-323) (Secret-RD)

13. Doll, "Air Pressure vs Time" Annex 1, Operation TUMBLER Preliminary Report (Project 1.2) 9 May 1952 (Secret-RD)

14. Aronson et al, "Free Air and Ground Level Pressure Measurements" Annex II, Operation TUMBLER, Preliminary Report - 6 May 1952 (Secret-RD)

15. Hartmann and Kalavski, "The Optimum Height of Burst for High Explosives", NavOrd Report 2451, July 1952 (Confidential SI)

16. Army, Navy, Air Force (JCS) TM 23-200/OPNAV-P-36-00100/AFOAT 385.2. Supplement No. 1 dated 8 February 1952 (Secret)

17. Pike and Bird, "The Reduction in Blast from Bare Charges at High Altitudes" Armament Research Establishment Report No. 3/50, April, 1950 (Secret, Descreet)

18. Polacheck and Seeger, "Regular Reflection of Shocks in Ideal Gases" ERR No. 13 (Bureau of Ordnance) 12 February 1944 (Confidential)

19. Hartmann, "The Effect of Ambient Conditions on Air Blast" NavOrd Report 2482, 20 June 1952 (Confidential SI)

20. Fisher, "Spherical Cast TNT Charges, Air Blast Measurements on" NOLM No. 10,780 of 23 January 1950 (Confidential)

21. Kirkwood and Brinkley "Theoretical Blast-Wave Curves for Cast TNT" OSRD No. 5481 of August 1945 (Unclassified)

22. Sokolnikoff, "Higher Mathematics for Engineers and Physicists" McGraw-Hill 1941

23. Murphey, "Pressure-time vs Distance Measurements" Annex XIV, Operation TUMBLER Preliminary Report (Project 19.1) 11 May 1952 (Secret-RD)

24. Hartmann, Lampson, Aronson, "Summary Report on Blast Measurements at Eniwetok 1951" Draft of Annex 1.6, Part I of the Scientific Director's Report of Operation GREENHOUSE - dated 1 May 1952 (Secret-RD) (In publication)

REFERENCES (CONT.)

25. Kennard, "Underwater Explosions, A Summary of Results" Report C-334, David Taylor Model Basin, February, 1951, (Confidential)

26. Monahan et al, "The Effect of Thermal Radiation on Materials" Operation BUSTER, October-November 1951, Project 2.4-2 (Secret-SI)

27. Clarke and Eberhard, "Time Shock Arrival" Operation TUMBLER, Preliminary Report Annex III, Project 1.4, 8 May 1952 (Confidential SI)

28. Cook, "Air Blast Pressure Measurement" Operation TUMBLER, Preliminary Report - Annex IX, Project 1.13, 8 May 1952 (Confidential SI)

29. Hirschfelder and Curtiss, "Thermodynamic Properties of Air", Vol.II, University of Wisconsin (NRL) 21 Dec 1948 (Unclassified)

30. Currie and Smith, "Flow Characteristics of Organopoly-siloxane Fluids and Greases" Industrial and Engineering Chemistry, Vol. 42, Page 2457, December, 1950 (Unclassified)

31. Arons and Yennie, "Long Range Shock Propagation in Underwater Explosion Phenomena, I", NavOrd 424, 27 April 1949 (Unclassified)

32. Rayleigh, "Theory of Sound", Vol. II, Second Edition p.78-88, Dover Publications, 1945

33. For the theory of the precursor beyond the critical angle, see Ott, Annalen der Physik, Vol. 41, 1942, p.443; for observations see Schmidt, Zeits. für tech. Phys. Vol. 19, p.554, and Physik. Zeits., Vol 39, 1938, p.868.

34. Broida, Broido, and Willoughby, "Air Temperature in the Vicinity of a Nuclear Detonation", Operation TUMBLER Preliminary Report, Annex XI (Project 8.2), 14 May 1952 (Confidential SI)

35. "Effects of Atomic Weapons", Edited under supervision of LASL, Government Printing Office, September, 1950 (Unclassified)

36. Jacobs and Liddiard, "The Observation of Precursors Near the Boundary of Two Liquids", NavOrd 2602, now in publication (Unclassified)

37. Murphey, "Some Measurements of Overpressure - Time vs Distance for Air Burst Bombs", Operation BUSTER-JANGLE, (WT-304) 4 March 1952 (Secret SI)

TABLE 1.1

Characteristics of TUMBLER Shots 1 through 4

Characteristics	Symbol	Shot 1	Shot 2	Shot 3	Shot 4
Location	--	FF Area	T-7	T-7	T-7
Nominal Ground Zero	--	F-200	7-200	7-200	7-200
Direction of Blast Line from Zero Tower	--	West from F-200	S 9°56'06" W from 7-200		
Location of Bendix Gages Relative to Blast	--	35 feet to right of blast line (facing zero) except for stations 7Q1* and 7Q2*.			
Actual Ground Zero from Station 200	GZ	122'N 67'E	143'S 84'E	80'S 124'W	140'S 153'W
Actual Height in feet	h	793	1109	3447	1040
Radio Chemical KT	W_{RC}	1.05	1.15	30.0	19.6
Pressure on Ground before Shot	P_{oG}	914 mb 13.26 psi	878 12.73	873 12.66	877 12.72
Pressure at Burst Height before Shot	P_o	888.5 mb 12.89 psi	842 12.21	770 11.17	845 12.26
Actual Temperature on Ground before Shot	T_{oG}	58°0F 14.4C	54°1F 12.3C	66°7F 19.3C	62°6F 17.0C
Actual Temperature at Burst Height	T_o	56°5F 13.6C	48°4F 9.1C	45°7F 7.6C	59°0F 15.0C
Factor to Multiply Pressures to Correct to Sea-Level	$S_p = \frac{14.7}{P_o}$	1.140	1.204	1.316	1.199
Factor to Multiply Distance to Correct to Sea-Level	$S_d' = \left(\frac{P_o}{14.7}\right)^{1/3}$	0.957	0.940	0.913	0.941
Factor to Multiply Distance to Correct to 1 KT at Sea-Level	$S_d = \left(\frac{P_o}{14.7 W_{RC}}\right)^{1/3}$	0.942	0.897	0.294	0.349
Factor to Multiply Time by to Correct to 1 KT at Sea-Level	$S_T = \left(\frac{T_o+273}{293}\right)^{1/2} \left(\frac{P_o}{14.7}\right)^{1/3} \left(\frac{1}{W_{RC}}\right)^{1/3}$	0.931	0.880	0.288	0.346
Factor to Multiply Impulse by to Correct to 1 KT at Sea-Level	$S_I = S_T S_P = \left(\frac{T_o+273}{293}\right)^{1/2} \left(\frac{14.7}{P_o}\right)^{2/3} \left(\frac{1}{W_{RC}}\right)^{1/3}$	1.061	1.060	0.379	0.415
Reduced Height in feet	$H = \frac{h}{(W_{RC})^{1/3} \left(\frac{P_o}{14.7}\right)^{1/3}}$	747	995	1012	363

* Stations 7Q1 and 7Q2 were used on Shots 3 and 4 only and were located relative to Station 7-200 as follows:

7Q1: 2917 feet; S 5°10'0" E
7Q2: 3686 feet; S 3°31'30" E

TABLE 2.1

Carbon Paper Distribution

Station	TUMBLER 1			TUMBLER 2			TUMBLER 3			TUMBLER 4		
	Normal Incidence Thermal Energy	Possible Minimum Energy	Over Gage Inlet / Test Only	Normal Incidence Thermal Energy	Possible Minimum Energy	Over Gage Inlet / Test Only	Normal Incidence Thermal Energy	Possible Minimum Energy	Over Gage Inlet / Test Only	Normal Incidence Thermal Energy	Possible Minimum Energy	Over Gage Inlet / Test Only
	cal/cm^2			cal/cm^2			cal/cm^2			cal/cm^2		
200	54.0	53.0	●	28.0	27.8	●	65.0	64.9	●	500.0	488.0	●
212				27.0	26.3	●	64.5	64.2	●	490.0	475.0	●
201	47.0	43.0		22.0	19.1	●	63.5	62.3	●	360.0	311.0	●
213				16.1	11.9	●	61.0	58.4	●	255.0	186.0	●
202	36.5	29.0		11.4	7.2	●	57.0	52.8	●	180.0	110.0	●
203	26.5	18.3		6.4	3.0	●	48.0	40.7	●	95.0	42.3	●
204	19.8	11.7		3.85	1.38		37.5	28.7	●	54.0	18.6	●
205	14.8	7.5		2.6	0.76		30.5	20.9	●	36.0	10.0	●
206	11.6	5.2		1.21	0.30	o	25.0	15.4	●	35.2	5.9	●
207	9.2	3.7					20.0	11.1		18.2	3.64	●
208	7.2	2.6					16.0	8.1		14.0	2.46	●
209	5.0	1.45					11.8	4.98		9.0	1.26	o
210	3.7	0.93					8.6	3.10	●	6.2	0.72	
211	2.1	0.40										
*Revetment	1.45		●	0.25		o	4.7		●	3.5		o

* Nearly normal incidence was assured at this location
Thermal data from Reference 11

● Indicates carbon paper burned
o " " " did not burn

TABLE 2.2

TUMBLER 1 - Phase Durations, Positive Impulses, and Pressures
(Ground Level)

Station Number	Ground Range (ft)	Phase Durations		Positive Impulse (psi-sec)	Peak Pressures		
		Positive t_4 (sec)	Negative t_8 (sec)		Initial P_b (psi)	Positive P_c (psi)	Negative P_e (psi)
F-200	170.7	0.222	0.840	1.98	25.08	27.65	3.48
F-201	353.7	0.213	0.936	1.57	16.18	20.22	3.45
F-202	588.3	0.220	0.936	1.34	10.63	15.85	2.60
F-202T	588.3	0.230	0.856	1.39	11.40	15.15	3.15
F-203	831.9	0.231	0.970	1.07	9.74	12.00	2.49
F-204	1078.4	0.243	0.972	0.86		11.91	2.10
F-205	1326.3	0.255	0.981	0.74		10.24	1.74
F-206	1574.8	0.277	0.975	0.68		8.08	1.37
F-207	1823.7	0.299	0.947	0.60		7.05	1.27
F-208	2073.0	0.309	0.975	0.50		5.63	1.01
F-209	2571.7	0.337	0.984	0.42		3.92	0.78
F-209T	2571.7	0.326	1.006	0.42		3.87	0.84
F-210	3071.0	0.361	1.032	0.35		2.96	0.70
F-211	4070.0	0.390	1.033	0.27		2.00	0.49

TABLE 2.3

TUMBLER 1 - Distances and Times
(Ground Level)

Station Number	Range Distances		Arrival Time t_1 (sec)	Rise Times	
	Ground (ft)	Slant (ft)		Initial t_5 (msec)	Peak t_6 (msec)
F-200	170.7	811.1	0.330	1.6	5.6
F-201	353.7	868.3	0.368	1.7	6.9
F-202	588.3	987.4	0.448	1.7	12.9
F-202T	588.3	987.4	0.453	1.6	10.9
F-203	831.9	1149.3	0.569	1.6	9.9
F-204	1078.4	1338.7	0.718		1.5
F-205	1326.3	1545.3	0.882		1.3
F-206	1574.8	1763.2	1.053		1.6
F-207	1823.7	1988.7	1.232		1.3
F-208	2073.0	2219.4	1.427		1.2
F-209	2571.7	2691.2	1.819		1.4
F-209T	2571.7	2691.2	1.821		1.6
F-210	3071.0	3171.7	2.227		1.4
F-211	4070.0	4146.5	3.066		1.1

TABLE 2.4

TUMBLER 2 - Phase Durations, Positive Impulses, and Pressures

Station Number	Ground Range (Ft)	Phase Durations		Positive Impulse (psi-sec)	Peak Pressures		
		Positive t_4 (sec)	Negative t_8 (sec)		Initial P_b (psi)	Positive P_c (psi)	Negative P_e (psi)
7-200	145.6	0.250	1.296	1.21	9.14*	14.06	2.37
7-212	259.0	0.259	1.314	1.18	10.91	12.06	2.19
7-201	627.9	0.254	0.986	1.06	9.59	10.59	1.99
7-201T	627.9	0.265	1.036	1.02	9.89	10.84	1.91
7-213	1,001.3	0.267	1.060	0.802	7.62	7.77	1.71
7-202	1,375.6	0.283	0.998	0.644	6.08	6.38	1.53
7-203	2,124.9	0.324	0.935	0.477		5.32	0.96
7-204	2,874.6	0.345	0.936	0.365		3.59	0.70
7-205	3,624.4	0.371	0.962	0.296		2.78	0.57
7-206	4,374.3	0.363	0.959	0.250		2.06	0.54
7-206T	4,374.3	0.390	0.895	0.244		1.86	0.47

* Initial peak of the form of P_a.

TABLE 2.5

TUMBLER 2 - Distances and Times (Ground Level)

Station Number	Range Distances		Arrival Times		Rise Times	
	Ground (Ft)	Slant (Ft)	t_1 (sec)	t_2 (sec)	Initial t_5 (msec)	Peak t_6 (msec)
7-200	145.6	1,118.5	0.551	0.554	1.5*	3.4
7-212	259.0	1,138.8	0.567		1.5	3.7
7-201	627.9	1,274.4	0.672		1.3	6.2
7-201T	627.9	1,274.4	0.671		1.5	5.9
7-213	1,001.3	1,494.2	0.842		1.4	5.6
7-202	1,375.6	1,767.0	1.066		1.3	6.6
7-203	2,124.9	2,396.9	1.584			1.7
7-204	2,874.6	3,081.1	2.163			1.4
7-205	3,264.4	3,790.3	2.773			1.4
7-206	4,374.3	4,512.6	3.399			1.4
7-206T	4,374.3	4,512.6	3.399			1.2

* Rise time to initial peak of 9.14 psi.

TABLE 2.6

TUMBLER 3 - Phase Durations, Positive Impulses, and Pressures (Ground Level)

Station Number	Ground Range (ft)	Phase Durations		Positive Impulse (psi-sec)	Peak Pressures		
		Positive t_4 (sec)	Negative t_8 (sec)		Initial P_b (psi)	Positive P_c (psi)	Negative P_e (psi)
7-200	174.9	0.753	4.07	3.30	6.55	12.13	1.88
7-212	309.9	0.753	3.09	3.37	7.58	12.11	1.88
7-201	665.4				8.14	11.67	
7-201T	665.4	0.738	3.24	3.21	6.22	11.76	1.96
7-213	1034.8	0.755	3.63	3.19	7.73	11.13	1.85
7-202	1407.1	0.781	3.71	2.95	8.83	10.19	1.71
7-203	2154.6	0.825	3.57	2.74	5.54	8.55	1.52
7-204	2903.3	0.780	3.13	2.20	6.51	7.73	1.61
7-205	3652.6	0.832	3.97	1.97		6.52	1.29
7-206T	4402.1	0.879	3.51	1.76		5.87	1.11
7-207	5151.8	0.938	3.47	1.62		5.77	0.89
7-208	5901.5	0.968	3.85	1.53		5.72	0.90
7-209	7401.2	1.025	3.25	1.23		4.51	0.65
7-210	8901.0	1.041	5.05	1.05		3.26	0.60
7-211	11900.7	1.115	3.25	0.809		2.55	0.49
7-Q1	2851.1	0.821	3.88	2.26		9.77	1.37
7-Q2	3616.0	0.855	3.56	2.13		7.19	1.24

TABLE 2.7

TUMBLER 3 - Distances and Times
(Ground Level)

Station Number	Range Distances		Arrival Time t_1 (sec)	Rise Times	
	Ground (ft)	Slant (ft)		Initial t_5 (msec)	Peak t_6 (msec)
7-200	174.9	3451.4	1.705	1.8	27.2
7-212	309.9	3460.9	1.721	1.2	21.5
7-201	665.4	3510.6	1.760	1.2	12.5
7-201T	665.4	3510.6	1.758	1.2	16.4
7-213	1034.8	3599.0	1.832	1.3	7.5
7-202	1407.1	3723.1	1.926	1.5	11.2
7-203	2154.6	4065.0	2.200	1.7	7.8
7-204	2903.3	4506.8	2.566	1.5	8.5
7-205	3652.6	5022.3	2.987		1.4
7-206T	4402.1	5591.1	3.459		1.8
7-207	5151.8	6198.6	3.964		1.6
7-208	5901.5	6834.5	4.502		1.4
7-209	7401.2	8164.5	5.630		1.6
7-210	8901.0	9545.1	6.822		5.5
7-211	11900.7	12389.8	9.275		0.9
7-Q1	2851.1	4473.3	2.530		1.8
7-Q2	5816.0	4995.7	2.950		1.5

TABLE 2.8

TUMBLER 4 - Distances and Arrival Times
(Ground Level)

Station Number	Range Distances		Arrival Times			
	Ground (ft)	Slant (ft)	t_1 (sec)	t_2 (sec)	t_3 (sec)	t_9 (sec)
7-200	230.4	1065.2	0.224	0.234		
7-212	265.5	1073.4	0.235	0.250		
7-201	607.6	1204.6	0.283	0.301		
7-201T	607.6	1204.6	0.284	0.303		
7-213	974.2	1425.0	0.368	0.420		
7-202	1345.4	1700.5	0.486	0.608	1.089	
7-203	2091.9	2336.2	0.907	0.953	1.529	
7-204	2804.3	3024.7	1.430		2.064	3.351
7-205	3589.3	3737.0	1.973		2.631	4.056
7-206T	4338.7	4461.6	2.546		3.235	4.785
7-207	5088.3	5193.5	3.131		3.841	5.496
7-208	5837.9	5929.8	3.730		4.452	6.186
7-209	7337.5	7410.8	4.967		5.709	7.482
7-210	8837.2	8898.2	6.232			9.008
7-211	11836.8	11882.4	8.802			12.628
7-Q1	2795.8	2983.0	1.377		1.974	
7-Q2	3559.3	3708.1	1.936		2.602	4.030

TABLE 2.9

TUMBLER 4 - Positive Impulses and Pressures
(Ground Level)

Station Number	Ground Range (ft)	Positive Impulse (psi-sec)	Peak Pressures			
			Precursor P_a (psi)	Initial P_b (psi)	Positive P_c (psi)	Negative P_e (psi)
7-200	230.4	9.30	151.0		140.2	7.4
7-212	265.5	8.67	101.4		116.9	6.3
7-201	607.6	6.99	27.5		82.7	5.9
7-201T	607.6	7.37	29.2		82.4	6.0
7-213	974.2	5.25	10.6		43.6	5.47
7-202	1345.4	4.33	8.7		24.50	4.37
7-203	2091.9	3.27			9.84	2.65
7-204	2804.3	2.38		6.09	8.84	2.06
7-205	3589.3	2.00		5.47	6.39	1.50
7-206T	4338.7	1.71		4.24	4.80	1.23
7-207	5088.3	1.39			3.96	0.96
7-208	5837.9	1.25			3.24	0.95
7-209	7337.5	0.87			2.14	0.65
7-210	8837.2	0.78			1.53	0.59
7-211	11836.8	0.64			1.21	0.45
7-Q1	2795.8	2.49			7.72	1.88
7-Q2	3559.3	2.06		1.69	6.20	1.71

TABLE 2.10

TUMBLER 4 - Phase Durations and Rise Times
(Ground Level)

Station Number	Ground Range (ft)	Phase Durations		Rise Times		
		Positive t_4 (sec)	Negative t_8 (sec)	Initial t_5 (msec)	Precursor Peak t_7 (msec)	Peak t_6 (msec)
7-200	230.4	0.281	1.08		9.3	18.2
7-212	265.5	0.279	1.02		8.3	22.2
7-201	607.6	0.300	0.807		1.4	34.6
7-201T	607.6	0.303	0.922		1.6	35.0
7-213	974.2	0.414	1.133		23.2	74.8
7-202	1345.4	0.539			20.5	161.8
7-203	2091.9	0.702				57.2
7-204	2804.3	0.748		1.9		15.5
7-205	3589.3	0.807		1.4		6.4
7-206T	4338.7	0.877		1.6		11.5
7-207	5088.3	0.942				1.7
7-208	5837.9	0.988				1.5
7-209	7337.5	1.085				1.5
7-210	8837.2	1.196				1.3
7-211	11836.8	1.284				1.5
7-Q1	2795.8	0.747				36.0
7-Q2	3559.3	0.812		1.7		33.6

TABLE 3.1

Photographic Details

Shot	Film Number	Location (Station)	Camera	Effective Aperture	Effective Focal Length(mm)	Nominal Frame Rate(fps)	Vertical Aiming	Horizontal Aiming	Purpose
1	13081	F-361	MMH-4	f/8-15°	75.03	96	Level	0°-00'	Shock Velocity
	13082	F-361	MMH-8	f/4-15°	75.13	110	"	"	" "
	13083	F-362	MMH-1	f/4-15°	74.98	96	"	"	Particle Disp.
	13084	F-362	MMH-5	f/8-15°	74.88	96	"	6°-51'L	" "
2	13181	7-361	MMH-4	f/8-30°	100.0	---	Level	0°-00'	Shock Velocity
	13182	7-361	MMH-8	f/4-45°	75.13	77	"	"	" "
	13183	7-362	MMH-1	f/8-30°	74.98	91	"	7°-57'L	Particle Disp.
	13184	7-362	MMH-5	f/4-45°	50.11	98	"	"	" "
3	13281	7-361	MMH-4	f/25-30°	50.47	96	4°-00'	0°-00'	Shock Velocity
	13282	7-361	MMH-8	f/5.6-30°	34.62	96	Level	0°-00'	" "
	13283	7-362	MMH-1	f/25-30°	50.14	96	4°-00'	7°-51'L	Particle Disp.
	13284	7-362	MMH-5	f/5.6-30°	50.11	96	"	"	" "
4	13381	7-361	MMH-4	f/18-60°	100.01	100	Level	0°-00'	Shock Velocity
	13382	7-361	MMH-8	f/5.6-90°	74.85	100	"	"	" "
	13383	7-362	MMH-1	f/18-60°	75.03	96	"	7°-57'L	Particle Disp.
	13384	7-362	MMH-5	f/5.6-90°	50.11	96	"	"	" "

TABLE 3.2

Absolute Time-of-Arrival of Shock in Free Air and Mach Region - TUMBLER 1

Distance From Burst (Ft)	Distance From GZ (Ft)	Time (Sec)	Distance From Burst (Ft)	Distance From GZ (Ft)	Time (Sec)
123.216		0.0052490	850.130	281.464	0.3517802
163.080		0.0143395	859.190	312.268	0.3609295
229.218		0.0234318	877.310	335.220	0.3700802
261.230		0.0325258	889.390	375.990	0.3792324
289.618		0.0416213	913.550	435.182	0.3975419
317.100		0.0507183	940.126	489.844	0.4158576
343.978		0.0598169	966.400	527.896	0.4341796
368.138		0.0689169	990.560	579.236	0.4525078
387.164		0.0780187	1,013.814	619.100	0.4708422
411.928		0.0871221	1,040.390	661.380	0.4891829
431.256		0.0962269	1,063.946	700.036	0.5075298
447.564		0.1053332	1,089.314	732.652	0.5258825
467.496		0.1144409	1,101.394	755.000	0.5350612
484.710		0.1235503	1,117.400	775.234	0.5442417
497.998		0.1326610	1,126.158	789.730	0.5534236
519.440		0.1417730	1,138.540	809.360	0.5626073
535.748		0.1508868	1,150.318	825.970	0.5717925
550.848		0.1600020	1,162.700	844.694	0.5809792
566.552		0.1691188	1,175.082	860.700	0.5901675
584.370		0.1782371	1,186.860	877.310	0.5993572
598.262		0.1873571	1,201.054	893.920	0.6085486
613.060		0.1964786	1,208.906	906.000	0.6177418
628.160		0.2056016	1,220.080	922.610	0.6269364
643.260		0.2147262	1,236.086	939.220	0.6361324
657.152		0.2238522	1,260.548	970.024	0.6545293
673.460		0.2329799	1,286.218	1,002.640	0.6729324
688.258		0.2421090	1,294.674	1,017.740	0.6821364
715.740		0.2603721	1,330.310	1,060.624	0.7097574
741.108		0.2786415	1,356.584	1,094.750	0.7281791
773.120		0.2969171	1,380.140	1,123.138	0.7466068
798.790		0.3151988	1,402.790	1,150.016	0.7650411
809.360	105.398	0.3243419	1,414.870	1,174.176	0.7834813
819.326	173.650	0.3334866	1,449.600	1,208.000	0.8019278
835.936	234.654	0.3426328	1,469.834	1,230.650	0.8203804

TABLE 3.3

Peak Overpressure - Shock Velocity - Distance - TUMBLER 1

Distance From Burst (Ft)	Shock Velocity (Ft/Sec)	Peak Overpressure (psi)
200	5,500.8	348.5
300	3,149.7	106.0
400	2,295.5	49.3
500	1,896.7	28.9
600	1,663.2	18.8
700	1,527.3	13.5
800	1,454.2	10.8
900	1,418.7	9.5
1,000	1,387.7	8.4
1,100	1,356.6	7.4

TABLE 3.5

Peak Overpressure - Shock Velocity - Distance - TUMBLER 2

Distance From Burst (Ft)	Shock Velocity (Ft/Sec)	Peak Overpressure (psi)
400	2,278.8	46.6
450	2,084.4	36.7
500	1,926.9	29.3
550	1,802.5	23.9
600	1,698.1	19.5
650	1,614.1	16.3
700	1,554.7	14.0
800	1,468.1	10.9
900	1,403.1	8.7
1,000	1,355.5	7.2
1,100	1,322.1	6.1
1,200	1,301.2	5.4

TABLE 3.4

Absolute Time-of-Arrival of Shock in Free Air
TUMBLER 2

Distance From Burst (Ft)	Time (Sec)	Distance From Burst (Ft)	Time (Sec)	Distance From Burst (Ft)	Time (Sec)
368.410	0.0683803	787.788	0.3065203	1,119.080	0.5446603
397.772	0.0816103	806.624	0.3197503	1,132.930	0.5578903
427.134	0.0948403	828.230	0.3329803	1,152.320	0.5711203
457.050	0.1080703	850.390	0.3462103	1,172.264	0.5843503
481.980	0.1213003	865.902	0.3594403	1,185.560	0.5975803
510.234	0.1345303	886.400	0.3726703	1,207.166	0.6108103
534.056	0.1477603	908.560	0.3859003	1,214.368	0.6240403
559.540	0.1609903	920.748	0.3991303	1,238.744	0.6372703
575.606	0.1742203	939.030	0.4123603	1,257.580	0.6505003
603.860	0.1874503	958.420	0.4255903	1,289.158	0.6769603
624.358	0.2006803	976.702	0.4388203	1,310.764	0.6901903
648.180	0.2139103	997.754	0.4520503	1,328.492	0.7034203
666.462	0.2271403	1,013.266	0.4652803	1,358.962	0.7298803
691.392	0.2403703	1,030.994	0.4785103	1,393.864	0.7563403
708.012	0.2536003	1,049.830	0.4917403	1,430.982	0.7828003
729.064	0.2668303	1,067.004	0.5049703	1,460.344	0.8092603
750.116	0.2800603	1,080.300	0.5182003	1,493.030	0.8357203
768.398	0.2932903	1,096.920	0.5314303		

TABLE 3.6

Absolute Time-of-Arrival of Shock in Free Air
TUMBLER 3

Distance From Burst (Ft)	Time (Sec)	Distance From Burst (Ft)	Time (Sec)	Distance From Burst (Ft)	Time (Sec)
194.580	0.0028800	1,009.278	0.1653354	1,478.808	0.3755718
342.630	0.0124362	1,044.810	0.1748916	1,519.416	0.3946842
424.692	0.0219924	1,072.728	0.1844478	1,556.640	0.4137966
485.604	0.0315486	1,095.570	0.1940040	1,591.326	0.4329090
552.438	0.0411048	1,120.114	0.2035602	1,631.088	0.4520214
599.814	0.0506610	1,139.562	0.2131164	1,664.082	0.4711338
647.190	0.0602172	1,164.096	0.2226726	1,690.308	0.4902462
691.182	0.0697734	1,175.940	0.2322288	1,724.994	0.5093586
730.098	0.0793296	1,201.320	0.2417850	1,763.910	0.5284710
765.630	0.0888858	1,222.470	0.2513412	1,785.060	0.5475834
798.624	0.0984420	1,235.160	0.2608974	1,823.976	0.5666958
835.002	0.1079982	1,258.848	0.2704536	1,853.586	0.5858082
868.842	0.1175544	1,284.228	0.2800098	1,888.272	0.6049206
899.298	0.1271106	1,323.990	0.2991222	1,920.420	0.6240330
926.370	0.1366668	1,367.982	0.3182346	1,954.260	0.6431454
955.980	0.1462230	1,406.052	0.3373470	1,981.332	0.6622578
989.820	0.1557792	1,450.890	0.3564594		

TABLE 3.7

Peak Overpressure - Shock Velocity - Distance - TUMBLER 3

Distance From Burst (Ft)	Shock Velocity (Ft/Sec)	Peak Overpressure (psi)
525	6,385	447.0
575	5,581	339.0
650	4,499	217.6
700	4,066	177.8
800	3,593	129.6
900	3,184	100.5
1,000	2,855	77.7
1,100	2,565	59.9
1,400	2,039	32.4
1,500	1,936	27.9
1,550	1,891	26.1
1,600	1,842	24.0
1,650	1,792	22.1
1,700	1,751	20.4
1,750	1,715	19.1
1,800	1,683	17.9
1,850	1,656	16.9
1,900	1,632	16.0
1,950	1,612	15.3
2,000	1,594	14.6

TABLE 3.8

Absolute Time-of-Arrival of Shock in Free Air - TUMBLER 4

Distance From Burst (Ft)	Time (Sec)	Distance From Burst (Ft)	Time (Sec)	Distance From Burst (Ft)	Time (Sec)
206.164	0.0044500	1,064.689	0.2215460	1,547.291	0.4682460
325.968	0.0143180	1,087.972	0.2314140	1,583.275	0.4879820
398.359	0.0241860	1,107.446	0.2412820	1,608.675	0.5077180
464.822	0.0340540	1,131.153	0.2511500	1,644.235	0.5274540
517.316	0.0439220	1,152.319	0.2610180	1,678.526	0.5471900
562.613	0.0537900	1,174.756	0.2708860	1,714.509	0.5669260
606.217	0.0636580	1,193.806	0.2807540	1,744.143	0.5866620
643.470	0.0735260	1,212.433	0.2906220	1,763.996	0.6002851
682.840	0.0833940	1,230.213	0.3004900	1,778.009	0.6063980
717.554	0.0932620	1,250.957	0.3103580	1,794.017	0.6197273
748.881	0.1031300	1,267.467	0.3202260	1,807.643	0.6261340
782.324	0.1129980	1,286.940	0.3300940	1,829.749	0.6391694
811.534	0.1228660	1,309.377	0.3399620	1,853.556	0.6586116
839.474	0.1327340	1,331.390	0.3498300	1,883.031	0.6780537
861.488	0.1426020	1,348.324	0.3596980	1,913.074	0.6974958
889.005	0.1524700	1,365.257	0.3695660	1,947.651	0.7169380
916.521	0.1623380	1,384.731	0.3794340	1,979.960	0.7363801
944.038	0.1722060	1,402.934	0.3893020	2,012.270	0.7558222
969.322	0.1820740	1,437.224	0.4090380	2,041.179	0.7752644
994.839	0.1919420	1,479.558	0.4287740	2,077.456	0.7947065
1,020.239	0.2018100	1,509.191	0.4485100	2,108.632	0.8238697
1,041.405	0.2116780				

TABLE 3.9

Peak Overpressure - Shock Velocity - Distance
TUMBLER 4

Distance From Burst (ft)	Shock Velocity (ft/sec)	Peak Overpressure (psi)
400	7457	656.5
450	6137	441.8
500	5244	319.5
550	4625	245.0
600	4156	196.6
650	3804	158.7
700	3521	129.5
750	3147	103.2
800	2908	87.0
850	2763	74.8
900	2624	66.2
1000	2359	50.8
1050	2257	45.1
1100	2166	40.5
1150	2091	36.7
1200	2023	33.4
1250	1966	30.7
1300	1916	28.4
1350	1874	26.5
1400	1830.6	24.7
1500	1757.5	21.6
1600	1695.2	19.0
1700	1646.6	17.1
1800	1609.6	15.7
1900	1583.0	14.7

TABLE 3.10

X's and Z's in Feet(Film 13083)- TUMBLER 1

Z_n	Z_n (Ft)	Time (Seconds)								
		0.1574	0.1788	0.2123	0.2337	0.2658	0.2872	0.3193	0.3407	0.3728
		X(Ft)								
Z_1	413.3	493.6	503.9	521.6	526.8	533.4	539.3	543.7	545.2	544.5
Z_2	432.5	501.0	511.3	529.7	537.8	542.2	548.9	553.3	553.3	553.3
Z_3	449.4	509.1	520.1	540.0	548.1	552.6	559.9	564.3	567.3	565.1
Z_4	478.9	523.1	537.8	557.7	565.1	573.9	579.1	584.2	589.4	589.4
Z_5	510.6	537.8	553.3	574.7	583.5	592.3	600.4	607.1	610.8	613.7
Z_6	553.3	---	575.4	601.9	611.5	622.5	630.6	638.8	646.1	648.3
Z_7	604.1	---	---	629.9	641.0	655.7	666.0	677.1	683.7	688.1
Z_8	677.8	---	---	---	---	697.7	711.7	726.4	733.8	740.4
Z_9	783.2	---	---	---	---	---	---	797.2	806.7	820.0

TABLE 3.11

X's and Z's in Feet(Film 13383)- TUMBLER 4

Z_n	Z_n(Ft)	Time (Seconds)								
		0.3587	0.3829	0.4193	0.4436	0.4799	0.5406	0.5770	0.6012	0.6376
		X(Ft)								
Z_4	1,090.4	1,226.9	1,253.4	1,274.8	1,292.1	1,304.4	1,325.8	1,338.0	1,345.1	1,359.4
Z_5	1,135.2	1,248.3	1,271.7	1,294.2	1,310.5	1,323.7	1,350.2	1,363.5	1,374.7	1,385.9
Z_6	1,171.9	1,265.6	1,291.1	1,312.5	1,332.9	1,347.2	1,374.7	1,386.9	1,397.1	1,412.4
Z_7	1,226.9	1,286.0	1,312.5	1,339.0	1,362.4	1,377.7	1,408.3	1,422.6	1,432.8	1,447.0
Z_8	1,302.3	1,320.7	1,352.3	1,378.7	1,400.1	1,411.4	1,449.1	1,463.3	1,474.5	1,492.9
Z_9	1,393.0	---	---	1,420.5	1,449.1	1,461.3	1,499.0	1,513.3	1,529.6	1,553.0

TABLE 3.12

Z_n-Z_j, X_n-X_j in Feet - TUMBLER 1

Z_n-Z_j	ΔZ (Ft)	Time (Seconds)							
		0.2123	0.2337	0.2551	0.2765	0.2979	0.3193	0.3407	0.3728
		ΔX(Ft)							
Z_4-Z_1	65.6	34.0	37.0	39.0	40.0	41.0	42.0	43.0	45.0
Z_5-Z_2	78.1	45.0	49.0	50.0	54.0	56.0	57.0	58.0	62.0
Z_5-Z_3	61.2	34.0	38.0	39.0	42.0	44.0	43.0	45.0	48.0
Z_6-Z_3	103.9	58.0	65.0	68.0	72.0	74.0	75.0	78.0	82.0
Z_6-Z_4	74.4	42.0	46.0	48.0	51.0	52.0	55.0	56.0	58.0
Z_7-Z_4	125.2	68.0	74.0	78.0	84.0	87.0	92.0	95.0	99.0
Z_7-Z_5	93.5	50.0	55.0	59.0	63.0	65.0	69.0	72.0	75.0
Z_8-Z_6	124.5	--	--	70.0	76.0	82.0	86.0	89.0	93.0
Z_8-Z_7	73.7	--	--	40.0	43.0	47.0	49.0	50.0	52.0
Z_9-Z_7	179.1	--	--	--	--	--	119.0	125.0	131.0
Z_9-Z_8	154.0	--	--	--	--	--	70.0	75.0	79.0

TABLE 3.13

Z_n-Z_j, X_n-X_j in Feet - TUMBLER 4

Z_n-Z_j	ΔZ(Ft)	Time (Seconds)								
		0.3829	0.3950	0.4072	0.4314	0.4436	0.4557	0.4678	0.4799	0.5406
		ΔX(Ft)								
Z_9-7	166.1	--	--	--	85.6	89.7	91.7	93.8	94.8	94.8
Z_9-6	221.1	--	--	--	111.1	115.2	119.2	123.3	125.3	128.4
Z_9-5	257.8	--	--	--	131.4	135.5	140.6	143.7	145.7	151.8
Z_9-4	302.6	--	--	--	150.8	155.9	160.0	164.1	166.1	174.2
Z_8-6	130.4	58.1	60.1	62.2	66.2	67.2	68.3	71.3	71.3	74.4
Z_8-5	167.1	76.4	80.5	81.5	86.6	87.3	89.7	91.7	91.7	97.8
Z_8-4	212.0	96.8	99.9	100.9	106.0	108.0	109.0	112.1	112.1	120.2
Z_7-4	136.6	60.1	62.2	62.2	65.2	66.2	68.3	70.3	71.3	79.5

TABLE 3.14

Calculated K, $\left(\frac{\partial X}{\partial Z}\right)_t$ - TUMBLER 1

Z_n-Z_j	$\bar{Z}$(Ft)	Time (Seconds)							
		0.2123	0.2337	0.2551	0.2765	0.2979	0.3193	0.3407	0.3728
		K							
Z_4-Z_1	446.1	0.518	0.564	0.595	---	---	---	---	---
Z_5-Z_2	471.5	0.576	0.627	0.640	0.691	0.717	0.730	0.743	0.794
Z_5-Z_3	480.0	0.556	0.621	0.637	0.686	0.719	0.703	0.735	0.784
Z_6-Z_3	501.4	0.558	0.626	0.654	0.693	0.712	0.722	0.751	0.789
Z_6-Z_4	516.1	0.564	0.618	0.645	0.685	0.699	0.739	0.753	0.780
Z_7-Z_4	541.5	0.543	0.591	0.623	0.671	0.695	0.735	0.759	0.791
Z_7-Z_5	556.0	0.535	0.588	0.631	0.674	0.695	0.738	0.770	0.802
Z_8-Z_6	615.5	---	---	0.562	0.610	0.659	0.691	0.715	0.747
Z_8-Z_7	640.9	---	---	0.543	0.583	0.638	0.665	0.673	0.706
Z_9-Z_7	693.6	---	---	---	---	---	0.664	0.698	0.731
Z_9-Z_8	730.5	---	---	---	---	---	0.454	0.487	0.513

TABLE 3.15

Calculated K, $\left(\frac{\partial X}{\partial Z}\right)_t$ - TUMBLER 4

Z_n-Z_j	$\bar{Z}$ (Ft)	Time (Seconds)								
		0.3829	0.3950	0.4072	0.4314	0.4436	0.4557	0.4678	0.4799	0.5406
		K								
Z_9-Z_7	1,310.5	--	--	--	0.5153	0.5399	0.5521	0.5644	0.5705	0.5705
Z_9-Z_6	1,281.9	--	--	--	0.5023	0.5207	0.5392	0.5576	0.5668	0.5806
Z_9-Z_5	1,268.7	--	--	--	0.5099	0.5257	0.5454	0.5573	0.5652	0.5889
Z_9-Z_4	1,241.2	--	--	--	0.4983	0.5152	0.5286	0.5421	0.5488	0.5758
Z_8-Z_6	1,288.0	0.4453	0.4609	0.4766	0.5078	0.5156	0.5234	0.5469	0.5469	0.5703
Z_8-Z_5	1,218.8	0.4573	0.4817	0.4878	0.5183	0.5244	0.5366	0.5488	0.5488	0.5854
Z_8-Z_4	1,196.3	0.4567	0.4711	0.4760	0.5000	0.5096	0.5144	0.5288	0.5288	0.5673
Z_7-Z_4	1,158.6	0.4403	0.4552	0.4552	0.4776	0.4851	0.5000	0.5149	0.5224	0.5821

TABLE 3.16

Calculated Pressure, $P_{n,m}$, and Distance, X - TUMBLER 1

Z_n	K	P_n (psi)	Z_n (Ft)	$\frac{6P_o+P_n}{6P_n+P_o}$ *	$\left(\frac{Z_n}{\sqrt{Y_n}}\right)^2$	$\frac{6P_o+P_n}{6P_n+P_o}\left(\frac{Z_n}{\sqrt{Y_n}}\right)^{\frac{2}{K}}$	$\left[\frac{6P_o+P_n}{6P_n+P_o}\left(\frac{Z_n}{\sqrt{Y_n}}\right)^{\frac{2}{K}}\right]1.4$	$P_{n,m}$ (psi) = $\left[\frac{6P_o+P_n}{6P_n+P_o}\left(\frac{Z_n}{\sqrt{Y_n}}\right)^{\frac{2}{K}}\right]1.4P_n$	X (Ft)	Time (Sec)
Z_3	0.530	49.9	449.4	0.4100	0.6900	0.5338	0.4142	20.7	541.0	
Z_4	0.565	44.5	478.9	0.4355	0.7392	0.5698	0.4555	20.3	557.0	
Z_5	0.567	40.1	510.6	0.4635	0.7885	0.6046	0.5400	21.7	575.0	0.2123
Z_6	0.535	35.9	553.3	0.4963	0.8532	0.7915	0.7204	25.9	599.0	
Z_7	---	31.6	604.1	0.5383	-----	-----	-----	-----	----	
Z_8	---	27.7	677.8	0.5868	-----	-----	-----	-----	----	
Z_3	0.578	49.9	449.4	0.4100	0.6726	0.4771	0.3552	17.7	548.0	
Z_4	0.616	44.5	478.4	0.4355	0.7133	0.5043	0.3832	17.1	567.0	
Z_5	0.624	40.1	510.6	0.4635	0.7592	0.5639	0.4485	18.0	586.0	0.2337
Z_6	0.602	35.9	553.3	0.4963	0.8147	0.6716	0.5730	20.6	613.0	
Z_7	---	31.6	604.1	0.5383	-----	-----	-----	-----	----	
Z_8	---	27.7	677.8	0.5868	-----	-----	-----	-----	----	
Z_3	0.600	49.9	449.4	0.4100	0.6580	0.4496	0.3260	16.3	554.0	
Z_4	0.639	44.5	478.4	0.4355	0.6961	0.4744	0.3515	15.6	574.0	
Z_5	0.650	40.1	510.6	0.4635	0.7414	0.5287	0.4095	16.4	593.0	0.2551
Z_6	0.634	35.9	553.3	0.4963	0.7913	0.6194	0.5105	18.3	622.0	
Z_7	0.585	31.6	604.1	0.5383	0.8584	0.7099	0.7190	22.7	652.0	
Z_8	---	27.7	677.8	0.5868	-----	-----	-----	-----	----	
Z_3	---	49.9	449.4	0.4100	-----	-----	-----	-----	----	
Z_4	0.685	44.5	478.4	0.4355	0.6841	0.4349	0.3105	13.8	579.0	
Z_5	0.688	40.1	510.6	0.4635	0.7242	0.4879	0.3655	14.7	600.0	0.2765
Z_6	0.665	35.9	553.3	0.4963	0.7713	0.5756	0.4610	16.5	630.0	
Z_7	0.605	31.6	604.1	0.5383	0.8302	0.7387	0.6548	20.7	663.0	
Z_8	---	27.7	677.8	0.5868	-----	-----	-----	-----	----	
Z_3	---	49.9	449.4	0.4100	-----	-----	-----	-----	----	
Z_4	0.709	44.5	478.4	0.4355	0.6748	0.4145	0.2905	12.9	583.0	
Z_5	0.710	40.1	510.6	0.4635	0.7123	0.4650	0.3420	13.7	605.0	
Z_6	0.696	35.9	553.3	0.4963	0.7592	0.5414	0.4240	15.2	635.0	0.2979
Z_7	0.665	31.6	604.1	0.5383	0.8129	0.6580	0.5560	17.6	670.0	
Z_8	---	27.7	677.8	0.5868	-----	-----	-----	-----	----	
Z_3	---	49.9	449.4	-----	-----	-----	-----	-----	----	
Z_4	0.734	44.5	478.9	0.4355	0.6701	0.3976	0.2745	12.2	585.0	
Z_5	0.738	40.1	510.6	0.4635	0.7053	0.4430	0.3205	12.9	608.0	
Z_6	0.731	35.9	553.3	0.4963	0.7474	0.5074	0.3870	13.9	640.0	0.3193
Z_7	0.718	31.6	604.1	0.5383	0.7962	0.5969	0.4860	15.4	677.0	
Z_8	0.656	27.7	677.8	0.5868	0.8716	0.7797	0.7059	19.6	726.0	
Z_3	---	49.9	449.4	-----	-----	-----	-----	-----	----	
Z_4	0.748	44.5	478.9	0.4355	0.6632	0.3861	0.2641	11.8	588.0	
Z_5	0.760	40.1	510.6	0.4635	0.6984	0.4259	0.3021	12.1	611.0	
Z_6	0.786	35.9	553.3	0.4963	0.7382	0.4661	0.3440	12.3	644.0	0.3407
Z_7	0.744	31.6	604.1	0.5383	0.7823	0.5660	0.4515	14.3	683.0	
Z_8	0.700	27.7	677.8	0.5868	0.8551	0.7168	0.6279	17.4	733.0	
Z_3	---	49.9	449.4	-----	-----	-----	-----	-----	----	
Z_4	0.791	44.5	478.9	0.4355	0.6588	0.3627	0.2420	10.8	590.0	
Z_5	0.799	40.1	510.6	0.4635	0.6916	0.4012	0.2781	11.2	614.0	
Z_6	0.797	35.9	553.3	0.4963	0.7290	0.4540	0.3315	11.9	648.0	0.3728
Z_7	0.778	31.6	604.1	0.5383	0.7688	0.5319	0.4130	13.0	689.0	
Z_8	0.734	27.7	677.8	0.5868	0.8367	0.6689	0.5690	15.8	741.0	

* P_o = 12.9 PSI

TABLE 3.17

Calculated Pressure, $P_{n,m}$, and Distance, X, TUMBLER 4

Z_n	K	p_n (psi)	Z_n (Ft)	$\frac{6P_o+P^*_n}{6P_n+P_o}$	$\left(\frac{Z_n}{X_n}\right)^2$	$\frac{6P_o+P_n}{6P_n+P_o}\left(\frac{Z_n}{X_n}\right)^2\frac{1}{K}$	$\left[\frac{6P_o+P_n}{6P_n+P_o}\left(\frac{Z_n}{X_n}\right)^2\frac{1}{K}\right]^{1.4}$	$P_{n,m}$ (psi) = $\left[\frac{6P_o+P_n}{6P_n+P_o}\left(\frac{Z_n}{X_n}\right)^2\frac{1}{K}\right]^{1.4}(P_n)$	X (Ft)	Time (Sec)
Z_8	---	40.4	1,314	0.4474	----	----	----	----	1,335.9	
Z_7	0.448	44.2	1,238	0.4243	0.8904	0.8433	0.7879	34.8	1,300.3	0.3708
Z_6	0.450	47.2	1,183	0.4086	0.8383	0.7612	0.6825	32.2	1,279.9	
Z_8	---	40.4	1,314	0.4474	----	----	----	----	1,348.2	
Z_7	0.457	44.2	1,238	0.4243	0.8752	0.8126	0.7335	32.4	1,311.5	0.3829
Z_6	0.454	47.2	1,183	0.4086	0.8252	0.7427	0.6590	31.1	1,290.1	
Z_8	---	40.4	1,314	0.4474	----	----	----	----	1,360.4	
Z_7	0.474	44.2	1,238	0.4243	0.8604	0.7715	0.6952	30.7	1,322.7	0.3950
Z_6	0.472	47.2	1,183	0.4086	0.8122	0.7031	0.6110	28.8	1,300.3	
Z_8	---	40.4	1,314	0.4474	----	----	----	----	1,370.6	
Z_7	0.485	44.2	1,238	0.4243	0.8486	0.7424	0.6595	29.1	1,331.9	0.4072
Z_6	0.476	47.2	1,183	0.4086	0.8021	0.6885	0.5930	28.0	1,308.4	
Z_8	0.489	40.4	1,314	0.4474	0.8883	0.8127	0.7480	30.2	1,381.8	
Z_7	0.498	44.2	1,238	0.4243	0.8370	0.7131	0.6230	27.5	1,341.0	0.4193
Z_6	0.485	47.2	1,183	0.4086	0.7923	0.6675	0.5680	26.8	1,316.6	
Z_8	0.505	40.4	1,314	0.4474	0.8765	0.7766	0.7019	28.4	1,391.0	
Z_7	0.509	44.2	1,238	0.4243	0.8257	0.6883	0.5930	26.2	1,350.2	0.4314
Z_6	0.495	47.2	1,183	0.4086	0.7825	0.6459	0.5421	25.6	1,324.7	
Z_8	0.526	40.4	1,314	0.4474	0.8664	0.7370	0.6521	26.3	1,399.1	
Z_7	0.524	44.2	1,238	0.4243	0.8170	0.6616	0.5602	24.8	1,357.3	0.4436
Z_6	0.506	47.2	1,183	0.4086	0.7742	0.6252	0.5179	24.4	1,331.9	
Z_8	0.542	40.4	1,314	0.4474	0.8577	0.7081	0.6170	24.9	1,406.3	
Z_7	0.540	44.2	1,238	0.4243	0.8073	0.6343	0.5295	23.4	1,365.5	0.4557
Z_6	0.521	47.2	1,183	0.4086	0.7670	0.6015	0.4910	23.2	1,338.0	
Z_8	0.558	40.4	1,314	0.4474	0.8477	0.6797	0.5822	23.5	1,411.4	
Z_7	0.550	44.2	1,238	0.4243	0.7989	0.6163	0.5082	22.5	1,372.6	0.4678
Z_6	0.531	47.2	1,183	0.4086	0.7387	0.5684	0.4540	22.2	1,345.1	
Z_8	0.567	40.4	1,314	0.4474	0.8405	0.6633	0.5630	22.7	1,420.5	
Z_7	0.556	44.2	1,238	0.4243	0.7907	0.6034	0.4925	21.8	1,379.8	0.4799
Z_6	0.537	47.2	1,183	0.4086	0.7545	0.5741	0.4565	21.5	1,349.2	
Z_8	0.578	40.4	1,314	0.4474	0.8077	0.6252	0.5180	20.9	1,449.1	
Z_7	0.576	44.2	1,238	0.4243	0.7590	0.5591	0.4435	19.6	1,408.3	0.5406
Z_6	0.570	47.2	1,183	0.4086	0.7268	0.5210	0.4010	18.9	1,374.7	
Z_8	0.576	40.4	1,314	0.4474	0.7767	0.6033	0.4924	19.9	1,477.6	
Z_7	0.616	44.2	1,238	0.4243	0.7302	0.5030	0.3825	16.9	1,435.8	0.6012
Z_6	0.626	47.2	1,183	0.4086	0.7026	0.4582	0.3357	15.8	1,398.1	
Z_8	0.615	40.4	1,314	0.4474	0.7600	0.5529	0.4362	17.2	1,493.9	
Z_7	0.633	44.2	1,238	0.4243	0.7200	0.4822	0.3600	15.9	1,446.0	0.6376
Z_6	0.637	47.2	1,183	0.4086	0.6894	0.4419	0.3200	15.1	1,411.4	

* P_o = 12.25 PSI

TABLE 3.18

Free-air Pressure-Time, TUMBLER 1

R = 590 Ft		R = 690 Ft	
P(psi)	T(Sec)	P(psi)	T(Sec)
19.5#	0.0000	14.2#	0.0000
11.0	0.0323	11.1	0.0111
5.5	0.0537	8.2	0.0325
3.3	0.0751	5.3	0.0539
1.3	0.0965	3.2	0.0753
0.2	0.1179	1.4	0.0967
-0.6	0.1393	0.2	0.1288
-1.1	0.1607		
-2.1	0.1928		

TABLE 3.19

Free-air Pressure-Time, TUMBLER 4

R = 1350 Ft		R = 1410 Ft	
P(psi)	T(Sec)	P(psi)	T(Sec)
26.5#	0.0000	24.2#	0.0000
25.2	0.0088	21.5	0.0122
22.2	0.0204	19.6	0.0243
19.8	0.0330	17.3	0.0364
17.9	0.0452	14.5	0.0486
16.0	0.0573	13.1	0.0607
14.2	0.0694	11.3	0.0728
12.6	0.0816	10.0	0.0849
11.0	0.0937	7.5	0.1456
10.0	0.1058	4.1	0.2065
9.2	0.1179	3.0	0.2426

Taken from shock velocity data; arrival time taken as zero time.

TABLE 3.20

Decay Parameter, θ, for TUMBLER 1 and 4

TUMBLER 1			TUMBLER 4		
Radial Distance (ft)	* θ_{sv} (msec)	** θ_{pd} (msec)	Radial Distance (ft)	* θ_{sv} (msec)	** θ_{pd} (msec)
575	39.2	44.9	1350	96.9	96.0
590	42.0	46.5	1410	110.4	108.0
690	64.5	53.0	1550	141.9	140.0

* θ_{sv} is based on shock velocity pressure-distance results.

** θ_{pd} is based on particle displacement pressure-time results.

TABLE 4.1

TUMBLER 1 Data Reduced to 1 KT at Sea Level(Ground Level)

Station	Range* (Ft)	Pressure (psi)	Positive Impulse (psi-sec)	Negative Pressure (psi)	Arrival Time t_1 (sec)	Positive Duration t_4 (sec)	Negative Duration t_8 (sec)
F-200	161 764	31.52	2.10	3.97	0.307	0.207	0.782
F-201	333 818	23.05	1.67	3.93	0.343	0.198	0.871
F-202	554 930	18.07	1.42	2.96	0.422	0.205	0.871
F-202T	554 930	17.27	1.47	3.59	0.417	0.214	0.797
F-203	783 1,083	13.68	1.14	2.84	0.530	0.215	0.903
F-204	1,015 1,261	13.58	0.91	2.39	0.668	0.226	0.905
F-205	1,249 1,456	11.67	0.79	1.98	0.821	0.237	0.913
F-206	1,483 1,661	9.21	0.72	1.56	0.980	0.258	0.908
F-207	1,717 1,873	8.04	0.64	1.45	1.147	0.278	0.882
F-208	1,952 2,091	6.42	0.53	1.15	1.329	0.288	0.908
F-209	2,422 2,535	4.47	0.45	0.89	1.693	0.314	0.916
F-209T	2,422 2,535	4.41	0.45	0.96	1.695	0.304	0.937
F-210	2,892 2,988	3.37	0.37	0.80	2.073	0.336	0.961
F-211	3,833 3,906	2.28	0.29	0.56	2.854	0.363	0.962

* Ground Range
Slant Range

TABLE 4.2

TUMBLER 2 Data Reduced to 1 KT at Sea Level (Ground Level)

Station	Range* (Ft)	Pressure (psi)	Positive Impulse (psi-sec)	Negative Pressure (psi)	Arrival Time t_1 (sec)	Positive Duration t_4 (sec)	Negative Duration t_8 (sec)
7-200	131 1,003	16.93	1.28	2.85	0.485	0.220	1.140
7-212	232 1,021	14.52	1.25	2.64	0.499	0.228	1.156
7-201	563 1,143	12.75	1.12	2.40	0.591	0.224	0.868
7-201T	563 1,143	13.05	1.08	2.30	0.590	0.233	0.912
7-213	898 1,340	9.36	0.850	2.06	0.741	0.235	0.933
7-202	1,234 1,585	7.68	0.683	1.84	0.938	0.249	0.878
7-203	1,907 2,185	6.41	0.506	1.16	1.394	0.285	0.823
7-204	2,579 2,763	4.32	0.387	0.84	1.903	0.304	0.824
7-205	3,252 3,400	3.35	0.314	0.69	2.440	0.326	0.847
7-206	3,925 4,048	2.48	0.265	0.65	2.991	0.319	0.844
7-206T	3,925 4,048	2.24	0.259	0.57	2.991	0.343	0.788

* Ground Range / Slant Range

TABLE 4.3

TUMBLER 3 Data Reduced to 1 KT at Sea Level(Ground Level)

Station	Range* (Ft)	Pressure (psi)	Positive Impulse (psi-sec)	Negative Pressure (psi)	Arrival Time t_1 (sec)	Positive Duration t_4 (sec)	Negative Duration t_8 (sec)
7-200	51 1,015	15.96	1.25	2.47	0.491	0.217	1.172
7-212	91 1,018	15.94	1.28	2.47	0.496	0.217	0.890
7-201	195 1,032	15.36	----	----	0.507	-----	-----
7-201T	195 1,032	15.48	1.22	2.58	0.506	0.213	0.933
7-213	304 1,058	14.65	1.21	2.43	0.528	0.217	1.045
7-202	413 1,095	13.41	1.12	2.25	0.555	0.225	1.068
7-203	632 1,195	11.25	1.04	2.00	0.634	0.238	1.028
7-204	853 1,325	10.17	0.83	2.12	0.739	0.225	0.901
7-205	1,073 1,477	8.58	0.75	1.70	0.860	0.240	1.143
7-206T	1,293 1,644	7.72	0.67	1.46	0.996	0.253	1.011
7-207	1,513 1,822	7.59	0.61	1.17	1.142	0.270	0.999
7-208	1,733 2,009	7.53	0.58	1.18	1.297	0.279	1.109
7-209	2,174 2,400	5.94	0.47	0.86	1.621	0.295	0.936
7-210	2,614 2,806	4.29	0.40	0.79	1.965	0.300	1.454
7-211	3,495 3,643	3.36	0.31	0.64	2.671	0.321	0.936
7-Q1	837 1,315	12.86	0.86	1.80	0.729	0.236	1.117
7-Q2	1,062 1,469	9.46	0.81	1.63	0.852	0.246	1.025

* Ground Range / Slant Range

TABLE 4.4

TUMBLER 4 Data Reduced to 1 KT at Sea Level(Ground Level)

Station	Range* (Ft)	Pressure (psi)	Positive Impulse (psi-sec)	Negative Pressure (psi)	Arrivel Time t_1 (sec)	Positive Duration t_4 (sec)	Negative Duration t_8 (sec)
7-200	80 372	168.1	3.86	8.9	0.081	0.097	0.374
7-212	93 375	140.2	3.60	7.6	0.087	0.097	0.353
7-201	212 420	99.2	2.90	7.1	0.104	0.104	0.279
7-201T	212 420	98.8	3.06	7.2	0.105	0.105	0.319
7-213	340 497	52.3	2.18	6.56	0.145	0.143	0.392
7-202	470 594	29.38	1.80	5.24	0.210	0.186	
7-203	730 815	11.80	1.36	3.18	0.330	0.243	
7-204	979 1,056	10.60	0.99	2.47	0.495	0.259	
7-205	1,253 1,304	7.66	0.83	1.80	0.683	0.279	
7-206T	1,515 1,557	5.76	0.71	1.47	0.881	0.303	
7-207	1,776 1,812	4.75	0.58	1.15	1.083	0.326	
7-208	2,038 2,070	3.88	0.52	1.14	1.291	0.342	
7-209	2,561 2,586	2.57	0.36	0.78	1.719	0.375	
7-210	3,085 3,106	1.83	0.32	0.71	2.156	0.414	
7-211	4,132 4,147	1.45	0.27	0.54	3.045	0.444	
7-Q1	976 1,041	9.26	1.03	2.25	0.476	0.258	
7-Q2	1,243 1,294	7.43	0.85	2.05	0.670	0.281	

* Ground Range
Slant Range

TABLE 4.5

Reduced Time-of-Arrival of Shock in Free Air and Mach Region
TUMBLER 1
(For 1 KT(RC) at Sea Level)

Reduced Distance From Burst (Ft)	Reduced Distance From GZ (Ft)	Reduced Time (Sec)	Reduced Distance From Burst (Ft)	Reduced Distance From GZ (Ft)	Reduced Time (Sec)
116.070		0.0048868	800.823	265.139	0.3275074
153.621		0.0133501	809.357	294.156	0.3360254
215.923		0.0218150	826.426	315.777	0.3445447
246.079		0.0302815	837.805	354.183	0.3530654
272.820		0.0387494	860.564	409.941	0.3701115
298.708		0.0472187	885.987	461.433	0.3871634
324.027		0.0556895	910.349	497.278	0.4042212
346.786		0.0641616	933.108	545.640	0.4212848
364.709		0.0726354	955.013	583.192	0.4383541
388.036		0.0811107	980.048	623.020	0.4554293
406.243		0.0895872	1,002.237	659.434	0.4725102
421.605		0.0980052	1,026.134	690.158	0.4895966
440.381		0.1065445	1,037.513	711.210	0.4981420
456.597		0.1150253	1,052.591	730.270	0.5066890
469.114		0.1235074	1,060.841	743.926	0.5152374
489.313		0.1319907	1,072.505	762.417	0.5237874
504.420		0.1404756	1,083.600	778.064	0.5323388
518.899		0.1489619	1,095.263	795.702	0.5408916
533.692		0.1574496	1,106.927	810.779	0.5494459
550.477		0.1659387	1,118.022	826.426	0.5580016
563.563		0.1744295	1,131.313	842.073	0.5665588
577.503		0.1829216	1,138.790	853.452	0.5751176
591.727		0.1914151	1,149.994	869.099	0.5836778
605.951		0.1999101	1,164.393	884.745	0.5922393
619.037		0.2084064	1,187.436	913.763	0.6093668
634.399		0.2169043	1,211.617	944.487	0.6265001
648.339		0.2254035	1,219.583	958.711	0.6350690
674.227		0.2424064	1,253.152	999.108	0.6607841
698.124		0.2594152	1,277.902	1,031.255	0.6779347
728.279		0.2764298	1,300.092	1,057.996	0.6950909
752.000		0.2934501	1,321.428	1,083.315	0.7122533
762.417	99.285	0.3019623	1,332.808	1,106.074	0.7294211
771.805	154.158	0.3104760	1,365.523	1,137.936	0.7465948
787.452	221.044	0.3189911	1,384.584	1,159.272	0.7637742

TABLE 4.6

Reduced Time-of-Arrival of Shock in Free Air - TUMBLER 2
(For 1 KT(RC) at Sea Level)

Reduced Distance From Burst (Ft)	Reduced Time (Sec)	Reduced Distance From Burst (Ft)	Reduced Time (Sec)	Reduced Distance From Burst (Ft)	Reduced Time (Sec)
330.464	0.0601747	706.646	0.2697379	1,003.815	0.4793011
356.801	0.0718171	723.542	0.2813803	1,016.238	0.4909435
383.139	0.0834595	742.922	0.2930227	1,033.631	0.5025859
409.974	0.0951019	762.800	0.3046651	1,051.521	0.5142283
432.336	0.1067443	776.714	0.3163075	1,063.447	0.5258707
457.680	0.1183867	795.101	0.3279499	1,082.828	0.5375131
479.048	0.1300291	814.978	0.3395923	1,089.288	0.5491555
501.907	0.1416715	825.911	0.3512347	1,111.153	0.5607979
516.319	0.1533139	842.310	0.3628771	1,128.049	0.5724403
541.662	0.1649563	859.703	0.3745195	1,156.375	0.5957251
560.049	0.1765987	876.102	0.3861619	1,175.755	0.6073675
581.417	0.1882411	894.985	0.3978043	1,191.657	0.6190099
597.816	0.1998835	908.900	0.4094467	1,218.989	0.6422947
620.179	0.2115259	924.802	0.4210891	1,250.296	0.6655795
635.087	0.2231683	941.698	0.4327315	1,283.591	0.6888643
653.970	0.2348107	957.103	0.4443739	1,309.929	0.7121491
672.854	0.2464531	969.029	0.4560163	1,339.248	0.7354339
689.253	0.2580955	983.937	0.4676587		

TABLE 4.7

Reduced Time-of-Arrival of Shock in Free Air - TUMBLER 3
(For 1 KT(RC) at Sea Level)

Reduced Distance From Burst (Ft)	Reduced Time (Sec)	Reduced Distance From Burst (Ft)	Reduced Time (Sec)	Reduced Distance From Burst (Ft)	Reduced Time (Sec)
57.207	0.0008294	296.728	0.0476166	434.770	0.1081647
100.733	0.0035816	307.174	0.0503688	446.708	0.1136690
124.859	0.0063338	315.382	0.0531210	457.652	0.1191734
142.768	0.0090860	322.098	0.0558732	467.850	0.1246778
162.417	0.0118382	329.314	0.0586253	479.540	0.1301822
176.345	0.0145904	335.031	0.0613775	489.240	0.1356865
190.274	0.0173426	342.244	0.0641297	496.951	0.1411909
203.208	0.0200947	345.726	0.0668819	507.148	0.1466953
214.649	0.0228469	353.188	0.0696841	518.590	0.1521996
225.095	0.0255991	359.406	0.0723863	524.808	0.1577040
234.795	0.0283513	363.137	0.0751385	536.249	0.1632084
245.491	0.0311035	370.101	0.0778906	544.954	0.1687128
255.440	0.0338557	377.563	0.0806428	555.152	0.1742171
264.394	0.0366079	389.253	0.0861472	564.603	0.1797215
272.353	0.0393600	402.187	0.0916516	574.552	0.1852259
281.058	0.0421122	413.379	0.0971559	582.512	0.1907302
291.007	0.0448644	426.562	0.1026603		

TABLE 4.8

Reduced Time-of-Arrival of Shock in Free Air - TUMBLER 4
(For 1 KT(RC) at Sea Level)

Reduced Distance From Burst (Ft)	Reduced Time (Sec)	Reduced Distance From Burst (Ft)	Reduced Time (Sec)	Reduced Distance From Burst (Ft)	Reduced Time (Sec)
71.951	0.0015397	371.576	0.0766549	540.005	0.1620131
113.763	0.0049540	379.702	0.0800692	552.563	0.1688418
139.027	0.0083684	386.499	0.0834836	561.428	0.1756704
162.223	0.0117827	394.772	0.0868979	573.838	0.1824991
180.543	0.0151970	402.159	0.0903122	585.805	0.1893277
196.352	0.0186113	409.990	0.0937266	598.364	0.1961564
211.570	0.0220257	416.638	0.0971409	608.706	0.2029851
224.571	0.0254400	423.139	0.1005552	615.634	0.2076986
238.311	0.0288543	429.344	0.1039415	620.525	0.2098137
250.426	0.0322687	436.584	0.1073839	626.112	0.2144256
261.359	0.0356830	442.346	0.1107982	630.867	0.2166424
273.031	0.0390973	449.142	0.1142125	638.582	0.2211526
283.225	0.0425116	456.973	0.1176269	646.891	0.2278796
292.977	0.0459260	464.655	0.1210412	657.178	0.2346066
300.659	0.0493403	470.565	0.1244555	667.663	0.2413335
310.263	0.0527546	476.475	0.1278698	679.730	0.2480605
319.866	0.0561689	483.271	0.1312842	691.006	0.2547875
329.469	0.0595833	489.624	0.1346985	702.282	0.2615145
338.293	0.0629976	501.591	0.1415271	712.371	0.2682380
347.199	0.0664119	516.366	0.1483558	725.032	0.2749684
356.063	0.0698263	526.708	0.1551845	735.126	0.2850589
363.451	0.0732406				

TABLE 4.9*

Reduced Time-of-Arrival of Shock in Free Air

GREENHOUSE (DOG)

Reduced Distance From Burst (Ft)	Reduced Time (Sec)
14.60	0.0
31.75	0.0001437
41.61	0.0002915
45.62	0.0004358
52.56	0.0005778
67.52	0.0012776
91.97	0.0019738
106.57	0.0032188
116.79	0.0045926
128.10	0.0059579
140.15	0.0073147
151.10	0.0086617
157.67	0.0100009
175.92	0.0126520

TABLE 4.10**

Reduced Time-of-Arrival of Shock in Free Air

GREENHOUSE (EASY)

Reduced Distance From Burst (Ft)	Reduced Time (Sec)
79.585	0.001765
164.244	0.012062
229.561	0.024934
271.414	0.037805
315.805	0.050677
340.536	0.063548
374.780	0.076419
405.852	0.089291
435.659	0.099588
462.926	0.112459
507.317	0.130479
530.780	0.143351
556.145	0.156222
569.464	0.166519

* Taken from Table 3.1, Ref. (2) and reduced to 1 KT_{RC}.

** " " " 3.5 " " " " " 1 "

TABLE 4.11

Reduced Free-air Overpressure vs Distance, TUMBLER 1

Distance Reduced to Sea Level (ft)	Distance Reduced to Sea Level and 1 KT(RC) (ft)	Pressure Reduced to Sea Level (psi)
191	188	397.3
287	283	120.8
383	377	56.2
479	471	32.9
574	565	21.4
670	659	15.4
766	754	12.3
861	848	10.8
957	942	9.6
1053	1036	8.4

TABLE 4.12

Reduced Free-air Overpressure vs Distance, TUMBLER 2

Distance Reduced to Sea Level (ft)	Distance Reduced to Sea Level and 1 KT(RC) (ft)	Pressure Reduced to Sea Level (psi)
376	359	56.1
423	404	44.2
470	449	35.3
517	493	28.8
564	538	23.5
611	583	19.6
658	678	16.9
752	718	13.1
846	807	10.5
940	897	8.7
1034	987	7.3
1128	1076	6.5

TABLE 4.13

Reduced Free-air Overpressure vs Distance - TUMBLER 3

Distance Reduced to Sea Level (ft)	Distance Reduced to Sea Level and 1 KT(RC) (ft)	Pressure Reduced to Sea Level (psi)
479	154	588
525	169	446
593	191	286
639	206	234
730	235	171
822	265	132
913	294	102
1004	323	78.8
1278	412	42.6
1370	441	36.7
1415	456	34.3
1461	470	31.6
1506	485	29.1
1552	500	26.8
1598	515	25.1
1643	529	23.6
1689	544	22.2
1735	559	21.1
1780	573	20.1
1826	588	19.2

TABLE 4.14

Reduced Free-air Overpressure vs Distance - TUMBLER 4

Distance Reduced to Sea Level (ft)	Distance Reduced to Sea Level and 1 KT(RC) (ft)	Pressure Reduced to Sea Level (psi)
376	140	787
423	157	530
471	175	383
518	192	294
565	209	236
612	227	190
659	244	155
706	262	124
753	279	104
800	297	89.7
847	314	79.4
941	349	60.9
988	366	54.1
1035	384	48.6
1082	401	44.0
1129	419	40.0
1176	436	36.8
1223	454	34.1
1270	471	31.8
1317	489	29.6
1412	524	25.9
1506	558	22.8
1600	593	20.5
1694	628	18.8
1788	663	17.6

TABLE 4.15

Composite Free-Air Peak Overpressure and Distance Reduced to 1 KT(RC) at Sea Level

Reduced Distance (Ft)	Overpressure (psi)
150	632.5
200	256.2
300	88.0
400	44.6
500	27.4
600	19.3
700	14.3
800	11.1
900	8.9
1000	7.4
1100	6.6

TABLE 4.16

Reduced Free-Air Overpressure vs Distance*
GREENHOUSE (DOG)

Distance at Sea Level (ft)	Distance Reduced to Sea Level and 1 KT(RC) (ft)	Pressure (psi)
300	68.7	10,616
400	91.6	2,647
500	114.5	1,264
600	137.4	788
700	160.3	558
800	183.2	448

* Original Data taken from Table 3.2, reference (2)

Reduced Free-Air Overpressure vs Distance*
GREENHOUSE (EASY)

Distance at Sea Level (ft)	Distance Reduced to Sea Level and 1 KT(RC) (ft)	Pressure (psi)
500	139.0	774.2
600	166.8	459.4
700	194.6	288.2
800	222.4	187.4
900	250.2	148.8
1000	278.0	117.6
1100	305.8	97.2
1300	361.4	71.4
1500	417.0	54.8
1800	500.4	42.6
2200	611.6	34.0

*Original data taken from Table 3.6 of reference (2)

TABLE 4.17

Free-Air Pressure-Time, Reduced to 1 KT(RC) at Sea Level

TUMBLER 1 and 4

TUMBLER 1*		TUMBLER 4**	
P(psi)	T(Sec)	P(psi)	T(Sec)
23.9#	0.0000	24.4#	0.0000
10.5	0.0357	22.1	0.0034
5.2	0.0556	14.5	0.0244
3.2	0.0755	9.2	0.0454
0.9	0.0954	7.4	0.0580

Taken from shock velocity data; arrival time taken as zero time.
REDUCTION FACTORS: * Distance: 0.9417, Time: 0.931, Pressure: 1.140
** Distance: 0.3491, Time: 0.346, Pressure: 1.199

TABLE 4.18*

Values of Decay Parameter, θ, Reduced to 1 KT(RC) at Sea Level

Pentolite Curve from Fig. 4.14, Ref.(24)		Composite P-D Curve, Shock Velocity		P-t Curve Particle Displacement		P-D Curve Shock Velocity	
		Zone 1		TUMBLER 1		TUMBLER 1	
R	θ	R	θ	R	θ	R	θ
91.0	1.64	200	3.69	541.4	41.67	541.4	36.50
182.0	4.91	300	11.82	555.1	43.13	555.1	39.10
273.0	10.56	400	23.45	649.7	49.23	649.7	60.05
364.0	18.66	500	39.37				
455.0	31.40						
546.0	45.50	Zone 2		TUMBLER 4		TUMBLER 4	
637.0	51.42	600	60.35	471.4	33.31	471.4	33.52
728.0	63.24	700	64.73	493.2	37.49	493.2	38.20
819.0	74.62	800	71.44	541.4	48.50	541.4	49.10
910.0	85.50	900	85.03				
1092.0	105.56						

* All values reduced to 1 KT(RC) at sea level
R in (Ft), θ in (msec)

TABLE 5.1

Distances at which Pressures Occur
Reduced to 1 KT(RC) at Sea Level

Pressure (psi)	TUMBLER				Jangle "S" 0 (a)
	1	2	3	4	
	Height of Burst in Feet for 1 KT(RC)				
	747	995	1012	363	
3	3,100	3,460		2,310	2,150
4	2,530	2,800		1,960	1,810
5	2,220	2,430		1,690	1,580
6	2,000	2,160		1,500	1,420
8	1,680	1,150		1,240	1,210
10	1,410	850		1,060	1,080
12	1,180	630		720	985
15	710	220		620	885
20	440	---		555	775
25	280	---		505	705
30	180	---		465	650
40	---	---		405	580
50	---	---		350	535

(a) Derived from Figure 3.3 of reference 12

TABLE 5.2

Optimum Height of Burst for 1 KT(RC) at Sea Level

Pressure (psi)	$H_{oP} = \frac{15,380}{14.7+p}$ (Ft)	$H'_{oP} = \frac{19,890}{14.7+p}$ (Ft)
3	---	1,125
4	813	1,066
5	780	1,010
6	746	963
8	678	878
10	622	807
12	576	746
15	518	670
20	---	575

H_{oP} = From equation for Pentolite given in reference 15.
H'_{oP} = Empirical based on Figure 5.1

TABLE 5.3

Data for Figure 5.2

Heights*		Pressures vs Distances in Reduced Feet							
		4 psi		6 psi		10 psi		15 psi	
$\mu = \frac{Ft}{Lbs^{1/3}}$	$H = \frac{Ft}{(KT)^{1/3}}$ $\mu \times 91$	1 Lb Pent. (λ)	1 KT(RC) $\lambda \times 91$	1 Lb Pent. (λ)	1 KT(RC) $\lambda \times 91$	1 Lb Pent. (λ)	1 KT(RC) $\lambda \times 91$	1 Lb Pent. (λ)	1 KT(RC) $\lambda \times 91$
0.0	0	14.8	1,347	11.5	1,047	8.8	801	7.2	655
2.27	207	18.7	1,702	14.5	1,320	11.0	1,001	9.0	819
3.29	299	18.8	1,711	15.8	1,438	11.8	1,074	9.4	855
4.44	404	20.2	1,838	16.1	1,465	11.5	1,047	9.0	819
5.97	543	22.5	2,048	17.8	1,620	12.2	1,110	10.2	928
7.40	673	23.8	2,166	18.2	1,656	12.6	1,147	7.5	683
9.20	837	26.0	2,366	17.2	1,565	10.2	928	4.7	428
9.88	899	26.0	2,366	17.2	1,565	9.2	837	0.0	0
11.80	1,074	24.0	2,184	15.5	1,411	5.5	501	---	---
14.50	1,320	22.5	2,048	12.5	1,137	0.0	0	---	---
19.00	1,729	---	---	0.0	0	-----	---	---	---
19.93	1,814	15.5	1,411	---	---	-----	---	---	---
25.0	2,275	0.0	0	---	---	-----	---	---	---

* All gages were at a height 0.18 ($Ft/Lbs^{1/3}$) or 16.4 ($Ft/KT^{1/3}$).

NOTE: Curves are from Figure 19 and Table II of Navord 2451 (Reference 15).

Points are from Tables II[a], V[b], IX[c], and XII[d] of Annex I (SRI) of the Tumbler Preliminary Report (Reference 13) as corrected below to 1 KT(RC) at Sea Level

Pressure (psi)	TUMBLER			
	1	2	3	4
	Reduced Gage Height			
	9.4[a]	9.0[b]	14.7[c]	17.4[d]
4	2,370	2,410	2,530	1,850
6	1,760	1,470	1,600	1,470
10	1,110	815	655	810
15	565	---	---	595

TABLE 5.4

Arrival Time of Precursor and Reflected Shock, TUMBLER 4

Reflected Shock (East) (Ft)	Reflected Shock (West) (Ft)	Precursor (East) (Ft)	Precursor (West) (Ft)	Absolute Time (Sec)
269.4	240.9	-	-	.2512
329.1	324.0	-	-	.2610
394.0	404.6	532.1	506.5	.2709
469.0	455.8	614.4	577.3	.2808
475.8	473.7	662.1	666.0	.2906
520.5	538.5	675.8	726.5	.3005
588.4	572.6	758.5	741.9	.3104
655.7	652.8	840.8	840.4	.3301
721.4	763.6	859.5	924.8	.3498
823.7	819.9	1041.2	1010.5	.3696
865.9	851.9	1099.2	1078.7	.3893
937.6	925.6	1171.6	1161.9	.4090
965.7	976.8	1246.2	1191.3	.4288
1016.9	1030.5	1297.0	1285.5	.4485
1061.6	1055.2	1368.2	1317.9	.4682
1129.8	1126.9	1383.1	1364.3	.4880
1137.9	1159.3	1437.7	1409.1	.5077
1184.4	1228.3	1485.8	1457.3	.5274
1221.1	1257.8	1513.1	1508.4	.5472
1275.2	1294.9	1601.0	1558.3	.5669
1313.6	1317.9	1616.3	1608.6	.5867
1347.7	1355.4	1647.9	1616.7	.6064
1398.0	1404.5	1694.8	1649.2	.6261
1428.7	1467.1	1722.1	1707.6	.6459
1452.2	1423.6	1764.3	1738.7	.6656

TABLE 5.5

Overlap of Ground Level and Free-air Measurements

TUMBLER Shot No.	Region of Overlap	
	Slant Range (ft)	Ground Range (ft)
1	811-1,200	171-901
2	1,119-1,150	146-287
3	None	None
4	1,065-1,400	230-937

TABLE 5.6

TUMBLER 1 - Calculated vs Experimental Values of Reflected Pressure in the Regular Region

Range (Ft)		P_s(psi) Rocket Trails	α	P_f(psi)	
Slant	Ground			Measured	Calculated
811	171	10.1	12°10'	27.65	26.5
832	250	9.7	17°30'	23.5	25.0
868	353	8.9	24° 0'	20.22	22.2
912	450	7.8	29°34'	18.0	18.5
987	588	7.0	36°33'	15.85	16.2
1,058	700	6.2	41°26'	13.8	15.0
1,149	832	5.4	46°22'	12.0	13.8

TABLE 5.7

TUMBLER 2 - Calculated vs Experimental Values of Reflected Pressure in the Regular Region

Range (Ft)		P_s(psi) Rocket Trails	α	P_f(psi)	
Slant	Ground			Measured	Calculated
1,118.6	145.6	6.0	7°32'	14.06	14.4
1,123	175.0	5.9	8°58'	13.3	14.2
1,127	200.0	5.8	10°13'	12.9	13.8
1,132	225.0	5.8	11°28'	12.5	13.8
1,139	259.6	5.8	13°10'	12.06	13.8
1,143	275.9	5.7	13°56'	11.9	13.5

TABLE 5.8

TUMBLER 4 - Calculated vs Experimental Values of Reflected Pressure in the Regular Region

Range (Ft)		P_s(psi) Rocket Trails	α	P_f(psi)	
Slant	Ground			Measured	Calculated
1,065.2	230.4	43.5	12°30'	140.2	172
1,073.4	265.5	42.8	14°20'	116.9	164
1,097	350	41	18°36'	98.8	155.5
1,114	400	39.8	21° 2'	93	148
1,154	500	36.8	25°40'	87.0	131
1,204.6	607.6	32.9	30°18'	82.4	111.5
1,204.6	607.6	32.9	30°18'	82.7	111.5
1,425.0	974.2	24.3	43° 8'	43.6	-----

TABLE 5.9

$P_s = p_o \left(\frac{1}{\zeta} - 1 \right)$ for TUMBLER 1 where p_o = 12.89 psi

ζ	P_s(psi)	ζ	P_s(psi)
0.05	244.9	0.50	12.89
0.10	116.0	0.60	8.60
0.20	51.56	0.70	5.53
0.30	30.07	0.80	3.22
0.40	19.33	0.90	1.43

TABLE 5.10

$P_s = p_o \left(\frac{1}{\zeta} - 1 \right)$ for TUMBLER 2 where p_o = 12.21 psi

ζ	P_s(psi)	ζ	P_s(psi)
0.05	231.99	0.50	12.21
0.10	109.89	0.60	8.14
0.20	48.84	0.70	5.24
0.30	28.45	0.80	3.05
0.40	18.32	0.90	1.36

TABLE 5.11

$P_s = p_o \left(\frac{1}{\zeta} - 1 \right)$ for TUMBLER 4 where p_o = 12.26 psi

ζ	P_s(psi)	ζ	P_s(psi)
0.05	232.9	0.50	12.26
0.10	110.3	0.60	8.18
0.20	49.0	0.70	5.26
0.30	28.6	0.80	3.07
0.40	18.39	0.90	1.36

TABLE 5.12

$$P_f = p_o \left(\frac{\zeta'}{\zeta} - 1 \right)$$ for TUMBLER 1 where p_o = 12.89 psi

P_s (psi)	ζ	$\alpha = 12^\circ 10'$		$\alpha = 17^\circ 30'$		$\alpha = 21^\circ 0'$		$\alpha = 29^\circ 34'$		$\alpha = 36^\circ 33'$		$\alpha = 41^\circ 26'$		$\alpha = 46^\circ 22'$	
		ζ'	P_f(psi)	ζ'	P_f(psi)	ζ'	P_f(psi)	ζ'	P_f(psi)	ζ'	P_f(psi)	ζ'	P_f(psi)	ζ'	P_f(psi)
19.33	0.4	2.22	58.65	2.19	57.62	2.16	56.72	2.15	56.33	2.16	56.72	----	---	----	---
12.89	0.5	1.87	35.17	1.85	34.80	1.84	34.55	1.82	34.03	1.84	34.55	1.95	37.38	----	---
8.60	0.6	1.60	21.53	1.60	21.53	1.59	21.27	1.59	21.27	1.59	21.27	1.64	22.30	----	---
5.53	0.7	1.40	12.89	1.40	12.89	1.39	12.76	1.38	12.50	1.40	12.89	1.42	13.28	1.48	14.31
3.22	0.8	1.24	7.09	1.24	7.09	1.24	7.09	1.23	6.96	1.24	7.09	1.25	7.22	1.27	7.61
1.43	0.9	1.12	3.15	1.12	3.15	1.12	3.15	1.11	3.00	1.14	3.00	1.11	3.00	1.12	3.15

TABLE 5.13

$$P_f = p_o \left(\frac{\zeta'}{\zeta} - 1 \right)$$ for TUMBLER 2 where p_o = 12.21 psi

P_s (psi)	ζ	$\alpha = 7^\circ 32'$*		$\alpha = 13^\circ 10'$**	
		ζ'	P_f(psi)	ζ'	P_f(psi)
12.21	0.5	1.87	33.46	1.86	33.21
8.14	0.6	1.61	20.51	1.61	20.51
5.24	0.7	1.40	12.21	1.40	12.21
3.05	0.8	1.24	6.72	1.24	6.72

* ζ' and P_f under these conditions are the same for $\alpha = 7^\circ 32'$, $8^\circ 58'$, $10^\circ 13'$, $11^\circ 28'$
** ζ' " P_f " " " " " " " " $\alpha = 13^\circ 10'$, $13^\circ 56'$

TABLE 5.14

$$P_f = p_o \left(\frac{\zeta'}{\zeta} - 1 \right)$$ for TUMBLER 4 where p_o = 12.26 psi

P_s (psi)	ζ	$\alpha = 12^\circ 30'$		$\alpha = 14^\circ 20'$		$\alpha = 18^\circ 36'$		$\alpha = 21^\circ 2'$		$\alpha = 25^\circ 40'$		$\alpha = 30^\circ 18'$		$\alpha = 43^\circ 9'$	
		ζ'	P_f(psi)	ζ'	P_f(psi)	ζ'	P_f(psi)	ζ'	P_f(psi)	ζ'	P_f(psi)	ζ'	P_f(psi)	ζ'	P_f(psi)
110.3	0.1	4.81	577	4.77	572.5	----	---	4.61	552.9	----	---	4.34	519	----	---
49.0	0.2	3.48	201	3.36	193.7	3.41	196.8	3.37	194.3	3.30	190.0	3.22	185.1	----	---
28.6	0.3	2.71	98.4	2.70	98.1	2.67	96.85	2.65	96.00	2.61	94.4	2.57	92.8	----	---
18.39	0.4	2.24	56.6	2.20	55.2	----	---	2.17	54.56	----	---	2.14	53.3	----	---
12.26	0.5	1.87	33.6	1.86	33.3	----	---	1.84	32.86	----	---	1.83	32.6	----	---
8.18	0.6	1.60	20.47	1.60	20.47	----	---	1.60	20.47	----	---	1.58	19.98	1.68	22.07
5.26	0.7	----	---	----	---	----	---	----	---	----	---	----	---	1.44	13.00
3.07	0.8	----	---	----	---	----	---	----	---	----	---	----	---	1.26	7.11
1.35	0.9	----	---	----	---	----	---	----	---	----	---	----	---	1.11	2.82

TABLE 5.15

Distances at which Pressure Levels occur in Free Air for 1 KT(TNT) at Sea Level

Pressure in psi	Kirkwood-Brinkley (TNT) Feet for 1 KT at Sea Level	TUMBLER							
		Distance in Feet at Sea Level				Reduced Distance in Feet for 1 KT at Sea Level			
		Shot 1	Shot 2	Shot 3	Shot 4	Shot 1 @.486KT	Shot 2 @.525KT	Shot 3 @12.55KT	Shot 4 @8.08KT
700	145	-	-	-	390	-	-	-	194
600	160	-	-	470	409	-	-	202	203
500	179	-	-	505	430	-	-	218	214
400	204	191	-	540	465	243	-	233	231
300	241	209	-	585	515	266	-	252	256
200	295	238	-	675	595	302	-	291	296
150	334	264	-	775	660	335	-	334	328
100	393	306	-	920	765	389	-	396	381
80	430	332	-	1000	840	422	-	431	418
70	455	350	-	1050	890	445	-	453	443
60	480	372	-	1120	950	473	-	483	473
50	515	400	400	1210	1030	508	496	522	512
40	562	435	445	1310	1130	553	551	565	562
30	630	492	503	1470	1310	625	623	634	652
20	760	590	605	1760	1620	750	750	759	806
15	870	680	700	-	-	864	867	-	-
10	1060	900	865	-	-	1144	1072	-	-
8	1190	-	995	-	-	-	1233	-	-
7	1280	-	1080	-	-	-	1338	-	-
6	1410	-	-	-	-	-	-	-	-
5	1560	-	-	-	-	-	-	-	-

TABLE 5.16

Comparison of TUMBLER Data with TNT in Free Air

Over-Pressure	KT (TNT)				$\frac{KT(TNT)}{KT(RC)}$ x 100 = Blast Efficiency				
(psi)	T1	T2	T3	T4	T1	T2	T3	T4	Avg.
200	.526	-	12.0	8.12	50.1	-	40.0	41.4	43.8
150	.493	-	12.5	7.76	46.9	-	41.7	39.6	42.7
100	.473	-	12.8	7.41	45.0	-	42.7	37.8	41.8
80	.460	-	12.6	7.41	43.8	-	42.0	37.8	41.2
70	.455	-	12.3	7.53	43.3	-	41.0	38.4	40.9
60	.465	-	12.6	7.76	44.3	-	42.0	39.6	42.0
50	.469	.469	13.0	8.00	44.6	40.8	43.3	40.8	42.4
40	.464	.495	12.6	8.12	44.2	43.1	42.0	41.4	42.7
30	.476	.508	12.6	9.00	45.3	44.2	42.0	45.9	44.3
20	.467	.504	12.5	9.73	44.4	43.8	41.7	49.6	44.9
15	.478	.520	-	-	45.5	45.2	-	-	45.3
10	.612	.543	-	-	58.3	47.2	-	-	52.7
8	-	.584	-	-	-	50.8	-	-	50.8
7	-	.601	-	-	-	52.2	-	-	52.2
Avg.	.486	.525	12.55	8.08	46.3	45.9	41.8	41.2	44.9

TABLE 5.17

Comparison of TUMBLER Data with TNT for Reflected Pressures

Reflected Pressure	Per Cent Efficiencies			
	15 psi	10 psi	6 psi	4 psi
TUMBLER 1*	57	84	83	75
TUMBLER 2*	63	58	103	84
TUMBLER 3*	66	61	103	85
TUMBLER 4*	14	42	45	59
GREENHOUSE DOG**		61		
GREENHOUSE EASY**		53		
GREENHOUSE GEORGE**		67		
CROSS-ROADS ABLE**		67		
SANDSTONE X-RAY**		45		
SANDSTONE YOKE**		58		
SANDSTONE ZEBRA**		51		
TRINITY**		55		
JANGLE S***		78		
BUSTER BAKER****	37	45		
BUSTER CHARLIE****	14	14		
BUSTER EASY****		12		

* Note that TUMBLER measurements at ground level are being compared with HE measurements above ground level.
** From Table 4.5 of reference (24)
*** From Fig. 4.3 of reference (24)
**** Calculated from data given in reference (37)

TABLE 5.18

Comparison of Free-Air Positive Impulse Data for Scaled Nuclear and TNT Charges

TUMBLER 1		TUMBLER 1 Reduced to 1 KT(RC) at Sea Level*		Experimental Curve for TNT Scaled to 1 KT(RC) at Sea Level (Ref (20))	
R (ft)	I (psi-msec)	R (ft)	I (psi-msec)	R (ft)	I (psi-msec)
590.0	797.3	555.8	846.7	555.8	844.8
690.0	644.8	650.0	684.8	650.0	713.5

* See Table 1.1 for scaling factors.

TABLE 6.1

Summary of Free-air TNT Equivalents for TUMBLER

Shot	KT(RC)	KT(TNT)	Per Cent Efficiency	Ranges
T 1	1.05	0.49	46	200-[illegible]0 psi
T 2	1.15	0.53	46	50-[illegible] psi
T 3	30.0	12.6	42	200-20 psi
T 4	19.6	8.08	41	200-20 psi

TABLE A1

TUMBLER 3 - Peak Pressure

Station No.	Ground Range (feet)	Gage No.	Indicated Peak Pressure (psi)	Inductance Gage pressure (psi)
7-212	3.0	237 242 233 249 197 137	9.5 8.9 6.5 7.2 8.5 8.0	12.1
7-203	2155	171 138 253 183 271 67	2.6 6.9 6.9 6.2 6.3 bad	8.6
7-205	3653	321 210 112 170 307 154	4.4 5.8 5.6 5.3 5.2 5.2	6.5
7-207	5152	296 96 175 222 240 191	3.8 4.6 3.3 3.5 3.8 bad	5.8
7-209	7401	202 172 239 134 190 160	2.1 5.6 2.1 2.6 3.0 1.7	4.5
7-92	3616	158 256 88 56 273 74	5.1 4.3 2.8 4.8 4.9 3.0	7.2

TABLE A2

TUMBLER 4 - Peak Pressure

Station No.	Grd Range (ft)	Gage No.	Damping Oil Vis. (Cent.)	Orifice Plate Dia. (in.)	Indicated Peak Pressure (psi)	Inductance Gage Pressure (psi)
7-212	266	185	1,000,000	None	104	117 (8 msec duration)
		138	"	"	113	
		137	"	"	121	125 (1 msec duration)
		222	"	3/8	99	
		96	"	3/8	96	
		249	"	3/8	102	
		61	100,000	None	104	
		154	"	"	136	
		253	"	"	116	
		172	"	3/8	103	
		321	"	3/8	102	
		190	"	3/8	106	
7-213	974	158	1,000,000	None	39.5	
		233	"	"	37	44 (8 msec duration)
		256	"	"	52.5	49 (1 msec duration)
		56	"	3/8	42.5	
		112	"	3/8	36	
		273	"	3/8	39	
		88	100000	None	46.5	
		197	"	"	44	
		210	"	"	46.5	
		237	"	3/8	36	
		307	"	3/8	52	
		170	"	3/8	39	
7-207	5088	296	1,000,000	None	1.1	4.0
		202	"	"	1.7	
		183	"	"	1.5	
		242	"	3/8	3.2	
		134	"	3/8	2.3	
		240	"	3/8	0.5	
		271	100000	None	1.5	
		175	"	"	1.9	
		239	"	"	0.4	
		171	"	3/8	1.0	
		191	"	3/8	1.5	
		160	"	3/8	3.0	

DISTRIBUTION

Copy No.

ARMY ACTIVITIES

Asst. Chief of Staff, G-2, D/A, Washington 25, D. C.	1
Asst. Chief of Staff, G-3, D/A, Washington 25, D. C. ATTN: Dep. Asst. CofS, G-3, (RR&SW)	2
Asst. Chief of Staff, G-4, D/A, Washington 25, D. C.	3
Chief of Ordnance, D/A, Washington 25, D. C. ATTN: ORDTF-AR	4
Chief Signal Officer, D/A, P&O Division, Washington 25, D. C. ATTN: SIGOP	5- 7
The Surgeon General, D/A, Washington 25, D. C. ATTN: Chairman, Medical R&D Board	8
Chief Chemical Officer, D/A, Washington 25, D. C.	9- 10
Chief of Engineers, D/A, Military Construction Division, Protective Construction Branch, Washington 25, D. C. ATTN: ENGEB	11
Chief of Engineers, D/A, Civil Works Division, Washington 25, D. C. ATTN: Engineering Division, Structural Branch	12
The Quartermaster General, CBR, Liaison Office, Research and Development Division, D/A, Washington 25, D. C.	13
Office, Chief of Transportation, D/A, Washington 25, D. C. ATTN: Military Planning and Intelligence	14
Chief, Army Field Forces, Ft. Monroe, Va.	15- 17
Army Field Forces Board #1, Ft. Bragg, N. C.	18
Army Field Forces Board #2, Ft. Knox, Ky.	19
Army Field Forces Board #4, Ft. Bliss, Tex.	20
Commanding General, First Army, Governor's Island, New York 4, N. Y. ATTN: G-4, ACofS	21- 23
Commanding General, Second Army, Ft. George G. Meade, Md. ATTN: AIABB	24
Commanding General, Second Army, Ft. George G. Meade, Md. ATTN: AIAME	25
Commanding General, Second Army, Ft. George G. Meade, Md. ATTN: AIACM	26
Commanding General, Third Army, Ft. McPherson, Ga. ATTN: ACofS, G-3	27- 28
Commanding General, Fourth Army, Ft. Sam Houston, Tex. ATTN: G-3 Section	29- 30
Commanding General, Fifth Army, 1660 Hyde Park Blvd., Chicago 15, Ill. ATTN: ALFEN	31
Commanding General, Fifth Army, 1660 Hyde Park Blvd., Chicago 15, Ill. ATTN: ALFOR	32
Commanding General, Fifth Army, 1660 Hyde Park Blvd., Chicago 15, Ill. ATTN: ALFMD-O	33- 36

DISTRIBUTION (Continued)

	Copy No.
Commanding General, Sixth Army, Presidio of San Francisco, Calif. ATTN: AMGCT-4	37
Commander-in-Chief, European Command, APO 403, c/o PM, New York, N. Y.	38
Commander-in-Chief, U. S. Army Europe, APO 403, c/o PM, New York, N. Y. ATTN: OPOT Division, Com. Dev. Branch	39- 40
Commander-in-Chief, Far East Command, APO 500, c/o PM, San Francisco, Calif. ATTN: ACofS, G-3	41- 45
Commanding General, U. S. Army Alaska, APO 942, c/o PM, Seattle, Wash.	46
Commanding General, U. S. Army Caribbean, APO 834, c/o PM, New Orleans, La. ATTN: CG, USARCARIB	47
Commanding General, U. S. Army Caribbean, APO 834, c/o PM, New Orleans, La. ATTN: CG, USARFANT	48
Commanding General, U. S. Army Caribbean, APO 834, c/o PM, New Orleans, La. ATTN: Cml. Off., USARCARIB	49
Commanding General, U. S. Army Caribbean, APO 834, c/o PM, New Orleans, La. ATTN: Surgeon, USARCARIB	50
Commanding General, USAR Pacific, APO 958, c/o PM, San Francisco, Calif. ATTN: Cml. Off.	51- 52
Commanding General, Trieste U. S. Troops, APO 209, c/o PM, New York, N. Y. ATTN: ACofS, G-3	53
Commandant, Command and General Staff College, Ft. Leavenworth, Kan. ATTN: ALLIS(AS)	54- 55
Commandant, The Infantry School, Ft. Benning, Ga. ATTN: C.D.S.	56- 57
Commandant, The Artillery School, Ft. Sill, Okla.	58
Commandant, The AA&GM Branch, The Artillery School, Ft. Bliss, Tex.	59
Commandant, The Armored School, Ft. Knox, Ky. ATTN: Classified Document Section, Evaluation and Req. Division	60- 61
Commanding General, Medical Field Service School, Brooke Army Medical Center, Ft. Sam Houston, Tex.	62
Commandant, Army Medical Service School, Walter Reed Army Medical Center, Washington 25, D. C. ATTN: Dept. of Biophysics	63
The Superintendent, United States Military Academy, West Point, N. Y. ATTN: Professor of Ordnance	64- 65
Commanding General, The Transportation Corps Center and Ft. Eustis, Ft. Eustis, Va. ATTN: Asst. Commandant, Military Sciences and Tactics	66
Commandant, Chemical Corps School, Chemical Corps Training Command, Ft. McClellan, Ala.	67
Commanding General, Research and Engineering Command, Army Chemical Center, Md. ATTN: Special Projects Officer	68
RD Control Officer, Aberdeen Proving Ground, Md. ATTN: Director, Ballistics Research Laboratory	69- 70

DISTRIBUTION (Continued)

	Copy No.
Commanding General, The Engineer Center, Ft. Belvoir, Va. ATTN: Asst. Commandant, The Engineer School	71- 73
Chief of Research and Development, D/A, Washington 25, D. C.	74
Commanding Officer, Engineer Research and Development Laboratory, Ft. Belvoir, Va. ATTN: Chief, Technical Intelligence Branch	75
Commanding Officer, Picatinny Arsenal, Dover, N. J. ATTN: ORDBB-TK	76
Commanding Officer, Army Medical Research Laboratory, Ft. Knox, Ky.	77
Commanding Officer, Chemical Corps Chemical and Radiological Laboratory, Army Chemical Center, Md. ATTN: Technical Library	78- 79
Commanding Officer, Transportation R&D Station, Ft. Eustis, Va.	80
Commanding Officer, Psychological Warfare Center, Ft. Bragg, N. C. ATTN: Library	81
Asst. Chief, Military Plans Division, Rm 516, Bldg. 7, Army Map Services, 6500 Brooks Lane, Washington 25, D. C. ATTN: Operations Plans Branch	82
Director, Technical Documents Center, Evans Signal Laboratory, Belmar, N. J.	83
Director, Waterways Experiment Station, PO Box 631, Vicksburg, Miss. ATTN: Library	84
Director, Operations Research Office, Johns Hopkins University, 6410 Connecticut Ave., Chevy Chase, Md. ATTN: Library	85

NAVY ACTIVITIES

Chief of Naval Operations, D/N, Washington 25, D. C. ATTN: OP-36	86- 87
Chief of Naval Operations, D/N, Washington 25, D. C. ATTN: OP-51	88
Chief of Naval Operations, D/N, Washington 25, D. C. ATTN: OP-53	89
Chief of Naval Operations, D/N, Washington 25, D. C. ATTN: OP-374 (OEG)	90
Chief, Bureau of Medicine and Surgery, D/N, Washington 25, D. C. ATTN: Special Weapons Defense Division	91- 92
Chief, Bureau of Ordnance, D/N, Washington 25, D. C.	93
Chief, Bureau of Personnel, D/N, Washington 25, D. C. ATTN: Pers 15	94
Chief, Bureau of Personnel, D/N, Washington 25, D. C. ATTN: Pers C	95
Chief, Bureau of Ships, D/N, Washington 25, D. C. ATTN: Code 348	96

DISTRIBUTION (Continued) Copy No.

Chief, Bureau of Supplies and Accounts, D/N, Washington 25, D. C.	97
Chief, Bureau of Yards and Docks, D/N, Washington 25, D. C. ATTN: P-312	98
Chief, Bureau of Aeronautics, D/N, Washington 25, D. C.	99-100
Office of Naval Research, Code 219, Rm 1807, Bldg. T-3, Washington 25, D. C. ATTN: RD Control Officer	101
Commander-in-Chief, U. S. Atlantic Fleet, Fleet Post Office, New York, N. Y.	102-103
Commander-in-Chief, U. S. Pacific Fleet, Fleet Post Office, San Francisco, Calif.	104-105
Commander, Operation Development Force, U. S. Atlantic Fleet, U. S. Naval Base, Norfolk 11, Va. ATTN: Tactical Development Group	106
Commander, Operation Development Force, U. S. Atlantic Fleet, U. S. Naval Base, Norfolk 11, Va. ATTN: Air Department	107
Commandant, U. S. Marine Corps, Headquarters, USMC, Washington 25, D. C. ATTN: (A03H)	108-111
President, U. S. Naval War College, Newport, Rhode Island	112
Superintendent, U. S. Naval Postgraduate School, Monterey, Calif.	113
Commanding Officer, U. S. Naval Schools Command, Naval Station, Treasure Island, San Francisco, Calif.	114-115
Director, USMC Development Center, USMC Schools, Quantico, Va. ATTN: Marine Corps Tactics Board	116
Director, USMC Development Center, USMC Schools, Quantico, Va. ATTN: Marine Corps Equipment Board	117
Commanding Officer, Fleet Training Center, Naval Base, Norfolk 11, Va. ATTN: Special Weapons School	118-119
Commanding Officer, Fleet Training Center, (SPWP School), Naval Station, San Diego 36, Calif.	120-121
Commander, Air Force, U. S. Pacific Fleet, Naval Air Station, San Diego, Calif.	122
Commander, Training Command, U. S. Pacific Fleet, c/o Fleet Sonar School, San Diego 47, Calif.	123
Commanding Officer, Air Development Squadron 5, USN Air Station, Moffett Field, Calif.	124
Commanding Officer, Naval Damage Control Training Center, U. S. Naval Base, Philadelphia 12, Pa. ATTN: ABC Defense Course	125
Commanding Officer, Naval Unit, Chemical Corps School, Ft. McClellan, Ala.	126
Joint Landing Force Board, Marine Barracks, Camp Lejeune, N. C.	127

DISTRIBUTION (Continued) — Copy No.

Commander, U. S. Naval Ordnance Laboratory, Silver Spring 19, Md. ATTN: EE — 128
Commander, U. S. Naval Ordnance Laboratory, Silver Spring 19, Md. ATTN: Alias — 129
Commander, U. S. Naval Ordnance Laboratory, Silver Spring 19, Md. ATTN: Alias — 130
Commander, U. S. Naval Ordnance Test Station, Inyokern, China Lake, Calif. — 131
Officer-in-Charge, U. S. Naval Civil Engineering Research and Evaluation Laboratory, Construction Battalion Center, Port Hueneme, Calif. ATTN: Code 753 — 132-133
Commanding Officer, USN Medical Research Institute, National Naval Medical Center, Bethesda 14, Md. — 134
Director, U. S. Naval Research Laboratory, Washington 25, D. C. — 135
Commanding Officer and Director, USN Electronics Laboratory, San Diego 52, Calif. ATTN: Code 210 — 136
Commanding Officer, USN Radiological Defense Laboratory, San Francisco, Calif. ATTN: Technical Information Division — 137-138
Commanding Officer and Director, David W. Taylor Model Basin, Washington 7, D. C. ATTN: Library — 139
Commander, Naval Air Development Center, Johnsville, Pa. — 140
Commanding Officer, Office of Naval Research Branch Office, 1000 Geary St., San Francisco, Calif. — 141-142

AIR FORCE ACTIVITIES

Special Asst. to Chief of Staff, Headquarters, USAF, Rm 5E1019, Pentagon, Washington 25, D. C. — 143
Asst. for Atomic Energy, Headquarters, USAF, Washington 25, D. C. ATTN: DCS/O — 144
Asst. for Development Planning, Headquarters, USAF, Washington 25, D. C. — 145-146
Director of Operations, Headquarters, USAF, Washington 25, D. C. — 147-148
Director of Plans, Headquarters, USAF, Washington 25, D. C. ATTN: War Plans Division — 149
Directorate of Requirements, Headquarters, USAF, Washington 25, D. C. ATTN: AFDRQ-SA/M — 150
Directorate of Research and Development, Armament Division, DCS/D, Headquarters, USAF, Washington 25, D. C. — 151
Directorate of Intelligence, Headquarters, USAF, Washington 25, D. C. — 152-153
The Surgeon General, Headquarters, USAF, Washington 25, D. C. — 154-155

[redacted]

DISTRIBUTION (Continued) Copy No.

Commanding General, U. S. Air Forces Europe, APO 633, c/o PM, New York, N. Y.	156
Commanding General, Far East Air Forces, APO 925, c/o PM, San Francisco, Calif.	157
Commanding General, Alaskan Air Command, APO 942, c/o PM, Seattle, Wash. ATTN: AAOTN	158-159
Commanding General, Northeast Air Command, APO 862, c/o PM, New York, N. Y.	160
Commanding General, Strategic Air Command, Offutt AFB, Omaha, Neb. ATTN: Chief, Operations Analysis	161
Commanding General, Tactical Air Command, Langley AFB, Va. ATTN: Documents Security Branch	162-164
Commanding General, Air Defense Command, Ent AFB, Colo.	165-166
Commanding General, Air Materiel Command, Wright-Patterson AFB, Dayton, Ohio	167-169
Commanding General, Air Training Command, Scott AFB, Belleville, Ill.	170-171
Commanding General, Air Research and Development Command, PO Box 1395, Baltimore 3, Md. ATTN: RDDN	172-174
Commanding General, Air Proving Ground Command, Eglin AFB, Fla., ATTN: AG/TRB	175
Commanding General, Air University, Maxwell AFB, Ala.	176-180
Commandant, Air Command and Staff School, Maxwell AFB, Ala.	181-182
Commandant, Air Force School of Aviation Medicine, Randolph AFB, Tex.	183-184
Commanding General, Wright Air Development Center, Wright-Patterson AFB, Dayton, Ohio. ATTN: WCOESP	185-190
Commanding General, Air Force Cambridge Research Center, 230 Albany St., Cambridge 39, Mass. ATTN: Atomic Warfare Directorate	191
Commanding General, Air Force Cambridge Research Center, 230 Albany St., Cambridge 39, Mass. ATTN: CRTSL-2	192
Commanding General, AF Special Weapons Center, Kirtland AFB, N. Mex. ATTN: Chief, Technical Library Branch	193-195
Commandant, USAF Institute of Technology, Wright-Patterson AFB, Dayton, Ohio. ATTN: Resident College	196
Commanding General, Lowry AFB, Denver, Colo. ATTN: Dept. of Armament Training	197-198
Commanding General, 1009th Special Weapons Squadron, 1712 G St., NW, Washington 25, D. C.	199-201
The RAND Corporation, 1500-4th St., Santa Monica, Calif. ATTN: Nuclear Energy Division	202-203

OTHER DEPT. OF DEFENSE ACTIVITIES

Executive Secretary, Joint Chiefs of Staff, Washington 25, D. C. ATTN: Joint Strategic Plans Committee	204

[redacted]

DISTRIBUTION (Continued)

	Copy No.
Director, Weapons Systems Evaluation Group, OSD, Rm 2E1006, Pentagon, Washington 25, D. C.	205
Asst. for Civil Defense, OSD, Washington 25, D. C.	206
Chairman, Armed Services Explosives Safety Board, D/D, Rm 2403, Barton Hall, Washington 25, D. C.	207
Chairman, Research and Development Board, D/D, Washington 25, D. C. ATTN: Technical Library	208
Executive Secretary, Committee on Atomic Energy, Research and Development Board, Rm 3E1075, Pentagon, Washington 25, D. C.	209-210
Executive Secretary, Military Liaison Committee, PO Box 1814, Washington 25, D. C.	211
Commandant, National War College, Washington 25, D. C. ATTN: Classified Records Section, Library	212
Commandant, Armed Forces Staff College, Norfolk 11, Va. ATTN: Secretary	213
Commanding General, Field Command, AFSWP, PO Box 5100, Albuquerque, N. Mex.	214-219
Chief, AFSWP, PO Box 2610, Washington 13, D. C.	220-228
University of California Radiation Laboratory, PO Box 808, Livermore Calif. ATTN: Margaret Folden	229
Division of Military Application, U. S. Atomic Energy Commission, 1901 Constitution Ave., Washington 25, D. C.	230-232
Los Alamos Scientific Laboratory, Report Library, PO Box 1663, Los Alamos, N. Mex. ATTN: Helen Redman	233-235
Sandia Corporation, Classified Document Division, Sandia Base, Albuquerque, N. Mex. ATTN: Wynne K. Cox	236-255
Weapon Test Reports Group, TIS	256
Surplus in TISOR for AFSWP	257-305

AEC, Oak Ridge, Tenn., AM1964

[redacted]